

PREMIO TESI DI DOTTORATO

- 31 -

PREMIO TESI DI DOTTORATO

Commissione giudicatrice, anno 2012

Luigi Lotti, *Facoltà di Scienze Politiche* (Presidente della Commissione)

Fortunato Tito Arecchi, *Facoltà di Scienze Matematiche, Fisiche e Naturali*

Franco Cambi, *Facoltà di Scienze della Formazione*

Paolo Felli, *Facoltà di Architettura*

Michele Arcangelo Feo, *Facoltà di Lettere e Filosofia*

Roberto Genesio, *Facoltà di Ingegneria*

Mario Pio Marzocchi, *Facoltà di Facoltà di Farmacia*

Adolfo Pazzagli, *Facoltà di Medicina e Chirurgia*

Mario Giuseppe Rossi, *Facoltà di Lettere e Filosofia*

Salvatore Ruggieri, *Facoltà di Medicina e Chirurgia*

Saulo Sirigatti, *Facoltà di Psicologia*

Piero Tani, *Facoltà di Economia*

Fiorenzo Cesare Ugolini, *Facoltà di Agraria*

Vincenzo Varano, *Facoltà di Giurisprudenza*

Graziella Vescovini, *Facoltà di Scienze della Formazione*

Elisa Evangelisti

# **Structural and functional aspects of membranes: the involvement of lipid rafts in Alzheimer's disease pathogenesis**

**The interplay between protein oligomers  
and plasma membrane physicochemical features  
in determining cytotoxicity**

Structural and functional aspects of membranes :  
the involvement of lipid rafts in Alzheimer's disease  
pathogenesis : the interplay between protein oligomers  
and plasma membrane physicochemical features in  
determining cytotoxicity / Elisa Evangelisti. – Firenze :  
Firenze University Press, 2013.

(Premio FUP. Tesi di dottorato ; 31)

<http://digital.casalini.it/9788866554455>

ISBN 978-88-6655-444-8 (print)

ISBN 978-88-6655-445-5 (online)

#### *Peer Review Process*

All publications are submitted to an external refereeing process under the responsibility of the FUP Editorial Board and the Scientific Committees of the individual series. The works published in the FUP catalogue are evaluated and approved by the Editorial Board of the publishing house. For a more detailed description of the refereeing process we refer to the official documents published in the online catalogue of the FUP (<http://www.fupress.com>).

#### *Firenze University Press Editorial Board*

G. Nigro (Co-ordinator), M.T. Bartoli, M. Boddi, R. Casalbuoni, C. Ciappei, R. Del Punta, A. Dolfi, V. Fargion, S. Ferrone, M. Garzaniti, P. Guarneri, A. Mariani, M. Marini, A. Novelli, M. Verga, A. Zorzi.

© 2013 Firenze University Press

Università degli Studi di Firenze

Firenze University Press

Borgo Albizi, 28, 50122 Firenze, Italy

<http://www.fupress.com/>

*Printed in Italy*

# Contents

<b>Summary</b>	<b>9</b>
<b>Introduction</b>	<b>15</b>
1.1 Protein aggregation and amyloidoses	15
1.1.1 Mechanisms of amyloid fibril formation	17
1.1.2 Oligomer structural polymorphism: fibrillar and prefibrillar oligomers	19
1.1.3 Oligomer toxicity: common mechanism of pathogenesis	21
1.1.4 Amyloid formation is an inherent property of polypeptide chains: functional amyloid and disease unrelated amyloid	28
1.2 HypF-N: model protein of amyloid aggregation unrelated to disease	30
1.2.1 Function, structure and aggregation of HypF-N	30
1.2.2 HypF-N protofibrils interact with cell membranes originating a cytotoxic cascade	32
1.2.3 A causative link between the structure of HypF-N oligomers and their ability to cause cellular dysfunction	33
1.3 Alzheimer's disease	34
1.3.1 The Alzheimer phenotype	34
1.3.2 The elaborate processing of APP	35
1.3.3 The genetics of Alzheimer's disease	37
1.3.4 Peripheral cells as a tool to identify and test hypotheses on AD pathophysiology	38
1.3.5 Adult neurogenesis and stem cell technology for AD	39
1.4 Cholesterol and gangliosides in the central nervous system (CNS)	40
1.4.1 Brain cholesterol metabolism	40
1.4.2 Ganglioside metabolism	41
1.4.3 Lipid rafts	42
1.4.4 Role of cholesterol in AD	43
1.4.5 Role of gangliosides in AD	46
1.5 Aim of the study	49
<b>Materials &amp; Methods</b>	<b>51</b>
2.1 Materials	51
2.1.1 Chemicals	51
2.1.2 Fluorescent probes	51
2.1.3 Peptides and aggregation protocols	52

# Amyloid Cytotoxicity and Membrane Lipid Composition

2.2 Cell cultures	53
2.3 Methods	54
2.3.1 Separation processes	54
2.3.2 Differentiation of human mesenchymal stromal cells	55
2.3.3 Modulation of membrane cholesterol levels	56
2.3.4 Modulation of membrane GM1 levels	56
2.3.5 Cholesterol content measurements	56
2.3.6 GM1 content measurements	57
2.3.7 Cell exposure to peptide aggregates	58
2.3.8 Analysis of aggregate interaction with the cells	58
2.3.9 Analysis of aggregate interaction with GM1	59
2.3.10 Analysis of aggregate internalisation	60
2.3.11 Analysis of membrane permeability	60
2.3.12 Analysis of cytosolic $\text{Ca}^{2+}$ dyshomeostasis	60
2.3.13 Evaluation of ROS production	61
2.3.14 Analysis of lipid peroxidation	61
2.3.15 Cytotoxicity assay and cell death analysis: apoptotic and necrotic markers	62
2.3.16 Steady-state fluorescence anisotropy	63
2.3.17 Atomic force microscopy (AFM)	64
2.3.18 Measurements of the fluorescence intensities	65
2.3.19 Statistical analysis	66
<b>Results</b>	<b>67</b>
3.1 Results I	67
3.1.1 A protective role for lipid raft cholesterol against amyloid-induced membrane damage in human neuroblastoma cells	67
3.1.2 $\text{A}\beta_{42}$ oligomer binding to the cell surface and its cytotoxic effect are modulated by membrane cholesterol content	67
3.1.3 $\text{A}\beta_{42}$ oligomers colocalize with lipid rafts	69
3.1.4 Isolation and characterization of DRMs	70
3.1.5 Effects of ADDLs on lipid raft structural order	72
3.1.6 AFM imaging of supported DRMs purified from cells exposed to ADDLs	73
3.2 Results II	76
3.2.1 Lipid rafts mediate amyloid-induced calcium dyshomeostasis and oxidative stress in Alzheimer's disease	76
3.2.2 Lipid rafts are primary interaction sites for $\text{A}\beta_{42}$ oligomers at the plasma membrane	77
3.2.3 Cholesterol and GM1 mediate $\text{A}\beta_{42}$ accumulation at the plasma membrane	79
3.2.4 Cholesterol and GM1 mediate $\text{Ca}^{2+}$ dyshomeostasis and extensive membrane permeabilization induced by <b><math>\text{A}\beta_{42}</math> oligomers</b>	81
3.2.5 GM1 modulates lipid peroxidation and cytotoxicity induced by <b><math>\text{A}\beta_{42}</math> oligomers</b>	83
3.2.6 GM1 mediates $\text{A}\beta_{42}$ -induced $\text{Ca}^{2+}$ dyshomeostasis, lipid peroxidation and cytotoxicity in rat cortical neurons	85

<b>3.3 Results III</b>	<b>86</b>
3.3.1 Membrane lipid composition and its physicochemical properties define cell vulnerability to aberrant protein oligomers	86
3.3.2 Membrane cholesterol content modulates oligomer cytotoxicity	86
3.3.3 Membrane cholesterol modulates oligomer-induced alteration of intracellular $\text{Ca}^{2+}$ homeostasis and ROS levels	90
3.3.4 Cholesterol levels modulate membrane permeability to the oligomers	92
3.3.5 Membrane GM1 affects the cytotoxic and permeabilizing effects of HypF-N oligomers	96
3.3.6 GM1, rather than cholesterol, plays a dominant role in oligomer cytotoxicity and membrane permeability	99
<b>3.4 Results IV</b>	<b>102</b>
3.4.1 Neuronal differentiation of human mesenchymal stromal cells increases their resistance to $\text{A}\beta 42$ aggregate toxicity	102
3.4.2 Neuronal differentiation of hMSCs results in reduced levels of membrane GM1	102
3.4.3 Neuronal differentiation of hMSCs reduces the interaction of $\text{A}\beta 42$ oligomers with the cell surface	104
3.4.4 Neuronal differentiation of hMSCs reduces $\text{A}\beta 42$ oligomer-induced intracellular $\text{Ca}^{2+}$ dyshomeostasis and oxidative stress	104
3.4.5 Neuronal differentiation of hMSCs increases cell resistance to $\text{A}\beta 42$ aggregates	106
<b>Discussion</b>	<b>109</b>
4.1 A protective role for lipid raft cholesterol against amyloid-induced membrane damage in human neuroblastoma cells	109
4.2 Lipid rafts mediate amyloid-induced calcium dyshomeostasis and membrane permeabilization in Alzheimer's fibroblasts	112
4.3 Membrane lipid composition and its physicochemical properties define cell vulnerability to aberrant protein oligomers	114
4.4 Neuronal differentiation of human mesenchymal stromal cells increases their resistance to $\text{A}\beta 42$ aggregate toxicity	117
4.5 Concluding remarks	118
<b>Abbreviations</b>	<b>121</b>
<b>References</b>	<b>123</b>



## **Summary**

The conversion of peptides and proteins from their native states to highly structured fibrillar aggregates, that accumulate in the extracellular or in the intracellular space, is a defining characteristic of many human disorders, including Alzheimer's disease, Creutzfeldt-Jacob disease, type II diabetes and a number of systemic amyloidoses. It is generally thought that amyloid oligomers formed early in the process of protein aggregation, or released from mature amyloid fibrils, are the pathogenic species in protein deposition diseases. This pathological feature appears likely to result, at least in part, from the ability of oligomers to interact with cell membranes, modifying the properties of the phospholipid bilayer, the stabilities and functions of its associated proteins and to enter the cell, thus causing cell dysfunction. The N-terminal domain of the prokaryotic hydrogenase maturation factor (HypF-N) is a valuable model system for investigating the structural basis of the cellular impairment caused by misfolded protein oligomers. In fact, it can rapidly be converted into stable oligomers under conditions that promote its unfolding into partially folded species and can generate a cascade of events, resulting in cytotoxicity and death, when added to cells.

Alzheimer's disease (AD) is a common form of dementia that results in memory loss and impairment of cognitive function in the elderly. A major pathological hallmark of AD is the formation of extracellular senile plaques composed of aggregated amyloid  $\beta$ -peptide ( $A\beta$ ), which is generated by sequential enzymatic cleavage of the amyloid precursor protein (APP) by  $\beta$ -secretase and the  $\gamma$ -secretase complex. Several lines of evidence suggest that soluble oligomers may be the principal neurotoxic agent in AD. Indeed, amyloid-derived diffusible ligands (ADDLs) are found in the cerebrospinal fluid of AD patients and the ADDL content of human brains better correlates with disease severity than do classical amyloid plaques containing insoluble  $A\beta$  deposits. Moreover, there is a rising consensus on major role of membranes as initial triggers of the biochemical modifications culminating with neuronal death. In spite of the intense research carried out in recent times, the role of cholesterol as a risk factor for AD remains controversial. The content of membrane cholesterol can modulate  $A\beta$  peptide production, aggregation and clearance in various ways, particularly by affecting the stability of lipid rafts and other membrane domains where APP and some APP processing secretases are located, as well as the activity of raft associated proteins. Increasing evidence now shows that  $A\beta$  can tightly associate with GM1 ganglioside (a component of lipid rafts), and it was originally postulated that this may act as a seed for its accumulation and aggregation. These findings, to-

## Amyloid Cytotoxicity and Membrane Lipid Composition

gether with the presence, in the raft domains, of ligand-gated calcium channels (the AMPA and NMDA glutamate receptors) involved in  $\text{Ca}^{2+}$  influx into neuronal synaptic ends and in  $\text{Ca}^{2+}$  permeabilization of amyloid-exposed cells has implicated lipid rafts as likely primary interaction sites for ADDLs.

Taking into account these observations, the aim of the present study is to get clues into the molecular basis of amyloid cytotoxicity with particular interest in the interaction of different types of oligomers, related or not with diseases, with cell membrane (or its subfractions, as lipid rafts) and the resulting cascade of events, culminating in cellular dysfunction and death. We also focused our attention to the role of membrane cholesterol and GM1 as possible modulators of the interaction between amyloid aggregates and the plasma membrane of exposed cells. Finally, considering that cell therapy is a promising approach for the treatment of neurodegenerative conditions such as AD, we investigated the relative vulnerability of human mesenchymal stromal cells and their neuronally differentiated counterparts to  $\text{A}\beta 42$  oligomers in view of the presence of toxic aggregates in tissue, which raises the question of whether grafted stem cells are susceptible to amyloid toxicity before they differentiate into mature neurons.

The present studies provide evidence that:

I) Cell resistance to amyloid toxicity is strictly related to lipid raft cholesterol content in SH-SY5Y cells. In particular, in our model cells, membrane cholesterol modulation was achieved by supplementing the cell culture media with water soluble cholesterol (PEG-chol) to increase the levels of membrane cholesterol; on the other hand, cholesterol levels were diminished by using methyl- $\beta$ -cyclodextrin ( $\beta$ -CD) or mevastatin (Mev). A moderate enrichment of membrane cholesterol in PEG-chol treated cells appeared to reduce the ADDLs interaction with the monosialoganglioside GM1 while an increased colocalization was found in cholesterol depleted cells following treatment with  $\beta$ -CD or Mev.  $\text{A}\beta$  oligomers interact with the plasma membrane preferentially at the raft domains and any structural modification of the latter following increase or decrease of cell cholesterol results in alterations of ADDL-raft interaction. In addition, cholesterol enrichment protects lipid rafts from perturbation induced by  $\text{A}\beta 42$ , indeed cholesterol-enriched lipid rafts did not display any significant change of the structural order upon exposure to  $\text{A}\beta 42$  oligomers. On the contrary, cholesterol loss resulted in increased rigidity of rafts exposed to oligomers, which penetrated and stiffen the raft bilayer. Accordingly, as imaged by AFM, the presence of the peptide clearly altered DRM morphology, giving rise to the formation of cavities in all samples, whose depth and size were significantly reduced in cholesterol-enriched samples with respect to those displayed by cholesterol-depleted samples. These results showed that the content of cholesterol affects the ability of ADDLs to interact with the cell membrane by modulating membrane physical features at the raft level.

II) Two lipidic raft components, that are cholesterol and GM1, affect the susceptibility of Familial Alzheimer's Disease (FAD) fibroblasts to  $\text{A}\beta 42$  oligomers in opposite ways, by modulating amyloid binding to lipid rafts and its subsequent toxic

effects. In the present study, primary fibroblasts from FAD patients carrying APP or PS1 gene mutations, secreted elevated amounts of A $\beta$ 42 peptide and showed greater membrane permeability and lipid peroxidation with respect to fibroblasts obtained from healthy subjects, suggesting partial disruption of membrane integrity and chronic oxidative stress associated with enhanced A $\beta$  production. Lipoperoxidation was higher in DRMs compared to the entire cell membrane, pointing to lipid rafts as preferential sites for A $\beta$ 42 interaction at the cell surface. Indeed, as observed by contact mode AFM, the increased release of A $\beta$ 42 in FAD fibroblasts was associated with evident alteration of lipid raft morphology, resulting in the formation of steps/cavities in DRMs purified from FAD fibroblasts. Moreover, A $\beta$  treatment induced greater aggregate-ganglioside colocalization and DRM structure perturbation in FAD fibroblasts, with respect to WT controls. Moreover, in our model cells, membrane cholesterol modulation was achieved by supplementing the cell culture media with water soluble cholesterol (Chol) to increase the levels of membrane cholesterol; on the other hand, cholesterol levels were diminished by using mevastatin (Mev). In addition, an increase in GM1 content was achieved treating cells with GM1 from bovine brain (GM1), whereas GM1 depletion was obtained exposing cells to D-threo-1-phenyl-2-decanoylamino-3-morpholino-1-propanol (PDMP), a glucosylceramide synthase inhibitor that blocks the natural synthesis of GM1. The increase in cytosolic Ca<sup>2+</sup> content and alteration of membrane permeability was much smoother and milder in cholesterol-enriched or GM1-depleted fibroblasts exposed to amyloid oligomers with respect to similarly treated control cells with basal cholesterol or GM1 content. In contrast, membrane cholesterol depletion or GM1 enrichment triggered a greater increase in cytosolic Ca<sup>2+</sup> levels and membrane permeability. Even in primary rat cortical neurons membrane GM1 content influences A $\beta$ 42 toxicity and intracellular Ca<sup>2+</sup> homeostasis, corroborating our hypothesis at the neuronal level. Moreover, pre-treatment with anti-GM1 antibodies, cholera toxin subunit B – a specific GM1 ligand – or with NAA, an enzyme that leaves the content and structure of GM1 unchanged except for the removal of the negatively charged sialic acid moiety, completely suppressed A $\beta$ -induced Ca<sup>2+</sup> spikes and membrane damage, suggesting that the negative charge on GM1 is a key factor determining calcium dyshomeostasis and membrane permeabilization, which results in cell vulnerability to A $\beta$  oligomers. Overall, our data suggest that raft cholesterol and GM1, by modulating membrane fluidity and charge, respectively, may specifically influence the binding of A $\beta$ 42 oligomers, their insertion into the phospholipid bilayer and their ability to disrupt membrane structure, which ultimately triggers cell death.

III) The degree of toxicity of the oligomeric species results from a complex interplay between the structural and physicochemical features of both the oligomers and the cellular membrane. In particular, we modulated the structural rigidity and/or charge density of the plasma membrane by altering in a variety of ways the levels of either cholesterol or GM1, or of both at one time. We analyzed the cytotoxicity to cultured neuroblastoma cells with a normal or a rationally altered content of membrane lipids, of two types of pre-formed HypF-N oligomers that we previously found to display different structural features and toxicities. Our results show that

both type A and B oligomers were internalized and sorted into endocytotic vesicles in the exposed cells. However, interaction of oligomer with the cell membrane and internalisation were significantly decreased in cells enriched in membrane cholesterol or with a reduced content of GM1; in particular, type B oligomers, that were unable to cross the plasma membrane of SH-SY5Y cells with a basal lipid content, became increasingly internalised in cells with a reduced content of cholesterol. Moreover, the cytotoxicities of A $\beta$ 42 oligomers and of the two types of misfolded HypF-N oligomers used in this study were dramatically affected by the physicochemical features of the cell membrane. In particular, the oligomers found to be toxic to the cells with basal lipid content became increasingly significantly less toxic as the membrane cholesterol level was increased or that of GM1 was decreased, whereas the opposite effect was found with cells treated so as to reduce their content of membrane cholesterol. Conversely, the oligomers that were not toxic to untreated cells remained harmless to cells with an increased content of cholesterol or a reduced content of GM1, but became increasingly harmful as the content of cholesterol in the membrane was decreased or that of GM1 was increased, reaching levels of toxicity comparable to those shown by the toxic oligomers with untreated cells. A number of characteristic features known to underlie oligomer cytotoxicity were also found to be modified in the cells with an altered membrane lipid composition, including cell membrane permeability, the levels of intracellular Ca<sup>2+</sup> and ROS, and the apoptotic response. The data obtained using cells with an altered content of both membrane cholesterol and GM1 show that the alteration in the GM1 levels plays a dominant role in determining the resulting effects. The importance of GM1 relative to cholesterol in determining oligomer-mediated cytotoxicity is also supported by our findings of an inverse relationship between the content of cholesterol and of GM1 in the plasma membrane of our cell model. The data reported here, therefore, lead us to conclude that the level of cytotoxicity of a specific type of protein oligomer, or indeed of other amyloid-related structures, is the result of a complex interplay between two critical factors: the specific properties of the aberrant protein assemblies (e.g., relative stability, disorder, flexibility and exposure of hydrophobic surface) and the physicochemical features of the interacting cell membranes that are associated with their lipid composition (e.g. fluidity, electrostatic potential, curvature, lateral pressure).

IV) Neuronal differentiation of human mesenchymal stromal cells increases their resistance to A $\beta$ 42 aggregate toxicity. In this study, we investigated whether, and to what extent, undifferentiated human mesenchymal stromal cells (hMSCs) and their neuronally differentiated counterparts (hMSC-n) were affected by the of A $\beta$ 42 oligomer toxicity. Our data show that the two cell types displayed differential susceptibility to A $\beta$  aggregate-induced toxicity. We found that undifferentiated cells were much more vulnerable to A $\beta$ 42 oligomers than their differentiated counterparts. The more vulnerable, undifferentiated cells displayed significantly higher membrane GM1 content, thus explaining their ability to bind and to be permeabilized by A $\beta$ 42 oligomers, together with the resulting increase in Ca<sup>2+</sup> and ROS and loss of cell viability. We report that a neuronally differentiated cell model is intrinsi-

Elisa Evangelisti

cally more resistant to A $\beta$ 42 oligomer-induced cytotoxicity than the undifferentiated, cognate cell line, and that the molecular basis of this differential susceptibility can be traced, at least in part, to the GM1 content of the plasma membrane.



# Introduction

## 1.1 Protein aggregation and amyloidoses

A broad range of human diseases arises from the failure of a specific peptide or protein to adopt, or remain in, its native functional conformational state. These pathological conditions are generally referred to as protein misfolding (or protein conformational) diseases. The largest group of misfolding diseases, however, is represented by amyloidoses (Chiti and Dobson, 2006). These diseases are characterized by the presence of deposits of fibrillar aggregates found as intracellular inclusions or extracellular plaques whose main constituent is a specific peptide or protein, different in the varying disorders (Table I) (Stefani, 2004). These diseases include a range of sporadic, familial or transmissible degenerative diseases, some of which affect the brain and the central nervous system (e.g. Alzheimer's and Creutzfeldt-Jakob diseases), while others involve peripheral tissues and organs such as the liver, heart and spleen (e.g. systemic amyloidoses and type II diabetes) (Stefani and Dobson, 2003). In addition, there are others diseases (Parkinson's and Huntington's diseases) characterized by the presence of intracellular, rather than extracellular, deposits localized in the cytoplasm, in the form of specialized aggregates known as Lewy bodies, or in the nucleus (Table I).

Despite the large differences in the structures of the proteins and peptides aggregated in the assemblies found in the differing amyloidoses or produced *in vitro*, amyloid fibrils share basic structural features and an ordered core structure. A typical amyloid fibril is straight, unbranched, 6-12 nm in width and reaches around 1  $\mu\text{m}$  in length; it is formed by a variable number of elementary filaments (protofilaments) twisted around each other, typically 1.5-2.0 nm in diameter (Serpell *et al.*, 2000). The main structural hallmark of amyloid fibrils is the ordered core of their protofilaments. The latter results from a double beta sheet which extends along the main filament axis and whose beta strands provided by each monomer stacks in register and run perpendicular to the fibril axis (what is known as cross-beta structure, whose signatures are the reflections at 4.8 and 9.6-11 Å in X-ray diffraction patterns) (Nelson *et al.*, 2005). Moreover, this cross- $\beta$  structure confers to the amyloid fibrils specific biophysical characteristics and a variety of tinctorial properties, notably staining with thioflavin T (ThT) and Congo red (CR).

## Amyloid Cytotoxicity and Membrane Lipid Composition

Clinical syndrome	Fibril component
<i>Alzheimer's disease</i>	<i>A<math>\beta</math> peptides (1–40, 1–41, 1–42, 1–43); Tau</i>
<i>Spongiform encephalopathies</i>	<i>Prion protein (full-length or fragments)</i>
<i>Parkinson's disease</i>	<i><math>\alpha</math>-synuclein (wild type or mutant)</i>
<i>Fronto-temporal dementias</i>	<i>Tau (wild type or mutant)</i>
<i>Familial Danish dementia</i>	<i>ADan peptide</i>
<i>Familial British dementia</i>	<i>ABri peptide</i>
<i>Hereditary cerebral haemorrhage with amyloidoses</i>	<i>Cystatin C (minus a 10-residue fragment); A<math>\beta</math> peptides</i>
<i>Amyotrophic lateral sclerosis</i>	<i>Superoxide dismutase (wild type or mutant)</i>
<i>Dentatorubro-pallido-Luysian atrophy</i>	<i>Atrophin 1 (polyQ expansion)</i>
<i>Huntington disease</i>	<i>Huntingtin (polyQ expansion)</i>
<i>Cerebellar ataxias</i>	<i>Ataxins (polyQ expansion)</i>
<i>Kennedy disease</i>	<i>Androgen receptor (polyQ expansion)</i>
<i>Spino cerebellar ataxia 17</i>	<i>TATA box-binding protein (polyQ expansion)</i>
<i>Primary systemic amyloidosis</i>	<i>Ig light chains (full-length or fragments)</i>
<i>Secondary systemic amyloidosis</i>	<i>Serum amyloid A (fragments)</i>
<i>Familial Mediterranean fever</i>	<i>Serum amyloid A (fragments)</i>
<i>Senile systemic amyloidosis</i>	<i>Transthyretin (wild-type or fragments thereof)</i>
<i>Familial amyloidotic polyneuropathy I</i>	<i>Transthyretin (over 45 variants or fragments thereof)</i>
<i>Hemodialysis-related amyloidosis</i>	<i><math>\beta</math>2-microglobulin</i>
<i>Familial amyloid polyneuropathy III</i>	<i>Apolipoprotein A-1 (fragments)</i>
<i>Finnish hereditary systemic amyloidosis</i>	<i>Gelsolin (fragments of the mutant protein)</i>
<i>Type II diabetes</i>	<i>Pro-islet amyloid polypeptide (fragments)</i>
<i>Medullary carcinoma of the thyroid</i>	<i>Procalcitonin (full-length or fragment)</i>
<i>Atrial amyloidosis</i>	<i>Atrial natriuretic factor</i>
<i>Lysozyme systemic amyloidosis</i>	<i>Lysozyme (full-length, mutant)</i>
<i>Insulin-related amyloid</i>	<i>Insulin (full-length)</i>
<i>Fibrinogen <math>\alpha</math>-chain amyloidosis</i>	<i>Fibrinogen (<math>\alpha</math>-chain variants and fragments)</i>

Table I. A summary of the main amyloidoses and the proteins or peptides involved. Conditions affecting the central nervous system are written in italic. From (Stefani, 2004).

The cross- $\beta$  structure can be therefore considered as the main structural hallmark of the amyloid aggregates. (Fig. 1) (Chiti and Dobson, 2006).

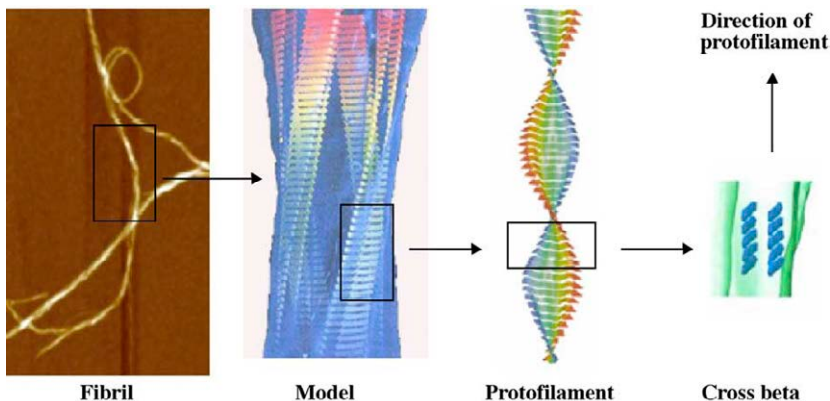


Figure 1. Close-up view of the structural organization of an amyloid fibril. The four protofilaments are wound around each other and their core structure is a row of  $\beta$ -sheets where each strand runs perpendicular to the fibril axis. From (Stefani, 2004).

### 1.1.1 Mechanisms of amyloid fibril formation

Protein folding and protein aggregation must be distinct but competing pathways the same polypeptide chain can undergo depending on the environmental conditions (Stefani, 2008). The view that protein folding and aggregation are competing paths considers both as distinct yet not mutually excluding processes relying on a more general energy landscape including conformational states not involved in protein folding, yet potentially accessible to a polypeptide chain (Jahn and Redford, 2008). The two sides of the protein energy landscape highlight the competition between intramolecular (folding) and intermolecular (aggregation) interactions, which increases considerably the roughness of the whole landscape (Fig. 2) (Stefani, 2008).

Moreover, protein folding and protein aggregation rely on similar physicochemical parameters of the polypeptide chain including a significant propensity to gain secondary structure, a low net charge, and a relatively high content of hydrophobic residues (Stefani, 2008). Any alteration of a protein's expression level or structure (increased synthesis or reduced degradation, presence of specific mutations or chemical modifications) or any minor, even subtle, change in the environmental conditions can trigger the build-up of the precursor, aggregation-prone, species that nucleate rapid growth of aggregates. The latter include heat shock, oxidative stress or chemical modifications, alterations of the intracellular macromolecular crowding, presence of suitable surfaces, absence of stabilizing ligands, any impairment of the quality control of protein folding in the cell, and others (reviewed in Chiti and Dobson, 2006; Stefani and Dobson, 2003; Stefani, 2010a). It is widely established that amyloid fibril formation has many characteristics of a “nucleated growth” mechanism. The time course of the conversion of a peptide or protein into its fibrillar form (measured by ThT fluorescence, light scattering, or other techniques) typically includes a lag phase that is followed by a rapid exponential growth phase (Pedersen *et al.*, 2004; Serio *et al.*, 2000). The lag phase is assumed to be the time required for

## Amyloid Cytotoxicity and Membrane Lipid Composition

“nuclei” to form. The lag phase can be shortened or eliminated by the addition of preformed aggregates to fresh solutions, a process known as seeding. Once a nucleus is formed, fibril growth is thought to proceed rapidly by further association of either monomers or oligomers with the nucleus. (Chiti and Dobson, 2006). The first phase in amyloid formation seems to involve the formation of soluble oligomers as a result of relatively non specific interactions, although, in some cases, specific structural transitions, such as domain swapping, might be important (Sirangelo *et al.*, 2004). The earliest species visible by electron or atomic-force microscopy (AFM) generally resemble small bead-like structures having a diameter of 2–5 nm, sometimes linked together, and often described as amorphous aggregates or as micelles. These early ‘prefibrillar aggregates’ then transform into species with more distinctive morphologies, often called ‘protofilaments’ or ‘protocellulins’ (Fig. 3).

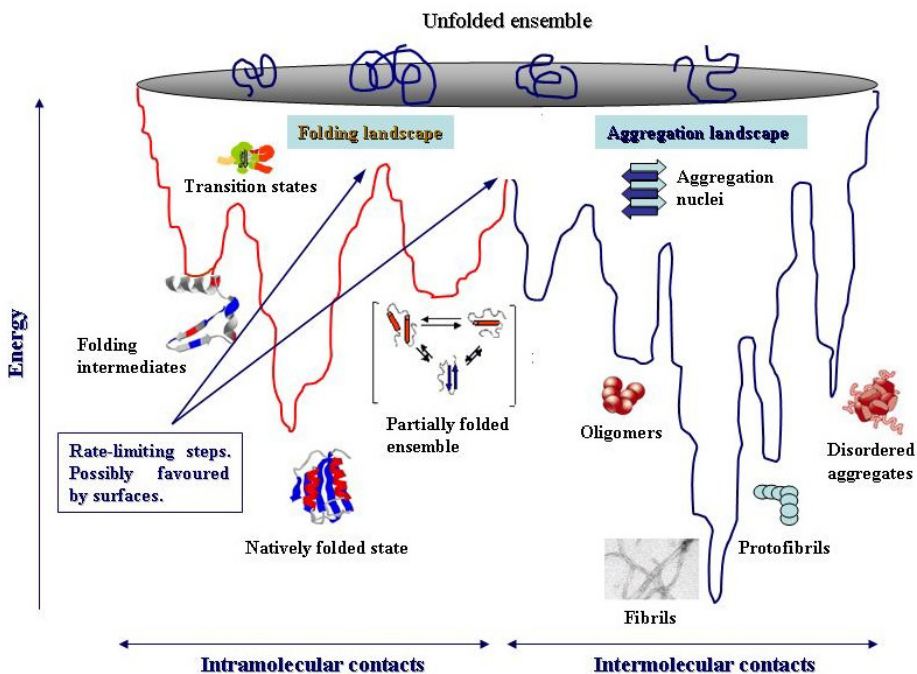


Figure 2. A combined energy landscape model for protein folding (left) and aggregation (right) starting from the unfolded ensemble. Both sides display considerable roughness, but amyloid fibrils display a remarkably higher stability and lower energy content than the natively folded structure. The picture highlights the multitude of the different conformational states available to a protein when they are stabilized by either intramolecular (monomeric protein) or intermolecular (aggregation intermediates and mature fibrils) contacts. The presence of intermolecular contacts increases dramatically the ruggedness of the landscape for protein aggregation with respect to what is shown in the folding side. From (Stefani, 2008).

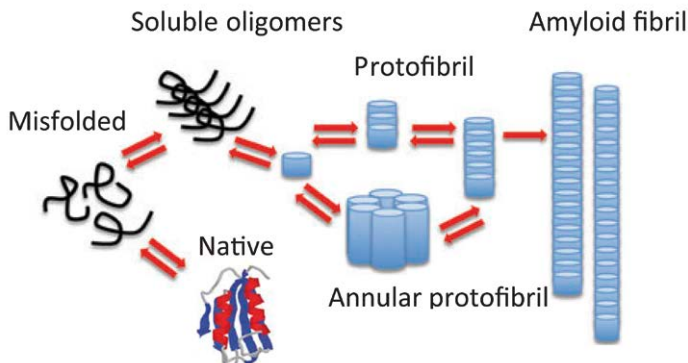


Figure 3. A schematic representation of the general mechanism of aggregation to form amyloid fibrils. Unfolded or partially unfolded proteins associate with each other to form small, soluble aggregates that undergo further assembly into protofibrils or protofilaments and then mature fibrils. Modified from (Williams and Serpell, 2011).

These structures are commonly short, thin, sometimes curly, fibrillar species that are thought to assemble into mature fibrils, perhaps by lateral association accompanied by some degree of structural reorganization. The nucleation-dependent polymerization mechanism of fibril growth, whose physical bases approach those of the ordered assembly occurring in crystal growth, also supports fibril stability and represents a key difference between protein folding and protein aggregation (Stefani, 2010a). The aggregates that form first are likely to be relatively disorganized structures that expose a variety of segments of the protein that are normally buried in the globular state (Bucciantini *et al.*, 2002). In some cases, however, these early aggregates appear to adopt quite distinctive structures, including well-defined annular species (Dobson, 2003; Lashuel *et al.*, 2002). Analogous spherical and chain-like protofibrillar structures have been observed for many systems, including amyloid- $\beta$  peptide ( $A\beta$ ) peptide (Harper *et al.*, 1997; Walsh *et al.*, 1999)  $\alpha$ -synuclein (Conway *et al.*, 2000), amylin (Kayed *et al.*, 2004), the immunoglobulin light chain (Ionescu-Zanetti *et al.*, 1999), transthyretin (Quintas *et al.*, 2001), polyQ-containing proteins (Kayed *et al.*, 2004),  $\beta 2$ -microglobulin (Gosal *et al.*, 2005). These species are generally characterized by extensive  $\beta$ -structure and sufficient structural regularity to bind ThT and CR (Chiti and Dobson, 2006).

### 1.1.2 Oligomer structural polymorphism: fibrillar and prefibrillar oligomers

The heterogeneity, remarkable instability and intrinsically disordered nature of oligomeric species makes it very difficult to get solid data on their conformational features. An important contribution on this issue has come from the use of antibodies raised against amyloid fibrils and their precursors that are able to recognise spe-

## Amyloid Cytotoxicity and Membrane Lipid Composition

cific structural features present in different forms of these assemblies and hence to discriminate among them. A previous study reported the generation of two conformational antibodies, A11 and OC, recognising oligomers and fibrils, respectively (Glabe, 2008; Kayed *et al.*, 2003; O’Nuallain *et al.*, 2002). It has been proposed two distinct types of oligomers: prefibrillar oligomers that are A11-positive and OC-negative, and fibrillar oligomers that are A11-negative and OC-positive (Fig. 4) (Glabe, 2008; Kayed *et al.*, 2003). As prefibrillar oligomers are not recognized by the fibril-specific antibodies, and are considered to be transient intermediates in the fibril formation process, a conformational change is necessary for them to become fibrils. It should be noted that the oligomer specific A11 antibody also recognizes soluble oligomers from various proteins, such as those from  $\alpha$ -synuclein, islet amyloid polypeptide, polyglutamine (PolyQ), lysozyme, human insulin and fragment of prion protein (PrP 106–126) (Kayed *et al.*, 2003).

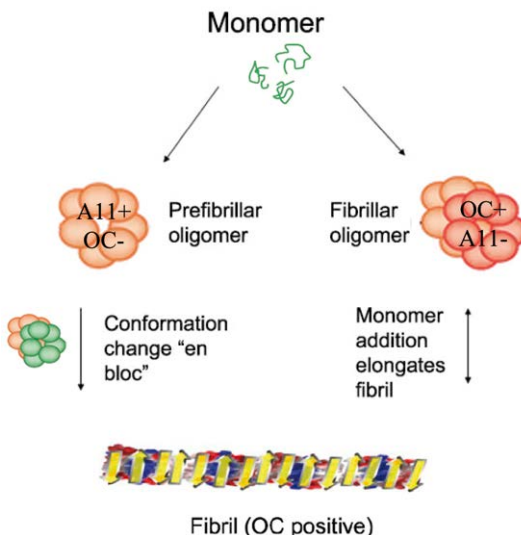


Figure 4. Schematic representation of the distinct types of amyloid oligomers and fibrils. The aggregation pathway can diverge into two paths depending on which conformation it adopts. Monomers can aggregate to form prefibrillar oligomers that are A11-positive and OC-negative (left pathway). These prefibrillar oligomers may then undergo a concerted conformation change “en bloc” to form fibrils. In the other pathway, monomers aggregate to form a fibrillar conformation that is OC-positive and A11-negative (right pathway). These fibrillar oligomers may represent fibril nuclei or seeds that are aggregates capable of elongating by recruiting additional monomers at their ends. Fibrils may be distinct from fibrillar oligomers on the basis of their content of multiple protofilaments. Modified from (Glabe, 2008).

These findings suggest that various proteins may form prefibrillar oligomers that share a common structure regardless of their amino acid sequence (Chiti and Dobson, 2006; Glabe, 2008; Kayed *et al.*, 2003; Sakono and Zako, 2010). However, be-

cause the fibrillar oligomers are recognized by the fibril-specific antibody, but not by A11, they at least possess the structural characteristics of fibrils. Thus, it is plausible that the fibrillar oligomer might represent fibril nuclei to which the monomers can attach before elongation (Glabe, 2008). A $\beta$  oligomers formed at a low pH, but not those formed at a neutral pH, are recognized by the 6E10 antibody (Necula *et al.*, 2007). These results strongly suggest the existence of a structural polymorphism of A $\beta$  oligomers. These data suggest the existence of at least two alternative aggregation nuclei for amyloid fibrils: one type evolving into mature fibrils directly but only after extensive structural reorganization and another type, possibly the true fibril precursor, growing into increasingly sized aggregates where added monomers acquire a new structure when incorporated into the oligomer. In general, the use of conformational antibodies raised specifically to amyloid oligomers, prefibrillar assemblies and mature fibrils has provided an invaluable tool to distinguish these distinct entities, clearly showing the existence of differences in their structural features (Glabe *et al.*, 2004; Kayed and Glabe, 2006; Kayed *et al.*, 2007; Mamikonyan *et al.*, 2007). It has also provided knowledge to show that the same protein/peptide at the onset of aggregation can generate oligomeric and prefibrillar assemblies with clearly different structural features (Kumar and Udgaonkar, 2009), thus providing a tool to investigate the conformational modifications underlying the hierarchical growth of amyloid fibrils as well as oligomer structural heterogeneity. Overall, these findings indicate that prefibrillar aggregates of different proteins and peptides share some basic structural features that are different from those displayed by the folded monomers or their fibrillar counterparts. These features can include the different exposure to the aqueous environment of hydrophobic patches normally buried into the compact structure of the monomeric protein following protein unfolding. On this aspect, chemical modifications and, more generally, environmental conditions can play a pivotal role not only in promoting/hindering protein misfolding and aggregation, but also in affecting the structural features of the aggregation nuclei, thus targeting them to organize into fibril precursors and mature fibrils with different structures, stabilities and cytotoxicities (Bravo *et al.*, 2008; Chen and Kokholyan, 2005; Danzer *et al.*, 2007). The structural features of amyloid oligomers, besides explaining the intrinsic instability of the latter, also provide clues to explain the tendency of amyloid oligomers and other unstable prefibrillar aggregates to interact inappropriately with cellular components and, accordingly, their toxic potential.

### 1.1.3 Oligomer toxicity: common mechanism of pathogenesis

The presence of highly organized and stable fibrillar deposits in the organs of patients suffering from protein deposition diseases led initially to suggest a causative link between protein misfolding, aggregation and pathological symptoms, often known as the “amyloid hypothesis”. Until recently, mature amyloid fibrils were considered the key agents responsible for cell damage and tissue impairment since they were the form of the aggregates commonly found in the pathological deposits (extracellular plaques or intracellular inclusions). Therefore, it appeared that the patho-

genic features of amyloid diseases resulted from the interaction with cell components of the deposits of the aggregated material. By providing a theoretical frame to understand the molecular basis of amyloid diseases, such a view stimulated the exploration of therapeutic approaches to amyloidoses mainly aimed at hindering fibrillar aggregate growth and deposition. However, the idea that mature fibrils are the main agents responsible of cell demise in the affected tissues is presently challenged by an impressive body of experimental data (reviewed in Stefani, 2010a). The different assemblies grown in the fibrillization path differ greatly not only in their cytotoxic potential but also in the cellular mechanisms and functions they interfere with, that appear to be specific for the aggregation state. For example, small A $\beta$ 42 oligomers found in the brains of Alzheimer's disease (AD) people impair long-term potentiation (Klyubin *et al.*, 2005; Walsh *et al.*, 2002) and raise endoplasmic reticulum stress (Chafekar *et al.*, 2007) whereas the neuroinflammatory response in AD brain appears more specifically associated to the presence of fibrillar A $\beta$  (Eikeleboom *et al.*, 2002). Moreover, at least in the case of the A $\beta$  peptides, cytotoxicity appears to be mediated by aggregation state-specific uptake; in fact, oligomer internalization by endocytosis into lysosomes appears associated with oligomer toxicity, whereas harmless amyloid fibrils are not internalized (Chafekar *et al.*, 2008). Actually, although in some cases mature amyloid fibrils can impair directly cell viability (Gharibyan *et al.*, 2007; Novitskaya *et al.*, 2006), most often the oligomeric assemblies transiently arising in the path of fibrillization of several peptides and proteins are the main or even the sole cytotoxic species (Lambert *et al.*, 1998; Reixach *et al.*, 2004; Walsh *et al.*, 1999; Walsh *et al.*, 2002). The idea that prefibrillar aggregates are the most highly toxic species among amyloids has led to consider mature fibrils as substantially inert, harmless deposits of the toxic precursors and their growth as a cell defense mechanism; it can also explain the lack of direct correlation between amyloid load in the brains of AD patients and severity of their clinical symptoms (Dickson, 1995). Recent studies on this issue indicate that amyloid oligomers are highly flexible and dynamic assemblies growing as in-path or off-path intermediates of amyloid fibrils. In general, they expose patches of hydrophobic residues on their surface and in differing environmental conditions they can exhibit remarkable structural differences even when they are grown from the same peptide/protein underlying their growth into mature fibrils with different structural, physical and morphological features (reviewed in Stefani, 2010a). Although most of these fibrillar amyloids assemblies are considered intermediates in the path of fibrillization, some of them, such as the frequently imaged small annular oligomers ("doughnuts"), could be "dead end" products of the process or, at any rate, structurally and functionally distinct types of amyloid oligomers (Kayed *et al.*, 2009). Finally, soluble oligomers grown in the fibrillization path of several peptides and proteins have also been repeatedly detected in, and purified from, cultured cells and tissues where the monomeric precursors are expressed (Billings *et al.*, 2005; Cleary *et al.*, 2005; Koffie *et al.*, 2009; Lesné *et al.*, 2006). These data reinforce the idea that amyloid oligomers are really formed *in vivo* and are directly associated with cell/tissue impairment (Koffie *et al.*, 2009).

The presence of toxic aggregates inside or outside cells can impair a number of cell functions that ultimately lead to cell death by an apoptotic mechanism. Recent research suggests, however, that in most cases initial perturbations to fundamental cellular processes underlie the impairment of cell function induced by aggregates (Stefani and Dobson, 2003).

### **1.1.3.1 Biological surfaces as primary sites of amyloid aggregation, interaction and toxicity**

Peptides and proteins can interact with, and be actively recruited by, inorganic, synthetic, or biological surfaces, in particular membranes (Bokvist *et al.*, 2004), but also macromolecules (Bravo *et al.*, 2008; Cherny *et al.*, 2004; Relini *et al.*, 2006; Suk *et al.*, 2006), thus modifying their conformational states, resulting in non-native, aggregation-prone conformations. Such a view has led to the proposal that surfaces can catalyse amyloid aggregate nucleation and growth by a mechanism substantially different from that observed in the bulk solution (reviewed in Sethuraman and Belfort, 2005; Stefani, 2007; Stefani, 2010b). Surfaces, apart from populating aggregation-prone conformers possibly different from those arising in solution, can also strongly increase the local concentration of the latter, thus speeding up aggregate nucleation, possibly accompanied by structural alterations of membrane integrity (Porat *et al.*, 2003). These considerations account for the increasing interest in the investigation of the physicochemical features of protein interaction with, and aggregation on, artificial or natural surfaces, even in relation to the structure and lipid composition of the latter. Apart from favouring protein misfolding and aggregation, synthetic and natural phospholipid bilayers can also be key interaction sites with prefibrillar aggregates (reviewed in Stefani, 2007; Stefani, 2010b). In general, protein aggregation onto, or aggregate interaction with, cell membranes results in lipid extraction, loss of membrane integrity, derangement of selective permeability and impairment of specific membrane-bound protein function and signalling pathways (reviewed in Stefani, 2007; Stefani, 2010b). In the past, several cell surface proteins have been considered as possible candidate receptors of A $\beta$  aggregates. These receptors could be specific for the shared cross- $\beta$  fold rather than for any peculiar structural feature of the A $\beta$  peptides although, in some cases, they could also be monomer-specific, as in the  $\beta$ -amyloid precursor protein (APP) or Abeta-TNFR1 (tumour-necrosis factor receptor-1) interactions proposed to be at the origin of A $\beta$  cytotoxicity (He *et al.*, 2004; Shadek *et al.*, 2006). Since 1996, the receptor for advanced glycation end products (RAGE) has been proposed as a major candidate as amyloid receptor (Yan *et al.*, 1996). RAGE is increased in systemic amyloidoses, is able to interact with amyloid assemblies made from serum amyloid A, amylin and prion-derived peptides (Yan *et al.*, 2000) and appears involved in Alzheimer's and Creutzfeldt-Jacob diseases (Sasaki *et al.*, 2002; Yan *et al.*, 1998). In addition to RAGE, several cell surface proteins, including the cellular, non-infectious form of prion protein (PrPc) (Chen *et al.*, 2010; Lauren *et al.*, 2009) voltage-gated (Hou *et al.*, 2007) or ligand-gated calcium channels such as the glutamate N-methyl d-aspartate (NMDA) receptors and  $\alpha$ -

amino-3-hydroxy-5-methyl-4-isoxazolepropionic acid receptor (AMPA) receptors have also been considered as possible receptors or specific interaction sites for amyloids (De Felice *et al.*, 2007; Pellistri *et al.*, 2008). In addition, tissue-type plasminogen activator (tPA) has also been proposed as a multi-ligand specific for the cross- $\beta$  structure (Kranenburg *et al.*, 2002). The presence of specific effects mediated through the preferential, or even specific, interaction with membrane proteins could, at least in part, explain the variable vulnerability to amyloids of different cell types (Cecchi *et al.*, 2005). However, in spite of these and other data on specific interaction sites for amyloids, the tendency of early amyloid aggregates to interact with synthetic lipid membranes supports the idea that the interaction can be non-specific but, possibly, modulated by the membrane lipid content (Stefani, 2008). This is confirmed by the key well-known role of anionic surfaces (anionic phospholipid-rich liposomes, glycosaminoglycans, nucleic acids, natural membranes) both as triggers of protein/peptide fibrillization and as potent inductors of  $\beta$ -sheet structures (reviewed in Stefani, 2007; Stefani, 2010b). It has been suggested that a shared fold in amyloid aggregates grown from different peptides and proteins could recognize, although with different efficiency, clusters of negative charges in cell membranes (Zhao *et al.*, 2004). In addition cholesterol and gangliosides could also play a role in modulating protein aggregation at, and aggregate interaction with, cell membranes. Actually, the biochemical and biophysical features of the cell membrane can affect the conformation, distribution and proteolytic processing of membrane proteins involved in neurodegenerative conditions such as AD or prion disease; in addition, the protein/peptide interaction, with the cell surface is considered an important requirement for cytotoxicity (reviewed in Stefani, 2007; Stefani and Liguri, 2009; Wakabayashi and Matsuzaki, 2007). Overall, the data presently available support the idea that membrane cholesterol and gangliosides can modulate conformational changes and aggregation of specific protein/peptides (Wakabayashi and Matsuzaki, 2009), even though it may affect protein/peptide oligomerization into amyloids in several ways (reviewed in Stefani and Liguri, 2009). Conflicting results have indicated that cholesterol can either inhibit (Curtain *et al.*, 2003) or promote (Qiu *et al.*, 2009) A $\beta$ 40 penetration into model liposomes, depending on the molar ratio of cholesterol in the membrane. The enhanced binding of A $\beta$  and acceleration of fibril formation with ganglioside-containing membranes has been reported by several studies (Butterfield and Lashuel, 2010; Matsuzaki, 2007; Okada *et al.*, 2007; Okada *et al.*, 2008). In fact, ganglioside clusters have been proposed by Matsuzaki to form sites on the cell membrane that are designated for the sequestering of A $\beta$  after cleavage from the APP and the seeding of its fibril formation (Fig. 5). The binding of A $\beta$  to ganglioside-containing membranes induces a random-coil-to  $\beta$ -sheet transition, which then triggers fibril formation (Fig. 5) (Okada *et al.*, 2007).

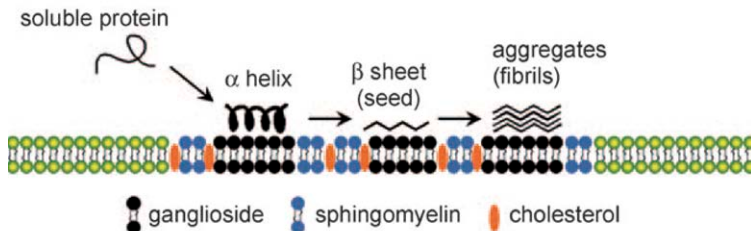


Figure 5. Templating of A $\beta$ -fibril formation on ganglioside clusters in lipid rafts. From (Butterfield and Lashuel, 2010)

### 1.1.3.2 Calcium homeostasis

To explain the genesis of Ca<sup>2+</sup> dysregulation in diseases associated to misfolding and aggregation of amyloid proteins, three main mechanisms have been postulated: the activation of pre-existing ion channels, the formation of calcium-permeable amyloid pores and the disruption of membrane lipid integrity (Fig. 6).

Interaction with several Ca<sup>2+</sup>-permeable channels has been described for amyloid proteins, potentially leading to an intracellular Ca<sup>2+</sup> rise. The glutamatergic system has been thoroughly studied, on the basis of the role played by glutamate receptors in the excitotoxic neuronal cell damage, whose over stimulation leads to excessive intracellular Ca<sup>2+</sup> rise (Choi, 1992). Several *in vitro* studies showed that incubation of neuronal cultures with A $\beta$  oligomers increased Ca<sup>2+</sup> influx through NMDA receptors. The moderate-affinity, uncompetitive NMDA receptor antagonist memantine protects against A $\beta$  oligomer toxicity by attenuating intracellular Ca<sup>2+</sup> increase (De Felice *et al.*, 2007). Currently, memantine is the only approved treatment for AD, besides acetylcholinesterase inhibitors, although the therapeutic efficacy is limited (Mayeux, 2010). Interactions of A $\beta$  with other Ca<sup>2+</sup> permeable channels have been documented, such as voltage-gated Ca<sup>2+</sup> channels (MacManus *et al.*, 2000; Rovira *et al.*, 2002) nicotinic acetylcholine (Dougherty *et al.*, 2003; Liu and Zhao, 2004; Mehta *et al.*, 2009) catecholamine (Fu *et al.*, 1998), serotonin and intracellular inositol trisphosphate (IP3Rs) receptors (Ju Yeon and Yeon Hee, 2005). A role for calcium-permeable channel has been described for other amyloid proteins. Ca<sup>2+</sup> influx via N-type voltage dependent Ca<sup>2+</sup> channels has been described following  $\alpha$ -synuclein treatment in rat synaptosomes (Adamczyk and Strosznajder, 2006). Over activation of NMDA receptors, followed by an abnormal neuronal Ca<sup>2+</sup> signaling, is believed to play a role in Huntington disease(HD) pathogenesis (Bezprozvanny and Hayden, 2004; Demuro *et al.*, 2010; Fan *et al.*, 2007; Zhang *et al.*, 2008).

## Amyloid Cytotoxicity and Membrane Lipid Composition

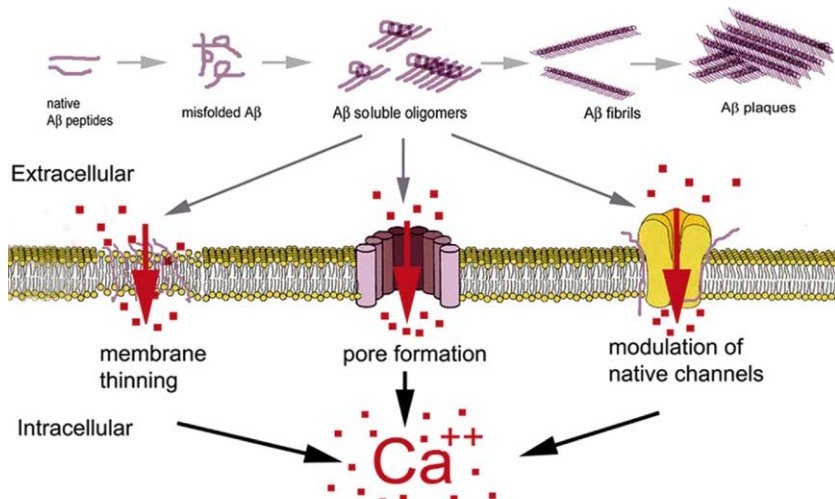


Figure 6. Schematic representation of the mechanisms proposed to explain  $\text{Ca}^{2+}$  dysregulation in diseases associated to misfolding and aggregation of amyloid proteins. From (Demuro et al., 2010).

Increasing evidence indicates that the toxicity of amyloid forming proteins is directly correlated with their shared ability to disrupt the membrane barrier function. Since 1993 it was proposed by Arispe and co-workers the “channel hypothesis” of amyloid toxicity: A $\beta$  exhibits ion-channel activity in planar lipid bilayers led to early proposals that the toxicity of A $\beta$  is based on an ion-channel mechanism that causes membrane depolarization,  $\text{Ca}^{2+}$  leakage, and a disruption of ionic homeostasis (Arispe et al., 1993; Lin et al., 2001; Pollard et al., 1995; Kagan et al., 2004). Channel activity was later reported for a number of other amyloidogenic proteins, including islet amyloid polypeptide (IAPP) (Mirzabekov et al., 1996),  $\alpha$ -synuclein (Kim et al., 2009, Volles and Lansbury, 2002), polyglutamine (Monoi et al., 2000), and prion-derived peptides (Kourie et al., 2001). Thus, the toxicity of these proteins may be related to their shared capabilities to form channels or pores in membranes and to enable unregulated ion leakage in analogy to the mode of action of the pore-forming toxins, which permeabilize membranes forming oligomeric pores characterized by  $\beta$ -sheet structure (Kagan et al., 2004; Lashuel and Lansbury, 2006). Morphological studies at transmission electron microscopy (TEM) and AFM levels have shown that oligomers of many amyloid proteins, such as A $\beta$  and  $\alpha$ -synuclein (Volles et al., 2001), serum amyloid A, amylin (Quist et al., 2005), and calcitonin (Diociaiuti et al., 2006), have a characteristic annular morphology, reminiscent of cation permeable membrane pores (Kagan and Thundimadathil, 2010). Furthermore, TEM analysis has also revealed the presence of A $\beta$  pore-like structures in the cell membrane of brains from AD patients but not from age-matched healthy patients (Inoue, 2008). Cells exposure to a wide range of oligomeric, but not fibrillary, amyloid proteins, in-

cluding A $\beta$ , prion peptide, IAPP, polyglutamine, and lysozyme, induced increase in intracellular calcium. The increase could not be attributed to activation of endogenous Ca $^{2+}$  channels, because the responses were unaffected by the potent endogenous Ca $^{2+}$  channel blocker cobalt (Demuro *et al.*, 2005).

Recently, Sokolov *et al.* showed that purified preparations of A $\beta$  oligomers, which stained positive with anti-oligomer antibodies, also caused a general increase in model bilayer conductivity in a concentration-dependent manner when added externally to the bilayer, without single-channel current jumps supportive of ion-channel formation (Sokolov *et al.*, 2006). These studies support a model in which amyloid oligomers bind to the membrane surface and disrupt lipid packing to cause membrane thinning and an increase in membrane leakiness without the formation of defined pores (Sokolov *et al.*, 2006). The different hypotheses are not mutually exclusive and can cooperate towards Ca $^{2+}$  dysregulation. Recently, it has been proposed that amyloid oligomers may act at two steps, separated in time, a first, very rapid step, where Ca $^{2+}$  increases due to glutamate receptor stimulation by the oligomers, followed by a second, delayed step, where oligomers permeabilize non specifically the cell membrane, possibly via the formation of amyloid pores (Malchiodi-Albedi *et al.*, 2011; Pellistri *et al.*, 2008)

### 1.1.3.3 Reactive oxygen species (ROS) and oxidative stress

There is accumulating evidence that suggests a key role of oxidative stress in the pathophysiology of AD and in other age-related neurodegenerative disorders. Oxidative stress is caused by an imbalance in the free radicals and antioxidant systems. Oxidative stress may cause lipid peroxidation, protein, DNA and RNA oxidation. A modification of the intracellular redox status in cells exposed to aggregates is associated with a sharp increase in the quantity of reactive oxygen species (ROS). In addition, changes have been observed in reactive nitrogen species, lipid peroxidation, deregulation of nitric oxide (NO) metabolism (Kourie, 2001), protein nitrosylation (Guentchev *et al.*, 2000) and upregulation of heme oxygenase-1, a specific marker of oxidative stress (Choi *et al.*, 2000). It is not clear why protein aggregation is followed, even *in vitro*, by production of ROS. In the case of A $\beta$ 42, Met35, Gly29 and Gly33 have been suggested to be involved (Brunelle and Rauk, 2002); a role has also been proposed for metal ions such as Fe, Cu and Zn, for example, through the generation of hydroxide radicals from hydrogen peroxide (Tabner *et al.*, 2002). An up-regulation of the activity of hydrogen peroxide-producing membrane enzymes, such as plasma membrane nicotinamide adenine dinucleotide phosphate-oxidase (NADPH oxidase) and endoplasmic reticulum cytochrome P450 reductase, has also been reported in A $\beta$ -induced neurotoxicity in microglia and in cortical neurons (Pappolla *et al.*, 2001; Qin *et al.*, 2002). More generally, intracellular oxidative stress could be related to some form of destabilisation of cell membranes by toxic species leading to a failure to regulate appropriately plasma membrane proteins such as receptors and ion pumps and/or to impairment of mitochondrial function (Mattson, 1999). Mitochondria play a well recognised role in oxidative stress and apoptosis; in

this regard, a key factor in A $\beta$  peptide neurotoxicity could be the opening of mitochondrial permeability transition pores by Ca $^{2+}$  entry in neuronal mitochondria followed by release of cytochrome c, a strong inducer of apoptosis (Moreira *et al.*, 2002). It has been suggested that intracellular ROS elevation following exposure to amyloid aggregates is a consequence of Ca $^{2+}$  entry into cells followed by stimulation of oxidative metabolism aimed at providing the ATP needed to support the activity of membrane ion pumps involved in clearing excess Ca $^{2+}$  (Squier, 2001). ROS elevation would in turn oxidise not only the proteins involved in ion transfer but also proteins such as calmodulin that when oxidised is unable to activate the Ca $^{2+}$ -ATPase (Squier, 2001). The down-regulation of the Ca $^{2+}$ -ATPase activity would then reduce the need for ATP, and hence ATP synthesis and ROS production by oxidative metabolism, leading to an increase in intracellular Ca $^{2+}$  concentration (Squier, 2001). The same could happen in old age, where the ATP levels tend to be lower resulting in an energy deficiency. This hypothesis can explain the relationship between ROS, apoptosis, mitochondrial damage and intracellular free Ca $^{2+}$  increase shown by cells exposed to toxic amyloid aggregates (Kawahara *et al.*, 2000; Kourie and Henry, 2002; Selkoe, 2001; Wyttenbach *et al.*, 2001). Indeed, many studies have suggested a close relationship between Alzheimer's, Parkinson's and prion diseases and the dysregulation of calcium homeostasis. The increase in intracellular free Ca $^{2+}$  levels is thought to be a consequence of the impairment of membrane permeability; the latter may be a consequence of the presence into the membrane of aspecific amyloid pores or may follow oxidative stress, membrane lipid peroxidation producing reactive alkenals such as 4-hydroxynonenal, and the chemical modification of membrane proteins acting as ion pumps (Butterfield *et al.*, 2001; Varadarajan *et al.*, 2000).

### **1.1.4 Amyloid formation is an inherent property of polypeptide chains: functional amyloid and disease unrelated amyloid**

An increasing number of proteins with no link to protein deposition diseases has been found to form, under some conditions *in vitro*, fibrillar aggregates that have the morphological, structural, and tinctorial properties that allow them to be classified as amyloid fibrils (Chiti and Dobson, 2006; Stefani and Dobson, 2003). This finding has led to the idea that the ability to form the amyloid structure is an inherent or generic property of polypeptide chains, although the propensity to form such a structure can vary dramatically with sequence. This generic ability can increasingly be seen to have been exploited by living systems for specific purposes, as some organisms have been found to convert, during their normal physiological life cycle, one or more of their endogenous proteins into amyloid fibrils that have functional rather than disease-associated properties. One particularly well-studied example of functional amyloid is that of the proteinaceous fibrils formed from the protein curlin that are used by *Escherichia Coli* to colonize inert surfaces and mediate binding to host proteins. Consistent with the characteristics of other amyloid structures, these fibrils are 6–12 nm in diameter, possess extensive  $\beta$ -sheet structure, as revealed by circular dichroism (CD) spectroscopy, and bind to CR and ThT (Chapman *et al.*, 2002). A

second example involves the filamentous bacterium *Streptomyces coelicolor* that produces aerial hyphae, which allow its spores to be dispersed efficiently; a class of secreted proteins called chaplins has been identified in the hyphae of this organism with the ability to form amyloid fibrils that act cooperatively to bring about aerial development (Claessen *et al.*, 2003). As well as these examples from bacteria, the formation of functional amyloid like structures has recently been observed in a mammalian system. The melanosomes, lysosome-related organelles that differentiate in melanocytes to allow the epidermal production of the melanin pigment, are characterized by intraluminal fibrous striations upon which melanin granules form. This fibrous material, sharing significant analogies with amyloid fibrils, is assembled from the intra-luminal domain of the membrane protein Pmel17 that is proteolyzed by a proprotein convertase (Berson *et al.*, 2003). This result is a direct indication that even in higher organisms amyloid formation can be physiologically useful for specific and specialized biological functions, provided it is regulated and allowed to take place under highly controlled conditions.

Until 1998 it was commonly believed that the ability to polymerize into ordered fibrillar aggregates of amyloid type was a shared property of the few proteins and peptides found aggregated in tissue in the various amyloid diseases possibly arising from some structural peculiarity. However, in 1998 it was found that two proteins, unrelated to any amyloid pathology, the SH3 domain from bovine phosphatidyl-inositol-3'-kinase (PI3-SH3) and fibronectin type III, were able to aggregate *in vitro* into fibrillar assemblies undistinguishable from the classical amyloid fibrils (Guixarro *et al.*, 1998; Litvinovich *et al.*, 1998). Amyloid aggregation could be achieved deliberately by a rational choice of solution conditions (Chiti *et al.*, 1999; Chiti *et al.*, 2001). Since then a substantial number of similar studies have been reported (Chiti *et al.*, 2001 and references therein). In each case aggregation of a full-length protein to form amyloid fibrils was found to require solution conditions (such as low pH, lack of specific ligands, high temperature, moderate concentrations of salts or co-solvents such as trifluoroethanol) such that the native structure was partially or completely disrupted but under which interactions such as hydrogen-bonding were not completely inhibited. It was also found that many peptides, both fragments of natural proteins or artificially designed sequences, that were unable to fold to stable globular structures readily formed fibrils (Tjernberg *et al.*, 2002). These results provided strong support for the suggestion that the ability to form amyloid fibrils is a generic property of peptides and proteins, and that the structures were the result of the inherent physico-chemical properties of the polypeptide main-chain rather than the specific interactions of side-chains. The tendency to aggregate arises from the primordial tendency of polypeptide chains to self-organize into polymeric assemblies stabilized by hydrogen bonds between parallel or anti-parallel polypeptide stretches in the  $\beta$ -strand conformation provided by the monomers. The resulting polymers display the ordered cross- $\beta$  structure that characterizes the amyloid fold (reviewed in Stefani and Dobson, 2003). This does not imply that the side chains of the polypeptide chain are not important; rather, they determine the environmental conditions under which the polypeptide chain can undergo aggregation. This view

considers natural proteins as a group of evolved amino acid polymers whose the amino acid sequences disfavour aggregation whilst favouring folding into compact states resulting mainly from the tertiary interactions among the side chains that shield the peptide backbone. Conversely, protein aggregation into amyloid, which is mainly stabilized by secondary interactions, is considered the expression of the intrinsic primordial tendency of the peptide backbone to give secondary intermolecular interactions between backbone groups (reviewed in Stefani and Dobson, 2003).

## 1.2 HypF-N: model protein of amyloid aggregation unrelated to disease

### 1.2.1 Function, structure and aggregation of HypF-N

The N-terminal domain of the prokaryotic protein HypF is a peptide with no link to protein deposition diseases able to form, under various conditions *in vitro*, fibrillar aggregates characterized by the morphological, structural, and tinctorial properties typical of the amyloid fibrils (Stefani and Dobson, 2003). HypF, a large protein of about 82 KDa that assists the folding of [NiFe]-hydrogenases, key enzymes in the hydrogen metabolism of prokaryotes (Colbeau *et al.*, 1998). In their fully functional forms, the iron atoms of the active sites of these [NiFe]-hydrogenases are stabilized in the low oxidation state ( $\text{Fe}^{2+}$ ) by binding to the carbon monoxide (CO) and cyanide (CN<sup>-</sup>) ligands (Nicolet *et al.*, 1999). Both molecules have been shown to originate from the processing of carbamoylphosphate (Paschos *et al.*, 2001). Thus, the assembly of the complex hydrogenase system requires the coordinated action of different maturation and regulatory factors. Indeed, hydrogenase operons contain a number of accessory genes (HypA-F) encoding maturation and regulatory proteins, including the essential maturation factor HypF (Casalot and Rousset, 2001). *E. coli*, as any other prokaryote, expresses a HypF protein, that contains an N-terminal acylphosphatase-like domain (residues 1-91) (HypF-N) (Fig. 7).

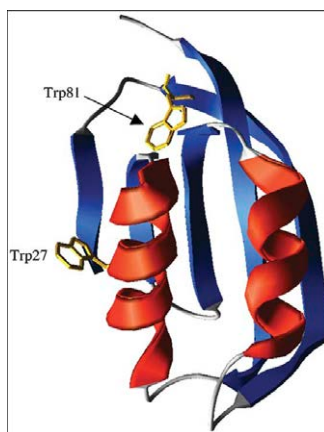


Figure 7. Three-dimensional structure of native HypF-N from X-ray crystallography. The red and blue colours indicate  $\alpha$ -helices and  $\beta$ -strands, respectively. From (Marcon *et al.*, 2005).

The HypF-N displays sequence and structural homology with other members of the acylphosphatase-like structural family. Acylphosphatases (AcPs) are small enzymes specifically catalysing the hydrolysis of carboxyl-phosphate bonds in acylphosphates such as carbamoylphosphate, succinylphosphate and 1,3-bisphosphoglycerate (Stefani *et al.*, 1997). Recent experiments shed light on the role of *E. coli* HypF in the conversion of carbamoylphosphate into CO and CN<sup>-</sup>, and on the coordination of these ligands to the assembled hydrogenase metal cluster (Reissmann *et al.*, 2003). According to these results, HypF-N acts as a carbamoyltransferase that transfers the carbamoyl moiety of carbamoyladenylate to the C-terminal cysteine of the partner protein HypE, forming an enzyme-thiocarbamate. HypE dehydrates the S-carbamoyl moiety in an ATP-dependent process to yield the enzyme thiocyanate. Finally, the cyano group can be nucleophilically transferred to an iron complex (Reissmann *et al.*, 2003). The structure of HypF-N has been resolved by X-ray crystallography and is well defined for residues 5-91 (Fig. 7) (Rosano *et al.*, 2002). The domain has a ferredoxin-like fold, which consists in a  $\alpha/\beta$  sandwich, with  $\beta\alpha\beta\beta\alpha\beta$  topology. Following the sequence identity with AcPs, it has been assigned to the acylphosphatase-like structural family. The five  $\beta$ -strands of the domain form a slightly twisted  $\beta$ -sheet ( $\beta_4-\beta_1-\beta_3-\beta_2-\beta_5$  strand arrangement), which faces on one side two  $\alpha$ -helices; the other side is instead fully solvent-exposed. Overall, the domain has a size of about 43x28x27 Å. This compact globular state displays the main structural strategies exploited by all- $\beta$  and  $\alpha/\beta$  proteins to escape amyloid aggregation (Richardson and Richardson, 2002). HypF-N forms amyloid-like fibrils under conditions that promote its partial unfolding, such as in the presence of trifluoroethanol (TFE) or following a decrease of pH. Formation of amyloid-like fibrils has been obtained initially at pH 5.5 with 30% (v/v) TFE or at pH 3.0 in citric acid (Chiti *et al.*, 2001). The formation of a partially folded state is a key event in the aggregation pathway of this protein *in vitro*, even under mild destabilising conditions in which the folded state is by far the predominant species. Indeed, under mild denaturing conditions generated by moderate concentrations of TFE [6–12% (v/v)], the native state of HypF-N is in rapid equilibrium with a partially unfolded state, whose population is about 1–2%; a kinetic analysis has shown that amyloid aggregation under these conditions arises from molecules accessing this amyloidogenic state (Campioni *et al.*, 2010). Recently, new aggregation conditions for HypF-N, enabling the characterization of the partially folded state populated prior undergoing aggregation, have been described, such as at pH 5.5 in the presence of 12% (v/v) TFE, or at pH 1.7 in the presence of salts (NaCl). A detailed structural investigation of this partially folded state has also been performed and achieved by means of different biophysical and biochemical techniques. (Canale *et al.*, 2006). The resulting species have been imaged with tapping mode AFM, have been shown to increase the fluorescence of ThT, indicating the presence of intermolecular  $\beta$ -sheet structure typical of amyloid aggregates. In general, the data obtained suggest that the aggregation process of this protein starts from a partially folded state that can be either fully populated or in rapid equilibrium with the native state when the latter is destabilized by mutations and/or mild unfolding conditions (Marcon *et al.*, 2005). The results support an aggregation

pathway in which the native protein first converts into a partially folded state separated from the native state by an energy barrier comparable to that of (un)folding. This monomeric state converts into globular small aggregates and small beaded fibrils that further associate into ring-like structures. Finally, the ring-like structures convert into ribbon-like fibrils that associate into fibrillar tangles (Relini *et al.*, 2004). As many disease-involved systems aggregate following similar pathways, HypF-N represents a useful model system to determine the common principles underlying amyloid formation.

### **1.2.2 HypF-N protofibrils interact with cell membranes originating a cytotoxic cascade**

It is increasingly suggested that the oligomers formed by proteins that are not related to any human disease can be toxic when added to the extracellular medium of cultured cells, whereas the same proteins in monomeric or fibrillar forms are not (Bucciantini *et al.*, 2002). The observation that the oligomers formed from such a heterogeneous group of proteins impair cell viability suggests that these species share the ability to “misinteract” with the macromolecular components of living organisms, such as membranes and proteins, and interfere with their normal function. The early prefibrillar aggregates of HypF-N formed in 30% TFE were shown to be able to interact with, insert into, and eventually disassemble synthetic membranes and supported phospholipid bilayers (Canale *et al.*, 2006; Relini *et al.*, 2004). Moreover, these species can interact with the plasma membrane of cultured cells and be internalized inside the cytoplasm, resulting in cell impairment and death (Bucciantini *et al.*, 2005; Cecchi *et al.*, 2005). Recently, it was found that their interaction with cell membranes is disfavoured by a high membrane cholesterol content (Cecchi *et al.*, 2006; Cecchi *et al.*, 2008a,b). Similarly to the prefibrillar aggregates of disease-related proteins and peptides, treatment of the cells with HypF-N protofibrils leads to an increase of ROS and free  $\text{Ca}^{2+}$  levels inside the cells, which ultimately die by apoptosis or necrosis (Bucciantini *et al.*, 2005; Cecchi *et al.*, 2005). Moreover, the increase of intracellular  $\text{Ca}^{2+}$  levels is associated with both the activation of plasma membrane receptors with  $\text{Ca}^{2+}$  channel activity, such as AMPA and NMDA, and unspecific membrane permeabilization, with the former effect being more important at early times (Pellistri *et al.*, 2008). The susceptibility of different cells to HypF-N aggregates was shown to depend on their ability to counteract these early impairments, which increases during cell differentiation (Cecchi *et al.*, 2005; Cecchi *et al.*, 2008a). Remarkably, HypF-N protofibrils can also induce a loss of cholinergic neurons when injected into rat brains, demonstrating that these species can act as toxins even in higher organisms (Baglioni *et al.*, 2006). These data strongly support the hypothesis that a common mechanism of cytotoxicity exists, which is related to the misfolded nature and oligomeric state of a protein rather than to its sequence. In spite of this advancement, a structural characterization of the conformational properties of the oligomers finalized to an understanding of the relationship with their toxic effect is still lacking, mainly due to the fact that the transient formation of these species and

their structural heterogeneity have hampered considerably their investigation. The structural determinants of the protein oligomers that are responsible for cell dysfunction are starting, only these days, to be elucidated. Recently, the functional and structural properties of the spherical aggregates formed by HypF-N in two distinct environmental conditions can be compared. It is therefore nowadays essential to determine in detail the structure of the toxic oligomeric species in order to identify new therapeutical targets, and to understand whether it represents a single common fold or rather exhibits some polymorphism.

### **1.2.3 A causative link between the structure of HypF-N oligomers and their ability to cause cellular dysfunction**

It is well known that incubation of the same protein/peptide under different experimental conditions causes the formation of oligomers or fibrils with different morphologies and that such differences result in different degrees of toxicity (Kayed *et al.*, 2009; Lee *et al.*, 2007; Petkova *et al.*, 2005). Similarly, mutations or covalent modifications result in different levels of oligomers or different fibrillar structures with completely different toxicities (Hung *et al.*, 2008). However, little experimental information is available on the structural features of oligomers grown under different conditions and on the relationship between their structure and their ability to cause cell dysfunction. Recently, it has been found that oligomers formed from the same protein (HypF-N) under different conditions (pH 5.5 in the presence of 12%(v/v) TFE or pH 1.7 in the presence of 330 mM NaCl) exhibited similar morphological and tinctorial properties, yet differed in their molecular structure. Comparisons of the two types of aggregates indicated that their structural differences resulted from different degrees of packing of the hydrophobic residues within their cores with a consequent different level of structural flexibility and solvent-exposure of such residues (Campioni *et al.*, 2010). Thus, whilst the ability to form amyloid-like structures is generic to polypeptide chains, whether or not such species are pathogenic will depend on their structural features, notably the extent to which hydrophobic residues are flexible and exposed on their surfaces within the environment of a living organism. These findings, however, do not seem to be limited to the HypF-N aggregates, and could indeed explain the toxic properties of the oligomers formed by disease-related systems. In fact, several studies indicated a correlation between the size and surface hydrophobicity of A $\beta$ 40 aggregates and their ability to decrease the bilayer fluidity of model membranes (Kremer *et al.*, 2000), suggesting that the exposure to the solvent of hydrophobic surfaces determines the ability of these species to interact with cell membranes. A correlation between hydrophobicity, tendency to form aggregates and aggregate cytotoxicity has also been observed in comparative studies where the behavior of different homopolymeric amino acid (HPAA) stretches was investigated (Oma *et al.*, 2005). It has been recently reported that expanded huntingtin-exon1 forms fibrillar aggregates at two different temperatures that have different structural and physical properties as well as different cytotoxicities (Petkova *et al.*, 2005). The structures and toxicities of both forms of the aggre-

gates are comparable with those extracted from regions of mouse brains affected to different extents by huntingtin deposition. In both pairs of structures a direct relationship between structural flexibility and cytotoxicity of amyloid assemblies was found, supporting the generality of previous conclusions (Petkova *et al.*, 2005). Finally, all these data lend support to the idea that a key feature in the generation of toxicity is the conversion of a species of aggregates where stability is associated with extreme burial of hydrophobic residues to one where such residues are substantially exposed and disorganized (Cheon *et al.*, 2007). Recently, it has been suggested that for therapeutic purposes the toxicity can be dramatically reduced if the hydrophobic residues are incorporated to a greater extent within the interior of the oligomeric assemblies, even in the absence of an effective change in morphology (Campioni *et al.*, 2010). Approaches of this type will facilitate the elucidation of the causative link between the molecular structure of aberrant protein oligomers and their ability to cause cell dysfunction, with the aim of understanding the pathogenesis of protein deposition diseases and identifying therapeutic strategies to combat them. Moreover, a detailed understanding of the forces that determine the structure of amyloid-like oligomers will also enable to identify the factors that can modulate it, and eventually alter the biological activities of these species.

### 1.3 Alzheimer's disease

#### 1.3.1 The Alzheimer phenotype

AD is a complex disorder, representing the most common form of dementia among the elderly population and the fourth leading cause of death in Western countries. AD is characterized by a well defined neuropathological profile which includes intracellular neurofibrillary tangles (NFT), extracellular  $\beta$ -amyloid-containing plaques, reduced synaptic density and neuronal loss in selected brain areas. NFT has been detected in distal dendrites as neuropil threads, and in the abnormal neurites that are associated with some  $\beta$ -amyloid plaques (neuritic plaques). Their major proteinaceous component are abnormal filaments which are termed either straight (SF) or paired helical filaments (PHF) (Crowther and Wischik, 1985; Wischik *et al.*, 1985). The core protein of these filaments is tau, a microtubule-associated protein (Goedert *et al.*, 1988). In the course of the disease tau becomes abnormally phosphorylated, it adopts an altered conformation and is re-localized from axonal to somato-dendritic compartments. The most relevant protein kinases involved in tau modifications in neurofibrillary degeneration are GSK3 $\beta$  (Imahori and Uchida, 1997; Ishiguro *et al.*, 1992; Takashima *et al.*, 1993) and Cdk5 (Alvarez *et al.*, 1999; Michel *et al.*, 1998; Patrick *et al.*, 1999; Tsai *et al.*, 1994). Phosphorylation tends to dissociate tau from microtubules. Since this increases the soluble pool of tau it might be an important first step in the assembly of tau filaments (Buee *et al.*, 2000; Chen *et al.*, 2004; Goedert *et al.*, 1995; Götz, 2001; Götz *et al.*, 2004; Lee *et al.*, 2001; Lichtenberg *et al.*, 1988; Schweers *et al.*, 1994). Physiological functions of tau include the assembly and stabilization of microtubules. Additional roles have been assigned

to tau in signal transduction, organization of the actin cytoskeleton, intracellular vesicle transport, and anchoring of phosphatases and kinases (Anderton *et al.*, 2000; De Ferrari and Inestrosa, 2000; Ebneth *et al.*, 1998; Flanagan *et al.*, 1997; Jenkins and Johnson, 1998; Lee and Rook, 1992; Maas *et al.*, 2000; Morishima-Kawashima and Kosik, 1996; Reszka *et al.*, 1995; Sontag *et al.*, 1999). In adult human brain, six tau isoforms are produced by alternative mRNA splicing of exons 2, 3 and 10. All six brain tau isoforms are found in neurofibrillary lesions of AD brains (Goedert *et al.*, 1992).

The other major lesion is the amyloid plaque. These are extracellular deposits of insoluble, 8–10-nm amyloid fibrils that are polymers of A $\beta$  (Glenner and Wong, 1984; Masters *et al.*, 1985). There are two major varieties of A $\beta$  plaques: neuritic/cored and diffuse plaques. The natural evolution of plaque morphology appears to be from diffuse to mature cored plaques. A $\beta$  is a naturally occurring peptide present in the brain and cerebrospinal fluid (CSF) of healthy individuals (Sjogren *et al.*, 2001). Whilst the etiology of AD still remains controversial, the most widely accepted theory is the amyloid cascade hypothesis which has provided the intellectual foundation for many AD clinical trials (Masters *et al.*, 2006). Although the hypothesis continues to evolve, its core principle has remained essentially unaltered in that A $\beta$  plays a central role in the etiology of AD. The theory entails that AD is a result of an imbalance between A $\beta$  production and clearance. This affects A $\beta$  stability or aggregation and leads to its accumulation in the brain, which initiates a multistep cascade, involving gliosis, inflammatory changes, excitotoxicity, formation of neurofibrillary tau tangles, oxidative stress, synaptic and neuronal dysfunction. This ultimately results in the memory loss and impaired cognitive functions of dementia (Masters *et al.*, 2006).

### **1.3.2 The elaborate processing of APP**

A $\beta$  is a 38–43-residue proteolytic fragment of APP (Kang *et al.*, 1987) that is generated normally throughout life by virtually all mammalian cells (Haass *et al.*, 1992; Seubert *et al.*, 1992; Shoji *et al.*, 1992) (Fig. 8). APP is a ubiquitous Type I membrane glycoprotein that occurs as a heterogeneous group of polypeptides arising from alternative splicing, N- and O-linked glycosylation, phosphorylation, sulphation, glycosaminoglycan addition and complex proteolysis. The processing of APP takes place along the secretory pathway and in endosomes after endocytosis. APP can be cleaved, within the A $\beta$  domain, by  $\alpha$ -secretase, a member of the disintegrin and metalloprotease (ADAM) family, leading to the release of the  $\alpha$ -sAPP (Buxbaum *et al.*, 1998; Koike *et al.*, 1999; Postina *et al.*, 2004). The resultant transmembrane C83 fragment is cleaved by  $\gamma$ -secretase, a transmembrane protein complex that includes presenilin-1 (PS1) or presenilin-2 (PS2), nicastrin, anterior pharynx-defective-1, and PS enhancer 2, originating the extracellular p3 and the APP intracellular C-terminal domain (AICD) fragment (Fig. 8) (De Strooper, 2003). AICD can migrate to the nucleus leading to gene transcription and thus activating signal transduction pathways (Leisring *et al.*, 2002). This corresponds to the non-

## Amyloid Cytotoxicity and Membrane Lipid Composition

amyloidogenic pathway because it precludes the formation of A $\beta$ . APP can also be processed through an amyloidogenic pathway, which involves the cleavage by  $\beta$ -secretase, such as the  $\beta$ -site APP-cleaving enzyme (BACE, also known as memapsin 2, a type I transmembrane aspartic protease) 1 (Repetto *et al.*, 2004) or BACE2 (Farzan *et al.*, 2000), originating the N-terminal soluble extracellular  $\beta$ -secretase-cleaved APP ( $\beta$ -sAPP) and the transmembrane C99 fragment. Cleavage of C99 by  $\gamma$ -secretase results in generation of A $\beta$  peptide and AICD. The APP cleavage by  $\alpha$ - or  $\beta$ -secretases is a prerequisite for  $\gamma$ -secretase cleavage. Some studies show that  $\alpha$ - and  $\beta$ -secretases may compete for APP substrate and, thus, increased activity of one pathway results in a decreased APP processing by the other (Skovronsky *et al.*, 2000).

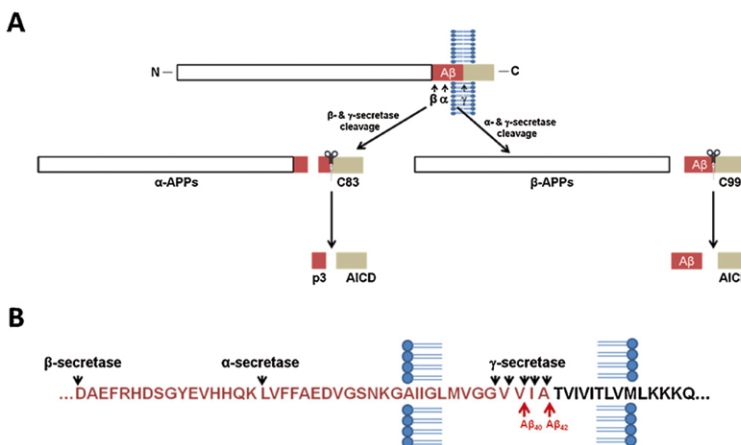


Figure 8. Schematic representation of the amyloid precursor protein (APP) and its metabolic derivatives. (A) Diagram of APP showing a large extracellular domain and short intracellular segment. Cleavage of APP by either  $\alpha$ - or  $\beta$ -secretases produces large soluble N-terminal fragments,  $\alpha$ -APPs or  $\beta$ -APPs and 10 and 12 kDa membrane-bound C-terminal fragments, C83 and C99, respectively. Both C83 and C99 can be further cleaved by  $\gamma$ -secretase leading to the release and secretion of non-pathogenic p3 peptide or A $\beta$ . (B) Amino acid sequence of A $\beta$  showing the most common APP secretase cleavage sites, including sites for A $\beta$ 40 and A $\beta$ 42 generation, as indicated by arrows. From (Fodero-Tavoletti *et al.*, 2011).

In normal cells, the non-amyloidogenic pathway predominates.  $\gamma$ -secretase can cleave APP successively beginning in amino acid 43 until amino acid 36 of A $\beta$  peptide; however, it stops the cleavage mainly at amino acid 42 or 40. In the amyloidogenic pathway, A $\beta$  with 40 amino acids is formed in higher quantity (about 90%) than A $\beta$  isoform with 42 amino acids (about 10%). Furthermore, A $\beta$ 42 has a greater tendency to aggregate and is more toxic to neurons than A $\beta$ 40. However, for some authors, the sequence of amino acids 25 to 35 of A $\beta$  (GSNKGAIGLM) is the responsible for the toxicity of the native full length peptide (Kaneko *et al.*, 2001), leading to increased rate of A $\beta$  aggregation (Liu *et al.*, 2004), induction of neuronal cell

death (Resende *et al.*, 2007), neuritic atrophy and synaptic loss (Grace *et al.*, 2002), and inhibition of neurogenesis (Li and Zuo, 2005).

### 1.3.3 The genetics of Alzheimer's disease

The familial form of Alzheimer's disease (FAD) accounts for nearly 5–10% of all cases of AD and is characterized by early manifestations of dementia, in some cases in patients approximately 40 years of age (Rosenberg, 2000). Four genes that confer increased susceptibility to this disease have been unequivocally confirmed, and mutations or polymorphisms in them either enhance A $\beta$  production, or interfere with its clearance (Table II).

Chromosome	Gene defect	Phenotype
21	APP mutations	Increased production of A $\beta$ , or A $\beta_{42}$
19	ApoE4 polymorphism	Increased density of A $\beta$ plaques
14	Presenilin 1 mutations	Increased production of A $\beta_{42}$
1	Presenilin 2 mutations	Increased production of A $\beta_{42}$

Table II. The four confirmed genetic determinants of increased susceptibility for Alzheimer's disease. From (Selkoe, 2007).

The apolipoprotein E (ApoE) polymorphism is associated with late-onset AD in a significant proportion of cases (Corder *et al.*, 1993; Poirier *et al.*, 1993), and appears to promote the formation of insoluble A $\beta$  oligomers and plaques (Holtzman *et al.*, 2000). Missense mutations in the APP gene have been found in a small number of families with early-onset AD, and are associated with increased production of A $\beta$  (Cai *et al.*, 1993; Citron *et al.*, 1994; Goate *et al.*, 1991; Scheuner *et al.*, 1996; Suzuki *et al.*, 1996). Trisomy of chromosome 21, on which the APP gene is located, is also associated with an AD-like pathology (Wisniewski *et al.*, 1985). The most aggressive forms of the disease, however, are associated with mutations in the PS1 and PS2 genes, located on chromosomes 14 and 1, respectively (Levy-Lahad *et al.*, 1995; Sherrington *et al.*, 1995). Mutations of PS1 and PS2 are associated with increased production of the most damaging form of the A $\beta$ -protein, A $\beta$ 42. Increased production of A $\beta$ 42 is thought to be the critical change that initiates AD as it has been shown to be the initial constituent of plaques in AD and is thought to trigger conformational changes in other A $\beta$  species rendering them prone to aggregation into plaques (Jarrett *et al.*, 1993; Younkin, 1998). Plasma concentrations of A $\beta$ 42 were significantly elevated in subjects with familial AD-linked PS1 and PS2 mutations compared with controls, as well as in subjects with APP mutations, as were A $\beta$ 42 concentrations in fibroblast media from subjects with PS1 and PS2 mutations (Scheuner *et al.*, 1996). Cellular production of A $\beta$ 42 was also significantly increased in hamster ovary cells transfected with mutant PS1 or PS2 (Xia *et al.*, 1997). Finally, brain A $\beta$ 42 was increased in mice that overexpress mutant PS1, but not those that overexpress wild-type PS1 (Duff *et al.*, 1996). The significance of PS1 in the pathogenesis of AD be-

came apparent when it was identified as the active site of the  $\gamma$ -secretase enzyme (Wolfe *et al.*, 1999). Deletion of the PS1 gene in mice greatly reduces  $\gamma$ -secretase activity (De Strooper *et al.*, 1998), and mutation of either of two fully conserved intramembrane aspartate residues in PS1 substantially reduces A $\beta$  production (Wolfe *et al.*, 1999).

#### **1.3.4 Peripheral cells as a tool to identify and test hypotheses on AD pathophysiology**

The use of peripheral cells is based on the hypothesis that AD might be a systemic disease that affects several tissues in the body. The specific brain damage could be the expression of a greater sensitivity to injury in postmitotic cells of the brain. Furthermore, a potential genetic defect underlying the disease may be manifest in several body tissues that express the gene involved. Peripheral tissues suitable for exploring pathophysiological hypotheses and possibly for providing a useful biological marker for diagnosis of AD include skin fibroblasts, platelets, lymphocytes, as well as body fluids such as plasma or CSF (Gasparini *et al.*, 1998). Among these tissues, cultured skin fibroblasts have been successfully used to elucidate the molecular and biochemical bases of many inborn errors of metabolism that cause neurological disease. Moreover, fibroblasts are an appropriate model for studies of those genetic diseases of the nervous system, including FAD, because they can be easily cultured, stored and contain the complete genomic information of the organism. Growth properties and *in vitro* aging of AD and control fibroblast cultures do not differ under standard conditions (Tesco *et al.*, 1993), although this topic is still controversial. Since growth properties and biological age in culture can have profound effects on the properties of cells cultured from skin, including the expression of genes (which could be related to AD) (Adler *et al.*, 1991), reproducible and interpretable results with the AD fibroblasts model require attention to the reproducibility of culture conditions including, but not limited to, matching AD and control cells for age, sex of the donors, and biological age in culture.

Alzheimer's disease diagnosis appears to be the major challenge posed by AD in its sporadic late-onset form, which still represents the vast majority of all cases. On the other hand, data obtained using fibroblasts from individuals with known gene defects, although representing only a small proportion of all AD cases, could be very informative about the cellular pathophysiology of AD. Fibroblast lines from FAD patients can therefore be classified according to the specific gene defect to see whether a particular genetic abnormality alters cellular function in a unique manner. Peripheral cells are therefore useful in identifying and testing hypotheses on the primary pathophysiological mechanisms leading to AD and for avoiding variables derived from a postmortem state. On the other hand, peripheral cells cannot be used to answer other clinically relevant questions that require an intact organism. Low or absent expression of neuronal proteins by peripheral cells cultured under standard conditions is an important limiting factor. In the study of AD and other neurological diseases, affecting either the central nervous system (CSN) and other tissues, periph-

eral cells are however a useful adjunct, providing the tools to study *in vitro* the dynamic alteration of metabolic processes that neuropathological examination indicates might be targets of the disease (Gasparini *et al.*, 1998).

### 1.3.5 Adult neurogenesis and stem cell technology for AD

Several evidence have demonstrated that, in adulthood, neurogenesis operates mainly in two areas of the mammalian CNS, in the anterior part of the subventricular zone (SVZ) along the lateral ventricles, and in the subgranular zone (SGZ) of the dentate gyrus (DG) of the hippocampus (Abrous *et al.* 2005; Colucci-D'Amato *et al.*, 2006; Taupin and Gage, 2002). In both areas, neurogenesis progresses as a complex multi-stage process, which starts with the proliferation of neural precursors residing in the SVZ and the SGZ (Abrous *et al.* 2005; Taupin and Gage, 2002). These areas (also known as neurogenic niches) contain multipotent neural stem cells (NSCs) (Seaberg and van der Kooy, 2002; Taupin and Gage, 2002). The NSCs that exhibit slow self-renewal produce neural progenitor cells (NPCs) with a faster dividing cell cycle, which ultimately differentiate into neurons or neuroglia; the differentiation process is regulated by numerous trophic factors (Abrous *et al.*, 2005; Lois and Alvarez-Buylla, 1993; Seaberg and van der Kooy, 2002). Another important pool of neural precursor cells is represented by astrocytes residing in the germinal centres of the adult brain; these astrocytes retain the stem cell properties throughout the life span, and are involved in both neuro- and glio-genesis (Alvarez-Buylla *et al.*, 2001; Doetsch *et al.*, 1999; Gotz and Huttner, 2005; Mori *et al.*, 2005). In addition, astrocytes appear to regulate the rate of proliferation of hippocampal stem cells, and favour the generation of new neurons (Song *et al.*, 2002). Immature neurons generated in the SVZ migrate via the rostral migratory stream to the olfactory bulb, where they differentiate into local interneurons (Lledo and Gheusi, 2003). Although many thousands of new neurons are generated in the SVZ and in the SGZ daily, only a minority of them survive and acquire adult neuronal properties (Abrous *et al.*, 2005; Lois and Alvarez-Buylla, 1993; Seaberg and van der Kooy, 2002). These newly generated neurons receive synaptic inputs, extend axons along the mossy fibres tract that pass through the hilus and exhibit electrophysiological properties similar to those of mature dentate granule cells (Levison and Goldman, 1993; Paterson *et al.*, 1973). In addition, these newly generated neurons express the full complement of ionotropic and metabotropic membrane receptors (Kempermann and Gage, 1999). Incidentally, those cells may act as neuronal replacements after injury or disease (Brandt and Storch, 2008). From a functional point of view, CNS neurogenesis and, more specifically, hippocampal neurogenesis, play an important role in structural plasticity and network maintenance. Therefore, it is likely to contribute to information storage, as well as learning and memory processes (Abrous *et al.*, 2005; Kempermann and Gage, 1999; Levison and Goldman, 1993; Paterson *et al.*, 1973).

The hippocampus is affected early in AD. Therefore, the pathological process associated with AD is likely to impinge upon neurogenesis. Impaired neurogenesis, in turn, can be relevant for the disease progression arguably being involved in the cog-

nitive impairments linked with neurodegeneration (Chevallier *et al.*, 2005; Haughey *et al.*, 2002; Jin *et al.*, 2004; Lopez-Toledano and Shelanski, 2007; Rodriguez *et al.*, 2009; Verret *et al.*, 2007; Zhao *et al.*, 2008). Current treatment options for AD are centered on regulating neurotransmitter activity. Enhancing cholinergic function improves AD behavioral and cognitive defects (Lunn *et al.*, 2011). Targeting the cholinergic system using stem cell therapies may provide environmental enrichment. Since that neurogenesis in the hippocampus decreases as we age and is exacerbated in AD (Drapeau and Nora Abrous, 2008; Shruster *et al.*, 2010); therefore, cellular therapies that enhance neurogenesis or replace lost neurons may also delay the progression of AD. Enhancing brain-derived neurotrophic factor (BDNF) levels, which are decreased with age and in AD, promotes neurogenesis and protects neuronal function (Li *et al.*, 1999). Rodent AD models receiving NPC grafts demonstrate increased hippocampal synaptic density and increased cognitive function associated with local production of BDNF (Blurton-Jones *et al.*, 2009). Similarly, BDNF up-regulation along with NPC transplants also improves cell incorporation and functional outcomes in an AD rat model (Xuan *et al.*, 2008). Many studies have shown that bone marrow-derived mesenchymal stromal cells (MSCs) can be used for neural cell regeneration. MSCs are an alternative source of multipotent self-renewing cells and are derived from adult bone marrow. Naturally, they differentiate to produce osteoblasts, chondrocytes, and adipocytes; however, there is evidence that they can transdifferentiate to a neural lineage (Satija *et al.*, 2009). MSCs provide an accessible alternative to embryonic stem (ES) cells and potentially circumvent the need for immunosuppression in cellular therapies because they are derived from an autologous source. Combining engineered growth factor overexpression with the benefits of stem cells integration into neural networks may provide an enhanced approach to treating AD. Furthermore, given the widespread neuronal loss involved in AD pathogenesis, targeting multiple systems simultaneously may be advantageous.

### 1.4 Cholesterol and gangliosides in the central nervous system (CNS)

#### 1.4.1 Brain cholesterol metabolism

Cholesterol is an essential component of the plasma membrane of all cells, where it increases membrane rigidity reducing lipid disorder; together with sphingolipids and gangliosides, is concentrated in detergent-resistant membrane fractions (lipid rafts) and plays key roles in neuronal development as well as in the maintenance of neuronal plasticity and function (reviewed in Ledesma and Dotti, 2006). The brain synthesizes essentially all of its cholesterol and does not appear to depend on the circulating pool of the steroid; actually, the plasma lipoproteins do not cross the blood-brain barrier (BBB) and do not deliver significant amounts of cholesterol to the CNS (Turley *et al.*, 1996). Neuronal cells appear to synthesize cholesterol during development, whereas mature neurons progressively lose such ability, getting cholesterol from glial cells, particularly astrocytes (Pfrieger, 2003; Poirier *et al.*, 1993). The rate-limiting step of cholesterol synthesis is the reaction catalyzed by 3-hydroxy-3-

methylglutarylCoA reductase (HMGCoAR), whose activity is controlled by the levels of cholesterol itself. Thus HMGCoAR has been a good candidate for pharmacological treatment of hypercholesterolemia using statins, chemical analogues of cholesterol. In the adult brain, the astrocytes not only synthesize, but also internalize and recycle the cholesterol released from degenerating nerve terminals to deliver it back to neurons (Jurevics and Morell, 1995); this activity requires cholesterol binding to one of the variants of ApoE, a major lipoprotein in the CNS (Mahley, 1988). ApoE is a ligand for cell surface lipoprotein receptors such as the LDLR (LDL-receptor) and the LDLR-related proteins (LRP); ApoE also regulates lipid transport to neurons and clears cholesterol from the extracellular space (Poirier, 2003). The fusion with lysosomes of the internalized endosomes containing ApoE-cholesterol-phospholipid complexes results in the intracellular release of cholesterol, with reduction of endogenous synthesis by HMGCoAR inhibition and storage upon fatty acid esterification by acylCoA:cholesterol acyltransferase (ACAT) (Poirier, 2003). The main product of brain cholesterol metabolism is the 24-hydroxy derivative (24SOH-Chol) that is translocated to the circulating blood through the BBB which hinders the direct passage to the CNS of the blood cholesterol and limits the reverse passage of cholesterol from the CNS to the venous circulation. Since most of the circulating 24SOH-Chol arises from brain cholesterol, its levels can be considered a measure of cholesterol turnover in the CNS (Kölsch *et al.*, 2004). Finally, a fraction of brain cholesterol could be translocated to the blood by transport systems involving ATP-binding cassette membrane transport proteins such as ABCA1.

#### **1.4.2 Ganglioside metabolism**

Gangliosides are sialic acid-containing glycosphingolipids that are expressed in the outer leaflet of the plasma membrane of all vertebrate cells. Gangliosides are involved in a variety of functions, including serving as antigens, receptors for bacterial toxins, mediators of cell adhesion, and mediators and modulators of signal transduction (Hakomori, 2003). About 200 gangliosides are known today, differing in their carbohydrate components (Yu *et al.*, 2007). Gangliosides are most abundant in the nervous system. Their expression in the nervous system is cell specific and developmentally regulated, and their quantities and species undergo dramatic changes during differentiation of the cell (Ngamukote *et al.*, 2007; Yanagisawa and Yu, 2007; Yu, 1994). Gangliosides also play an important role in the pathogenic mechanisms of many immune-mediated neurological disorders, such as Guillain-Barre' syndrome (Yu *et al.*, 2006). GM1 ganglioside is present in endocytic organelles, in the trans-Golgi network, and in the plasma membranes. More recently, it has been demonstrated that GM1 ganglioside is also present in nuclear membranes, adding another interesting facet to the myriad biological functions of gangliosides (Ledeen and Wu, 2007). In the plasma membrane, where the bulk of GM1 is deposited, GM1 is not distributed uniformly but is more concentrated in non-coated invaginations (Parton, 1994). Gangliosides are also known to exist in clusters and to form microdomains or lipid rafts on the surface of the plasma membrane (Simons and Toomre,

2000). This specific localization of gangliosides enables them to interact with a variety of bio-effectors, such as glycoproteins, antibodies, peptide hormones, and growth factors (Ariga *et al.*, 2001; Yang *et al.*, 1996). Furthermore, gangliosides can promote cell differentiation and induce neuritogenesis (Hakomori and Igarashi, 1995; Ledeen *et al.*, 1998). Gangliosides are also known to provide a neuroprotective role in *in vivo* and *in vitro* models of neuronal injury (Hadjiconstantinou and Neff, 1998). The mechanisms of the neuroprotective effect of GM1 and related gangliosides, however, are still obscure (Sokolova *et al.*, 2007).

#### 1.4.3 Lipid rafts

Lipid rafts are dynamic highly ordered membrane microdomains enriched in cholesterol, gangliosides, particularly GM1, sphingolipids and saturated phospholipids distinct from the surrounding bilayer of mostly unsaturated phospholipids. Biochemically, lipid rafts are defined by their relative insolubility in non-ionic detergents at low temperature, conferring upon them the alternative name, detergent-resistant membranes (DRMs). Lipid rafts are particularly enriched in glycosyl-phosphatidylinositol (GPI)-anchored and acylated proteins due to the preferential intercalation of the saturated acyl chains into the liquid-ordered environment (Simons and Ikonen, 1997). Other proteins can also associate with lipid rafts either directly or through binding to other cofactors or ligands (Allen *et al.*, 2007). The dynamic clustering and pinching off of lipid rafts regulates the spatial and temporal assembly of signalling and trafficking molecules, forming short-lived but vital signalling platforms (Allen *et al.*, 2007). Lipid rafts are implicated in various essential cellular functions, including signal transduction, cell adhesion and protein/lipid sorting (Lewis and Hooper, 2011). Of particular relevance are cell signalling, sorting and axon guidance, as these processes are essential for neural development and synaptic plasticity (Guirland and Zheng, 2007; Kamiguchi, 2006). Indeed, lipid rafts serve to compartmentalise cellular processes by concentrating certain proteins and lipids within the same microenvironment serving as platforms regulating the induction of signaling pathways, owing to their ability to recruit or exclude specific lipids and proteins (Simons and Ikonen, 1997; Simons and Toomre, 2000). They are often thought to exert a positive effect by maintaining various signaling components (receptors, coupling factors, enzymes and substrates) in a restricted domain, thus inducing a more rapid and efficient coupling. Lipid rafts play a more subtle regulatory role due to the fact that different signaling components can be localized in both the raft and non-raft parts of the membrane (Harder and Engelhardt, 2004; Pike, 2003). The fact that lipid microdomains are dynamic structures in which both lipids and proteins can move with different kinetics is essential for their role in signal transduction, but this dynamism has also made it exceedingly difficult to study their functional presence in living cell membranes. Thus, controversy has arisen concerning their size and even their existence under steady-state conditions (resting cells) *versus* the activated state (Kenworthy *et al.*, 2004). Crucially, neuronal lipid rafts are also required for the maintenance of dendritic spines and healthy synapses, which are vi-

tal for neural communication including learning and memory; processes which fail in AD (Hering *et al.*, 2003). The observation that lipid rafts are much more abundant in mature hippocampal neurons than in other cell types emphasises their physiological importance within the memory centre of the healthy brain, and may explain why hippocampal neurons are a primary target for A $\beta$  oligomer toxicity and destruction in AD (Malchiodi-Albedi *et al.*, 2011).

#### **1.4.4 Role of cholesterol in AD**

In spite of the intense research carried out in recent times, the role of cholesterol as a risk factor for AD remains controversial (reviewed in Koudinov and Koudinova, 2005; Puglielli *et al.*, 2003; Shobab *et al.*, 2004; Sjögren *et al.*, 2006; Stefani and Liguri, 2009). In the past 15 years, several epidemiological studies have stressed an association between high plasma cholesterol, mainly in mid age, and increased susceptibility to sporadic late-onset AD (reviewed in Shobab *et al.*, 2004). The lack of a direct effect of circulating cholesterol on AD risk is further supported by the notion that there is very little exchange between circulating and brain cholesterol thus questioning the importance of statins (inhibitor of the geranylgeranyl isoprenoids synthesis) able to cross the BBB (including atorvastatin, simvastatin and lovastatin) as possible drugs for AD therapy (reviewed in Ledesma and Dotti, 2005). The use of statins as possible pharmacological agents in the treatment of AD stems from retrospective clinical studies indicating that individuals chronically treated with these drugs display lower risk of developing late-onset AD (Zandi *et al.*, 2005). However, recent studies do not support these conclusions (reviewed in Ledesma and Dotti, 2005; Shobab *et al.*, 2004) and other prospective studies failed to show a beneficial effect of statins in AD treatment (MRC/BHF Heart Protection Study, 2002).

The content of membrane cholesterol can modulate A $\beta$  peptide production, aggregation and clearance in various ways, particularly by affecting the stability of lipid rafts and other membrane domains where APP and some APP processing secretases are located, as well as the activity of raft associated proteins. In particular, the following effects/actions have been highlighted: (i.) membrane cholesterol can affect the cellular localization and the activity of the APP and the secretases modulating APP processing through the amyloidogenic or the non-amyloidogenic pathway; (ii.) membrane cholesterol can affect the way A $\beta$  peptides interact with the plasma membrane favouring or disfavouring aggregate nucleation; (iii.) membrane cholesterol can hinder the interaction of A $\beta$  oligomers with the cell membrane thus avoiding their cytotoxic effects.

##### **1.4.4.1 Membrane cholesterol modulates A $\beta$ production affecting the amyloidogenic and the non-amyloidogenic pathways**

Lipid rafts harbour many membrane proteins including APP and some secretases (Ehehalt *et al.*, 2003; Kakio *et al.*, 2003; Lee *et al.*, 2003). The content of membrane cholesterol and the functional organization of lipid rafts appear to markedly

affect the way APP is processed by the  $\alpha$ -,  $\beta$ -, and  $\gamma$ -secretases thus favouring the non-amyloidogenic or the amyloidogenic pathway, with increased or reduced A $\beta$ 40/42 production (Abad-Rodriguez *et al.*, 2006; Cramer *et al.*, 2006; Kojro *et al.*, 2001). The raft dependence of the generation of amyloidogenic derivatives of proteins and peptides does not appear to be limited to APP and A $\beta$  peptides. Actually, several lines of evidence support the idea that the pathological conversion of the cellular prion protein (PrP) to the infectious scrapie (PrP<sup>sc</sup>) form of the prion protein occurs at the lipid rafts (Harris, 1999; Prusiner *et al.*, 1998). However, conflicting data have been reported on the effect of membrane cholesterol on APP processing; two models have been proposed. The “high neuronal membrane cholesterol models of AD pathogenesis” postulates that two pools of APP do exist in the cells, one associated with membrane rafts and another out of rafts, where  $\alpha$ -cleavage occurs, suggesting that only the raft-localized APP processing results in A $\beta$  generation (Ehehalt *et al.*, 2003). Such a scenario would be favoured by high levels of brain cholesterol possibly associated with the ApoE4 phenotype or during lipid rafts co-clustering in the endocytic process (Fig. 9A). Several data indicate that in peripheral and neuronal cell lines low membrane cholesterol and increased membrane fluidity stimulate the non-amyloidogenic pathway ( $\alpha/\gamma$ -secretase cleavage); this could result from reduced activity of BACE, the enzyme starting the amyloidogenic pathway, and from increased  $\alpha$ -secretase activity and APP content in the cell membrane, where it can undergo  $\alpha$ -secretase cleavage (Kojro *et al.*, 2001). Moreover, in the hippocampus of both humans and transgenic mice only a very moderate amount of APP and BACE is found in the same membrane environment; these co-localized APP and BACE fractions increase markedly in AD patients and in rodents with a moderate reduction of brain cholesterol (Abad-Rodriguez *et al.*, 2004).

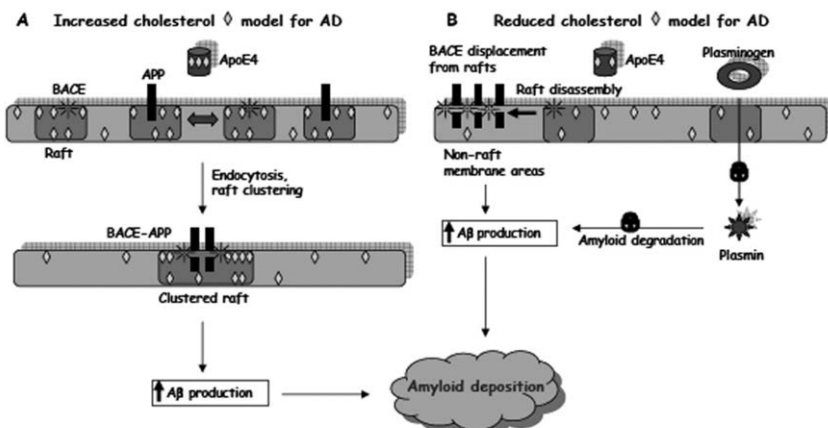


Figure 9. The high (A) and low (B) neuronal membrane cholesterol models of AD pathogenesis. The high cholesterol model assumes that low neuronal membrane cholesterol is protective against AD. In fact, high membrane cholesterol would result in increased lipid raft co-clustering and APP-BACE co-localization thus favouring the amyloidogenic pathway of APP

processing with increased A $\beta$  production. On the contrary, the low membrane cholesterol model envisages a protective role of relatively high amounts of membrane cholesterol assuming that APP is located in non-raft membrane domains. High membrane cholesterol would maintain APP and BACE separated into different membrane domains thus reducing A $\beta$  generation. Under low cholesterol conditions, following lipid raft disassembly BACE would translocate to non raft domains thus favouring its association with APP and starting the amyloidogenic pathway of APP processing. Under these conditions, the production of A $\beta$  peptides would be further increased by the reduced activation of plasminogen to plasmin, a raft-associated event (Stefani and Liguri, 2009).

The opposite “low neuronal membrane cholesterol models of AD pathogenesis” claims that BACE, but not APP, is localized in lipid rafts (Abad-Rodriguez *et al.*, 2004). As a consequence, a moderate loss of membrane cholesterol would result in raft disassembly and increased BACE-APP co-localization in non-raft membrane domains, with increased  $\beta$ -cleavage (Fig. 9B). The protective effect of cell cholesterol against A $\beta$  production and cytotoxicity is convincingly confirmed by more recent investigations on the relation between Seladin-1 (DHCR24, 3- $\beta$ -hydroxysterol delta-24-reductase, which catalyzes the reduction of the  $\Delta$ 24 double bond in desmosterol to produce cholesterol), cholesterol levels and A $\beta$  generation in neuronal cells. Indeed, the beneficial effect of increased cholesterol following Seladin-1 over expression has recently been reported in a study showing that cultured cells enriched in membrane cholesterol by Seladin-1 over expression display reduced ability to bind externally supplied A $\beta$  oligomers with increased resistance to their cytotoxic effects, whereas the opposite was seen in the same cells made poor in cholesterol following treatment with the Seladin-1 inhibitor desmosterol (Cecchi *et al.*, 2008b). These data, together with those indicating a specific down-regulation of Seladin-1 (Greeve *et al.*, 2000) and a reduced level of cholesterol in the brains of AD patients (Mason *et al.*, 1992), establish a role of this enzyme in lipid raft formation, modulation of APP processing, A $\beta$  generation and clearance, and cell resistance to A $\beta$  oligomer cytotoxicity.

#### **1.4.4.2 Membrane cholesterol modulates A $\beta$ aggregation**

In solution, A $\beta$  peptides display a substantially unfolded conformation with reduced content of secondary structure; however, the latter increases considerably in phospholipid vesicles particularly when enriched in cholesterol thus underscoring the role of membranes in modulating peptide structure and aggregation (Choo-Smith *et al.*, 1997; Ji *et al.*, 2002). Actually, structural perturbations may be expected to occur in proteins/peptides following their interaction with membranes thus enhancing their rate of fibrillization (reviewed in McLaurin *et al.*, 2000). Therefore, it is not surprising that membrane lipid composition affects remarkably the effect of a membrane on a protein/peptide structure and aggregation propensity. The ability of A $\beta$  peptides to insert into the membrane seems to depend on the membrane cholesterol:phospholipids ratio. In synthetic, low cholesterol dimyristoylphosphatidylcholine (DMPC) vesicles, A $\beta$  preferentially localizes at the membrane surface exhibiting

an aggregation-prone  $\beta$ -structure; on the contrary, in the same vesicles containing 33% cholesterol the C-terminal tail of the peptide inserts into the membrane with an altered,  $\alpha$ -helix rich structure that hinders peptide aggregation (Ji *et al.*, 2002). These data support the idea that the content in cholesterol affects the way A $\beta$  peptides interact with the phospholipid bilayer and their ability to insert in the latter, modulating its aggregation into fibrillar assemblies.

### 1.4.4.3 Membrane cholesterol modulates A $\beta$ cytotoxicity

A $\beta$  oligomer toxicity has been associated basically with the ability of these assemblies to interact with the cell membranes. Such an interaction results in loss of membrane integrity, derangement of selective ion permeability and impairment of specific membrane-bound protein function (De Felice *et al.*, 2007; Kourie and Henry, 2002; Mattson, 1999; Resende *et al.*, 2007), and appears modulated by the content of cholesterol in the membrane, increasing in cholesterol-poor membranes and vice versa (Cecchi *et al.*, 2005; Cecchi *et al.*, 2008c, Pensalfini *et al.*, 2011). Actually, many data support the idea that A $\beta$  oligomer cytotoxicity following association with the cell membrane depends on membrane physical features including fluidity, compactness, curvature and others, resulting from lipid composition. Since differing cell types display different average membrane lipid composition, for example in terms of cholesterol or ganglioside content, this could contribute to explain the variable susceptibility to the same toxic oligomeric species of varying cell types in culture and in tissue, or of the same cells in different differentiation stages or cell cycle phases (Cecchi *et al.*, 2005; Cecchi *et al.*, 2008c). Membrane cholesterol can modulate aggregate-cell interaction by affecting the physical state of the rafts harbouring for example glutamatergic calcium channels such as the AMPA and NMDA receptors, which have been suggested to act a binding site for A $\beta$  oligomers (De Felice *et al.*, 2007; Resende *et al.*, 2007).

### 1.4.5 Role of gangliosides in AD

In brain cells, ganglioside and lipid abnormalities, in addition to pathogenic A $\beta$  production, may contribute to the pathological conditions found in AD (Mutoh *et al.*, 2006). Several earlier studies showed alterations in ganglioside metabolism in AD brain (Kalanj *et al.*, 1991; Kracun *et al.*, 1992; Svennerholm and Gottfries, 1994). This is manifested as reductions in gangliosides in the majority of brain regions, including the cerebral cortex, hippocampus, basal telencephalon, and frontal white matter, and especially in the frontal cortex and white matter (Kalanj *et al.*, 1991). The pattern of ganglioside alterations in AD differs according to age of onset (Ariga *et al.*, 2008). A fundamental question concerning the pathogenic mechanism of AD is how non toxic A $\beta$  is converted to its toxic aggregates in the brain (Yanagisawa, 2007). Yanagisawa *et al.* (Yanagisawa *et al.*, 1995) found that GM1 ganglioside bound to A $\beta$ 42, to form a complex termed “GA $\beta$ ” in AD brains. GA $\beta$  has unique characteristics, including an extremely high aggregation potential and an altered pat-

tern of immunoreactivity, which results in seeding for amyloid fibril formation in brains. The formation of GA $\beta$  serves as one of the critical factors in the development of AD and may provide new insights into its pathophysiology (Yanagisawa, 2007) (Fig. 10).

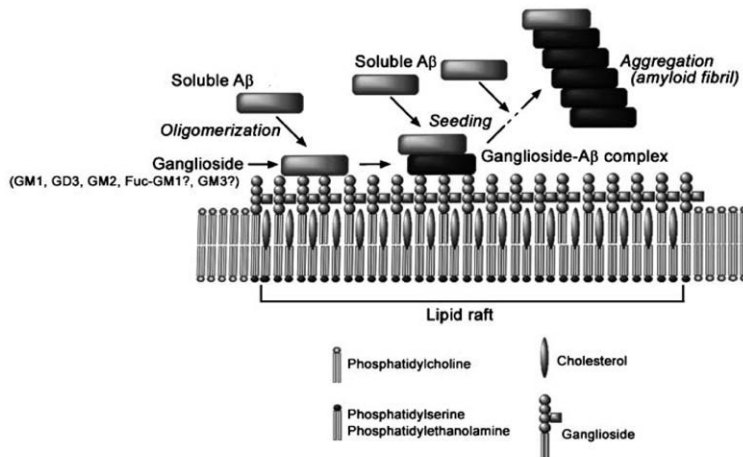


Figure 10. Interactions of gangliosides and amyloid  $\beta$ -proteins in lipid rafts. Form (Ariga et al., 2008).

In addition, several evidence confirmed that A $\beta$  binds to membranes containing ganglioside GM1, and upon binding, undergoes a conformational transition from random coil to an ordered structure rich in  $\beta$ -sheet. This interaction appears to be ganglioside specific because no changes in A $\beta$ 40 conformation were found in the presence of various phospholipids or sphingomyelin. The peptide binds selectively to membranes containing gangliosides with a binding affinity ranging from  $10^{-6}$  to  $10^{-7}$  M, depending on the type of the ganglioside sugar moiety (Choo-Smith *et al.*, 1997; McLaurin and Chakrabarty, 1996; Terzi *et al.*, 1995). Thus, favourable interactions between A $\beta$  and GM1 in the cell membrane provide a mechanism for A $\beta$  fibrillogenesis *in vivo*, and A $\beta$ -induced disruption of the cell membrane may provide a pathway by which A $\beta$  exerts toxicity (Chi *et al.*, 2007). Indeed, surface-associated,  $\beta$ -sheet-rich, peptide micro-aggregates could then act as a specific template ("seed") to recruit additional peptide molecules from solution and promote fibril formation by a  $\beta$ -sheet augmentation mechanism (Choo-Smith *et al.*, 1997) (Fig. 10). A $\beta$  aggregation in brain is accelerated through an increase in the level of GM1 in neuronal membranes (Yamamoto *et al.*, 2004). Further studies have demonstrated that GM1 and trisialoganglioside GT1b promote the aggregation and cytotoxicity of A $\beta$ 40, and these gangliosides, especially GM1, catalyze the formation of neurotoxic fibrils (Okada *et al.*, 2007). This effect is dose dependent. Using surface plasmon resonance (SPR) it has been demonstrated that A $\beta$ 40 binds to a number of gangliosides with

## Amyloid Cytotoxicity and Membrane Lipid Composition

the following order of binding strength: GQ1b $\alpha$  > GT1a $\alpha$  > GQ1b > GT1b > GD3 > GD1a = GD1b > LM1 > GM1 > GM2 = GM3 > GM4 (Ariga *et al.*, 2001). The ganglioside sugar moiety, specifically the sialic acid, plays an important role in the A $\beta$ -gangliosides interaction. The sialic acid residue of the ganglioside head-group is important for determining the nature of the conformational change in A $\beta$  peptides following its binding to ganglioside (Mandal and Pettegrew, 2004; Williamson *et al.*, 2006).

Gangliosides are enriched in the lipid rafts of brains of AD patients (Molander-Melin *et al.*, 2005). It has been reported the presence of gangliosides in DRMs isolated from 10 AD and 10 age-matched control brains. DRMs from the frontal and temporal cortices of AD brains contained a significantly higher concentration of gangliosides GM1 and GM2 (Molander-Melin *et al.*, 2005). The DRMs derived from temporal cortex of AD patients were depleted of cholesterol compared with control subjects. However, it has been reported that seeding formation is facilitated by cholesterol; A $\beta$  binding to GM1 is markedly accelerated in a cholesterol-rich environment at lipid rafts level (Kakio *et al.*, 2001; Mizuno *et al.*, 1999). According some researchers, increases in intramembrane cholesterol content, which are likely to occur during aging, appear to be a risk factor for amyloid fibril formation (Kakio *et al.*, 2001). Lipid rafts containing ganglioside clusters may serve as a conformational catalyst to generate a membrane-active form of A $\beta$  with seeding ability rather than providing a specific binding site for the protein (Kakio *et al.*, 2003).

Administration of GM1 have been used to inhibit progression of AD, but this treatment is still at an experimental stage, as are efforts to prevent the formation of amyloid plaques (Gottfries, 1994). *In vivo* GM1 administration may reduce or prevent brain amyloidosis (Matsuoka *et al.*, 2003). This anti-amyloidogenic effect could be attributed to a “peripheral sink” effect, i.e., that GM1-bound A $\beta$  alters central/peripheral dynamics, drawing A $\beta$  out of the brain. In addition, GM1-bound A $\beta$  in the blood is no longer available to BBB and incorporate into plaques centrally. Thus, peripheral administration of GM1 may be effective in reducing amyloid aggregation in AD. A potential difficulty, however, in tapping the neuroprotective effects of GM1 is the low level of gangliosides that can enter into the brain. In this regard, it has been reported that only 1% of peripherally administered GM1 crosses the BBB to enter the brain (Saulino and Schengrund, 1994). Exogenous GM1 treatment has also been used to treat symptoms of Parkinson’s disease, in both human and animal models (Fazzini *et al.*, 1990; Pope-Coleman *et al.*, 2000; Rothblat and Schneider, 1999; Schneider *et al.*, 1992). In addition, it has been developed a novel monoclonal antibody raised against purified GA $\beta$  from AD brain, which substantially inhibits *in vitro* A $\beta$  assembly (Hayashi *et al.*, 2004). These findings add a new dimension to the development of novel therapeutic strategies by targeting seeded A $\beta$  in the brain, which selectively inhibits the initial step of the pathological process of AD (Kimura and Yanagisawa, 2007; Yanagisawa, 2007). Recent studies suggest that A $\beta$  aggregation occurs in lipid rafts mediated by a cluster of GM1 (Yuyama *et al.*, 2006). Interestingly, rifampicin and nordihydroguaiaretic acid have been shown to inhibit binding of A $\beta$  to GM1 liposomes by competitively binding to the membranes and/or di-

rect interaction with A $\beta$  in solution, thus at least partly preventing fibrils from forming. These small compounds can therefore be utilized for therapeutics. With the finding that GA $\beta$  has a conformation distinct from that of soluble A $\beta$ , it may be possible to develop a novel therapeutic strategy to specifically inhibit the initiation of oligomerization polymerization of A $\beta$  in the brain (Hayashi *et al.*, 2004; Yamamoto *et al.*, 2005).

### 1.5 Aim of the study

Increasing evidence supports the idea that the initial events of A $\beta$  oligomerization and cytotoxicity in Alzheimer's disease involve the interaction of amyloid A $\beta$ -derived diffusible ligands (ADDLs) with the cell membrane. This also indicates lipid rafts, ordered membrane microdomains enriched in cholesterol, sphingolipids and gangliosides, as likely primary interaction sites of ADDLs. To shed further light on the relation between ADDL-cell membrane interaction and oligomer cytotoxicity, we investigated the dependence of ADDLs binding to lipid rafts on membrane cholesterol content in human SH-SY5Y neuroblastoma cells (Results I). Confocal laser and contact mode atomic force microscope analyses, anisotropy fluorescence measurements suggest that cholesterol reduces amyloid-induced membrane modifications at the lipid raft level by altering raft physicochemical features.

These results were also confirmed in primary fibroblasts from FAD bearing APP Val717Ile, PS1 Leu392Val or PS1 Met146Leu gene mutations (Results II). In addition, A $\beta$  has been found to be tightly associated with GM1 and it was originally postulated that this interaction might act as a seed for A $\beta$  accumulation and aggregation. However, no clear mechanistic evidence regarding the relationship between lipid raft content and amyloid toxicity is currently available. In this regards the modulation of specific raft physicochemical properties, such as mild depletion of GM1 content and interference with GM1 exposure or negative charge, was tested analyzing the interaction of amyloid aggregates with the plasma membrane and the resulting cell damage in FAD fibroblasts and in primary cortical neurons from rat brains (Results II). These findings suggest a specific role for raft domains, as primary mediators of amyloid toxicity in AD neurons.

In view of the undoubtedly importance of the structural features of amyloid oligomers in determining their pivotal role as major cytotoxic species, several recently reported studies have tried to assess the oligomer structure-toxicity relationship by focusing on features of the oligomers, including stability and exposure of hydrophobic surfaces. In particular, it has been recently published that two types of stable oligomers generated from the small prokaryotic protein HypF-N under different destabilising conditions differ significantly in their sub-microscopic structural properties and cytotoxicities, though displaying similar morphological and tinctorial properties. To study the relationship between the physicochemical properties of the protein aggregates and physicochemical features of the cell membranes with which the oligomers interact, membrane cholesterol and GM1 content has been modulated in SH-SY5Y neuroblastoma cells before exposure to the two types of oligomers of

## Amyloid Cytotoxicity and Membrane Lipid Composition

HypF-N. The results, confirmed using oligomers formed by A $\beta$  peptide associated with Alzheimer's disease, reveal that toxicity is not inherent to protein oligomers only, but results from a complex interplay between the structural and physicochemical features of both the oligomers and the cell membrane (Results III).

Cell therapy is a promising approach for the treatment of neurodegenerative conditions such as Alzheimer's and Parkinson's diseases. However, the presence of toxic aggregates in tissue raises the question of whether grafted stem cells are susceptible to amyloid toxicity before they differentiate into mature neurons. To address this question, we investigated the relative vulnerability of human mesenchymal stromal cells and their neuronally differentiated counterparts to A $\beta$ 42 oligomers and whether susceptibility correlates with membrane GM1 content, a key player in oligomer toxicity. We found that our cell model was highly susceptible to aggregate toxicity, whereas neuronal differentiation induced resistance to amyloid species (Results IV). This data correlated well with the content of membrane GM1, levels of which decreased considerably in differentiated cells. These findings extend our knowledge of stem cell vulnerability to amyloid species, which remains a controversial issue, and confirm that amyloid-GM1 interactions play an important role in cell impairment.

# Materials & Methods

## 2.1 Materials

### 2.1.1 Chemicals

All reagents were of analytical grade or the highest purity available. Media and sera for cell cultures, except from those for mesenchymal stromal cells (hMSC) cultures (Euroclone; Wetherby, West York, UK) and primary cultured cortical neurons (Life Technologies; Milan, Italy) were purchased from Sigma (Milan, Italy). Tissue plastic-ware was obtained from Steroglass (Perugia, Italy). 1,2-bis(2-aminophenoxy)ethane-N,N,N',N'-tetraacetic acid acetoxyethyl ester (BAPTA-AM), 1,6-diphenyl-1,3,5-hexatriene (DPH), dimethylsulfoxide (DMSO), disialoganglioside (GD1a), fetal bovine serum (FBS), filipin III, hexafluoro-2-isopropanol (HFIP), methyl- $\beta$ -cyclodextrin ( $\beta$ -CD), mevastatin (Mev), monosialotetrahexosyl-ganglioside (GM1), neuroaminidases (NAA), phosphate buffered saline (PBS), pluronics acid F-127, polyoxyetanyl-cholesteryl sebacate (PEG-cholesterol), trisialoganglioside (GT1b), vitamin E (Vit E), water-soluble cholesterol balanced with methyl- $\beta$ -cyclodextrin (40 mg of cholesterol per gram of  $\beta$ -CD-Chol) (Chol) and other chemicals were from Sigma (Milan, Italy). D-Threo-1-phenyl-2-decanoylamino-3-morpholino-1-propanol (PDMP) was obtained from Matreya LLC (PA, USA).

### 2.1.2 Fluorescent probes

2',7'-dichlorodihydrofluorescein diacetate (CM-H<sub>2</sub>DCFDA), 4,4-difluoro-3a,4a-diaza-*s*-indacene (BODIPY) 581/591 C<sub>11</sub>, Alexa Fluor 647- and 555-conjugated cholera toxin subunit B (CTX-B), Alexa Fluor 633- and fluorescein- conjugated wheat germ agglutinin (WGA), calcein acetoxyethyl ester (calcein-AM), fluo3 acetoxyethyl ester (fluo3-AM), N-(3-triethylammoniumpropyl)-4-(6-(4-diethylamino)phenyl)hexatrienylpyridinium dibromide (FM4-64) were from Molecular Probes (Eugene, OR). CM-H<sub>2</sub>DCFDA, BODIPY, calcein-AM, Fluo3-AM and FM4-64 were prepared as stock solutions in DMSO, dried under N<sub>2</sub> and stored in light-protected vessels at -20 °C until use.

### 2.1.3 Peptides and aggregation protocols

$\text{A}\beta_{42}$  and  $\text{A}\beta_{42-1}$  reverse peptides (as trifluoroacetate salts) were purchased from Sigma (Milan, Italy) and from Bachem (Bübendorf, Switzerland), respectively;  $\text{A}\beta_{42}$  amine-reactive succinimidyl esters of carboxyfluorescein ( $\text{A}\beta_{42}\text{-FAM}$ ) was from AnaSpec (San Jose, CA, USA). Lyophilized  $\text{A}\beta_{42}$ ,  $\text{A}\beta_{42}\text{-FAM}$  and  $\text{A}\beta_{42-1}$  were initially incubated 1.0 mM in HFIP at least for 1 h at room temperature to allow complete peptide monomerization. Then, aliquots of peptide solutions were dried under  $\text{N}_2$  and stored at  $-80^\circ\text{C}$ . Prefibrillar aggregates of the  $\text{A}\beta_{42}$  peptide were obtained according to Lambert's protocol (Lambert *et al.*, 2001). Briefly, aliquots of  $\text{A}\beta_{42}$  were dissolved in DMSO to a final concentration of 5.0 mM, incubated in ice-cold F12 medium to a concentration of 100  $\mu\text{M}$  at  $4^\circ\text{C}$  for 24 h and then centrifuged at 14,000  $\times g$  for 10 min to remove insoluble structures. The supernatant, defined as the amyloid  $\beta$ -derived diffusible ligand (ADDL) preparation, consisted of a fibril-free solution of globular assemblies, as assessed by AFM (Cecchi *et al.*, 2009). Fluorescein-labeled  $\text{A}\beta_{42}\text{-FAM}$  aggregates were prepared as described above, except that the aggregation mixture contained a combination of  $\text{A}\beta_{42}\text{-FAM}$  peptide with 2 molar equivalents of unlabeled  $\text{A}\beta_{42}$  peptide (at a 1:2 ratio) to minimize possible interference of the fluorophore with the aggregation, while retaining sufficient fluorescence signal (Simakova and Arispe, 2007). For fibrillar conditions, 10 mM HCl was added to bring the peptide to a final concentration of 100  $\mu\text{M}$ , and the peptide was incubated for 24 h at  $37^\circ\text{C}$  (Dahlgren *et al.*, 2002).

HypF-N protein, expressed and purified as previously reported (Marcon *et al.*, 2005), was converted into stable oligomers by incubation to 48  $\mu\text{M}$  for 4 h at  $25^\circ\text{C}$  in two different experimental conditions: 50 mM acetate buffer, 12% (v/v) trifluoroethanol (TFE), 2 mM dithiothreitol (DTT), pH 5.5 (condition A) and 20 mM trifluoroacetic acid (TFA), 330 mM NaCl, pH 1.7 (condition B) (Campioni *et al.*, 2010). Both types of HypF-N oligomers were centrifuged at 16,100  $\times g$ , dried under  $\text{N}_2$  to remove the TFE and TFA when necessary, dissolved in the appropriate culture media at 48  $\mu\text{M}$  concentration and immediately added to cultured cells at 12  $\mu\text{M}$  final concentrations. Native HypF-N was tested by diluting the protein stock solution in the same cell media. Tapping-mode AFM revealed the presence of spherical bead-like aggregates with heights in the range of 2-6 nm and 2-7 nm under conditions A and B, respectively (Campioni *et al.*, 2010). For the internalization experiment, monomeric HypF-N was labelled with fluorescein-5-isothiocyanate (5-FITC) using AnaTag<sup>TM</sup> 5-FITC Microscale Protein Labeling Kit (AnaSpec, San Jose, CA, USA) and then converted into oligomers. These oligomeric species did not re-solubilize when placed under physiological conditions, as indicated by the preservation of their ability to bind ThT (Campioni *et al.*, 2010). Moreover, neither type of oligomer underwent any detectable structural reorganization following re-suspension in cell culture medium (Campioni *et al.*, 2010).

Prion protein fragment 106-126 (PrP 106-126), as a trifluoroacetate salt, was purchased from Bachem. Lyophilized PrP 106-126 was dissolved 1.0 mM in HFIP and incubated for 10 min at room temperature. Aliquots of protein were ten-fold

diluted, incubated for 15 min at room temperature and then centrifuged for 15 min at  $14,000 \times g$ . The supernatant were dried under  $N_2$  to eliminate HFIP. Samples were then heated for 30 min at 65 °C and stirred for 6 h at 22 °C to obtain soluble oligomers (Demuro *et al.*, 2005).

## 2.2 Cell cultures

Human SH-SY5Y neuroblastoma cells (A.T.C.C., Manassas, VA, USA) were cultured in Dulbecco's Modified Eagle's Medium (DMEM)/F-12 Ham with 25 mM N-2-hydroxyethylpiperazine-N-2-ethanesulfonic acid (HEPES) and  $NaHCO_3$  (1:1) supplemented with 10% FBS, 1.0% glutamine and 1.0% antibiotics. The cell culture was maintained in a 5.0%  $CO_2$  humidified atmosphere at 37 °C and grown until 80% confluence for a maximum of 20 passages.

Fibroblasts were obtained from three patients belonging to Italian families bearing the APP Val717Ile mutation (mean  $\pm$  SD age = 53.3  $\pm$  7.1 years) and from three patients belonging to other Italian families bearing the PS1 Leu392Val and Met146Leu mutations (mean  $\pm$  SD age = 56.7  $\pm$  8.6 years), respectively. They underwent clinical assessment according to published guidelines and the AD diagnosis fulfilled the Diagnostic and Statistical Manual of Mental Disorders criteria (DSM-IV) (American psychiatric association, 1994; The dementia study group of the Italian neurological society, 2000). Primary fibroblasts were also obtained from three age-matched healthy subjects (mean  $\pm$  SD age = 49.7  $\pm$  8.3 years), carrying neither APP or PS1 mutations nor diagnosis of neurological disorders. The local ethical committee approved the protocol and written consent was obtained from all subjects or, where appropriate, their caregivers. Skin biopsies of 3 mm punch were obtained from the volar side of the upper arm of FAD patients and healthy controls. The cells were grown in DMEM supplemented with 10% FBS, 1.0% glutamine and 1.0% antibiotics and harvested in T-25 flasks until confluence, 7 days after previous subculture (Pensalfini *et al.*, 2011). All nine fibroblast lines were subjected to an equal number of passages (ranging from 10 to 18) and analyzed in three different experiments before confluence. The release of endogenous A $\beta$ 42 into the cell culture media was quantified using an A $\beta$ 42 ELISA kit (Molecular Probes).

Primary cortical neurons were obtained from embryonic day (ED)-17 Sprague-Dawley rats (Harlan, Italy). The experimental procedure was in accordance with the standards set forth in the Guide for the care and use of laboratory animals (published by the National Academy of Science, National Academy Press, Washington, DC, USA). The uteri were removed from the gravid rat under anesthesia. Cerebral cortices were dissociated in sterile Dulbecco's PBS (D-PBS; Sigma), and neurons isolated in the same medium containing trypsin (0.5% in sterile Dulbecco's phosphate-buffered saline) for 10 min at 37 °C. After centrifugation, dissociated neurons were re-suspended in neurobasal medium (NBM) supplemented with 2.0% B-27 and 0.5 mmol/L glutamine, and then plated in poly-L-lysine-coated 24-well plates at a density of approximately  $4.5 \times 10^4$ /well. Cultures were maintained in NBM at 37 °C in a 5.0%  $CO_2$ -humidified atmosphere for 14 days after plating.

## Amyloid Cytotoxicity and Membrane Lipid Composition

Human mesenchymal stromal cells (hMSCs) were obtained from the iliac crest of healthy donor marrow aspirates, as previously reported (Benvenuti *et al.*, 2006). Permission was obtained from all subjects and the protocol approved by the local ethical committee. Cells were cultured at  $10^4$  cells/cm<sup>2</sup> in 100-mm dishes in DMEM supplemented with 50 µg/ml gentamycin and 10% FBS at 37 °C in a humidified atmosphere containing 95% air and 5.0% CO<sub>2</sub>.

### 2.3 Methods

#### 2.3.1 Separation processes

##### 2.3.1.1 Cell lysis

Total cell lysates were obtained from cells by three freeze-thaw cycles followed by 5 s ultrasonication in ice in 20 mM Tris-HCl buffer, pH 8.0, containing 1.0% Triton X-100, 137 mM NaCl, 10% glycerol, 6.0 M urea, 0.1 mM PMSF, 10 µg/ml leupeptin, 10 µg/ml aprotinin and by centrifugation at 14,000 × g for 10 min at 4 °C. Protein content was measured in cytosolic and nuclear fractions according to the colorimetric method of Bradford (Bradford, 1976). Briefly, the method involves the binding of Coomassie Brilliant Blue to protein and it is based on the observation that Coomassie Brilliant Blue exists in two different color forms, red and blue. The red form is converted to the blue form upon binding of the dye to protein. This binding causes a shift in the absorption maximum of the dye from 365 to 595 nm, and it is the increase in absorption at 595 nm which is monitored (Bradford, 1976).

##### 2.3.1.2 Membrane purification

The cells were homogenized in PBS containing 9.0% sucrose with three freeze-thaw cycles, 5 s sonication in ice and centrifugation at 700 × g for 10 min at 4 °C (Cecchi *et al.*, 2008b). The membrane fractions were pelleted by a further supernatant centrifugation at 110,000 × g for 1 h at 4 °C. Protein content was measured by the method of Bradford (Bradford, 1976).

##### 2.3.1.3 Purification of DRMs

The cells were washed twice with ice-cold PBS, scraped, and collected by centrifugation at 1,000 × g. To purify detergent-resistant membrane fractions (DRMs), the cells were dispersed in a 10 mM Tris-HCl buffer, pH 7.5, containing 150 mM NaCl, 5.0 mM EDTA, 1.0 mM Na<sub>3</sub>VO<sub>4</sub>, 1.0% Triton X-100 (TNE buffer), protease inhibitors (10 µg/ml leupeptin and 10 µg/ml aprotinin) and incubated in ice for 20 min (Romiti *et al.*, 2001). The cells were disrupted in a Dounce homogenizer (80 strokes) and centrifuged at 1,500 × g for 5 min at 4 °C to obtain the post-nuclear fraction. The post-nuclear lysate was adjusted to 40% (w/v) sucrose by 1:1 addition of 80% sucrose prepared in TNE buffer, placed at the bottom of an ultracentrifuge tube and overlaid with two layers of 30% and 5.0% sucrose in TNE buffer. The sucrose gradi-

ent was centrifuged at 170,000 × g for 22 h at 4 °C using a Beckman SW50 rotor. Fractions were then collected from the top of the gradient as follow: 0.5 ml for fraction 1, 0.25 ml for fractions 2 to 11, 1 ml for fractions 12 and 13, while the pellet was dissolved in 0.08 ml of TNE buffer (fraction 14) (Cecchi et al., 2009). A representative amount of each fraction was subjected to immunoblot analysis of flotillin-1 marker on a 12% (w/v) sodiumdodecylsulfate polyacrylamide gel electrophoresis (SDS/PAGE), blotted onto a polyvinylidene difluoride (PVDF) Immobilio-P transfer membrane, incubated with 1:500 diluted mouse monoclonal anti-flotillin-1 antibodies (BD Biosciences, San Diego, CA) and 1:5000 anti-mouse antibodies. The flotillin-1-rich fractions were pooled as DRMs and extensively dialyzed against TNE buffer to remove sucrose. The amount of sphingomyelin in lipid rafts was assayed using a photometric method with the Sphingomyelin Assay Kit (Cayman Chemical, Ann Arbor, MI, USA). Briefly, sample sphingomyelin was hydrolyzed by sphingomyelinase to phosphorylcholine and ceramide for 60 min at 37 °C. The choline resulting from the subsequent incubation of phosphorylcholine with alkaline phosphatase was oxidized by choline oxidase with production of H<sub>2</sub>O<sub>2</sub>. The latter was reacted in the presence of peroxidase with N-ethyl-N-(2-hydroxy-3-sulfopropyl)-3,5-dimethoxyaniline (DAOS) and 4-aminoantipyrine, yielding a blue color product with an optimal absorption at 595 nm (Hojjati and Jiang, 2006). Sphingomyelin was quantified by comparison with a reference curve built by assaying known amounts of sphingomyelin (25–800 ng).

### 2.3.2 Differentiation of human mesenchymal stromal cells

To induce differentiation towards a neuronal phenotype (hMSC-n), an aliquot of cultured hMSC cells was pre-incubated for 24 h in NBM containing 1.0 mM β-mercaptopropanoic acid (BME) and 10 ng/ml basic fibroblast growth factor (bFGF), and subsequently cultured for a further 48 h in NBM containing 10% FBS, 10 mM BME. To assess the differentiated phenotype, cells were photographed using a phase contrast microscope (Nikon, Diaphot TMD-EF). hMSCs and hMSC-n cells were assessed for the expression of neuronal specific markers by quantitative real time RT-PCR. Total RNA isolation, cDNA synthesis and real time PCR conditions were as previously reported (Dal Pozzo et al., 2010). Primers and probes were TaqMan gene expression assays: for tau protein assay ID Hs00902193\_m1; for microtubule associated protein 2 (MAP2) assay ID Hs00159041\_m1; for synaptophysin assay ID Hs00300531\_m1 (Applied Biosystems, Foster City, CA, USA). Each measurement was carried out in triplicate. mRNA quantification was carried out using a comparative Ct method according to the manufacturer's instructions (Applied Biosystems). Data was normalized to ribosomal 18S RNA expression (assay ID Hs99999901\_s1; Applied Biosystems) and reported as a fold increase vs. hMSCs. Immunostaining for neurofilament M (NF-M) was performed as previously reported (Benvenuti et al., 2006), using 1:500 diluted polyclonal primary antibodies (NF-M, rabbit anti-neurofilament M C-terminal Ab, Chemico, Billerica, MA, USA).

### 2.3.3 Modulation of membrane cholesterol levels

The increase in membrane cholesterol content was also achieved by supplementing SH-SY5Y cell and FAD fibroblasts culture media with 0.1 mM PEG-cholesterol for 1 h at 37 °C or with 0.2 mg/ml soluble cholesterol (Chol) for 3 h at 37 °C, respectively. In a series of experiment, the increase of membrane cholesterol content was achieved by supplementing SH-SY5Y cell culture media with Chol at three different concentrations (0.05; 0.2; 0.5 mg/ml) for 3 h at 37 °C. Membrane cholesterol depletion was obtained by incubating SH-SY5Y cells with 1.0 mM  $\beta$ -CD for 30 min at 37°C in serum-free media. Membrane cholesterol depletion was also performed by incubating SH-SY5Y cells and fibroblasts with 10  $\mu$ M Mev for 48 h at 37 °C in the presence of 1.0% FBS. Cells were then extensively washed with PBS and exposed to peptide oligomers. In a series of experiments cholesterol depletion was achieved SH-SY5Y cells by supplementing the culture medium with  $\beta$ -CD at three different concentrations (0.2; 1.0; 2.0 mM) for 30 min at 37 °C in serum-free media (Yancey et al., 1996) or with Mev at three different concentrations (1.0; 5.0; 10  $\mu$ M) for 48 h at 37°C in the presence of 1.0% FBS (Endo et al., 1976).

### 2.3.4 Modulation of membrane GM1 levels

In fibroblasts and SH-SY5Y cells, an increase in membrane GM1 content was achieved by adding 32  $\mu$ M bovine brain-derived GM1 to cell culture media for 48 h, while neurons were treated with 100  $\mu$ M GM1 for 24 h. GM1 depletion was achieved by inhibiting cell glucosylceramide synthase with 25  $\mu$ M D-threo-1-phenyl-2-decanoylamoно-3-morpholino-1-propanol (PDMP) for 48 h in fibroblasts and SH-SY5Y cells or for 24 h in neurons. Hydrolysis of the sialic acid moiety from gangliosides was achieved by exposing cells to an NAA cocktail (117 mU/ml of *V. cholerae* NAA and 33 mU/ml of *A. ureafaciens* NAA, Sigma) for 1 h at 37 °C (Malchiodi-Albedi et al., 2010).

### 2.3.5 Cholesterol content measurements

#### 2.3.5.1 Microscope analysis

A labeling of membrane cholesterol was achieved using the fluorescent probe filipin III. The cells seeded on glass coverslips were fixed in 4.0% buffered paraformaldehyde for 20 min at 0 °C and then were incubated with 0.25 mg/ml cholesterol binding agent (filipin III) in PBS for 24 h at 37 °C. After washing, the cells were fixed again in 4.0% buffered paraformaldehyde for 20 min at 0 °C. The distribution of membrane cholesterol was investigated by using confocal scanning microscopy. The emitted fluorescence was detected after excitation at 355 nm using a confocal Leica TCS SP5 scanning microscope (Mannheim, Germany) equipped with an argon laser source. A series of optical sections (1024  $\times$  1024 pixels) 1.0  $\mu$ m in thickness was taken through the cell depth for each sample using a Leica Plan Apo 63 $\times$  oil immersion

objective and projected as a single composite image by superimposition (Pensalfini et al., 2011).

### **2.3.5.2 Enzymatic assay**

The amount of cholesterol in membrane fractions and in purified lipid rafts was assessed using the sensitive fluorimetric Amplex Red Cholesterol Assay Kit (Molecular Probes). Sample cholesterol was oxidized by 1.0 U/ml cholesterol oxidase for 30 min at 37 °C to yield H<sub>2</sub>O<sub>2</sub> and the corresponding ketone product. In the presence of 1.0 U/ml horseradish peroxidase (HRP), H<sub>2</sub>O<sub>2</sub> reacted with 150 µM 10-acetyl-3,7-dihydroxyphenoxyazine (Amplex Red reagent) with a 1:1 stoichiometry to generate the highly fluorescent resorufin (Mohanty et al., 1997). At the end of the incubation, sample fluorescence was measured at 544 nm excitation and at 590 nm emission. Cholesterol content was determined by comparison with a reference curve built by assaying various cholesterol amounts (0.05-1.0 µg) (Amundson and Zhou, 1999).

### **2.3.6 GM1 content measurements**

#### **2.3.6.1 Microscope analysis**

GM1 distribution in the plasma membrane was monitored in cells seeded on glass coverslips using 1:100 diluted rabbit polyclonal anti-GM1 antibodies (Calbiochem; EMD Chemicals Inc., Darmstadt, Germany) and with 1:1000 diluted Alexa Fluor 488-conjugated anti-rabbit antibody or with 4.5 µg/ml CTX-B. The emitted fluorescence was detected after excitation at 488 nm and 647 nm, respectively, by the confocal scanning system described above.

#### **2.3.6.2 Dot-blot analysis**

The GM1 content in membrane fractions was investigated by dot blot analysis using 20 µg membrane proteins spotted onto a PVDF membrane; the membrane was then incubated overnight at 4 °C with 1:500 rabbit polyclonal anti-GM1 antibodies and with 1:1000 peroxidase-conjugated anti-rabbit antibodies (Pierce, Rockford, IL, USA) for 1 h at room temperature and detected with a Super Signal West Dura (Pierce). All spot densities were measured as densitometric units using the image analysis and densitometric program Quantity One (Biorad, Milan, Italy). For each spot of interest, values of treated cells were calculated as a percentage relative to cells with basal GM1 content taken to be as 100%. To exclude a potential cross-reactivity of the anti-GM1 antibodies against other neuronal gangliosides, we carried out a dot-blot analysis. Briefly, 2.0 µl of a 0.05 mg/ml solution of GM1, GD1a and GT1b were spotted onto PVDF, and then incubated overnight at 4 °C with 1:500 rabbit polyclonal anti-GM1 antibodies and the signals detected and quantified as described above.

### 2.3.6.3 Flow cytometric analysis

The membrane GM1 content was also monitored in cells loaded with 2.25 µg/ml CTX-B by using a FACSCanto flow cytometer (Beckton Dickinson Biosciences, San Jose, CA, USA).

### 2.3.7 Cell exposure to peptide aggregates

SH-SY5Y cells, FAD and wild-type fibroblasts with different cholesterol and GM1 content, were exposed to 1.0 µM Aβ42 oligomers for 30 min. In a series of experiments SH-SY5Y cells were exposed to 12 µM Aβ42 prefibrillar aggregates obtained according to Lambert's protocol as above reported (Lamber *et al.*, 2001). Primary cortical neurons, hMSC and their neuronally differentiated counterparts hMSC-n were exposed to 5.0 µM or 10 µM Aβ42, respectively. In a set of experiments, hMSC and hMSC-n were treated with different final concentration of Aβ42 oligomers or with 50 µM PrP 106-126 oligomers. Aliquots of solutions containing native or aggregated HypF-N in pre-fibrillar forms (condition A and B) were centrifuged, dried under N<sub>2</sub> to remove the TFE or TFA when necessary, dissolved in the appropriate cell media at 48 µM concentration and immediately added to SH-SY5Y in basal condition or upon cholesterol or GM1 modulation at 12 µM final concentration. The cells were incubated in the presence of the aggregates for 1 h. In a set of experiments were used fluorescent oligomers obtained from HypF-N 5-FITC or Aβ-FAM. In some experiments, the oligomers were added to cell culture media to appropriate final concentrations for differing lengths of time. Neither disassembly nor microscopic differences in the aggregate structure were observed following dilution in the cell culture media. Aggregate concentration was calculated as monomeric peptide concentration. In some experiments cells were also exposed to Aβ42-1 reversed sequence peptide, as negative control, processed as above reported for Aβ42 peptides.

### 2.3.8 Analysis of aggregate interaction with the cells

The interaction of Aβ42 aggregates with plasma membranes was monitored in cholesterol-enriched, cholesterol-depleted SH-SY5Y cells, in hMSC and hMSC-n cells by confocal scanning microscopy. Briefly, SH-SY5Y and hMSC cells exposed for 30 min to 1.0 µM ADDLs, or for 0, 10, 30 and 60 min to 10 µM Aβ42 oligomers, respectively; were counterstained with fluorescein-conjugated WGA (5.0 µg/ml) for 10 min to detect the plasma membrane profiles. In another set of experiments, hMSC and hMSC-n, cultured on glass coverslips, were pre-incubated for 20 min in the absence or in the presence of 1:100 diluted rabbit polyclonal antibodies against GM1, exposed to 10 µM Aβ42 aggregates for 1 h and then counterstained as above reported. After washing, the coverslips were incubated with mouse monoclonal anti-Aβ antibodies 6E10 (Signet, DBA, Italy) 1:1000 diluted in PBS with 1.0% FBS for 60 min. The immunoreaction was revealed by incubation for 90 min with Texas Red-conjugated anti-mouse secondary antibodies (Vector Laboratories, DBA, Italy), 1:1000 diluted in PBS containing 1.0% FBS. The emitted fluorescence was detected

after double excitation at 488 nm and 633 nm using the confocal scanning microscope described above and in all images, green and red fluorescence indicates cell profiles and aggregates, respectively. Aggregate-cell interactions were also analyzed by exposing SH-SY5Y cells with different cholesterol content to 3.0  $\mu$ M A $\beta$ 42-FAM oligomers and counterstaining the plasma membranes with Alexa Fluor 633-conjugated WGA (5.0  $\mu$ g/ml), but without fixing cells in buffered paraformaldehyde, without permeabilizing the plasma membrane and without using antibodies. The emitted fluorescence was detected after double excitation at 488 nm and 633 nm using the confocal scanning microscope described above and in all images, red and green fluorescence indicates cell profiles and aggregates, respectively. The internalisation of HypF-N and A $\beta$ 42 oligomers into the cytosol of the exposed SH-SY5Y cells with different cholesterol or GM1 content was monitored by confocal scanning microscopy in cells seeded on glass coverslips. After aggregate exposure, the cells were counterstained with 5.0  $\mu$ g/ml Alexa Fluor 633-conjugated WGA, fixed in 2.0% buffered paraformaldehyde for 10 min at room temperature, permeabilized with a 3.0% glycerol solution for 5 min and then the aggregates were detected with 1:1000 diluted rabbit polyclonal anti-HypF-N antibodies and with 1:1000 diluted Alexa Fluor 488-conjugated anti-rabbit antibodies; A $\beta$ 42 oligomers were detected with mouse monoclonal 6E10 antibodies and with 1:1000 diluted fluorescein-conjugated anti-mouse antibodies. The emitted fluorescence was detected after double excitation at 488 nm and 633 nm by the confocal scanning system. In all images, red and green fluorescence indicates cell profiles and aggregates (HypF-N or A $\beta$ 42), respectively.

### 2.3.9 Analysis of aggregate interaction with GM1

The colocalization of A $\beta$ 42 aggregates with the GM1, marker of lipid rafts, was monitored in fibroblasts and neuroblastoma cells with different cholesterol content seeded on glass coverslips using mouse monoclonal 6E10 anti-A $\beta$  antibodies and with 1:1000 diluted fluorescein-conjugated anti-mouse antibodies and 4.5  $\mu$ g/ml Alexa Fluor 647-conjugated CTX-B. The emitted fluorescence was detected by the confocal scanning system after double excitation at 488 nm and 647 nm for fluorescein and Alexa Fluor 647-conjugated CTX-B, respectively.

#### 2.3.9.1 FRET analysis

The colocalization of A $\beta$ 42 oligomers with GM1 was also analyzed in cholesterol-enriched or cholesterol-depleted fibroblasts, hMSCs and hMSC-n, seeded on glass coverslips, by fluorescence resonance energy transfer (FRET) analysis. Cells were exposed to A $\beta$ 42-FAM oligomers for 30 min and then fixed in 2.0% buffered paraformaldehyde for 10 min at room temperature. After washing, cell surface GM1 was counterstained with 4.5  $\mu$ g/ml Alexa Fluor 555-conjugated CTX-B, re-suspended in cell culture medium, for 20 min at room temperature. An acceptor bleaching protocol was employed to measure FRET efficiency, as previously described (Day, *et al.*, 2001; Kenworthy *et al.*, 2000; Kinoshita *et al.*, 2003). Acceptor bleaching was accom-

plished using the TCS SP5 confocal system described above using the implemented FRET acceptor photobleaching wizard. Pre-bleach and post-bleach images were serially recorded, with A $\beta$ -FAM and cell surface GM1 excited at 488 nm (donor) and 555 nm (acceptor), respectively, using an argon laser and appropriate emission bands. Low laser intensities were used to avoid acquisition bleaching. The acceptor was bleached at high intensity at 555 nm. FRET efficiency is displayed in pseudocolour for better visualization.

### 2.3.10 Analysis of aggregate internalisation

To investigate the mechanism of HypF-N oligomer internalization, cholesterol-depleted SH-SY5Y cells were incubated with 12  $\mu$ M 5-FITC-labelled oligomers and 5.0  $\mu$ g/ml FM4-64 for 1 h at 37 °C as previously reported (Kaminski Schierle *et al.*, 2011). The images were recorded using the 488 nm laser line to excite 5-FITC-labelled oligomers and the 543 nm laser line to excite FM4-64, a widely used marker for endocytotic vesicles. In all images, red and green fluorescence indicates vesicles and aggregates, respectively.

### 2.3.11 Analysis of membrane permeability

In order to assess whether A $\beta$ 42 or HypF-N aggregates disrupt cell membrane integrity, neuroblastoma cells and fibroblasts with different cholesterol or GM1 content were pre-treated for 20 min at 37 °C with 2.0  $\mu$ M calcein-AM, dissolved in DMSO and re-suspended in cell culture medium (Cecchi *et al.*, 2008b). The decay in fluorescence was analyzed by confocal microscopy after excitation at 488 nm in cell exposed to A $\beta$ 42 or HypF-N aggregates. In another set of experiments, fibroblasts were exposed to calcein-AM and then incubated for 20 min in the absence or in the presence of 4.5  $\mu$ g/ml Alexa Fluor 647-conjugated CTX-B or 1:100 diluted rabbit polyclonal anti-GM1 antibodies, before treatment with A $\beta$ 42 aggregates.

### 2.3.12 Analysis of cytosolic Ca<sup>2+</sup> dyshomeostasis

The effect of A $\beta$ 42 or HypF-N aggregates on cytosolic free Ca<sup>2+</sup> levels was analyzed in fibroblasts and SH-SY5Y cells with different cholesterol or GM1 content, in GM1-enriched or depleted primary cortical neurons, hMSC and hMSC-n cells, plated on glass coverslips and loaded with Fluo3-AM, a Ca<sup>2+</sup>-specific fluorescent probe. The cells were first exposed to A $\beta$ 42 aggregates or to HypF-N aggregates for differing length of times at 37 °C. Cytosolic Ca<sup>2+</sup> levels were also examined in fibroblasts and neurons pre-treated for 20 min in the absence or in the presence of 1:100 diluted rabbit polyclonal anti-GM1 antibodies, before treatment with A $\beta$ 42 aggregates. The cells were then loaded for 30 min at 37 °C with 10  $\mu$ M Fluo3-AM, 0.01% (w/v) pluronic acid F-127 in Hank's Balanced Salt Solution (HBSS) and subsequently fixed in 2.0% buffered paraformaldehyde for 10 min at room temperature. Fluorescence was detected after excitation at 488-nm by collecting the emitted fluorescence with the confocal scanning system described above.

### **2.3.13 Evaluation of ROS production**

Intracellular ROS production was detected by using CM-H<sub>2</sub>DCFDA, a ROS-sensitive fluorescent dye. CM-H<sub>2</sub>DCFDA esterified derivative is loaded more effectively within the cytoplasm of the cells because it is more cell permeant before ester groups are hydrolyzed by the cellular esterases. Only a negligible leakage of the probe occurred, since chloromethyl-DCF is negatively charged at physiological intracellular pH. Cholesterol-enriched, cholesterol-depleted and basal SH-SY5Y cells, hMSC and hMSC-n were first cultured on glass coverslips and exposed to Aβ42 or HypF-N aggregates for different times at 37 °C. The cells were then incubated with 5.0 μM CM-H<sub>2</sub>DCFDA, dissolved in 0.1% DMSO and Pluronic acid F-127 (0.01% w/v), in the final 10 min of aggregate exposure. The cells were then fixed in 2.0% buffered paraformaldehyde for 10 min at room temperature and the emitted CM-H<sub>2</sub>DCFDA fluorescence was detected after 488-nm excitation by the confocal scanning microscope described above.

### **2.3.14 Analysis of lipid peroxidation**

#### **2.3.14.1 Measurement of lipid peroxidation products**

To assess the rate of lipid peroxidation after Aβ42 cell treatment, the levels of 8-OH isoprostanate were measured photometrically in fibroblasts and hMSC cell lysates and in lipid rafts fraction purified from fibroblasts at 405 nm using the 8-isoprostanate EIA kit (Cayman Chemical Company, Ann Arbor, MI, USA) (Pensalfini *et al.*, 2011).

#### **2.3.14.2 Confocal microscope analysis**

Lipid peroxidation after cell exposure to Aβ42 aggregates was also investigated in fibroblasts and neurons by confocal scanning microscope analysis, using the fluorescent probe BODIPY 581/591 C<sub>11</sub>, which is intrinsically lipophilic thus mimicking the properties of natural lipids (Naguib, 1998). In particular, BODIPY 581/591 C<sub>11</sub> can be used to measure antioxidant activity in lipid environments since it behaves as a fluorescent lipid peroxidation reporter that shifts its fluorescence from red to green when challenged with oxidizing agents (Drummen *et al.*, 2004). FAD, wild-type fibroblasts and neurons with differing GM1 content were cultured on glass coverslips and exposed to 1.0 μM (fibroblasts) or 5.0 μM (neurons) Aβ42 aggregates for 30 min at 37 °C. In a set of experiments, fibroblasts and neurons, cultured on glass coverslips, were pre-incubated for 20 min in the absence or in the presence of 4.5 μg/ml Alexa Fluor 647-conjugated CTX-B or 1:100 diluted rabbit polyclonal antibodies against GM1 and then exposed to Aβ42 aggregates for 1 h. Lipid peroxidation was also examined in fibroblast and neurons exposed to aggregates in Ca<sup>2+</sup>-free medium. Dye loading was achieved by adding 5.0 μM fluorescent BODIPY, dissolved in 0.1% DMSO, to the cell culture media for 30 min at 37 °C. The cells were fixed in 2.0% buffered paraformaldehyde for 10 min and the BODIPY fluorescence was

measured by simultaneous acquisition of the green (ex 485nm/em 520nm) and red signal (ex 581nm/em 591nm), by confocal microscope analysis, as described above.

### 2.3.15 Cytotoxicity assay and cell death analysis: apoptotic and necrotic markers

#### 2.3.15.1 MTT test

The toxic effect of the differing aggregates on metabolic cell functions was assessed in cell models by the 3-(4,5-dimethylthiazol-2-yl)-2,5-diphenyltetrazolium bromide (MTT) assay in 96-well plates. Cholesterol-enriched, cholesterol-depleted and basal neuroblastoma cells were exposed to 1.0  $\mu\text{M}$  A $\beta$ 42 oligomers for 24 h at 37 °C; fibroblasts and neurons following GM1 modulation were exposed to 1.0 (fibroblasts) or 5.0 (neurons)  $\mu\text{M}$  A $\beta$ 42 oligomers for 24 h at 37 °C. SH-SY5Y cell, upon membrane cholesterol and/or GM1 modulation were treated with 12  $\mu\text{M}$  HypF-N or A $\beta$ 42 oligomers. hMSC and hMSC-n were treated with A $\beta$ 42 oligomers (0.1, 1.0, 10, 25, 50  $\mu\text{M}$  final concentration), 10  $\mu\text{M}$  A $\beta$ 42 fibrils, 10  $\mu\text{M}$  A $\beta$ 42-1 reverse peptides and 50  $\mu\text{M}$  PrP 106-126 oligomers. As a negative control, neuroblastoma cells were pre-treated with 100  $\mu\text{M}$  Vit E for 24 h at 37 °C, before aggregate or H $_2$ O $_2$  exposure. In a series of experiments, fibroblast, primary cortical neurons, hMSC and hMSC-n, were pre-incubated for 20 min in the absence or in the presence of 4.5  $\mu\text{g/ml}$  Alexa Fluor 647-conjugated CTX-B or 1:100 diluted rabbit polyclonal antibodies against GM1 and then exposed to A $\beta$ 42 aggregates for 24 h. After cell treatments, 100  $\mu\text{l}$  of 0.5 mg/ml MTT solution in PBS was added to the cell cultures and the samples were incubated for 4 h at 37 °C. Finally, 100  $\mu\text{l}$  of cell lysis buffer (20% SDS, 50% N,N-dimethylformamide, pH 4.7) was added to each well and the samples were incubated for at least 3 h at 37 °C in a humidified incubator, before determination of absorbance value of blue formazan at 590 nm with an ELISA plate reader. Cell viability was expressed as a percentage of MTT reduction in aggregate or H $_2$ O $_2$ -exposed cells compared to untreated cells (assumed as 100%).

#### 2.3.15.2 Hoechst staining

Nuclear alterations eventually induced by the amyloid aggregates were investigated by Hoechst 33342 dye staining. Briefly, cholesterol-enriched cholesterol-depleted and basal neuroblastoma cells were exposed to A $\beta$ 42 or HypF-N oligomers for 24 h at 37 °C. Human mesenchymal stromal cells, cultured on glass coverslips, were pre-incubated for 20 min in the absence or in the presence of 1:100 diluted rabbit polyclonal antibodies against GM1 and then exposed to A $\beta$ 42 aggregates for 24 h. Then, the cells were incubated with 20  $\mu\text{g/ml}$  Hoechst for 15 min at 37 °C and fixed in 2.0% buffered paraformaldehyde for 10 min at room temperature. Blue fluorescence micrographs of cells were obtained under UV illumination in an epifluorescence inverted microscope (Nikon, Diaphot TMD-EF) with an appropriate filter set.

### 2.3.15.3 Caspase-3 activity

The extent of the apoptotic program activation in SH-SY5Y and hMSC cells was evaluated by confocal microscope analysis of caspase-3 activity, which is the main effector caspase in apoptosis. Neuroblastoma cells upon cholesterol modulation and hMSC cells pre-incubated for 20 min in the absence or in the presence of 1:100 diluted rabbit polyclonal antibodies against GM1, were exposed to 12  $\mu$ M HypF-N or 10.0  $\mu$ M A $\beta$ 42 oligomers, respectively for 24 h at 37 °C. In a series of experiments, neuroblastoma cells depleted in cholesterol following treatment with 2.0 mM  $\beta$ -CD were pre-treated with 10  $\mu$ M BAPTA-AM for 30 min, extensively washed and then exposed for 3 h to either type of HypF-N oligomers in culture media with or without Ca $^{2+}$ . After the appropriate treatment, the culture media were removed and replaced with FAM-FLICA Caspases 3&7 solution (Caspase 3&7 FLICA kit; FAM-DEVD-FMK; Immunochemistry Technologies, LLC, Bloomington, MN, USA) for 30 min, following the manufacturer's instructions. The cells were fixed on glass coverslips in 2.0% buffered paraformaldehyde for 10 min at room temperature and then fluorescence was detected after 488 nm excitation, by the confocal scanning system, as described above.

### 2.3.15.4 LDH release

The presence of necrotic cells was assessed by measuring the activity of lactate dehydrogenase (LDH), a typical necrotic marker released into the cell culture medium after plasma-membrane rupture. LDH activity was measured in the culture media of cholesterol-enriched, cholesterol-depleted or basal SH-SY5Y cells after exposure to 1.0  $\mu$ M A $\beta$ 42 aggregates for 48 h at 37 °C using a fluorimetric LDH assay kit (Roche Diagnostics, Mannheim, Germany) at 490 nm, after blank subtraction at 595 nm.

### 2.3.16 Steady-state fluorescence anisotropy

Fluorescence anisotropy ( $r$ ) of DPH was used to measure the structural order of the hydrophobic region of the purified lipid rafts under steady-state conditions (Lentz, 1989; Shinitzky and Barenholz, 1974). Anisotropy measurements were performed at 37 °C by a Perkin-Elmer LS 55 luminescence spectrometer equipped with manual polarisers with excitation and emission wavelengths set at 360 nm and 425 nm, and with a slit-width of 2.5 nm and 4 nm, respectively. Our system was initially calibrated using DPH in mineral oil, which should give an anisotropy value of 1.0. The  $g$  factor was calculated using horizontally polarized excitation and subsequent comparison of the horizontal and vertical emissions. Lipid rafts purified from neuroblastoma cells or fibroblast were incubated for 10 min in the absence or in the presence of 1.0  $\mu$ M A $\beta$ 42 aggregates or A $\beta$ 42-1 reverse peptide and then further incubated for 30 min with DPH at a 1:250 probe-to-lipid ratio. In another set of experiments, lipid rafts were incubated for differing times (10, 30, 60 min) in the presence of 1.0  $\mu$ M A $\beta$ 42 aggregates before dye loading. Fluorescence intensity was measured

with the excitation polariser in the vertical position and the analysing emission polariser in both the vertical ( $I_{VV}$ ) and the horizontal ( $I_{VH}$ ) positions; the anisotropy constant,  $r$ , was calculated using the equation:

$$r = \frac{I_{VV} - gI_{VH}}{I_{VV} + 2gI_{VH}}$$

### 2.3.17 Atomic force microscopy (AFM)

AFM analyses were performed in collaboration with the group of Prof.ssa Alessandra Gliozi, of the Department of Physics of the University of Genoa. AFM analysis was carried out on 50  $\mu\text{l}$  aliquots of the purified DRMs deposited on freshly cleaved mica, incubated for 1 h and then rinsed with Milli-Q water. AFM measurements were performed using a Dimension 3100 scanning probe microscope (Digital Instruments, Veeco, Santa Barbara, CA, USA) equipped with a Nanoscope IIIa controller and a “G” scanning head (maximum scan size 100 x 100  $\mu\text{m}$ ). Tapping mode AFM would be expected to minimize lateral forces and allow better imaging of soft samples. Raft membranes were an exception, as we could not image them in tapping mode, even using different cantilevers and solution conditions. It is possible that when operating in tapping mode an oscillation is also induced in the sample. This would explain why tapping mode imaging of DRMs was impossible. On the other hand, when operating in contact mode, a force is steadily applied to the sample, resulting in an improved stability of the system. Thus images were acquired in contact mode in liquid by using V-shaped non-conductive silicon nitride cantilevers (type DNP, Veeco; 115  $\mu\text{m}$  length, nominal spring constant 0.58 N/m) with pyramidal tips (nominal curvature radius in the 20-60 nm range) and scan rate in the 0.5-2.0 Hz range. Images were captured as 512  $\times$  512 pixel images. The minimum force employed in contact mode imaging was 0.3 nN. The morphological features of the samples were analyzed in terms of height and width in cross section in the topographic AFM images. The heights of the steps associated either to membrane domains or to cavities were measured with respect to the background. The sizes of each domain (or hollow) were the mean of the widths measured along the major diameter of the domain (or hollow) and the corresponding in-plane perpendicular direction. Due to tip size effects, which cause an apparent increase of the size of the imaged object in the image plane, domain sizes are overestimated respect to the real ones. To evaluate the expected widths,  $w$ , we modelled the domain as a flat object with half-spherical edges, using the equation:

$$w = w_{app} + 2h - 2\sqrt{2hR_T + h^2}$$

where  $w_{app}$  and  $h$  are the measured width and height, respectively, and  $R_T$  is the AFM tip radius. We used a silicon calibration grating with ultrasharp tips (NT-MDT TGT01, Silicon-MDT Ltd., Moscow, Russia) to measure the curvature radius  $R_T$  for four tips of the same type and we obtained a mean value of  $25\pm7\text{nm}$ . This value, which is within the range provided by the manufacturer, has been used to evaluate the correction for tip enlargement effects, according to the procedure quoted above. The possible changes in neuroblastoma or fibroblasts raft morphology induced by the interaction with A $\beta$ 42 oligomers were investigated in samples prepared as described above incubated for 30 min in the presence of 1.0  $\mu\text{M}$  ADDLs, rinsed with Milli-Q and imaged in liquid. To check the presence of the GM1 ganglioside, after deposition on the mica substrate the DRMs were incubated for 30 min with rabbit polyclonal anti-GM1 antibodies, diluted 1:1000. The presence of flotillin-1 in the samples deposited on the mica substrate was assessed by incubating the rafts with 0.5  $\mu\text{g}/\text{ml}$  mouse anti-flotillin-1 antibodies for 30 min. The domains imaged in the DRMs samples were better characterized by incubation with a mixture of carboxy-peptidase Y from baker's yeast, thermolysin from *Bacillus thermoproteolyticus rokko* Type X and  $\alpha$ -chymotrypsin from bovine pancreas Type VII (Sigma; Milan, Italy), at final concentrations of 1.0 mg/ml, 5.0 mg/ml and 5.0 mg/ml, respectively. Protease digestion was carried out by incubating the rafts with the protease mixture for 2 h either before or after sample deposition on the mica substrate. To characterize morphologically the A $\beta$ 42 aggregates, 20  $\mu\text{l}$  aliquots of ADDLs, obtained as reported above, were deposited on freshly cleaved mica substrates and dried under mild vacuum. The images were acquired in tapping mode in air using a Dimension 3100 AFM microscope (as detailed above) and a multimode scanning probe microscope equipped with an "E" scanning head (maximum scan size 10  $\mu\text{m}$ ). Single beam uncoated silicon cantilevers (type OMCL-AC, Olympus, Japan) were used. The drive frequency was around 300 kHz and the scan rate was in the 0.3-0.8 Hz range.

### 2.3.18 Measurements of the fluorescence intensities

To quantify the signal intensity of each fluorescent probe, a variable number of cells (10 to 22) were analyzed in each experiment using ImageJ software (NIH, Bethesda, MD, USA), and the fluorescence intensities expressed as fractional changes above the resting baseline,  $\Delta F/F$ , where  $F$  is the average baseline fluorescence in control cells (assumed as 100%) and  $\Delta F$  represents the fluorescence changes over the baseline in cells exposed to different treatments. In the quantification of the fluorescence intensity of intracellular A $\beta$ 42 oligomers in human mesenchymal stromal cells, fluorescence signals are expressed as  $\Delta F$  ( $F_1 - F_0$ ), where  $F_1$  represents the fluorescence in A $\beta$ 42 oligomer-treated cells and  $F_0$  the fluorescence in untreated cells. GM1-A $\beta$ 42 aggregates and endocytotic vesicles-HypF-N oligomers colocalization was estimated for regions of interest (in 12–13 cells), in three different experiments, using the ImageJ (NIH, Bethesda, MD, USA) and JACOP plugin (rsb.info.nih.gov) software (Rasband, 1997).

### 2.3.19 Statistical analysis

Except the AFM and hMSC-n neuronal markers expression data, which are expressed as mean  $\pm$  standard error (SE), all other data are expressed as mean  $\pm$  standard deviation (SD). Comparisons between the different groups were performed by ANOVA followed by Bonferroni's t-test. A p value  $< 0.05$  was considered statistically significant. AFM data concerning sample morphological features are over an ensemble of at least 100 measurements. All the statistical analyses had a confidence level  $\geq 95\%$ .

## Results

### 3.1 Results I

#### 3.1.1 A protective role for lipid raft cholesterol against amyloid-induced membrane damage in human neuroblastoma cells

Increasing evidence supports the idea that the initial events of A $\beta$  oligomerization and cytotoxicity in Alzheimer's disease involve the interaction of amyloid A $\beta$ -derived diffusible ligands (ADDLs) with the cell membrane. This also indicates lipid rafts, ordered membrane microdomains enriched in cholesterol, sphingolipids and gangliosides, as likely primary interaction sites of ADDLs. To shed further light on the relation between ADDL-cell membrane interaction and oligomer cytotoxicity, in the first part of the result section was investigated the dependence of ADDLs binding to lipid rafts on membrane cholesterol content in human SH-SY5Y neuroblastoma cells. Confocal laser microscopy showed that A $\beta$ 42 oligomers markedly interact with membrane rafts and that a moderate enrichment of membrane cholesterol prevents their association with the monosialoganglioside GM1. Moreover, anisotropy fluorescence measurements of flotillin-1-positive rafts purified by sucrose density gradient suggested that the content of membrane cholesterol and membrane perturbation by ADDLs are inversely correlated. Finally, contact mode atomic force microscope images of lipid rafts in liquid showed that ADDLs induce changes in raft morphology with the appearance of large cavities whose size and depth were significantly reduced in similarly treated cholesterol-enriched rafts. Our data suggest that cholesterol reduces amyloid-induced membrane modifications at the lipid raft level by altering raft physicochemical features.

#### 3.1.2 A $\beta$ 42 oligomer binding to the cell surface and its cytotoxic effect are modulated by membrane cholesterol content

In previous studies we showed that the interaction of amyloid aggregates of different peptides and proteins with the plasma membranes of several types of cultured cells is significantly inversely correlated to the membrane content of cholesterol (Cecchi *et al.*, 2005; Cecchi *et al.*, 2008b; Cecchi *et al.*, 2008c; Pensalfini *et al.*, 2011). Here, we modulated the cholesterol content in human neuroblastoma cells by incubating the cells in the presence of polyoxyetanyl-cholesteryl sebacate (PEG-cholesterol), methyl- $\beta$ -cyclodextrin ( $\beta$ -CD) or mevastatin (Mev). Cell treatment with PEG-cholesterol significantly increased the content of cholesterol in the cell

## Amyloid Cytotoxicity and Membrane Lipid Composition

membrane ( $13.55 \pm 0.68 \mu\text{g}/\text{mg}$  protein,  $p \leq 0.05$ ) *versus* control cells ( $10.84 \pm 0.54 \mu\text{g}/\text{mg}$  protein) as assayed by the Amplex Red Cholesterol Assay Kit. Conversely, membrane cholesterol content was significantly reduced by cell treatment with  $\beta$ -CD ( $7.26 \pm 0.73 \mu\text{g}/\text{mg}$  protein,  $p \leq 0.05$ ) and Mev ( $9.71 \pm 0.46 \mu\text{g}/\text{mg}$  protein,  $p \leq 0.05$ ) *versus* control cells. These data were confirmed by confocal analysis of the sensitive fluorescent probe filipin III (Fig. 11A).

Then, we evaluated the ability of our ADDLs to bind to the plasma membrane of neuroblastoma cells after a 30 min period of exposure by qualitative confocal microscope analysis of anti-A $\beta$ 42 antibody fluorescence (Fig. 11B). To exclude any possible interference of the cell fixation favoring the intracellular uptake of ADDLs, the distribution of fluorescein-labeled A $\beta$ 42-FAM aggregates was analyzed in unfixed neuroblastoma cells. Green fluorescence signal confirmed the different membrane distribution of ADDLs at our experimental conditions (Fig. 11B).

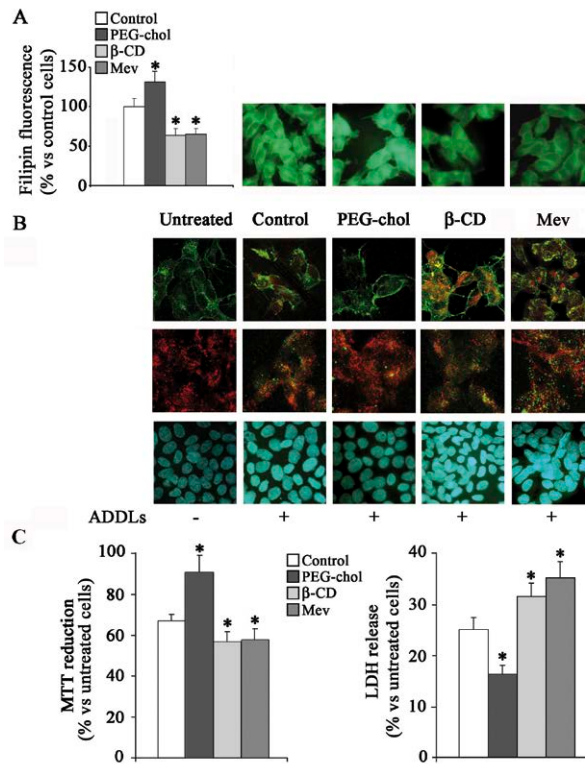


Figure 11. (A) Representative confocal microscope analysis of membrane cholesterol content in SH-SY5Y neuroblastoma cells probed by the fluorescent dye filipin III. (B) Representative confocal microscope images showing aggregates penetrating into the plasma membrane of neuroblastoma cells treated with  $1.0 \mu\text{M}$  A $\beta$ 42 ADDLs (top) or with  $3.0 \mu\text{M}$  A $\beta$ 42-FAM aggregates (middle) for 30 min. Representative blue fluorescence micrographs of Hoechst 33342 stained cells, after exposure to  $1.0 \mu\text{M}$  ADDLs for 24 h (bottom). (C) MTT and assays after exposure to  $1.0 \mu\text{M}$  A $\beta$ 42 aggregates

We also evaluated whether an increased content of membrane-cholesterol was able to prevent amyloid toxicity at our experimental conditions. As shown in Fig. 11C, the quantitative analysis of the ability of the treated cells to reduce MTT and the morphological evaluation of Hoechst 33342 stained cells revealed no marked characteristics of apoptosis in cells enriched in cholesterol after their exposure to ADDLs for 24 h. On the other hand, the loss of membrane cholesterol in cells treated with  $\beta$ -CD or Mev before exposure to the aggregates resulted in a marked increase in the number of cells displaying nuclear condensation and a significant impairment of viability respect to similarly exposed cells with basal cholesterol content. Finally, we investigated whether neuroblastoma cells exposed to ADDLs for 48 h underwent a necrotic cell death. As shown in Fig. 11C, a significant release of LDH in the cell culture media was observed in cells with basal and, to a greater extent, reduced cholesterol content exposed to ADDLs. Also in this case, cholesterol enriched cells displayed a higher resistance to amyloid toxicity, as compared to control cells, as revealed by the significant reduction of LDH release in the culture media.

### 3.1.3 A $\beta$ 42 oligomers colocalize with lipid rafts

Cholesterol is not uniformly distributed into the plasma membrane. In fact, it is concentrated in lipid rafts, which appear to exist in a liquid-ordered phase contributing to their partitioning from the surrounding liquid-disordered glycerophospholipid-rich environment. Lipid rafts are considered primary interaction sites of ADDLs (Williamson *et al.*, 2008). Therefore, we sought to assess whether the modified ability of our ADDLs to interact with normal, cholesterol-enriched or depleted cells implied the participation of lipid rafts. Confocal laser microscopy showed a marked colocalization of A $\beta$ 42 oligomers with GM1, a well known lipid raft marker, on the plasma membranes of neuroblastoma cells (Fig. 12). In particular, when the images were merged, a number of yellow areas representing the colocalization of membrane-bound ADDL with GM1 were seen. The scatter plots of fluorescence signals over the highlighted areas are shown in Fig. 12 (*right*). Two different algorithms, the Pearson's correlation coefficient and the overlap coefficient according to Manders gave similar results. In particular, the analysis over three different experiments yielded a colocalization of 43% between GM1 and ADDLs in control cells. Interestingly, a moderate enrichment of membrane cholesterol in PEG-chol treated cells appeared to reduce the ADDLs interaction with the monosialoganglioside GM1 as supported by the low degree of colocalization (19%), while an increased colocalization was found in  $\beta$ -CD (69%) and Mev (67%) treated cells.

Overall, our colocalization data show that A $\beta$  oligomers interact with the plasma membrane preferentially at the raft domains and that any structural modification of the latter following increase or decrease of cell cholesterol results in alterations of ADDL-raft interaction. These findings agree with previously reported data, showing that the content of cholesterol in cell membranes or in synthetic lipid vesicles modulates membrane-aggregate interaction (Arispe and Doh, 2002; Cecchi *et al.*, 2008b), pointing at the membrane rafts as the key sites where those modifications do occur.

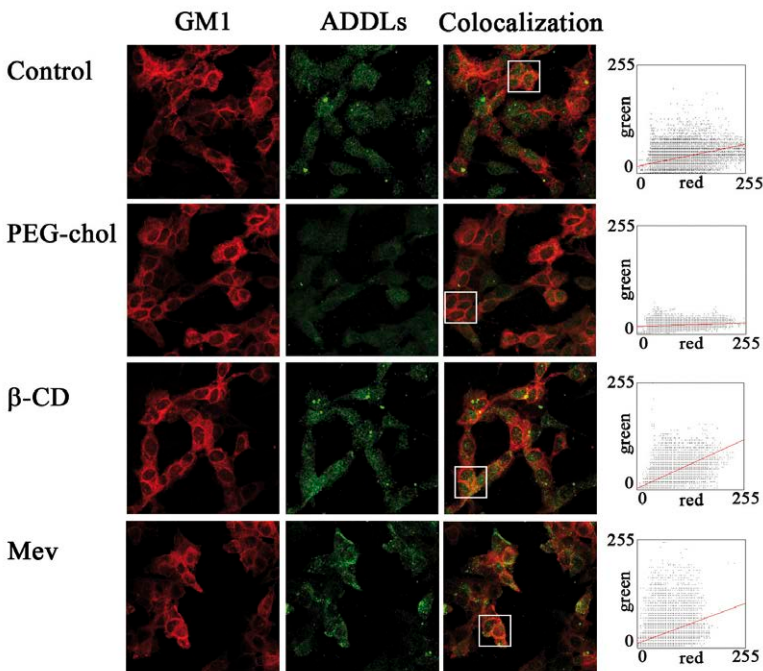


Figure 12. Representative confocal microscope images showing ADDL colocalization with GM1 (yellow), a typical marker of lipid rafts in neuroblastoma cells. Top, control cells; second row, PEG-chol treated cells; third and fourth row,  $\beta$ -CD and Mev treated cells, respectively. A $\beta$ 42 oligomers were labelled with monoclonal mouse 6E10 anti-A $\beta$  antibodies and fluorescein-conjugated anti-mouse antibodies (green), while GM1 was stained with fluorescent CTX-B conjugate as a probe (red). The scatter plots indicate the colocalization pattern over the selected area of each panel; the sampled pixels were plotted as a function of red ( $x$  axis) and green ( $y$  axis) fluorescence intensity, resulting in a partial (top), low (second row) or high (third and fourth row) GM1-ADDL colocalization.

### 3.1.4 Isolation and characterization of DRMs

After having analyzed the ADDL-raft interaction in normal, cholesterol-enriched, or depleted SH-SY5Y cells, we investigated by confocal microscopy the modification of lipid raft morphology and distribution in the plasma membranes of cells enriched or depleted in cholesterol by labelling the cell surface GM1. GM1-positive membrane domains did not appear uniformly distributed on the plasma membranes and some more brightly stained domains were observed in control cells (Fig. 13). PEG-cholesterol treatment apparently increased the brightness of GM1-rich domains, without any evident alteration of their surface distribution. On the

other hand, a substantially reduced CTX-B fluorescence was evident in cholesterol-depleted cells, confirming that the content of membrane cholesterol is crucial for lipid raft organization, possibly by regulating in a dose-dependent manner both their formation and function.

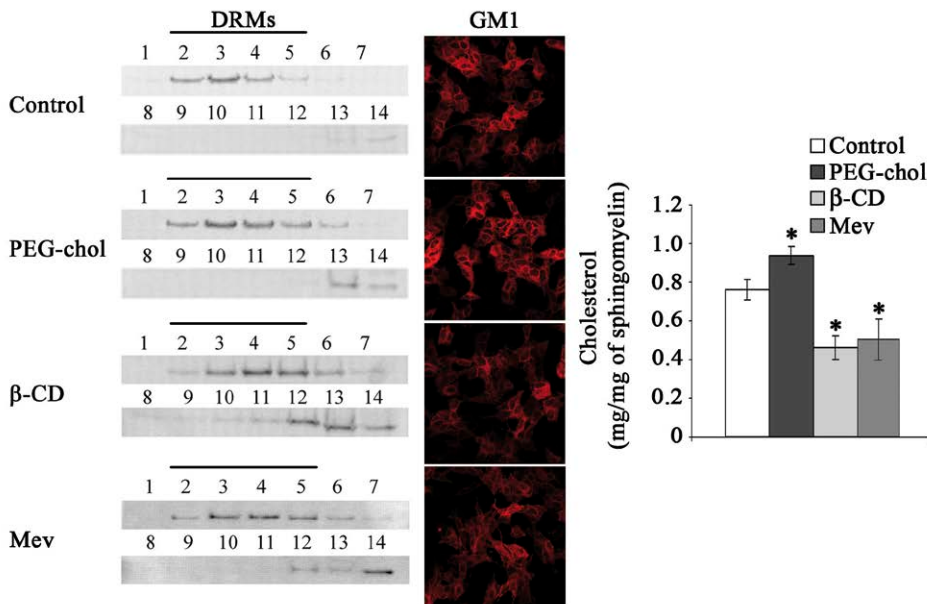


Figure 13. Representative immunoblot analysis of flotillin-1 levels in 14 sucrose gradient fractions collected from the top (low density) through the bottom (high density) of the gradient tube. An aliquot from each fraction was run on 12% SDS/PAGE, transferred onto a PVDF membrane and then incubated with mouse anti-flotillin-1 monoclonal antibodies. The amount of cholesterol in the DRM pools was determined by a fluorimetric assay and expressed as ratio to sphingomyelin content. On the right side of the figure, representative confocal analysis of the cell surface GM1 distribution in SH-SY5Y cells probed by the fluorescent CTX-B conjugate.

Next, we investigated the effects of the same treatments directly on lipid raft fractions isolated from treated or control neuroblastoma cells. Due to their insolubility in non-ionic detergents at low temperatures, lipid rafts have been defined as detergent-resistant membranes (DRMs). Because of their high lipid-to-protein ratio, DRMs display a low density and can be isolated by cell lysis with Triton X-100 and flotation on sucrose-density gradients. Sucrose gradient fractions, purified from human neuroblastoma cells untreated or treated with PEG-cholesterol or with  $\beta$ -CD or Mev, were analyzed by Western blot for the presence of flotillin-1, a lipid raft protein marker. As shown in Fig. 13, flotillin-1 was localized in low density fractions (2-5) in control cells. In agreement with confocal analysis, cholesterol

enrichment did not affect remarkably the DRM density distribution. On the contrary, in  $\beta$ -CD and Mev treated cells most of the flotillin-1 immunoreactivity was shifted to fractions 12-14. However, a minor flotillin-1 immunoreactivity was still present in fractions 2-5, suggesting that  $\beta$ -CD or Mev treatment led to a partial, not complete, disruption of the organization and/or the number of lipid rafts in our cell model. After extensive dialysis to remove sucrose, the amount of cholesterol was quantified in the pooled flotillin-1-positive fractions (2-5) purified from cells enriched or depleted in cholesterol or from control cells. The amount of cholesterol in the plasma membrane microdomains was significantly increased (+20% vs control cells) or reduced (-40% vs control cells) upon cell treatment with PEG-cholesterol or with  $\beta$ -CD and Mev, respectively (Fig. 13). No significant difference was observed in the total sphingomyelin levels among DRMs pools obtained from control cells ( $2.17 \pm 0.32$  ng/ $\mu$ l), cholesterol-enriched cells ( $2.09 \pm 0.23$  ng/ $\mu$ l) and cholesterol-depleted cells ( $1.94 \pm 0.45$  ng/ $\mu$ l).

### 3.1.5 Effects of ADDLs on lipid raft structural order

The effect of cholesterol on membrane fluidity is known to be complex; cholesterol can either enhance or decrease membrane fluidity depending on temperature, cholesterol concentration and bilayer composition (Wood *et al.*, 1999). However, under physiological conditions cholesterol is known to increase membrane rigidity. Thus, we evaluated the effect of cholesterol content on the structural order of the hydrophobic regions of lipid rafts by measuring the fluorescence anisotropy of 1,6-diphenyl-1,3,5-hexatriene (DPH) under steady-state conditions at 37 °C. The relative motion of the DPH dye molecule within the fatty acid acyl chain space of the lipid bilayer was determined by polarized fluorescence and expressed as  $r$ , the anisotropy constant, whose value is inversely proportional to the degree of membrane fluidity (Lentz, 1989; Shinitzky and Barenholz, 1974). In raft-enriched samples prepared from neuroblastoma cells a moderate cholesterol enrichment significantly increased the raft structural order, whereas cholesterol depletion resulted in a higher fluidity (Fig. 14).

We also investigated whether the content of cholesterol in lipid rafts modified the membrane perturbing effect of ADDLs. We found a rapid reduction of fluidity in control lipid rafts exposed to 1.0  $\mu$ M A $\beta$ 42 oligomers for various lengths of time (Fig. 14, *inset*). As the most ordered structure was reached in less than 10 min of exposure to the oligomers, we chose this incubation time for subsequent experiments. No evident difference in DPH fluorescence anisotropy was detected by exposing lipid rafts to A $\beta$ 42-1, suggesting that this effect is specific of the  $\beta$ -sheet structure found in ADDLs.

Cholesterol-enriched lipid rafts did not display any significant change of the anisotropy upon exposure to A $\beta$ 42 oligomers or to the reverse A $\beta$ 42-1 peptide, suggesting that cholesterol enrichment protects lipid rafts from perturbation by A $\beta$ 42. On the contrary, cholesterol loss resulted in increased rigidity of rafts exposed not only to A $\beta$ 42 ADDLs, as expected, but also to A $\beta$ 42-1 monomers, suggesting that the lat-

ter are able to penetrate and stiffen the raft bilayer as well, although with reduced efficiency.

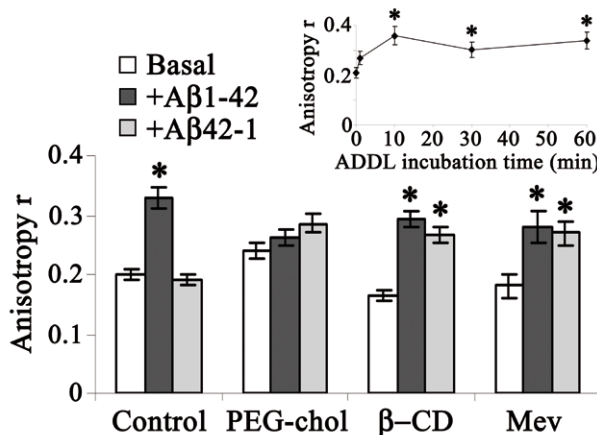


Figure 14. DPH fluorescence anisotropy,  $r$ , measured before and after DRM treatment with A $\beta$ 42 ADDLs or the reverse A $\beta$ 42-1 peptide. The measurements were performed on control, cholesterol-enriched and cholesterol-depleted samples. DPH fluorescence anisotropy,  $r$ , measured by incubating rafts for 2, 10, 30 and 60 min in the presence of 1.0  $\mu$ M A $\beta$ 42 oligomers. All the data are means  $\pm$  S.D. of six independent experiments. \* $p$  $\leq$ 0.05, significant difference vs untreated microdomain fluidity.

### 3.1.6 AFM imaging of supported DRMs purified from cells exposed to ADDLs

AFM analyses were performed in collaboration with the group of Prof.ssa Alessandra Gliozi, of the Department of Physics of the University of Genoa. The deposition of purified DRMs on mica substrates for AFM inspection resulted in the spontaneous formation of membrane multilayers, similarly to the behaviour observed when supported bilayers are formed from liposome deposition (Canale *et al.*, 2006; Egawa and Furusawa, 1999). The DRM multilayers completely covered the imaging field and there was no mica substrate exposed. However they did not appear homogeneous, with membrane domains sprouting from a uniform background (Fig. 15A). The background thickness with respect to the mica surface, measured by indenting the background in different points, corresponded to up to four double layers (each about 5 nm thick). The domains were stable upon scanning (Fig. 15B) and had a typical lateral size of a few hundred of nm. Their height with respect to the background was less than 2 nm (Table III). To check whether the sprouting domains had the same chemical nature of the background, we performed antibody labelling experiments to detect the presence of GM1 and flotillin-1, typical components of membrane rafts. Fig. 15D shows a representative image obtained in the presence of anti-GM1 antibodies.

## Amyloid Cytotoxicity and Membrane Lipid Composition

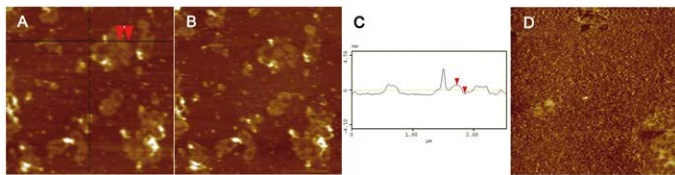


Figure 15. (A) Contact mode AFM image in liquid (height data) of DRMs extracted from control cells; (B) a subsequent scan of the same area showing reproducibility of domain imaging. The image in (B) was taken 15 min after that in (A); (C) height profile obtained from an image section along the horizontal line indicated in (A); (D) imaging of DRMs labeled with anti-GM1 antibodies. Scan size 2.5  $\mu$ m; Z range (A, B) 10 nm, (D) 5 nm.

A uniform distribution of granular structures located in the background is observed, indicating the presence of GM1 in this region. As the DRM multilayers completely covered the imaging field, we can rule out the possibility of any non-specific interaction of anti-GM1 antibodies with the mica. No granular structures were observed on the domain surface, although incubation with anti-GM1 antibodies resulted in domain fragmentation. To check whether proteins were the main component of these domains, we incubated the DRMs with a cocktail of proteases, as described in Materials and Methods section. DRM treatment with the proteases before deposition on the mica substrate resulted in the disappearance of membrane domains and the presence of a homogeneous sample surface. Conversely, when DRMs were incubated with proteases after deposition on the mica substrate, the domains originally present were very unstable upon scanning and disappeared after a few scans (Fig. 16A,B).

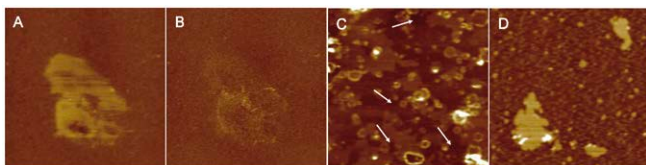


Figure 16. Contact mode AFM images in liquid (height data) showing the disrupting effect of proteases on DRM lipid domains (A, B): (A) first scan after a 2 h sample incubation in the presence of proteases; (B) second scan (about 15 min later); (C) DRMs purified from cells pretreated with A $\beta$ 42 oligomers. The white arrows indicate some of the cavities resulting from DRM interaction with ADDLs. (D) DRMs purified from cells pre-treated with A $\beta$ 42-1 oligomers. Scan size 2.5  $\mu$ m; Z range 10 nm.

As mentioned above, successive scans performed in the absence of proteases (Fig. 15A,B) showed that the domains can be reproducibly imaged and therefore their instability observed in the presence of proteases can actually result from the action of the latter. These results suggest that the background is composed by DRMs, while the slightly higher domains are formed by fluid phase-separated proteins or lipid-protein complexes present in the DRM preparations.

DRMs purified from cholesterol-enriched and cholesterol-depleted cells were also imaged by AFM. In samples purified from cholesterol-enriched cells the lateral size of the membrane domains appeared reduced as compared with that measured in control samples which, in turn, was reduced with respect to that measured in DRMs purified from cholesterol-depleted cells (Table III). This finding could be explained by the effect of cholesterol on membrane fluidity, resulting in decreased mobility, and therefore reduced coalescence, of fluid domains, in agreement with the fluorescence anisotropy data reported above.

Raft samples	Pore depth (nm)	Pore size (nm)	Domain size (nm)	Domain height (nm)
Control			$455 \pm 15$	$1.68 \pm 0.04$
Control + A $\beta$ 1–42	$1.50 \pm 0.04$	$420 \pm 20$	$218 \pm 12$	$0.68 \pm 0.02$
Chol-enriched			$356 \pm 16$	$1.78 \pm 0.03$
Chol-enriched + A $\beta$ 1–42	$1.03 \pm 0.03$	$370 \pm 30$	$332 \pm 18$	$0.81 \pm 0.04$
Chol-depleted			$540 \pm 40$	$1.17 \pm 0.06$
Chol-depleted + A $\beta$ 1–42	$1.30 \pm 0.03$	$450 \pm 30$	$261 \pm 11$	$1.22 \pm 0.04$
A $\beta$ 1–42 treated cells	$0.68 \pm 0.04$	$120 \pm 10$	$470 \pm 40$	$0.83 \pm 0.03$

Table III. Interaction with ADDLs affects the morphological features of DRMs. Each pore (or domain) size figure was the mean of the widths measured along the pore (or domain) major diameter and the corresponding in-plane perpendicular direction. Domain heights were measured with respect to the image background. The data are expressed as mean $\pm$ standard error over an ensemble of at least 100 measurements.

Next, we investigated the effect of cell exposure to ADDLs on DRM morphology. DRMs purified from cells treated with A $\beta$ 42 oligomers before raft extraction (Fig. 16C) displayed the presence of cavities, or hollows (white arrows), whose depth and size are reported in Table III. Corral-like structures ( $1.7 \pm 0.1$ ) nm high and ( $260 \pm 10$ ) nm in diameter were also observed (Fig. 16C). Both cavities and corral-like structures were absent in DRMs purified from cells treated with A $\beta$ 42-1 oligomers before raft extraction (Fig. 16D), suggesting a non generic interaction of A $\beta$ 42 with lipid rafts. Fig. 17 compares the morphologies of DRMs extracted from control (Fig. 17A), cholesterol-enriched (Fig. 17B) and cholesterol-depleted (Fig. 17C) cells before (-) and after (+) exposure to ADDLs. The latter are imaged in the inset in Fig. 17B. The presence of the peptide clearly altered DRM morphology, giving rise to the formation of cavities in all samples. The quantitative analysis of the images showed that the depth and size of the cavities observed in cholesterol-enriched samples were significantly reduced with respect to those displayed by cholesterol-depleted samples. All DRMs treated with A $\beta$ 42 oligomers after purification displayed cavities with depths and sizes significantly increased as compared to those found in DRMs purified from cells previously exposed to the same oligomers. In particular, a four-fold increase in the cavity sizes was observed (Table III). These results indicate that a reduced raft damage was caused by ADDLs in living cells with respect to that found in purified DRMs.

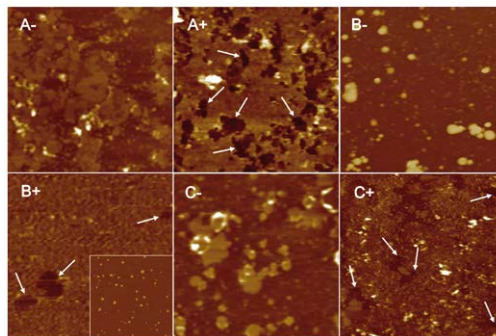


Figure 17. Contact mode AFM images in liquid (height data) of DRMs before (-) and after (+) 30 min incubation with 1.0  $\mu\text{M}$  A $\beta$ 42 ADDLs. (A+, A-) DRMs prepared from control cells; (B+, B-) cholesterol-enriched DRMs; (C+, C-) cholesterol-depleted DRMs. The white arrows indicate some of the cavities formed as a consequence of DRM interaction with ADDLs. Scan size 2.5  $\mu\text{m}$ ; Z range 10 nm. The inset in (B+) is a tapping mode AFM image of ADDLs. Scan size 1.0  $\mu\text{m}$ ; Z range 5.0 nm.

In addition to cavity formation, DRM exposure to ADDLs resulted in changes of domain morphology. In fact, exposure of DRMs purified from control and cholesterol-enriched cells to ADDLs resulted in a remarkable reduction of domain heights (as measured with respect to the image background) to values similar to those observed in DRMs purified from cells previously exposed to A $\beta$  oligomers. On the contrary, domain height was substantially unchanged in DRMs purified from cholesterol-depleted cells (Table III).

The domain lateral size in DRM preparations from control and cholesterol-depleted cells exposed to A $\beta$  oligomers was reduced, while that of DRMs from cholesterol-enriched cells was substantially unchanged, suggesting that cholesterol hinders the ADDL-DRM (and possibly raft) interaction. Furthermore, the domain size in DRMs purified from cells treated with A $\beta$ 1-42 oligomers was the same as that of the DRMs purified from control, not exposed, cells suggesting a possible recovery of the membrane structure *in vivo*.

### 3.2 Results II

#### 3.2.1 Lipid rafts mediate amyloid-induced calcium dyshomeostasis and oxidative stress in Alzheimer's disease

Several lines of evidence suggest that the initial events of A $\beta$  oligomerization and deposition in AD involve the interaction of soluble oligomers with neuronal membranes. In this second part of the result section, was shown that A $\beta$ 42 oligomers are recruited to lipid rafts, which are ordered membrane microdomains rich in cholesterol and gangliosides, resulting in lipid peroxidation, Ca $^{2+}$  dyshomeostasis and greater membrane permeability in primary fibroblasts from familial AD patients (FAD) bearing APP Val717Ile, PS1 Leu392Val or PS1 Met146Leu gene mutations.

Moreover, the presence of significantly higher levels of lipid peroxidation correlated with greater structural modification in detergent resistant domains (DRMs) isolated from APP and PS1 fibroblasts, compared to WT fibroblasts obtained from healthy subjects. The modulation of specific raft physicochemical properties, such as moderate increases in cholesterol content, modest depletion of GM1 content and interference with GM1 exposure or negative charge, precluded the interaction of amyloid aggregates with the plasma membrane and the resulting cell damage in FAD fibroblasts and cortical neurons from rat brains. These findings suggest a specific role for raft domains as primary mediators of amyloid toxicity in AD neurons.

### 3.2.2 Lipid rafts are primary interaction sites for A $\beta$ 42 oligomers at the plasma membrane

Mutations in PS1, PS2 or APP genes have been shown to increase production of 42-residue amyloid peptides, i.e. the most amyloidogenic form of A $\beta$  (Hardy and Selkoe, 2002). Accordingly, higher levels of A $\beta$ 42 peptide were found in the culture media of PS1 Leu392Val, PS1 Met146Leu and APPVal717Ile fibroblasts from FAD patients compared to WT fibroblasts from healthy subjects (Fig.18A left). APP fibroblasts, in particular, released significantly more A $\beta$ 42 than PS1 cells. Thus, we investigated whether FAD fibroblasts with altered proteolytic APP processing display increased oxidative damage. 8-OH isoprostane levels were significantly higher in PS1 and APP fibroblasts with respect to WT fibroblasts (Fig. 18A right).

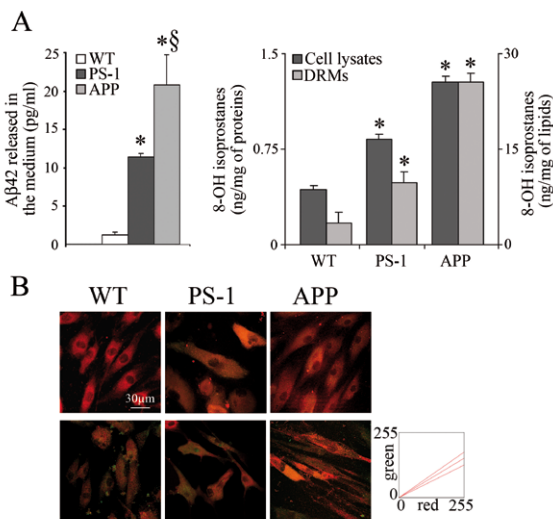


Figure 18. (A) A $\beta$ 42 levels in the cell culture media of WT, PS1 and APP fibroblasts were measured using a commercial ELISA kit. 8-OH isoprostane levels were quantified both in cell lysates and in the pooled flotillin-1-positive fractions (DRMs) purified from WT, PS1 and APP fibroblasts. (B) Representative confocal microscope images of lipid peroxidation in WT, PS1 and APP fibroblasts were achieved using the fluorescent probe BODIPY. Representative confocal microscope images showing A $\beta$ 42 colocalization with GM1 (yellow), a typical lipid raft marker.

## Amyloid Cytotoxicity and Membrane Lipid Composition

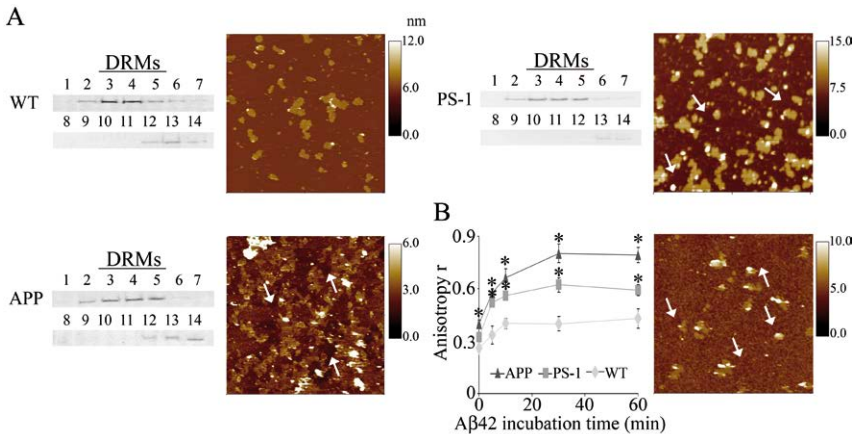


Figure 19 A $\beta$ 42-GM1 interactions induce structural modification of DRMs. (A) Representative Western blot analysis of flotillin-1 levels in WT, PS1 and APP fibroblasts, determined from 14 sucrose gradient fractions collected from the top (low density) to the bottom (high density) of the gradient tube. An aliquot from each fraction was run on 12% SDS/PAGE, transferred onto a PVDF membrane and then incubated with mouse monoclonal anti-flotillin-1 antibodies. Flotillin-1-positive fractions (DRMs) enriched in lipid raft microdomains (from 3 to 5) were pooled and analyzed using contact mode AFM in liquid with a scan size of 5  $\mu$ m. Steps or cavities were present in PS1 and APP DRMs (white arrows). (B) DPH fluorescence anisotropy,  $r$ , measured by incubating rafts from WT, PS1 and APP fibroblasts for 0, 5, 10, 30 and 60 min in the presence of 1.0  $\mu$ M A $\beta$ 42 oligomers, and then for 30 min with DPH. All data is mean  $\pm$  S.D. of four independent experiments. \* $p$   $\leq$  0.05, significant difference vs WT fibroblasts. AFM image of DRMs purified from WT fibroblasts after 30 min incubation with 1.0  $\mu$ M A $\beta$ 42 oligomers. Scan size 5  $\mu$ m.

Confocal microscope analysis confirmed the presence of enhanced cell-surface oxidation in FAD fibroblasts displaying greater basal A $\beta$  production, as assessed using the fluorescent probe BODIPY 581/591C<sub>11</sub> (Fig. 18B). Moreover, the increase in lipid peroxidation was higher in detergent-resistant membranes (DRMs) (Fig. 19A, left) compared to the entire membrane component (Fig. 18A, right), pointing to lipid rafts as a preferential site for A $\beta$ 42 interaction at the cell surface. Accordingly, we observed marked colocalization of A $\beta$ 42 oligomers with gangliosides in fibroblast membranes following exposure to A $\beta$ 42 aggregates (Fig. 18B). In particular, where green and red fluorescent signals were merged, a number of yellow areas, representing A $\beta$ 42-GM1 colocalization, were evident in PS1 and APP fibroblasts. Scatter plots of fluorescence signals, analyzed using Pearson's correlation coefficient and the overlap coefficient according to Manders, yielded about 65% A $\beta$ 42-GM1 colocalization in PS1 and APP fibroblasts and 50% in WT fibroblasts obtained from healthy subjects. Greater A $\beta$ 42-GM1 colocalization in FAD fibroblasts was associated with evident alteration of DRM morphology, as observed by contact mode AFM (Fig. 19A). In particular, steps/cavities (white arrows), which were absent in WT DRMs, were found in PS1 and, to a greater extent, in APP DRMs. Disruption of the plasma membrane is evident from its granular appearance, where multiple small defects are

formed. The greater membrane damage observed in APP samples correlates well with their increased release of A $\beta$ 42, compared to PS1 samples. Furthermore, exposure of DRMs purified from WT fibroblasts to A $\beta$ 42 oligomers for 30 min generated extensive small lesions in lipid rafts (Fig. 19B, white arrows). Similar behaviour was observed in DRMs extracted from SH-SY5Y cells (Cecchi *et al.*, 2009). Accordingly, the fluorescence anisotropy constant ( $r$ ) of 1,6-diphenyl-1,3,5-hexatriene (DPH), which is inversely proportional to the degree of membrane fluidity, was higher in DRMs from PS1 and APP fibroblasts than that in corresponding lipid rafts from WT fibroblasts (Fig. 19B). Moreover, DRMs obtained from PS1 and, to a greater extent, APP fibroblasts showed a greater increase in stiffness when exposed to A $\beta$ 42 oligomers, with respect to rafts purified from WT fibroblasts.

### 3.2.3 Cholesterol and GM1 mediate A $\beta$ 42 accumulation at the plasma membrane

Cholesterol and monosialoganglioside GM1 are two key components of lipid rafts, which are increasingly accepted as playing an important role in stimulating protein aggregation and forming interactions with protein oligomers (Ariga *et al.*, 2008; Ehehalt *et al.*, 2003; Malchiodi-Albedi *et al.*, 2010; Matsuzaki *et al.*, 2010). Hence, we investigated whether cholesterol may modulate A $\beta$ 42 interaction with these liquid-ordered structures in FAD and WT fibroblasts. Moderate enrichment of membrane cholesterol, as assessed by filipin staining (Fig. 20), reduced the interaction of A $\beta$ 42 oligomers with GM1, resulting in about 34% colocalization in PS1 and APP fibroblasts and 28% colocalization in WT cells, compared to similarly treated cells with basal cholesterol content (Fig. 18B and 21A).

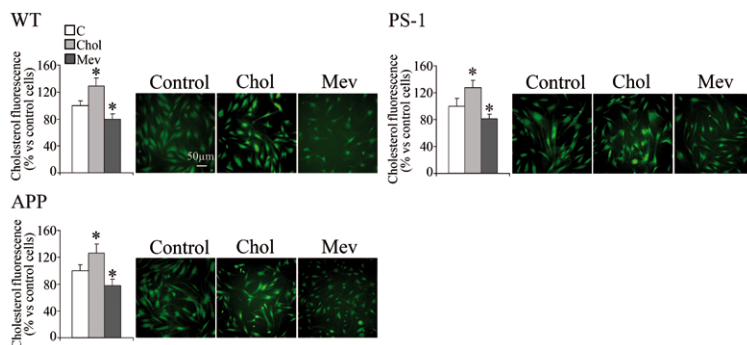


Figure 20. Modulation of membrane cholesterol in fibroblast cultures. Representative confocal microscope analysis of membrane cholesterol in WT and FAD fibroblasts displaying PS1 and APP gene mutations, probed using the fluorescent dye filipin III. Membrane cholesterol enrichment and depletion were achieved by supplementing fibroblast culture media with 0.2 mg/ml  $\beta$ CD-Chol (Chol) for 3 h at 37 °C, or with 10  $\mu$ M mevastatin (Mev) for 48 h at 37°C in the presence of 1% FBS, respectively. Filipin III fluorescence is expressed as a fractional change above the resting baseline,  $\Delta F/F$ , where  $F$  is the average baseline fluorescence in control cells (assumed to be 100%) and  $\Delta F$  represents the change in fluorescence with respect to baseline levels. The values shown are means  $\pm$  S.D. of three independent experiments. \* $p\leq 0.05$ , significant difference vs relative control cells with basal cholesterol levels.

## Amyloid Cytotoxicity and Membrane Lipid Composition

In contrast, an increase in A $\beta$ 42-GM1 colocalization (about 80%) in PS1 and APP and, to a lesser extent, in WT fibroblasts (59%), was observed after cholesterol depletion. Accordingly, robust FRET between A $\beta$ 42 oligomers and GM1 was observed in cholesterol-depleted fibroblasts (Fig. 21B), indicating that these two molecules directly interact with each other at the cell surface (Day, et al., 2001; Kenworthy et al., 2000). In particular, FRET was more detectable in FAD fibroblasts than in WT cells treated with mevastatin for 48 hours. In contrast, moderate enrichment of membrane cholesterol appeared to reduce A $\beta$ 42-GM1 interactions, as supported by the low intensity of colocalization signals (Fig. 21B). Accordingly, treatment with neuraminidase (NAA), which removes the sialic acid moiety from GM1, reduced the interaction of A $\beta$ 42 oligomers with GM1, resulting in about 20% colocalization in FAD fibroblasts and 15% colocalization in WT cells (Fig. 21C).

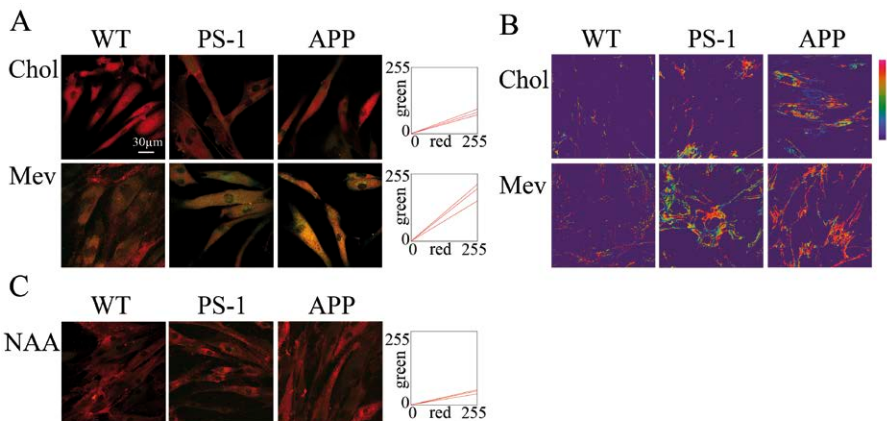


Figure 21. Cholesterol and GM1 mediate A $\beta$ 42 accumulation at the plasma membrane. (A) Representative confocal microscope images showing A $\beta$ 42 colocalization with GM1 (yellow). WT, PS1 and APP fibroblasts were treated with 1.0  $\mu$ M A $\beta$ 42 for 30 min and then labeled with mouse monoclonal 6E10 anti-A $\beta$ 42 and fluorescein-conjugated anti-mouse antibodies (green), while GM1 was stained with fluorescent CTX-B conjugate (red). Scatter plots compare A $\beta$ 42-GM1 colocalization in WT, PS1 and APP fibroblasts following treatment with Chol and Mev. Pixels were plotted as a function of red (x axis) and green (y axis) fluorescence intensity, resulting in little (top) or marked (bottom) A $\beta$ 42-GM1 colocalization. (B) Representative FRET images showing A $\beta$ 42-GM1 colocalization in fibroblasts exposed to 1.0  $\mu$ M A $\beta$ 42-FAM for 30 min following treatment with Chol and Mev. FRET efficiency images are presented using a pseudocolor scale for better visualization. The color of the bar represents the pixel density of the image and thus the intensity of interaction. (C) Representative confocal microscope images showing A $\beta$ 42-GM1 colocalization in fibroblasts depleted of sialic acid (by addition of NAA) and then exposed to 1.0  $\mu$ M A $\beta$ 42 for 30 min. A $\beta$ 42 oligomers were labeled with 6E10 antibodies (green), while GM1 was stained with Alexa Fluor 647-conjugated CTX-B (red). Pixels were plotted as above reported, resulting in little A $\beta$ 42-GM1 colocalization.

### 3.2.4 Cholesterol and GM1 mediate $\text{Ca}^{2+}$ dyshomeostasis and extensive membrane permeabilization induced by A $\beta$ 42 oligomers

Perturbation of ion distribution across the plasma membrane is one of the earliest modifications displayed by cells exposed to toxic amyloid aggregates (Arispe *et al.*, 2007; Decker *et al.*, 2010; Demuro *et al.*, 2010). Accordingly, a sharp increase in cytosolic  $\text{Ca}^{2+}$  was observed in FAD and WT fibroblasts exposed to A $\beta$ 42 oligomers (Fig. 22A). In particular, kinetic analysis revealed that the increase in intracellular  $\text{Ca}^{2+}$  levels in PS1 and APP fibroblasts, with rate constants ( $k_1, k_2$ ) of  $5.23(\pm 0.10) \times 10^{-3}$  seconds $^{-1}$ ,  $5.86(\pm 0.11) \times 10^{-3}$  seconds $^{-1}$ , was greater compared to WT cells ( $k_3$ ) of  $2.07(\pm 0.77) \times 10^{-3}$  seconds $^{-1}$ . Furthermore, the increase in cytosolic  $\text{Ca}^{2+}$  content was much smoother and milder in cholesterol-enriched fibroblasts exposed to amyloid oligomers with respect to similarly treated control cells with basal cholesterol content (Fig. 22A,B). In contrast, membrane cholesterol depletion, following cell treatment with mevastatin, triggered a greater increase in cytosolic  $\text{Ca}^{2+}$  levels.

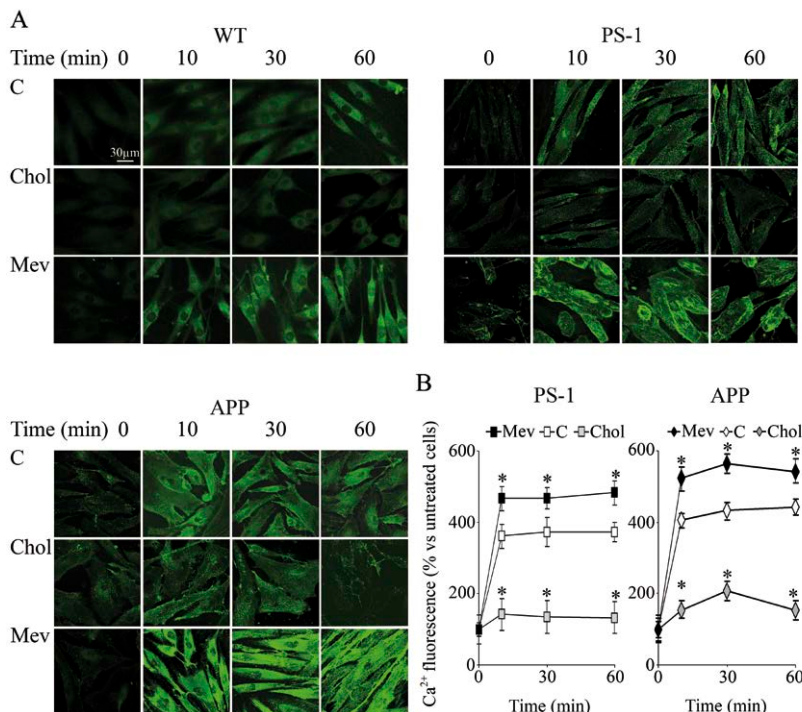


Figure 22. Cholesterol enrichment reduces A $\beta$ 42-induced  $\text{Ca}^{2+}$  dyshomeostasis. (A) Representative confocal microscope images of cytosolic  $\text{Ca}^{2+}$  levels in WT, PS1 and APP fibroblasts, under basal conditions or following treatment with Chol and Mev, treated with 1.0  $\mu\text{M}$  A $\beta$ 42 oligomers for 0, 10, 30 and 60 min at 37 °C. Cells were then treated for 30 min with 8.8  $\mu\text{M}$  fluo-3-AM. (B) Quantitative analysis of fluo-3 fluorescence. The values shown are means  $\pm$  S.D. of three independent experiments. \* $p\leq 0.05$ , significant difference vs relative control cells with basal cholesterol content.

## Amyloid Cytotoxicity and Membrane Lipid Composition

On the other hand, significant GM1 enrichment (Fig. 23A) induced a sharper rise in cytosolic  $\text{Ca}^{2+}$  levels than that observed in similarly exposed cells with basal GM1 levels (Fig. 23B). In contrast, a decrease in membrane GM1, following cell treatment with the glucosylceramide synthase inhibitor PDMP (Fig. 23A), prevented the  $\text{Ca}^{2+}$  spikes induced by A $\beta$ 42 oligomers (Fig. 23B). The binding of anti-GM1 antibodies ( $\text{Ab}_{\text{GM1}}$ ) to raft monosialoganglioside and sialic acid hydrolysis by NAA also precluded the increase in intracellular  $\text{Ca}^{2+}$ . In any case, no change in  $\text{Ca}^{2+}$  levels was observed when fibroblasts were treated with GM1 or PDMP in the absence of A $\beta$ 42 oligomers (Fig 23C).

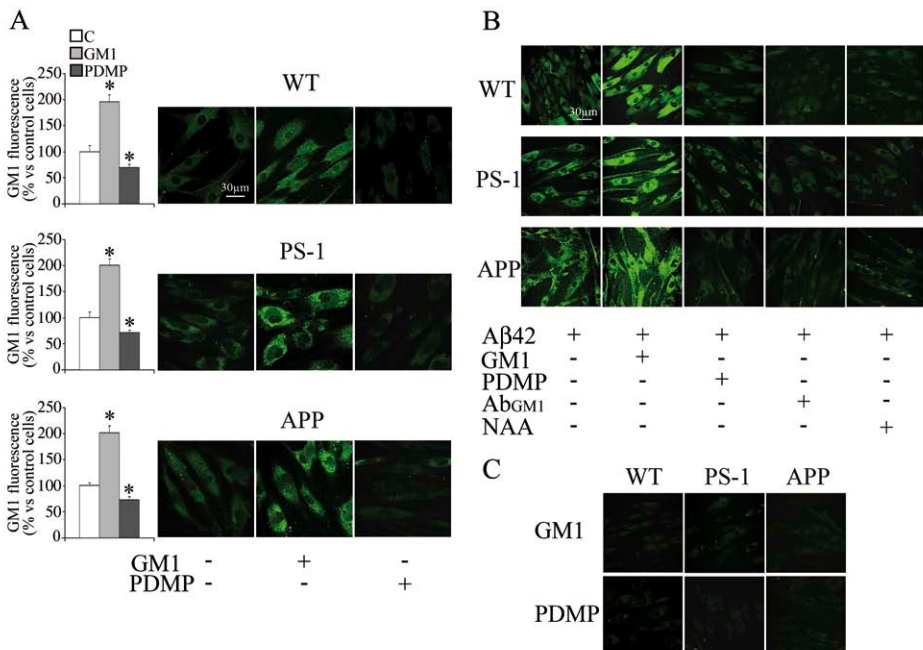


Figure 23. Depletion of GM1 reduces A $\beta$ 42-induced  $\text{Ca}^{2+}$  dyshomeostasis. (A) Representative confocal microscope images of GM1 content in WT, PS1 and APP fibroblasts under basal conditions, or following treatment with 50  $\mu\text{g}/\text{ml}$  GM1 or 25  $\mu\text{M}$  PDMP for 48 h at 37°C. Semi-quantitative values of the green fluorescent signal (rabbit polyclonal anti-GM1 antibodies) are shown on the left of each image. The values shown are means  $\pm$  S.D. of three independent experiments. \* $p \leq 0.05$ , significant difference vs relative control cells with basal GM1 levels. (B, C) Representative confocal microscope images of cytosolic  $\text{Ca}^{2+}$  levels in WT, PS1 and APP fibroblasts, under basal conditions or following treatment with GM1, PDMP, AbGM1 or a cocktail of NAA, exposed to 1.0  $\mu\text{M}$  A $\beta$ 42 aggregates for 0 and 30 min at 37 °C (B), or not treated with aggregates (C). Cells were then treated for 30 min with 8.8  $\mu\text{M}$  fluo-3-AM.

Moreover, the presence of A $\beta$ 42 aggregates in the cell culture media triggered a sharp decrease in cell calcein fluorescence, suggesting extensive A $\beta$ 42 oligomer-induced alteration of membrane permeability in fibroblasts (Fig. 24). The decrease in calcein fluorescence was less marked in A $\beta$ 42-exposed fibroblasts enriched in

membrane cholesterol, while greater calcein leakage was observed in APP and PS1 fibroblasts compared to WT controls, suggesting greater A $\beta$ 42 aggregate-induced alteration of membrane permeability in the former. Indeed, calcein-loaded APP and PS1 fibroblasts fluoresced less compared to WT fibroblasts, even prior to the exogenous addition of A $\beta$ 42 aggregates, perhaps reflecting greater amyloid-induced membrane damage in FAD cells displaying enhanced basal A $\beta$  production (Fig. 24). No decrease in calcein fluorescence was observed in A $\beta$ 42-exposed, GM1-depleted fibroblasts. In contrast, in cholesterol-depleted or GM1-enriched fibroblasts, marked calcein leakage was observed upon exposure to A $\beta$ 42 oligomers.

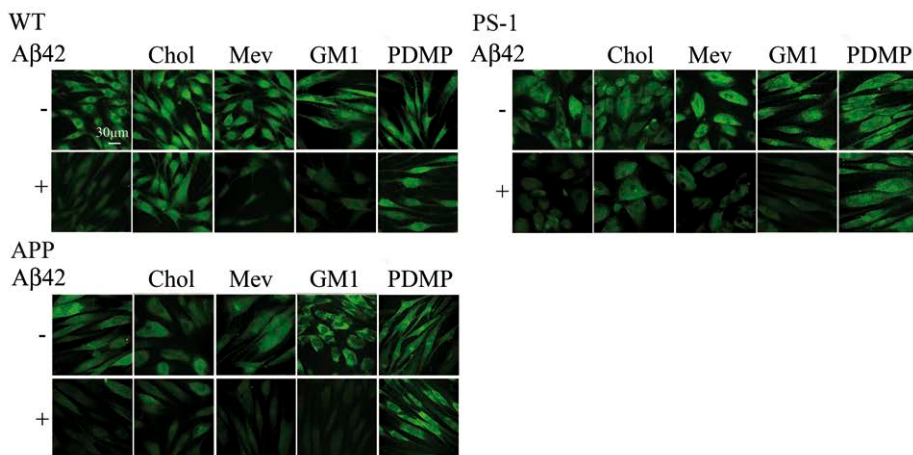


Figure 24. Cholesterol enrichment and GM1 depletion prevent membrane permeabilization induced by A $\beta$ 42 oligomers. Representative confocal microscope images showing cholesterol-enriched (Chol), cholesterol-depleted (Mev), GM1-enriched (GM1) or GM1-depleted (PDMP) fibroblasts loaded with 2.0  $\mu$ M calcein-AM for 20 min and then exposed to 1.0  $\mu$ M A $\beta$ 42 aggregates for 30 min at 37 °C.

### 3.2.5 GM1 modulates lipid peroxidation and cytotoxicity induced by A $\beta$ 42 oligomers

A $\beta$ 42 has been found to be tightly associated with monosialoganglioside GM1, implicating lipid rafts in the process of A $\beta$  aggregation and deposition (Ariga *et al.*, 2001; Ehehalt *et al.*, 2003). Accordingly, the binding of anti-GM1 antibodies (Ab<sub>GM1</sub>) and cholera toxin (CTX-B) to raft GM1 reduced the alteration of membrane permeability (as shown by decreased calcein leakage) and prevented the sharp increase in membrane oxidation (Fig. 25A,B). Calcein leakage was also prevented by treating fibroblasts with NAA (Fig. 25A). Moreover, BODIPY-loaded FAD fibroblasts showed a greater shift to green fluorescence than did WT cells when exposed to A $\beta$ 42 aggregates (Fig. 25B). However, this fluorescence shift was precluded by culturing cells in a Ca<sup>2+</sup>-free medium, suggesting that the influx of extracellular Ca<sup>2+</sup> is involved in the lipid peroxidation process induced by A $\beta$ 42 oligomers.

## Amyloid Cytotoxicity and Membrane Lipid Composition

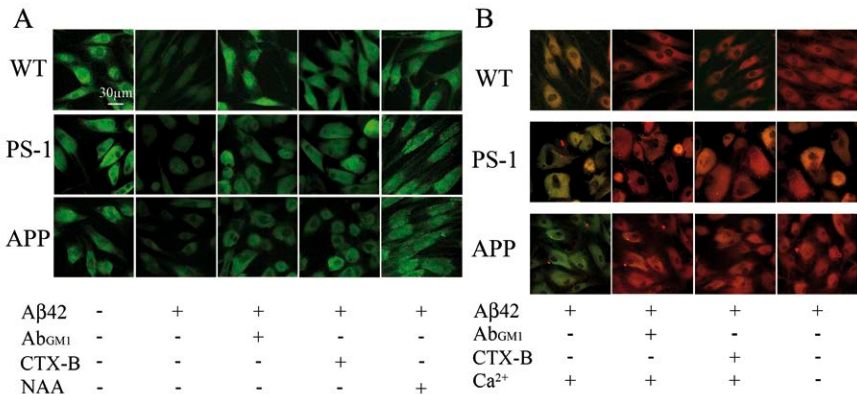


Figure 25 GM1 modulates membrane permeabilization, lipid peroxidation induced by A $\beta$ 42 oligomers. (A) Representative confocal microscope images of WT, PS1 and APP fibroblasts loaded with 2.0  $\mu$ M calcein-AM for 20 min. Cells were incubated in the absence or presence of Ab<sub>GM1</sub>, CTX-B or NAA, as reported above, and subsequently exposed to 1.0  $\mu$ M A $\beta$ 42 oligomers for 30 min. (B) Representative confocal microscope images of lipid peroxidation in fibroblasts pre-incubated for 20 min with Ab<sub>GM1</sub> or CTX-B and subsequently exposed to 1.0  $\mu$ M A $\beta$ 42 oligomers for 30 min. As a control, cells were also exposed to A $\beta$ 42 aggregates in a Ca<sup>2+</sup>-free medium. Lipid peroxidation was analyzed using the fluorescent probe BODIPY 581/591C<sub>11</sub>.

The MTT assay was then performed in fibroblasts previously modulated in GM1 content, structure or accessibility, following 24 h exposure to 1.0  $\mu$ M A $\beta$ 42 oligomers. As shown in Fig. 26, the increase in GM1 content triggered a slight increase in A $\beta$ 42 toxicity relative to that observed in fibroblasts with basal GM1 content. In contrast, membrane GM1 depletion, membrane binding with anti-Ab<sub>GM1</sub> or CTX-B, and GM1 charge modification improved fibroblast viability, suggesting a major role for GM1 raft domains in amyloid-induced cytotoxicity.

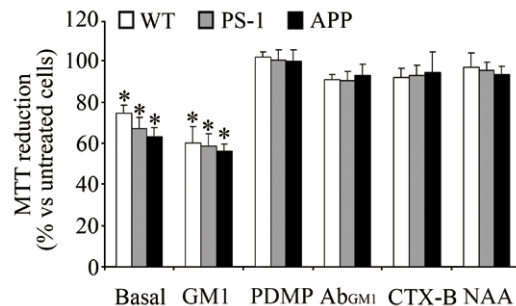


Figure 26 GM1 modulates A $\beta$ 42-induced cytotoxicity. Aggregate cytotoxicity in FAD and WT fibroblasts was assessed using the MTT assay. Cells were GM1-enriched (GM1), GM1-depleted (PDMP) or incubated for 20 min in the absence or presence of Ab<sub>GM1</sub>, CTX-B or NAA, prior to treatment with 1.0  $\mu$ M A $\beta$ 42 aggregates for 24 h at 37 °C. Cell viability was expressed as a percentage of MTT reduction in treated cells compared to corresponding untreated cells, where it was assumed to be 100%.

### 3.2.6 GM1 mediates A $\beta$ 42-induced Ca $^{2+}$ dyshomeostasis, lipid peroxidation and cytotoxicity in rat cortical neurons

We next investigated the effects of A $\beta$ 42 oligomers on intracellular Ca $^{2+}$  content and membrane lipoperoxidation in cultured rat cortical neurons with varying GM1 content. A moderate increase in membrane GM1 content, as assessed by confocal microscopy using Ab<sub>GM1</sub> antibodies (Fig. 27A), resulted in a sharper increase in cytosolic Ca $^{2+}$  (Fig. 27B) and membrane oxidation (Fig. 27C) in neurons, compared to that observed in A $\beta$ 42-exposed cells with basal GM1 content (Fig. 27B,C). In contrast, following GM1 depletion by PDMP treatment, the binding of Ab<sub>GM1</sub> to raft monosialoganglioside and sialic acid hydrolysis by NAA precluded the increase in intracellular Ca $^{2+}$  (Fig. 27B) and lipoperoxidation of the cell membrane (Fig. 27C). No change in cytosolic Ca $^{2+}$  levels was observed when rat neurons, in the absence of A $\beta$ 42 oligomers, were pre-treated so as to modulate GM1 content, exposure or charge. Moreover, membrane oxidation was prevented by culturing cells in a Ca $^{2+}$ -free medium, suggesting that the influx of extracellular Ca $^{2+}$  is involved in A $\beta$ 42 oligomer-induced lipid peroxidation (Fig. 27C).

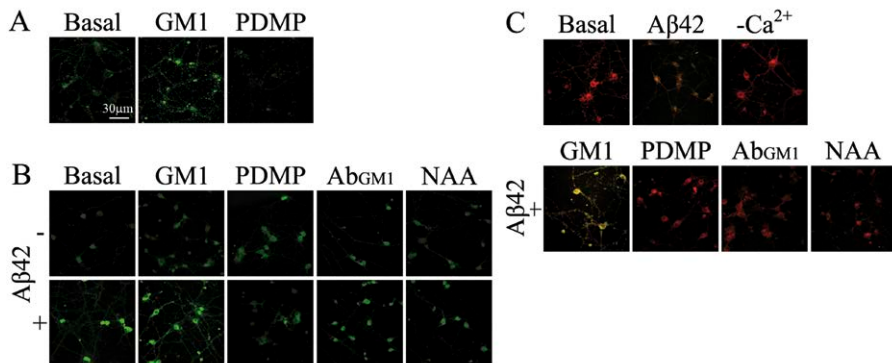


Figure 27. GM1 depletion reduces A $\beta$ 42-induced Ca $^{2+}$  dyshomeostasis and membrane lipoperoxidation in rat cortical neurons. (A) Representative confocal microscope images of GM1 content in neurons under basal conditions, or following treatment with 100  $\mu$ M GM1 or 25  $\mu$ M PDMP for 24 h at 37 °C. (B) Representative confocal microscope images of cytosolic Ca $^{2+}$  levels in neurons, under basal conditions or following treatment with GM1, PDMP, Ab $\beta$ GM1 or NAA, exposed to 5.0  $\mu$ M A $\beta$ 42 aggregates for 0 (-) and 30 (+) min at 37°C. (C) Representative confocal microscope images of lipid peroxidation in cells under basal conditions or pre-incubated with GM1, PDMP, Ab $\beta$ GM1 or NAA, and subsequently exposed to 5.0  $\mu$ M A $\beta$ 42 oligomers (+) for 30 min. As a control, cells were also exposed to A $\beta$ 42 aggregates in a Ca $^{2+}$ -free medium.

Next, we investigated whether changes in cytosolic calcium levels and membrane lipoperoxidation also resulted in neurotoxicity. As shown in Fig. 28, A $\beta$ 42 oligomers triggered a substantial decrease in MTT reduction, compared to untreated cells. Moreover, an increase in GM1 content triggered a slight increase in A $\beta$ 42 tox-

icity relative to that observed in neurons with basal GM1 content. In contrast, membrane GM1 depletion and GM1 charge modification improved neuron viability, confirming for the role of GM1 raft domains in amyloid-induced cytotoxicity.

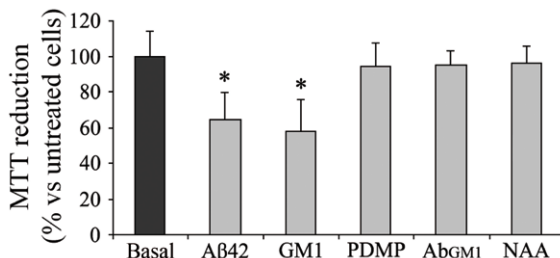


Figure 28. GM1 depletion reduces A $\beta$ 42-induced cytotoxicity in rat cortical neurons. MTT reduction assay carried out in cells pre-treated with GM1, PDMP, AbGM1 or NAA, prior to treatment with 5.0  $\mu$ M A $\beta$ 42 aggregates for 24 h at 37 °C. The reported values are means  $\pm$  S.D. of three independent experiments. \* $p\leq 0.05$ , significant difference vs relative control cells.

### 3.3 Results III

#### 3.3.1 Membrane lipid composition and its physicochemical properties define cell vulnerability to aberrant protein oligomers

Increasing evidence suggests that the interaction of misfolded protein oligomers with cell membranes is a primary event resulting in the cytotoxicity associated with many protein misfolding diseases, including neurodegenerative disorders.

In the third part of the result section are describe the relative contributions to toxicity of the physicochemical properties of both protein oligomers and the cell membrane with which they interact. We modulated the membrane content of cholesterol and the ganglioside GM1 in SH-SY5Y cells exposed to two types of oligomers of the prokaryotic protein HypF-N displaying different ultrastructural and cytotoxicity properties, and to oligomers formed by A $\beta$  peptide associated with Alzheimer's disease. The data reveal that the degree of toxicity of the oligomeric species results from a complex interplay between the structural and physicochemical features of both the oligomers and the cellular membrane.

#### 3.3.2 Membrane cholesterol content modulates oligomer cytotoxicity

We increased or decreased the membrane cholesterol content in human SH-SY5Y neuroblastoma cells by incubating the latter in solutions containing three different concentrations of either soluble cholesterol (Chol), methyl- $\beta$ -cyclodextrin ( $\beta$ -CD) or mevastatin (Mev) (Fig. 29);  $\beta$ -CD and Mev are known to remove cholesterol from the plasma membrane of cultured cells and to inhibit cholesterol biosynthesis, respectively (Endo *et al.*, 1976; Yancey *et al.*, 1996). Cell treatment with 0.2 or 0.5

mg/ml Chol significantly increased the content of membrane cholesterol (to  $13.01 \pm 0.92$  and  $15.66 \pm 1.53$   $\mu\text{g}/\text{mg}$  protein respectively) relative to untreated cells ( $9.85 \pm 1.13$   $\mu\text{g}/\text{mg}$  protein). Conversely, membrane cholesterol was significantly reduced by treatment with 1.0 or 2.0 mM  $\beta$ -CD (to  $6.75 \pm 0.49$  and  $5.78 \pm 0.23$   $\mu\text{g}/\text{mg}$  protein respectively) or with 5.0 or 10  $\mu\text{M}$  Mev (to  $7.82 \pm 0.42$  and  $6.58 \pm 0.35$   $\mu\text{g}/\text{mg}$  protein respectively) (Fig. 29A). These data were confirmed by confocal microscopy using the fluorescent probe filipin, whose fluorescence increases upon binding to cholesterol (Fig. 29B) (Drabikowski *et al.*, 1973).

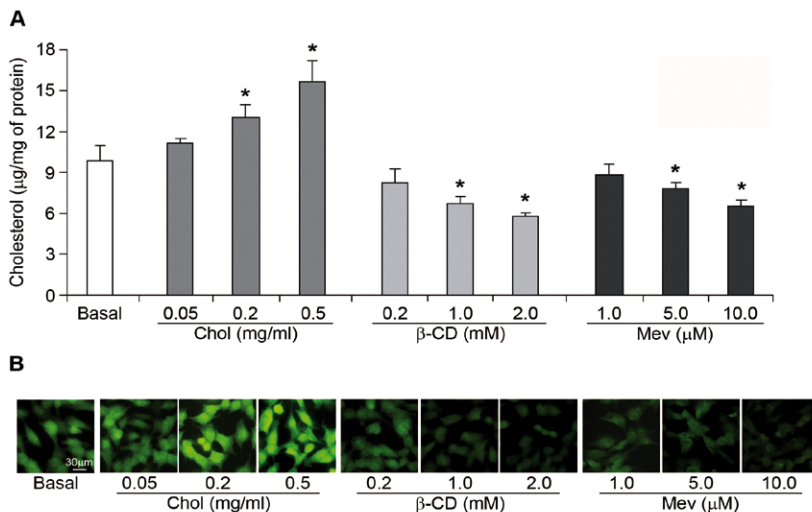


Figure 29. Modulation of cholesterol levels in human SH-SY5Y neuroblastoma cells. (A) The quantity of membrane cholesterol was determined by a fluorimetric assay. The asterisk indicates a significant difference relative to cells with basal cholesterol levels ( $p \leq 0.05$ ). (B) Representative confocal microscopy images showing the quantity of membrane cholesterol in SH-SY5Y cells, probed by the fluorescent dye filipin. The green fluorescence intensity in the images correlates with the amount of membrane cholesterol. In both panels the values reported are means  $\pm$  S.D. of four independent experiments.

Our recent results have shown that oligomers generated from the small prokaryotic protein HypF-N under different destabilising conditions (A or B) differ significantly in their sub-microscopic structural properties and cytotoxicities, though displaying similar morphological and tinctorial properties (Campioni *et al.*, 2010; Zampagni *et al.*, 2011). To assess the effects of the alteration of membrane cholesterol on the cytotoxicity of either form of HypF-N oligomer, we first evaluated their effects on cell viability parameters describing mitochondrial status and chromatin condensation using the MTT and Hoechst 33342 assays, respectively. As revealed by the MTT assay, Chol-enriched SH-SY5Y cells exposed to type A oligomers, which have been found to be highly toxic to cells with basal cholesterol content, showed significantly improved viability (Fig. 30), whereas similarly treated cells remained fully viable upon exposure to type B oligomers, that are also not toxic to cells with basal cholesterol content (Fig. 30).

## Amyloid Cytotoxicity and Membrane Lipid Composition

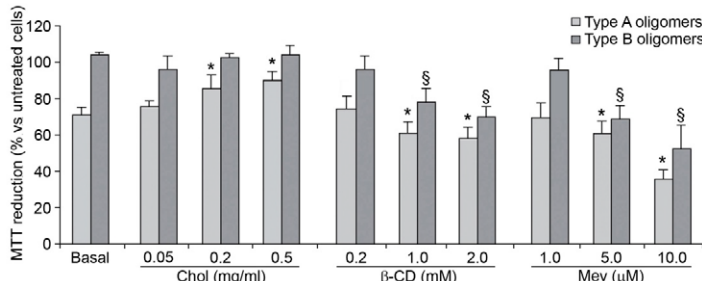


Figure 30. Cytotoxicity caused by type A and type B HypF-N oligomers in cells enriched with, or depleted in, cholesterol. MTT reduction assay carried out on basal, cholesterol-enriched (Chol) and cholesterol-depleted ( $\beta$ -CD or Mev) SH-SY5Y cells treated for 24 h with type A (light grey) or type B (dark grey) HypF-N oligomers (12  $\mu$ M monomer concentration). Cell viability was expressed as the percentage of MTT reduction in treated cells as compared to corresponding cells not exposed to the oligomers but treated with corresponding amounts of Chol,  $\beta$ -CD or Mev. The values reported are means  $\pm$  S.D. of six independent experiments. The symbols \* and  $\ddagger$  indicate significant differences relative to basal cells exposed to type A and B HypF-N oligomers, respectively ( $p \leq 0.05$ ).

By contrast, loss of membrane cholesterol following cell treatment with  $\beta$ -CD or Mev resulted not only resulted in a greater loss of cell viability in the presence of type A oligomers, but also in the appearance of significant cytotoxicity following the exposure to type B oligomers (Fig. 30). A similar modulation of oligomer cytotoxicity was observed for the cells with different cholesterol content when treated with A $\beta$ 42 oligomers (Fig. 31). Furthermore, we found that membrane cholesterol content did not influence the toxicity of H<sub>2</sub>O<sub>2</sub>. Indeed cholesterol-enriched, cholesterol-depleted or cells with basal content of cholesterol displayed the same degree of toxicity upon exposure to 150  $\mu$ M H<sub>2</sub>O<sub>2</sub>, suggesting that toxicity modulation by cholesterol is specific for protein oligomers (Fig. 31). By contrast, cell pre-incubation with 100  $\mu$ M vitamin E for 24 h induced a complete suppression of cytotoxicity following treatment with A $\beta$ 42 oligomers or H<sub>2</sub>O<sub>2</sub> (Fig. 31).

Taken together, these observations indicate that, in our system, oligomer toxicity depends not only on the type of oligomer but also on the amount of cholesterol in the cell plasma membrane.

The cells treated with Chol,  $\beta$ -CD and Mev were also stained with Hoechst 33342, a fluorescent marker that binds to the highly condensed chromatin present in the nuclei of apoptotic cells (Weisblum and Haenssler, 1974). Fluorescence microscopy images show that type A oligomers increased the apoptotic status of the SH-SY5Y cells, whereas neither type B oligomers nor the native protein had any effect, thus mirroring the data obtained with the MTT test (Fig. 32A,B). The images show that cholesterol modulates the apoptotic response induced by exposure to HypF-N oligomers; indeed, the cells enriched in cholesterol were resistant to type A oligomers, whereas the cells depleted in cholesterol by treatment with  $\beta$ -CD or Mev not only increased their apoptotic status when exposed to type A oligomers but also became apoptotic even in the presence of type B oligomers (Fig. 32C).

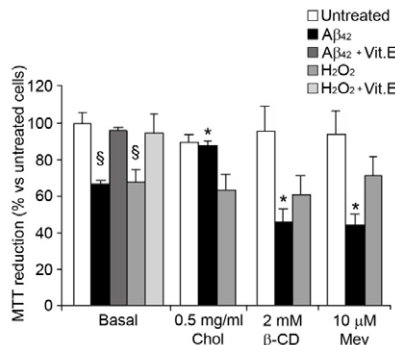


Figure 31. Cytotoxicity of A<sub>β</sub>42 oligomers and H<sub>2</sub>O<sub>2</sub> in cells enriched with, or depleted in, cholesterol. MTT reduction assay carried out on basal cells or on cells treated with 0.5 mg/ml Chol, 2.0 mM β-CD or 10 μM Mev and then exposed for 24 h to 12 μM A<sub>β</sub>42 or to 150 μM H<sub>2</sub>O<sub>2</sub> or pretreated for 48 h with 100 μM vitamin E prior to A<sub>β</sub>42 or H<sub>2</sub>O<sub>2</sub> exposure. The values reported are means ± S.D. of four independent experiments. Cell viability was expressed as the percentage of MTT reduction in treated cells as compared to corresponding cells not exposed to the oligomers but treated with corresponding amounts of Chol, β-CD, Mev. The symbols § and \* indicate significant differences relative to basal untreated cells and basal cells treated with A<sub>β</sub>42, respectively ( $p \leq 0.05$ ).

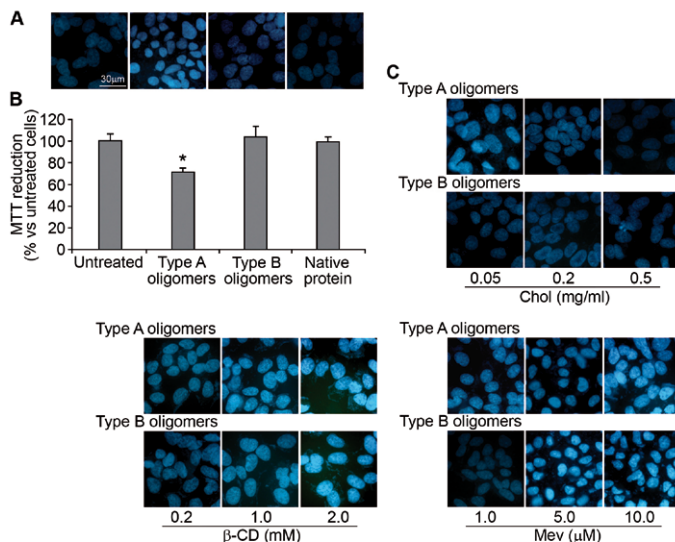


Figure 32. Chromatin condensation caused by type A or type B HypF-N oligomers in cells with different cholesterol content. Hoechst staining (A) and MTT reduction assay (B) carried out on basal cells exposed for 24 h to 12 μM type A or type B HypF-N oligomers or to native monomeric HypF-N. The blue fluorescence arises from Hoechst 33342 dye bound to apoptotic nuclei. The MTT values reported are means ± S.D. of six independent experiments. The symbol \* indicates significant differences relative to untreated cells ( $p \leq 0.05$ ). (C) Hoechst staining test showing apoptotic pathway activation induced by type A and B HypF-N oligomers in cells enriched with cholesterol (Chol) or depleted in cholesterol (β-CD or Mev) and exposed for 24 h to 12 μM type A or type B HypF-N oligomers.

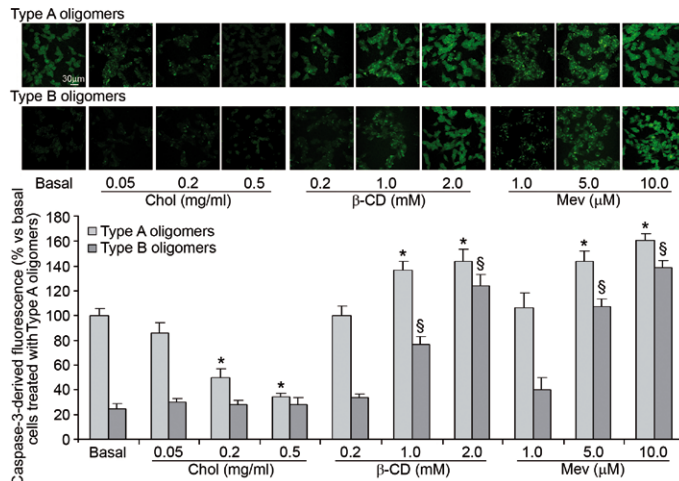


Figure 33. Caspase-3 activation caused by type A and type B HypF-N oligomers in cells enriched with, or depleted in, cholesterol. Representative confocal scanning microscopy images of basal, cholesterol-enriched and cholesterol-depleted cells showing caspase-3 activation following treatment for 24 h with type A (upper images) or type B (lower images) HypF-N oligomers (12  $\mu$ M). Caspase-3 activity was assessed using the fluorescent probe FAM-FLICA™ Caspase 3&7 (green). The presence and concentrations of Chol,  $\beta$ -CD and Mev, and the corresponding semi-quantitative values of the green fluorescence signal, are shown below each confocal image for type A (light grey) and type B (dark grey) oligomers. The values reported are means  $\pm$  S.D. of three independent experiments. The symbols \* and § indicate significant differences relative to basal cells exposed to type A and B HypF-N oligomers, respectively ( $p \leq 0.05$ ).

A similar trend was observed by measuring caspase-3 activity, a well recognised apoptotic marker. Indeed, when cells significantly enriched in membrane cholesterol were exposed to type A oligomers, a reduced caspase-3 activation was observed with respect to similarly treated cells with basal cholesterol content (Fig. 33). Under these conditions, type B oligomers induce no change in caspase-3 activity.

By contrast, type A oligomers triggered a significant increase in the activation of the apoptotic pathway in cells significantly depleted in membrane cholesterol relative to cells with basal cholesterol content (Fig. 33). In addition, similarly treated cells exposed to type B oligomers showed significant increases in caspase-3 activity, with respect to cells with basal cholesterol levels.

### 3.3.3 Membrane cholesterol modulates oligomer-induced alteration of intracellular $\text{Ca}^{2+}$ homeostasis and ROS levels

It is widely accepted that disruption of intracellular  $\text{Ca}^{2+}$  homeostasis and impairment of redox status are among the earliest biochemical consequences of the interaction of prefibrillar amyloid assemblies with cell membranes (Butterfield *et al.*, 2001; Hyun *et al.*, 2002; Kourie, 2001). We therefore investigated the effects of the two distinct types of HypF-N oligomers on the intracellular  $\text{Ca}^{2+}$  content and reactive oxygen

species (ROS) production in SH-SY5Y neuroblastoma cells with different cholesterol levels using confocal microscopy. When cells significantly enriched in membrane cholesterol content were exposed to type A oligomers, a smaller rise in cytosolic  $\text{Ca}^{2+}$  (Fig. 34A) and ROS (Fig. 34B) levels was observed with respect to cells with basal cholesterol content that were treated similarly. Under these conditions, type B oligomers do not induce any change in free  $\text{Ca}^{2+}$  or ROS, although type A oligomers were found to cause significant increases in the levels of both these species (Fig. 34A,B) in cells depleted in membrane cholesterol by treatment with 1.0 or 2.0 mM  $\beta$ -CD or with 5.0 or 10  $\mu\text{M}$  Mev relative to cells with basal cholesterol content. In addition, cells treated similarly exposed to type B oligomers showed significant increases in intracellular  $\text{Ca}^{2+}$  (Fig. 34A) and ROS (Fig. 34B), with respect to cells with basal cholesterol levels.

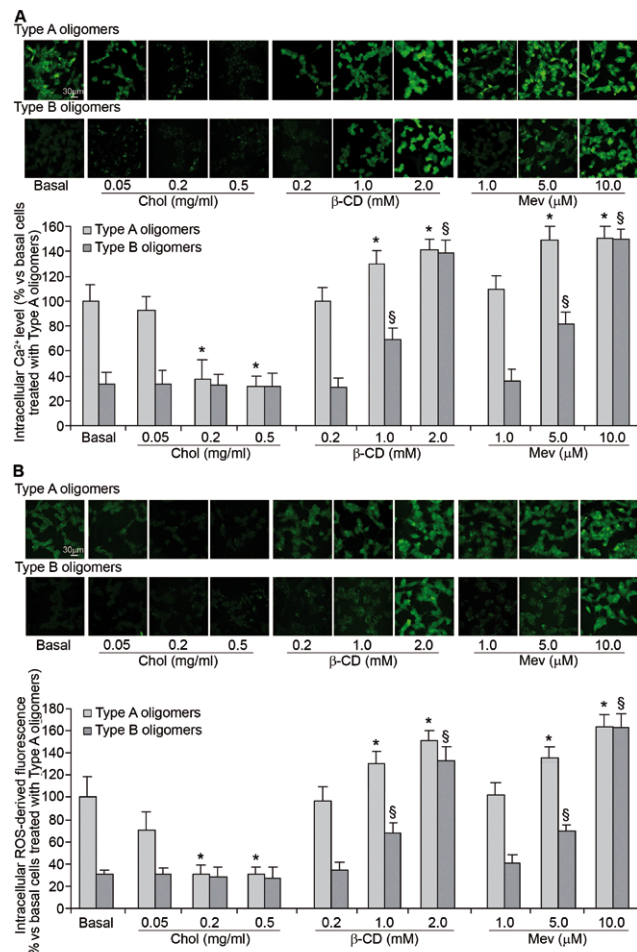


Figure 34. Cytosolic  $\text{Ca}^{2+}$  spikes and ROS production in cells with different cholesterol content exposed to type A and type B HypF-N oligomers. (A) Representative confocal scanning microscopy images of basal, cholesterol-enriched (Chol) and cholesterol-depleted ( $\beta$ -CD or

## Amyloid Cytotoxicity and Membrane Lipid Composition

Mev) cells showing levels of intracellular free Ca<sup>2+</sup> (A) or intracellular ROS production (B) following treatment for 1 h with type A (upper images) or type B (lower images) HypF-N oligomers (12 µM). The corresponding semi-quantitative values of the green fluorescence signal, are shown below each confocal image for type A (light grey) and type B (dark grey) oligomers. The symbols \* and § indicate significant differences relative to basal cells exposed to type A and B HypF-N oligomers, respectively ( $p\leq 0.05$ ).

To investigate whether or not the alteration of Ca<sup>2+</sup> levels triggered the apoptotic pathway, we measured caspase-3 activation in cholesterol-depleted cells exposed to aggregates either in the presence of the intracellular Ca<sup>2+</sup> chelator BAPTA-AM or in Ca<sup>2+</sup>-free medium. The early (3 h) increase in caspase-3 activity, following the addition of both types of oligomers, was prevented when the cells were pre-treated for 30 min with 10 µM BAPTA-AM or cultured in a Ca<sup>2+</sup>-free medium, suggesting a primary causative role for the influx of extracellular Ca<sup>2+</sup> in the apoptotic pathway (Fig. 35).

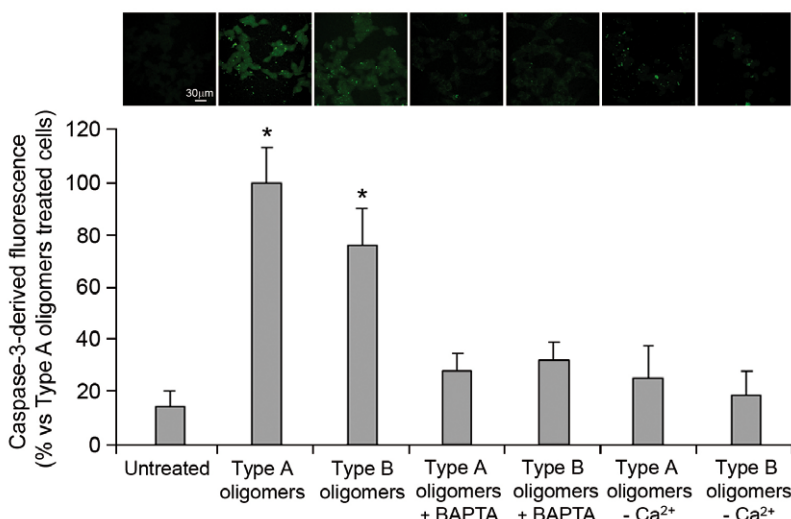


Figure 35. Ca<sup>2+</sup>-dependent caspase-3 activation induced by type A and type B HypF-N oligomers. Representative confocal scanning microscopy images showing caspase-3 activation in cholesterol-depleted cells (2.0 mM β-CD) exposed for 3 h to no oligomers, 12 µM type A or type B HypF-N oligomers after pre-treatment with 10 µM BAPTA-AM for 30 min or in culture media with or without free Ca<sup>2+</sup>. The corresponding semi-quantitative values of the signals, are shown below each confocal image. The values reported are means ± S.D. of three independent experiments. The symbol \* indicates significant differences relative to cholesterol-depleted cells treated with no oligomers ( $p\leq 0.05$ ).

### 3.3.4 Cholesterol levels modulate membrane permeability to the oligomers

Next, we sought to assess whether the modulation of membrane cholesterol levels affected the ability of either oligomer type to interact with the plasma membrane of SH-SY5Y cells, triggering loss of membrane integrity and inducing membrane

permeabilization. We found that the previously reported ability of SH-SY5Y cells with basal content of cholesterol to internalise type A oligomers (Campioni *et al.*, 2010; Zampagni *et al.*, 2011) was significantly increased when SH-SY5Y cells were treated with the highest concentrations of  $\beta$ -CD or Mev; conversely, oligomer internalisation was significantly reduced in cells most enriched in membrane cholesterol (Fig. 36). In contrast, type B oligomers, found to be unable to cross the plasma membrane of basal SH-SY5Y cells, became increasingly internalised in cells treated with  $\beta$ -CD or Mev, but not with Chol, as assessed by confocal microscope analysis (Fig. 36).

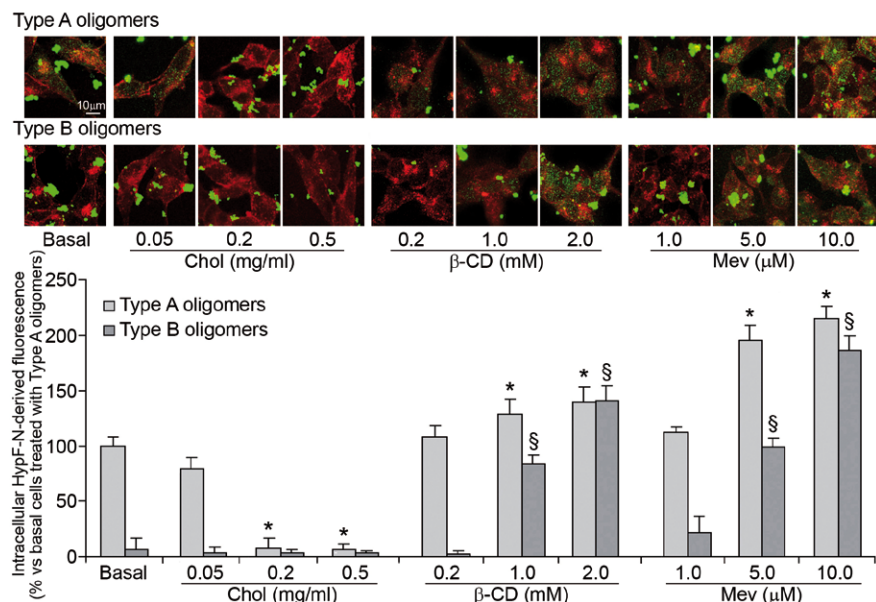


Figure 36. Interaction of type A and B HypF-N oligomers with the plasma membrane of cells enriched with, or depleted in, cholesterol. Representative confocal scanning microscopy z-stacks images of basal, cholesterol-enriched (Chol) and cholesterol-depleted ( $\beta$ -CD and Mev) cells treated for 1 h with 12  $\mu$ M type A (upper images) or type B (lower images) HypF-N oligomers. In all images, red and green fluorescence indicates cell profiles and HypF-N oligomers, respectively. The presence and concentrations of Chol,  $\beta$ -CD and Mev, and the corresponding semi-quantitative values of the green fluorescence signal arising from HypF-N oligomers inside the cells, are shown below each confocal image for type A (light grey) and B (dark grey) oligomers. The values reported are means  $\pm$  S.D. of three independent experiments. The symbols \* and § indicate significant differences relative to basal cells exposed to type A and B HypF-N oligomers, respectively ( $p \leq 0.05$ ).

The imaging of different optical sections (including basal, intermediate median and apical planes) of cholesterol-depleted cells revealed not only the presence of type A aggregates inside cells (median planes), but also of type B oligomers (Fig. 37A).

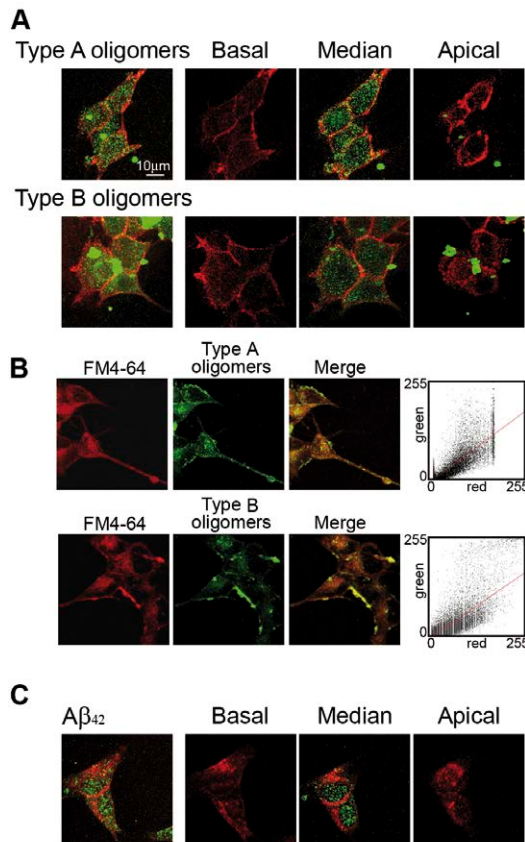


Figure 37. Aggregate internalisation by endocytosis, in cholesterol depleted cells. (A) Representative optical sections taken through 2.0 mM  $\beta$ -CD treated cells by confocal scanning microscopy after exposure for 1 h to HypF-N oligomers at basal, median and apical focal lengths, as indicated. (B) Representative confocal microscope images of live cells with reduced content of cholesterol incubated for 1 h with 5.0  $\mu\text{g}/\text{ml}$  FM4-64 (red) and with 5-FITC type A (upper images) and B (lower images) HypF-N oligomers (green). The overlay image shows that oligomers uptake is concomitant with the internalization of FM4-64, a lipophilic dye widely used as a marker of endocytotic vesicles. The scatter plots indicate the oligomers-vesicle colocalization pattern; the sampled pixels were plotted as a function of red (x axis) and green (y axis) fluorescence intensity. (C) Representative optical sections taken through 2.0 mM  $\beta$ -CD treated cells by confocal scanning microscopy after exposure for 1 h to  $\text{A}\beta_{42}$  oligomers at basal, median and apical focal lengths, as indicated.

Further experiments showed that both type A and B oligomers appeared to be internalized and sorted into endocytotic vesicles in live cells (Fig. 37B). Indeed, confocal laser microscopy showed a marked colocalization (by ~ 85%) of HypF-N 5-FITC-labelled oligomers with FM4-64, a widely used marker for endocytotic vesicles. In particular, when the images were merged, a large number of yellow areas representing the colocalization of endocytotic vesicles (red) with fluorescent oligomers

(green) was seen. The analysis over three different experiments yielded a similar degree of colocalization between endocytic vesicles and type A or type B oligomers in cholesterol depleted cells following treatment with 2.0 mM  $\beta$ -CD (Fig. 37B), as assessed by two different algorithms, the Pearson's correlation coefficient and the overlap coefficient according to Manders.

The modulation of the ability to internalise the oligomers by differently treated cells was also examined by measuring membrane permeability using calcein as a fluorescent probe. Analysis by confocal microscopy of SH-SY5Y cells pre-loaded with the calcein-AM fluorescent probe showed that cell exposure to type A oligomers resulted in a clear decrease of fluorescence intensity in cells with a high reduction of cholesterol content relative to those with basal cholesterol levels, indicating increased membrane permeabilization in the former (Fig. 38). By contrast, the reduction of calcein fluorescence was significantly less evident in cells that were enriched in cholesterol when exposed to type A oligomers, suggesting a reduced permeabilization. Moreover, membrane permeabilization was not observed in cells with normal or increased cholesterol content exposed to type B oligomers, whereas cells with a decreased cholesterol content exposed to the same oligomers showed a significant increase in membrane permeabilization with respect to cells with basal cholesterol levels (Fig. 38). Taken together, these results suggest that oligomer recruitment across the plasma membrane and the permeability of the membrane to cytosolic molecules are closely related to each other, and that membrane cholesterol modulation strongly affects the extent to which the different types of oligomers are able to induce both effects.

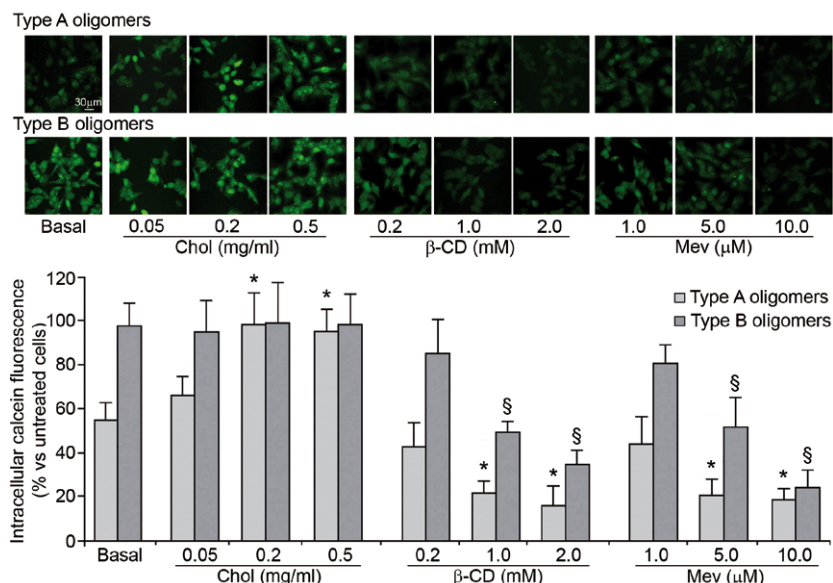


Figure 38. Membrane permeability induced by type A and B HypF-N oligomers in cells enriched with, or depleted in, cholesterol. Representative confocal scanning microscopy images showing basal, cholesterol-enriched (Chol) and cholesterol-depleted ( $\beta$ -CD and Mev) cells pre-loaded with calcein-AM and then exposed to type A (upper images) or type B (lower im-

ages) HypF-N oligomers (12 µM). The presence and concentrations of Chol, β-CD and Mev, and the corresponding semi-quantitative values of the calcein fluorescence intensity, are shown below each confocal image for type A (light grey) and B (dark grey) oligomers. The values reported are means ± S.D. of three independent experiments. The symbols \* and § indicate significant differences relative to basal cells exposed to type A and B HypF-N oligomers, respectively ( $p \leq 0.05$ ).

### 3.3.5 Membrane GM1 affects the cytotoxic and permeabilizing effects of HypF-N oligomers

Several studies have indicated that monomeric and oligomeric A $\beta$  bind preferentially to GM1, a monosialoganglioside that is abundant in neuronal cell membranes, particularly in lipid rafts. Binding to GM1 has also been found to stimulate fibril formation by A $\beta$  peptides (Ariga *et al.*, 2001; Kakio *et al.*, 2002; Malchiodi-Albedi *et al.*, 2010; Matsuzaki *et al.*, 2010; McLaurin *et al.*, 1998; Wakabayashi and Matsuzaki, 2007; Wang *et al.*, 2005); similar effects have been reported for other peptides such as amylin (Wakabayashi and Matsuzaki, 2009) and salmon calcitonin (sCTO) (Diociaiuti *et al.*, 2006). In addition, treatment with neuraminidase (NAA), which removes the sialic acid moiety from gangliosides, has been reported to inhibit sCTO neurotoxicity and its associated biochemical modifications (Malchiodi-Albedi *et al.*, 2010). Here, we studied the effects of membrane GM1 modulation on the cytotoxicity of either type of HypF-N oligomers. To this end, we incubated separate batches of SH-SY5Y cells with GM1 from bovine brain or with D-threo-1-phenyl-2-decanoylamino-3-morpholino-1-propanol (PDMP), a glucosylceramide synthase inhibitor that blocks the natural synthesis of GM1 (Tamboli *et al.*, 2005). Treatment of SH-SY5Y cells with GM1 significantly increased the GM1 content in the cell membrane, whereas PDMP treatment significantly reduced the membrane GM1 level, as assessed by dot blot, flow cytometry and confocal microscopy analyses using anti-GM1 antibodies and cholera toxin subunit B (CTX-B) (Fig. 39). The specificity of our antibodies to GM1 was confirmed by the lack of cross-reactivity with GD1a and GT1b neuronal gangliosides, as shown by dot blot analysis (Fig. 39, top right).

In our cell model, we found that the increase in membrane GM1 did not modify substantially the toxicity of type A oligomers, whereas it caused type B oligomers to become significantly toxic and able to induce caspase-3 activation (Fig. 40A,B). Conversely, a decrease in GM1 by cell treatment with PDMP or NAA did not modify cell resistance to type B oligomers, but suppressed cell vulnerability to type A oligomers (Fig. 40A;B).

A similar trend was observed when cells with different GM1 content were treated with A $\beta$ 42 aggregates (Fig. 41), suggesting that amyloid cytotoxicity generically depends on the GM1 content in the cell plasma membrane. By contrast, the modulation of membrane GM1 did not affect the toxicity of 150 µM H<sub>2</sub>O<sub>2</sub>, supporting a specific involvement of membrane GM1 in amyloid oligomer cytotoxicity (Fig. 41).

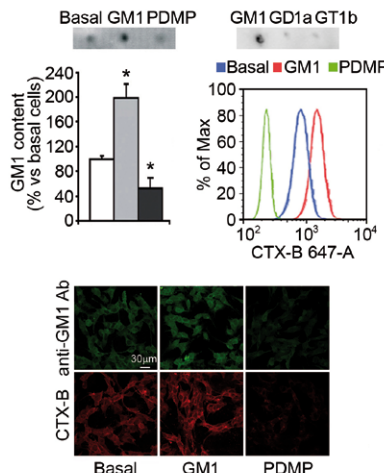


Figure 39. Dot-blot and the corresponding densitometric analysis (*top, left*) of the GM1 content in the membrane fraction of untreated cells or of cells pre-treated with 32  $\mu$ M GM1 or 25  $\mu$ M PDMP. The specificity of the antibodies to GM1 is shown by the lack of cross-reactivity to GD1a and GT1b gangliosides (dot-blot on the right). Flow cytometric analysis (*top, right*) of membrane GM1 content in untreated cells (blue) or in cells pre-treated with GM1 (red) or PDMP (green). After GM1 modulation, single-cell suspensions were incubated with the fluorescent probe CTX-B. The confocal microscopy images (*bottom*) show the cell surface GM1 distribution probed by anti-GM1 antibodies (green) or the CTX-B conjugate (red).

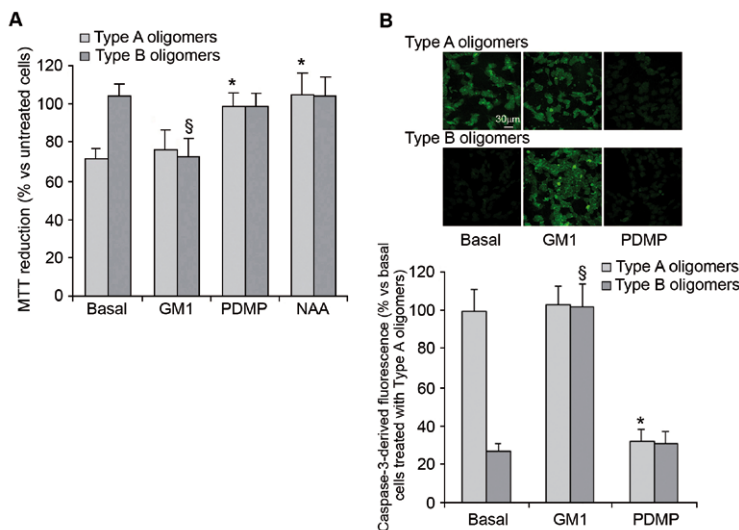


Figure 40. Cytotoxicity and caspase-3 activation caused by type A and type B HypF-N oligomers in cells enriched with, or depleted in, GM1. (A) MTT reduction assay carried out on untreated (basal), GM1-enriched (GM1), GM1-depleted (PDMP) and sialic-acid-depleted (NAA) cells exposed for 24 h to type A (light grey) or type B (dark grey) HypF-N oligomers

## Amyloid Cytotoxicity and Membrane Lipid Composition

(12  $\mu$ M). Cell viability was expressed as the percentage of MTT reduction in treated cells as compared to corresponding cells not exposed to the oligomers but treated with corresponding amounts of GM1, PDMP or NAA. The values reported are means  $\pm$  S.D. of three independent experiments. The symbols \* and § indicate significant differences relative to basal cells exposed to type A and B HypF-N oligomers, respectively ( $p \leq 0.05$ ). (B) Representative confocal scanning microscopy images and the corresponding semi-quantitative values of the fluorescent signals showing caspase-3 activation in untreated (basal), GM1-enriched (GM1) or GM1-depleted (PDMP) cells. Caspase-3 activity was assessed using the fluorescent probe FAM-FLICA™ Caspase 3&7 (green).

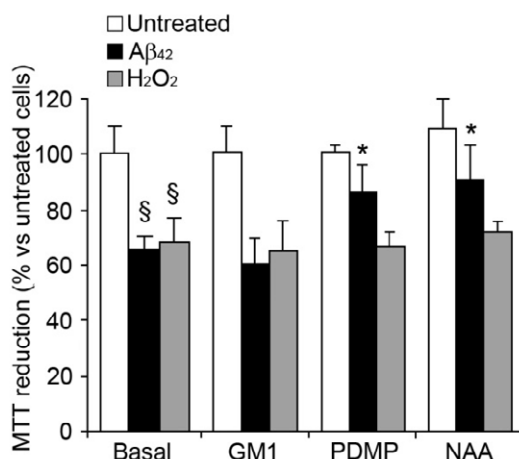


Figure 41. Cytotoxicity of  $\text{A}\beta_{42}$  oligomers and  $\text{H}_2\text{O}_2$  in cells enriched with, or depleted in GM1. MTT reduction assay carried out on GM1-enriched (GM1), GM1-depleted (PDMP) and sialic-acid-depleted (NAA) cells exposed for 24 h to 12  $\mu$ M  $\text{A}\beta_{42}$  or 150  $\mu$ M  $\text{H}_2\text{O}_2$ . The values reported are means  $\pm$  S.D. of four independent experiments. Cell viability was expressed as the percentage of MTT reduction in treated cells as compared to corresponding cells not exposed to the oligomers but treated with corresponding amounts of GM1, PDMP or NAA. The symbols § and \* indicate significant differences relative to basal untreated cells and basal cells treated with  $\text{A}\beta_{42}$ , respectively ( $p \leq 0.05$ ).

As with the results obtained by modulating the content of membrane cholesterol, these findings were confirmed by cell permeability data. Indeed, SH-SY5Y cells with increased GM1 content showed a significantly higher internalisation of type B oligomers into the cells and an enhanced membrane permeability to calcein with respect to cells with basal levels of GM1 (Fig. 42A,B). By contrast, cells pre-treated with PDMP or NAA displayed a significantly reduced entry of type A oligomers into the cells and a reduced membrane permeability to calcein with respect to cells with basal levels of GM1 (Fig. 42A,B).

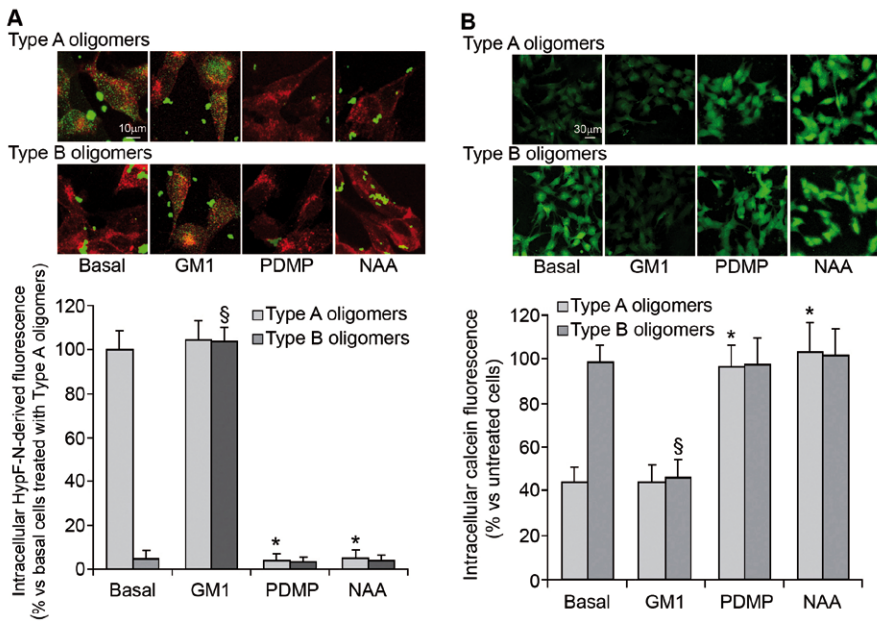


Figure 42. Penetration of, and membrane permeability induced by, type A and type B HypF-N oligomers in cells with altered GM1 content. (A) Representative confocal scanning microscopy images of basal, GM1-enriched (GM1), GM1-depleted (PDMP) and sialic-acid-depleted (NAA) cells exposed for 1 h to type A (upper images) or type B (lower images) HypF-N oligomers (12  $\mu$ M). In all images, red and green fluorescence indicates cell profiles and HypF-N oligomers, respectively. The semi-quantitative values of the green fluorescence intensity arising from HypF-N oligomers inside the cells are shown below each confocal image for type A (light grey) and type B (dark grey) oligomers. The values reported are means  $\pm$  S.D. of three independent experiments. (B) Representative confocal microscopy images showing basal, GM1-enriched (GM1), GM1-depleted (PDMP) and sialic-acid-depleted (NAA) cells pre-loaded with calcein-AM and then exposed to type A (upper images) or type B (lower images) HypF-N oligomers (12  $\mu$ M). The semi-quantitative values of the calcein fluorescence are shown below each confocal image for type A (light grey) and type B (dark grey) oligomers. The values reported are means  $\pm$  S.D. of three independent experiments. In both panels the symbols \* and § indicate significant differences relative to basal cells exposed to type A and type B HypF-N oligomers, respectively ( $p \leq 0.05$ ).

### 3.3.6 GM1, rather than cholesterol, plays a dominant role in oligomer cytotoxicity and membrane permeability

The observation of the opposite effects of membrane cholesterol and GM1 on the cytotoxicity of oligomers, and on their ability to interact with, and to permeabilize, the cell membrane, prompted us to explore the relative contributions of the two lipids to the overall effects described above. Initially, we modified the content of membrane cholesterol by incubating the cells in the presence of the different concentrations of Chol,  $\beta$ -CD or Mev used in the experiments reported above, and then

## Amyloid Cytotoxicity and Membrane Lipid Composition

evaluated the GM1 content in their plasma membrane. Cholesterol enrichment resulted in a dose-dependent decrease of membrane GM1 with respect to untreated cells, as assessed by flow cytometry analysis (Fig. 43A). In accord with these findings, confocal microscopy and dot blot analyses showed a marked decrease in the membrane content of GM1 (by ~ 30%) in cells with the highest Chol concentration relative to basal cells (Fig. 43B,C).

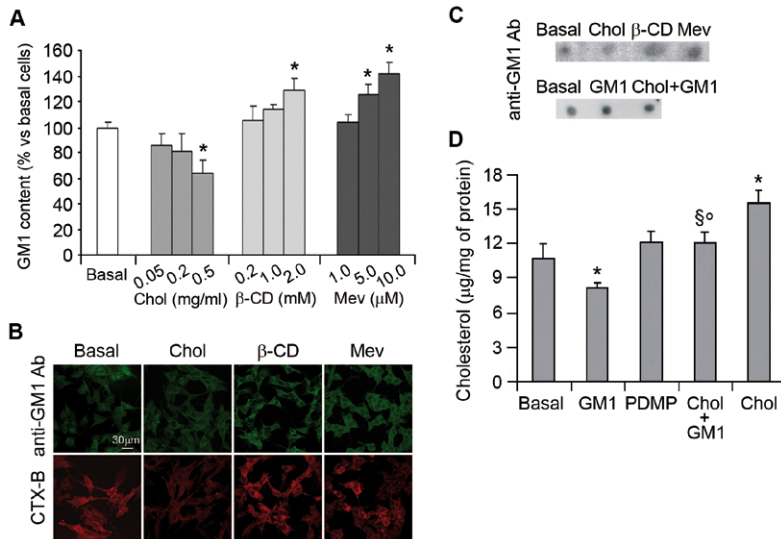


Figure 43. (A) Flow cytometric analysis of membrane GM1 content in basal, cholesterol-enriched (Chol) and cholesterol-depleted ( $\beta$ -CD or Mev) cells. (B) Representative confocal microscopy analysis of the cell surface GM1 distribution probed by anti-GM1 antibodies (green) or by the fluorescent CTX-B conjugate (red). (C) Dot blot analysis of the GM1 content in the membrane fraction of untreated cells (basal) or of cells treated with 0.5 mg/ml Chol, 2.0 mM  $\beta$ -CD, 10  $\mu$ M Mev, 32  $\mu$ M GM1 or with a mixture of 0.5 mg/ml Chol and 32  $\mu$ M GM1. (D) Membrane cholesterol in untreated cells (basal) or in cells pre-treated with 32  $\mu$ M GM1, 25  $\mu$ M PDMP, 0.5 mg/ml Chol and 32  $\mu$ M GM1 or 0.5 mg/ml Chol. The symbols \*, †, ‡ indicate a significant difference relative to basal, GM1 and Chol treated cells, respectively ( $p\leq 0.05$ ).

Conversely, cholesterol depletion following cell treatment with  $\beta$ -CD or Mev determined an inverse modulation of GM1, whose levels were significantly increased after exposure to the highest concentrations of  $\beta$ -CD (by ~ 30%) or Mev (by ~ 40%) (Fig. 43A,B,C). In a separate set of experiments, we measured the levels of cholesterol in cells with different GM1 content following treatment with GM1 or PDMP. We found that the increase in the GM1 level significantly decreased the content of cholesterol in the cell membrane (by ~ 25%) as compared to that measured in untreated cells; conversely, the cholesterol content was found to be slightly increased (by ~ 15%) in cells depleted in GM1 (Fig. 43D). These data indicate that the apparent biological effects of the perturbation of the levels of either lipid could be the result, at least in part, of the alteration of the other.

We therefore sought to assess the effect of the modification of both cholesterol and GM1 levels in the same cells. Cell exposure to both Chol and GM1 resulted in a remarkable increase of the GM1 content (by ~ 55%), as assessed by densitometric analysis of dot-blots (Fig. 43C) and a slight increase in cholesterol levels (by ~ 10%), as assessed by the fluorimetric assay (Fig. 43D). In particular, in cells treated with both lipids, the cholesterol content was significantly higher or lower relative to cells treated only with GM1 or Chol, respectively. These cells were significantly more susceptible to, and permeabilised by, type B oligomers with respect to basal cells (Fig. 44A,B); by contrast, loss of membrane cholesterol and sialic acid upon treatment with both Mev and NAA resulted in a significant decrease of cell vulnerability to, and permeabilisation by, type A oligomers *versus* basal cells (Fig. 44A,B). Accordingly, cholesterol and GM1 depletion following treatment with both Mev and PDMP, respectively, suppressed type A oligomer toxicity (Fig. 44A). Taken together, the two sets of data indicate that GM1, rather than cholesterol, plays a dominant role in mediating HypF-N oligomer cytotoxicity and that the effects observed by modifying the cholesterol content in the cell membrane can, at least in part, be the result of the associated inverse modulation of GM1.

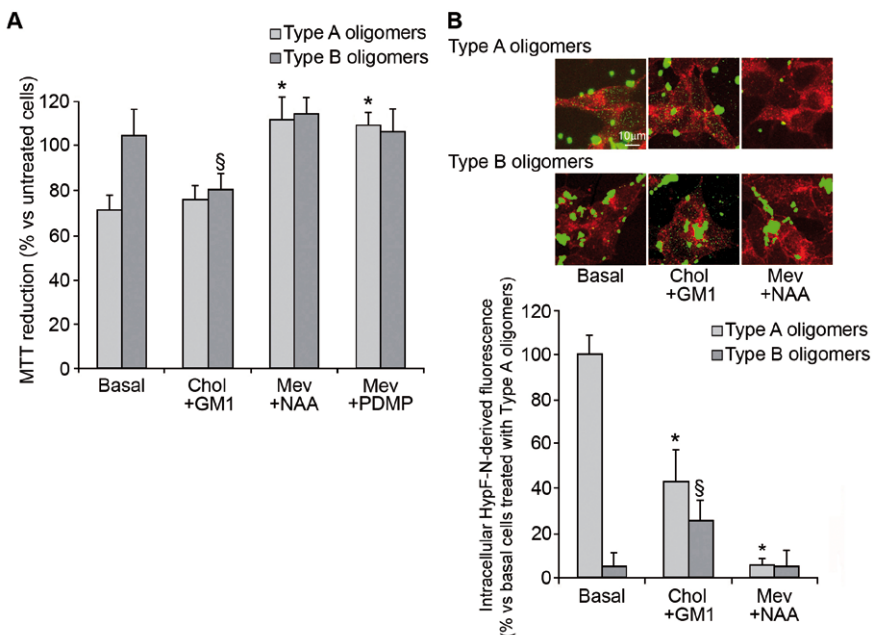


Figure 44. Cytotoxicity and penetration of type A and type B HypF-N oligomers in cells with altered content of both cholesterol and GM1. (A) MTT reduction assay in untreated cells (basal), in cells treated with both 0.5 mg/ml cholesterol and 32  $\mu$ M GM1 (Chol+GM1), in cells depleted both in cholesterol and in sialic acid using 10  $\mu$ M Mev, 117 mU/ml of *V. cholerae* NAA and 33 mU/ml of *A. ureafaciens* NAA (Mev+NAA), or in cells depleted both in cholesterol and in GM1 using 10  $\mu$ M Mev and 25  $\mu$ M PDMP (Mev+PDMP) and then exposed for 24 h to type A (light grey) or type B (dark grey) HypF-N oligomers (12  $\mu$ M). Cell viability was expressed as the percentage of MTT reduction in treated cells as compared to corresponding

cells not exposed to the oligomers but treated with corresponding amounts of Chol and GM1, Mev and NAA, Mev and PDMP. The values reported are means  $\pm$  S.D. of six independent experiments. (B) Representative confocal scanning microscopy images of untreated (basal), cholesterol- and GM1-enriched (Chol+GM1), or cholesterol- and sialic acid-depleted (Mev+NAA) cells exposed for 1 h to type A (upper images) or type B (lower images) HypF-N oligomers (12  $\mu$ M). In all images, red and green fluorescence indicates cell profiles and HypF-N oligomers, respectively. The presence of additives and the corresponding semi-quantitative values of the green fluorescence intensity arising from HypF-N oligomers inside the cells are shown below each confocal image for type A (light grey) and type B (dark grey) oligomers. The values shown are means  $\pm$  S.D. of three independent experiments. In both panels the symbols \* and § indicate significant differences relative to basal cells exposed to type A and B HypF-N oligomers, respectively ( $p \leq 0.05$ ).

### 3.4 Results IV

#### 3.4.1 Neuronal differentiation of human mesenchymal stromal cells increases their resistance to A $\beta$ 42 aggregate toxicity

Cell therapy is a promising approach for the treatment of neurodegenerative conditions such as Alzheimer's and Parkinson's diseases. However, the presence of toxic aggregates in tissue raises the question of whether grafted stem cells are susceptible to amyloid toxicity before they differentiate into mature neurons. To address this question, in this fourth part of the result section has been investigated the relative vulnerability of human mesenchymal stromal cells and their neuronally differentiated counterparts to A $\beta$ 42 oligomers and whether susceptibility correlates with membrane GM1 content, a key player in oligomer toxicity. Our cell model was highly susceptible to aggregate toxicity, whereas neuronal differentiation induced resistance to amyloid species. This data correlated well with the content of membrane GM1, levels of which decreased considerably in differentiated cells. These findings extend our knowledge of stem cell vulnerability to amyloid species, which remains a controversial issue, and confirm that amyloid-GM1 interactions play an important role in cell impairment.

#### 3.4.2 Neuronal differentiation of hMSCs results in reduced levels of membrane GM1

A neuronally differentiated phenotype (hMSC-n) was induced in human mesenchymal stromal cells (hMSCs) isolated from iliac crest aspirates of young volunteers, as previously reported (Benvenuti *et al.*, 2006). Following cell treatment, hMSCs underwent a morphological shift from a flat, fibroblast-like phenotype to a neuronal-like one characterized by prominent process-like extensions and positive staining for neurofilament M (NF-M) (Fig. 45A).

Expression of the neuronal markers synaptophysin, tau and microtubule associated protein 2 (MAP 2) was also significantly increased in hMSC-n compared to hMSCs (Fig. 45B). Numerous studies have shown that different gangliosides and their expression levels are cell type-specific and tightly controlled during cell devel-

opment and differentiation (Ariga *et al.*, 2008). To this end, we investigated the membrane content of monosialoganglioside GM1 during stromal cell differentiation. Dot blot analysis revealed a significant decrease in membrane GM1 (by ~ 75%) in hMSC-n with respect to hMSCs (Fig. 45C). This finding was confirmed by confocal microscope analysis using anti-GM1 antibodies or cholera toxin subunit B (CTX-B) (Fig. 45C).

We previously demonstrated that membrane cholesterol content is significantly higher in retinoic-acid-differentiated SH-SY5Y neuroblastoma cells compared to undifferentiated controls (Cecchi *et al.*, 2008a). Accordingly, neuronal differentiation of hMSCs results in a significant increase in membrane cholesterol content (from  $34.24 \pm 5.75$  to  $55.92 \pm 7.87 \mu\text{g}/\text{mg}$  protein).

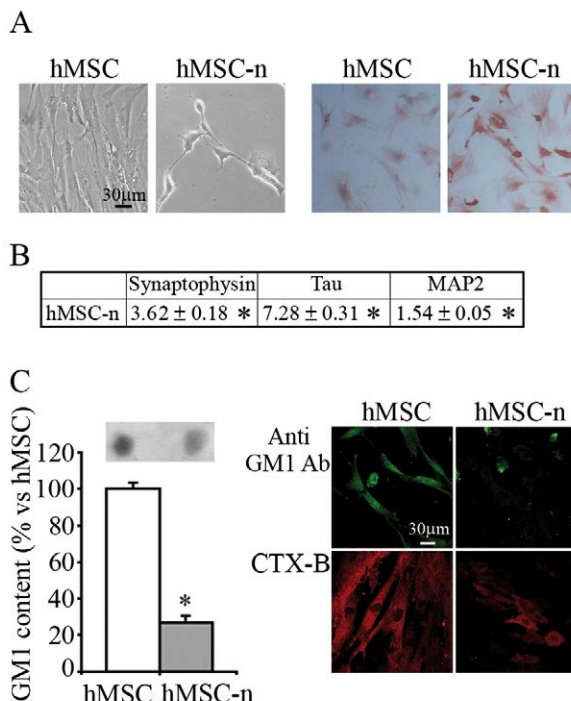


Figure 45. Neuronal differentiation reduces membrane GM1 levels in hMSC-n. A Left, Representative images of hMSCs and hMSC-n obtained by inverted phase contrast microscopy. Right, representative immunocytochemical staining of neurofilament M (NF-M) in hMSCs and hMSC-n. B Expression of neuronal markers in hMSC-n. The reported values (mean  $\pm$  s.e.) are representative of four independent experiments and indicate the increase in expression (fold) vs hMSCs, which was taken to be 1. \* Significant difference ( $p \leq 0.05$ ) vs. untreated cells. C Left, representative dot blot analysis and relative densitometric quantification of membrane GM1 content in hMSCs and hMSC-n. Right, representative confocal images showing cell surface distribution of GM1, probed with anti-GM1 antibodies (green) or with CTX-B conjugate (red). The reported values (mean  $\pm$  s.d.) are representative of three independent experiments. \*Significant difference ( $p \leq 0.05$ ) vs. untreated cells.

### 3.4.3 Neuronal differentiation of hMSCs reduces the interaction of A $\beta$ 42 oligomers with the cell surface

The interaction between amyloid aggregates and neuronal membranes is thought to play an important role in AD neuropathology (Stefani and Dobson, 2003; Stefani, 2007). In general, the idea that lipid bilayers affect protein/peptide aggregation, aggregate interaction with exposed cells and amyloid cytotoxicity has gained widespread acceptance (Ariga *et al.*, 2008; Arispe and Doh, 2002; Cecchi *et al.*, 2005). Similarly, recent evidence suggests that GM1 content plays a key role in modulating the interaction of amyloid oligomers with the cell membrane. Accordingly, different levels of membrane GM1 in undifferentiated hMSCs and differentiated hMSC-n prompted us to examine the effect of neuronal differentiation on the ability of exogenous A $\beta$ 42 oligomers to bind the cell surface. We used FRET microscopy to determine the intermolecular proximity of A $\beta$ 42 oligomers to membrane GM1 at the cell surface of hMSCs and hMSC-n (Kinoshita *et al.*, 2003). Interestingly, a stronger FRET signal was detected in hMSCs than in hMSC-n, suggesting greater proximity of A $\beta$ 42 oligomers to GM1 in the former compared to the latter (Fig. 46A). In line with this finding, the amount of A $\beta$ 42 oligomers inside cells increased quickly following addition of 10  $\mu$ M A $\beta$ 42 oligomers to the cell medium, reaching maximum levels after 30 min (Fig. 46B). Moreover, quantitative analysis of intracellular A $\beta$ 42 fluorescence showed that A $\beta$ 42 oligomers were internalized to a greater extent by undifferentiated cells than by neuronally differentiated counterparts (Fig. 46B). Imaging of different optical sections, including basal, apical and median planes of hMSCs and hMSC-n exposed to oligomers for 60 min, confirmed that more A $\beta$ 42 aggregates were present inside (median planes) hMSCs than in hMSC-n (Fig. 46C, *left panel*). We also found that A $\beta$ 42 internalization could be prevented by pre-incubating cells with anti-GM1 antibodies (Anti-GM1 Ab) (Fig. 46C, *right panel*). These findings tally with the recognized importance of GM1 as a key interaction site for amyloid oligomers at the membrane level.

### 3.4.4 Neuronal differentiation of hMSCs reduces A $\beta$ 42 oligomer-induced intracellular Ca $^{2+}$ dyshomeostasis and oxidative stress

The influx of Ca $^{2+}$  ions from the extracellular space into the cytosol and the generation of intracellular ROS are recognized as early biochemical modifications in cells exposed to amyloid oligomers (Canale *et al.*, 2006; Cecchi *et al.*, 2005; Demuro *et al.*, 2005; Orrenius *et al.*, 2003). Accordingly, we found that A $\beta$ 42 aggregates triggered a significant increase in intracellular Ca $^{2+}$  levels and ROS production in both hMSCs and hMSC-n, compared to unexposed control cells (Fig. 47A and B).

However, the increase in cytosolic Ca $^{2+}$  and ROS was significantly greater in undifferentiated cells than in neuronally differentiated counterparts. Moreover, the increase in 8-OH isoprostanate levels was much greater in hMSCs than in hMSC-n, following cell exposure to A $\beta$ 42 oligomers for 3 h (Fig. 47C). Overall, these findings suggest that neuronal differentiation of our stem cell model, which causes a decrease in membrane GM1, is associated with reduced susceptibility to Ca $^{2+}$  dyshomeostasis and lipid peroxidation upon exposure to toxic A $\beta$ 42 oligomers.

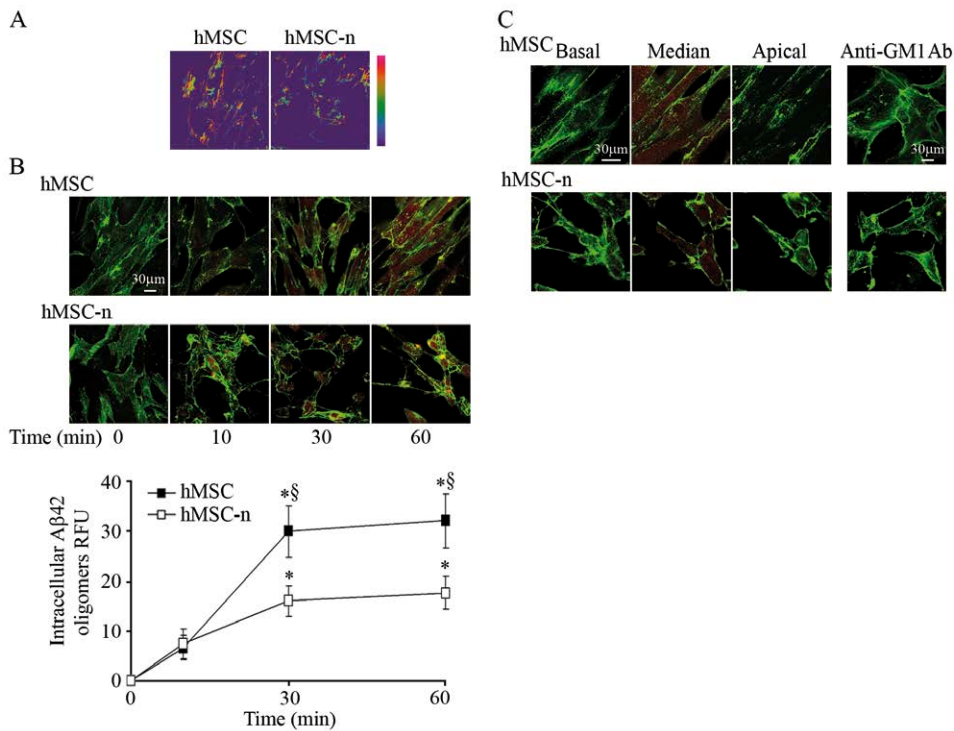


Figure 46. A Examples of FRET efficiency images, reflecting the colocalization of A $\beta$ 42 oligomers with GM1 in hMSCs and hMSC-n exposed to 10  $\mu$ M A $\beta$ 42-FAM for 30 min. B Representative confocal microscope images showing insertion of A $\beta$ 42 oligomers into the plasma membrane of hMSCs and hMSC-n exposed for differing lengths of time (0, 10, 30 and 60 min) to 10  $\mu$ M ADDLs. The plasma membrane profile was stained with fluorescein-conjugated WGA (green); A $\beta$ 42 aggregates were labelled with monoclonal anti-mouse 6E10 antibodies (red). The fluorescent intensity of intracellular A $\beta$ 42 oligomers was quantified and is shown below the images. C Left Optical sections (basal, median and apical focal lengths) of cells exposed for 60 min to 10  $\mu$ M A $\beta$ 42 oligomers. Right Representative confocal microscope images showing insertion of aggregates into the plasma membrane of hMSCs and hMSC-n pre-incubated for 20 min with 1:100 diluted polyclonal anti-GM1 antibodies prior to 30-min aggregate exposure. The reported values (mean  $\pm$  s.d.) are representative of three independent experiments. The symbols \* and § indicate significant differences vs. respective untreated cells and hMSC-n cells, respectively ( $p \leq 0.05$ ). A variable (10-22) number of cells were analyzed for each time point in all three experiments.

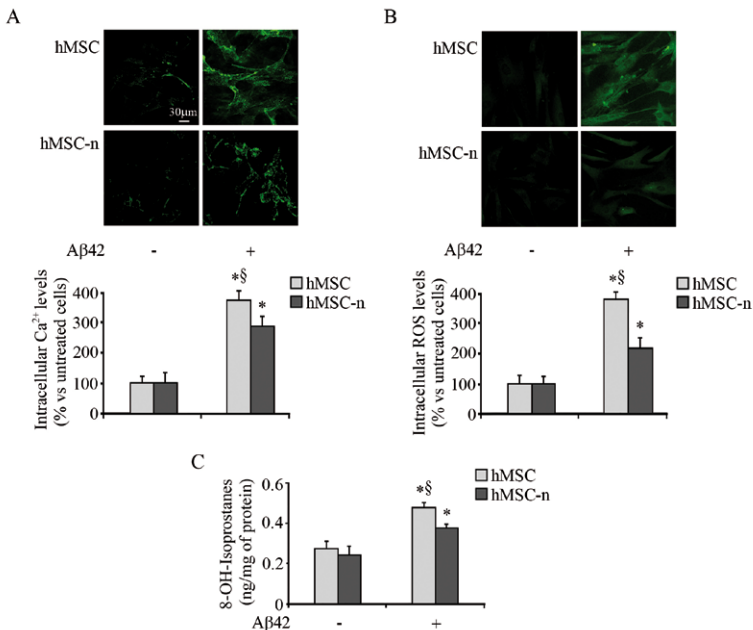


Figure 47 A Representative confocal microscope images showing intracellular  $\text{Ca}^{2+}$  levels in hMSCs and hMSC-n before and after exposure to 10  $\mu\text{M}$  A $\beta$ 42 oligomers for 10 min. B Representative confocal microscope images showing intracellular ROS levels in hMSCs and hMSC-n before and after exposure to 10  $\mu\text{M}$  A $\beta$ 42 oligomers for 10 min. C Lipid peroxidation was quantified by measuring 8-OH isoprostane levels in hMSCs and hMSC-n exposed to 10  $\mu\text{M}$  A $\beta$ 42 aggregates for 3 h. The values reported are mean  $\pm$  s.d. of three independent experiments. The symbols \* and § indicate significant differences ( $p \leq 0.05$ ) vs. untreated cells and hMSC-n, respectively.

### 3.4.5 Neuronal differentiation of hMSCs increases cell resistance to A $\beta$ 42 aggregates

It is widely accepted that impairment of function and viability in cells exposed to toxic amyloid aggregates results from early changes in membrane permeability and intracellular redox state. We therefore assessed the effect of neuronal differentiation and changes in membrane GM1 content on A $\beta$ 42 oligomer cytotoxicity, by analyzing cell viability parameters including mitochondrial status, chromatin condensation and activation of apoptosis. As revealed by the MTT assay, hMSC-n were more resistant than hMSCs when exposed to a wide range (0.1–50  $\mu\text{M}$ , monomer concentration) of A $\beta$ 42 oligomer concentrations (Fig. 48). The use of MTT data to plot a dose-response curve, which reached a plateau at the highest A $\beta$ 42 oligomer concentrations, allowed us to calculate the A $\beta$ 42 oligomer concentrations responsible for 50% of the observed effect (IC<sub>50</sub>). The IC<sub>50</sub> for hMSC-n was fifty fold higher (3.34  $\mu\text{M}$ ) than for hMSCs (0.06  $\mu\text{M}$ ). In addition, undifferentiated cells, but not their neuronally differentiated counterparts, displayed partial susceptibility to A $\beta$ 42 fibrils (10

$\mu\text{M}$ , monomer concentration), confirming the remarkable resistance of differentiated cells to A $\beta$ 42 aggregate-induced stress (Fig. 48). Furthermore, the absence of any cytotoxic effect in cells treated with the A $\beta$ 42-1 reverse peptide highlights the selectivity of the cellular response to A $\beta$ 42 aggregates. This differential susceptibility to amyloid oligomers was also observed by treating cells with 50  $\mu\text{M}$  PrP 106-126 (Fig 48). Moreover, treating cells with anti-GM1 antibodies prior to 10  $\mu\text{M}$  A $\beta$ 42 oligomer exposure improved cell viability, suggesting an important role for GM1 raft domains in amyloid-induced cytotoxicity (Fig. 48).

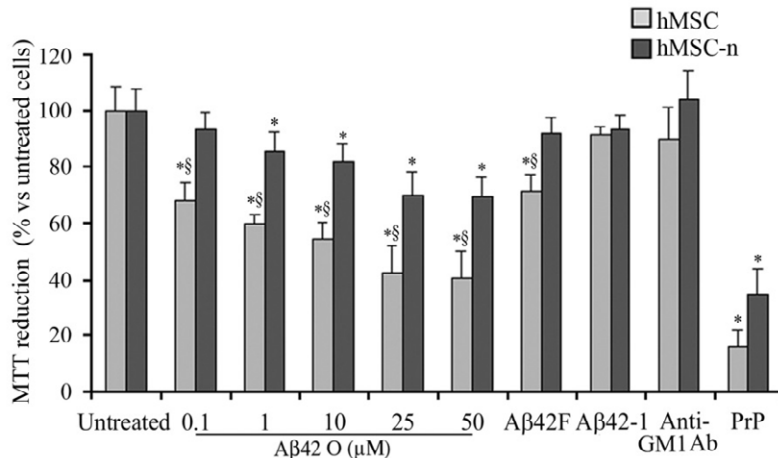


Figure 48. Neuronal differentiation of hMSCs protects against aggregates toxicity. Viability of hMSCs and hMSC-n exposed for 24 h to different concentrations of A $\beta$ 42 oligomers (0.1-50  $\mu\text{M}$ ), 10  $\mu\text{M}$  fibrils, 10  $\mu\text{M}$  A $\beta$ 42-1 reverse peptide or 50  $\mu\text{M}$  PrP 106-126. Values were calculated with respect to control experiments, which were carried out by culturing the same cells under the same conditions except that aggregates were replaced by vehicle. The reported values (mean  $\pm$  s.d.) are representative of three independent experiments carried out in triplicate. The symbols \* and § indicate significant differences vs. untreated cells and hMSC-n cells, respectively ( $p \leq 0.05$ ).

In contrast with 10  $\mu\text{M}$  A $\beta$ 42 oligomer-exposed hMSCs, negligible chromatin condensation was found in aggregate-exposed hMSC-n upon staining with Hoechst 33342, a fluorescent marker that binds to the highly condensed chromatin found in the nuclei of apoptotic cells (Figure 49B upper panel) (Cecchi *et al.*, 2008b). Treatment with anti-GM1 antibodies precluded apoptotic responses in both cell types (Figure 49B, right). Cells displayed a similar response with regards caspase-3 activity – a more specific apoptotic marker – when treated with 10  $\mu\text{M}$  A $\beta$ 42 oligomers or pre-treated with anti-GM1 antibodies prior to A $\beta$ 42 exposure (Fig 49B, lower panel). This data confirms that differentiated neuronal cells display greater resistance to A $\beta$ 42 oligomer toxicity and indicates that, in our model, cell impairment eventually culminates in apoptotic cell death, in agreement with previous findings in other cell systems exposed to different amyloid species (Cecchi *et al.*, 2005).

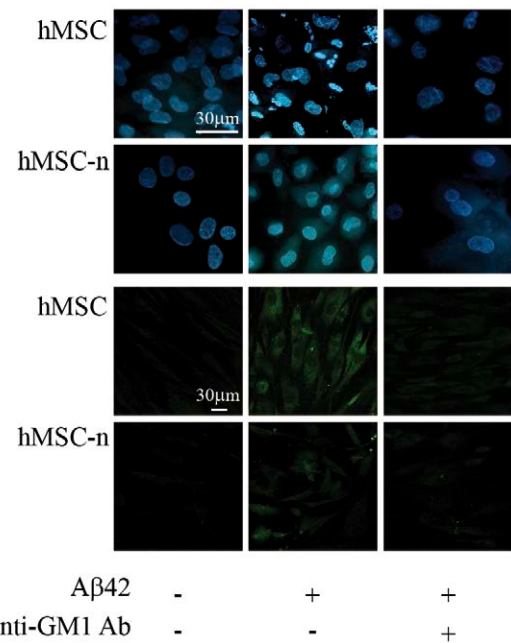


Figure 49. Neuronal differentiation of hMSCs increases cell resistance to A $\beta$ 42 aggregates. Left Hoechst staining (upper panel) and caspase-3 activation (lower panel) in hMSCs and hMSC-n, either untreated or exposed to 10  $\mu$ M A $\beta$ 42 oligomers for 24 h. Right Hoechst staining (upper panel) and caspase-3 activation (lower panel) in hMSCs and hMSC-n pre-incubated for 20 min with 1:100 diluted polyclonal anti-GM1 antibodies prior to 24-h oligomer exposure. All images were obtained using the same magnification.

## Discussion

### 4.1 A protective role for lipid raft cholesterol against amyloid-induced membrane damage in human neuroblastoma cells

In the present study we investigated whether membrane cholesterol can influence ADDL cytotoxicity to human neurotypic SH-SY5Y cells by modulating either the physical state of the cell membrane, mainly at the lipid raft level, or oligomer binding to the membrane itself, in most cases a key step in amyloid cytotoxicity. In PEG-cholesterol supplemented cells, the increase of plasma membrane cholesterol resulted in a reduced ADDL binding to the plasma membrane, as compared to control cells. Conversely, the same oligomers appeared to accumulate mostly at the cell plasma membrane when they were added to the culture medium of cells depleted in membrane cholesterol following treatment with  $\beta$ -CD or Mev. These results suggest that, in our neuronal cell model, the cholesterol content of the cell membrane is inversely correlated with the membrane perturbing effects of A $\beta$ 42 oligomers. These data agree with our previous findings, which show that neuroblastoma cells enriched in membrane cholesterol display higher resistance to A $\beta$ 42 oligomer toxicity than untreated or cholesterol-depleted cells (Cecchi *et al.*, 2008b). They are also consistent with previous reports showing that disruption of cholesterol homeostasis can be detrimental to cells because toxic A $\beta$  aggregates interact more easily with cholesterol-poor membranes (Arispe and Doh, 2002; Cecchi *et al.*, 2005; Cecchi *et al.*, 2008a; Yip *et al.*, 2001). In particular, our data agree with several reports indicating that the cholesterol content affects membrane physical features such as fluidity and density of lipid packing, hindering both aggregate recruitment at the cell membrane and membrane permeabilization (Arispe and Doh, 2002). In particular, the results we obtained in the presence of mevastatin -a specific inhibitor of cholesterol synthesis- support a cholesterol-dependent effect, rather than a generic lipid density-dependent effect at the plasma membrane level.

Previous reports suggest that A $\beta$  binding and aggregation, as detected by ThT or Congo Red staining, occur in lipid raft domains where it is favoured by clusters of the key component GM1 ganglioside (Yanagisawa, 2007; Williamson *et al.*, 2008). It has also been hypothesized that A $\beta$ 42 adopts an altered conformation upon binding to GM1 and that in such an altered conformation it can act as a seed for A $\beta$  fibrillogenesis in AD brain (Yanagisawa, 2007). Finally, previous findings indicate that GM1 clusters are affected by membrane cholesterol depletion (Fujita *et al.*, 2007). Actually, our confocal laser microscope analysis showed a marked ADDL-GM1 col-

ocalization on plasma membrane rafts in neuroblastoma cells. Furthermore, in our cell model, cholesterol-depleted lipid rafts displayed enhanced ADDL-GM1 colocalization with respect to control cells, whereas we found a significantly reduced ADDL binding to cholesterol-enriched rafts, as compared to control cells. Our data on ADDL-GM1 colocalization in cholesterol-enriched or -depleted cells agree with previously reported findings on the effect of cholesterol on amyloid aggregate binding to the cell membrane (Arispe and Doh, 2002; Kawahara *et al.*, 2000; Yip *et al.*, 2001) and suggest that a mild loss of neuronal membrane cholesterol results in an increased binding of ADDLs to neuronal lipid rafts.

There is no consensus on the steady state fraction of rafts in the cell membranes, their size, location and lipid/protein composition, which might reflect rapid raft dynamics accounting for intrinsic raft heterogeneity in different cultured or tissue cells. There are several procedures described in the literature allowing purification of lipid rafts and caveolae membranes, and the variability of the experimental result can depend on the method used. In this study we choose a widely used method to prepare membrane domains enriched in sphingolipids, monosialogangliosides and cholesterol (DRMs). This experimental approach provides a more appropriate mimic of the lipid rafts found *in vivo* than synthetic raft-like vesicles. However, whether, and to what extent, these isolated DRMs reflect the physical, chemical and biochemical organization of lipid rafts *in vivo* remains to be elucidated. Taking into account these caveats, we investigated the ability of ADDLs to interact with purified DRMs and the effect of such interaction on physical and morphological features of the latter.

Our anisotropy fluorescence measurements of sucrose density gradient-purified and flotillin-1-positive DRMs confirmed that there is an inverse relation between cholesterol content and membrane perturbing effects of ADDLs. The DPH probe partitions equally between the ordered and the disordered phases of membrane lipid domains (Lentz, 1989). It is evenly distributed throughout all the lipidic regions in the plasma membrane of a living cell (Companyó *et al.*, 2007; Lentz, 1993) and its location is similar in membranes with different content of cholesterol (Kaiser and London, 1998). Therefore, the cholesterol-induced effects on DPH fluorescence polarization here reported reflect differences in DPH motion, rather than in DPH distribution (Kaiser and London, 1998). By using such technique, we found that DRMs microdomains purified from cholesterol-enriched cells are less susceptible to the decrease of fluidity caused by A $\beta$  oligomers as compared to comparable preparations of DRMs purified from control cells. Conversely, the loss of cholesterol resulted in a higher susceptibility of disassembled lipid rafts, not only to A $\beta$ 42 oligomers but also to the A $\beta$ 42-1 reverse monomeric peptide. These results suggest that the more fluid the lipid raft membrane, the greater its ability to bind non-specifically A $\beta$ 42 and, possibly, other peptides. We therefore conclude that the presence of  $\beta$ -sheet structure appears to be required for the membrane perturbing properties of A $\beta$  oligomers only in DRMs mimicking raft microdomains with basal cholesterol content, but not in DRMs purified from cholesterol depleted plasma membranes, in agreement with previously reported evidences in synaptosomal plasma membranes (Eckert *et al.*, 2005).

AFM imaging in liquid, obtained in collaboration with the group of Prof.ssa Gliozzi, showed that treatment of DRMs with ADDLs resulted in the formation of large cavities, or hollows. The ADDL-lipid interaction may result in lipid depletion from the bilayer, with the formation of steps reflecting differences between the thickness of a standard bilayer and that of a thinner phase. Similar effects have been observed previously in supported lipid bilayers exposed to prefibrillar amyloid aggregates (Canale *et al.*, 2006). A thinner phase may result from lipid interdigitation, as observed in supported lipid bilayers interacting with transmembrane peptides (Rinia *et al.*, 2000). Alternatively, oligomer interaction with the bilayer may induce trans-gauche conformational changes of the lipids, giving rise to a reduced bilayer thickness (Teller *et al.*, 2000). The size and depth of the cavities were significantly reduced in DRMs purified from cholesterol-enriched cells, suggesting cholesterol may protect against amyloid-induced cell membrane damage at the lipid raft level. Overall, our results on DRM morphology agree with previous experimental data indicating a protective effect of cholesterol against membrane disassembly by prefibrillar aggregates of proteins and peptides (Arispe and Doh, 2000). The formation of cavities was observed also in DRMs purified from cells pre-treated with A $\beta$ 42 oligomers. However, in this case the depth and size of the cavities were significantly reduced, suggesting that living cells are able to resist, at least in part, ADDL-induced membrane damage.

A typical feature of DRM samples observed by AFM was the presence of domains protruding from the lipid surface. These domains were shown to consist of fluid protein or lipoprotein complexes. In fact, they disappeared in the presence of proteases and displayed higher adhesion forces than the background. We exploited the presence of these fluid domains to characterize the differences between samples with varying cholesterol content and to check the changes induced by their interaction with ADDLs. The domain size increased with decreasing cholesterol content (Table III), reflecting increased environment fluidity. Actually, increased mobility can favour fluid domain coalescence. On the contrary, domain height decreased with decreasing cholesterol content. The latter finding might be interpreted as the result of an increased compliance of the cholesterol-depleted DRM environment. Treatment of DRMs with ADDLs induced changes in domain morphology that appeared to depend on the content of cholesterol and suggested domain disassembly. In particular, in cholesterol-enriched samples the domain size was almost unaffected by treatment with ADDLs, while in control and cholesterol-depleted samples the domain size after raft treatment with ADDLs was almost half of that measured before treatment.

Domain heights were similar in DRMs purified from control cells and subsequently exposed to ADDLs and in DRMs purified from cells previously exposed to the same A $\beta$  oligomers, suggesting that domain modifications are similar when they occur in the whole intact plasma membrane or in purified membrane fractions. However, pre-treatment with A $\beta$  oligomers did not affect the domain size, which was compatible with that of untreated control cells.

Overall, our data on DRM domains provide information on the structural and morphological features of the cell plasma membrane and its cholesterol- and GM1 ganglioside-enriched raft domains. In particular, we showed that the content of cholesterol affects the ability of ADDLs to interact with the cell membrane by modulating membrane physical features at the raft level. In addition, as far as we know, we imaged for the first time by AFM the morphological features of raft domains purified from the plasma membrane of neurotypic model cells previously enriched or depleted in cholesterol and the different effects on their structure caused by exposure to ADDLs.

#### **4.2 Lipid rafts mediate amyloid-induced calcium dyshomeostasis and membrane permeabilization in Alzheimer's fibroblasts**

The pathogenesis of FAD, with regards to PS and APP mutations, has been attributed to toxic effects associated with the overproduction and aggregation of A $\beta$  peptides, particularly the more hydrophobic A $\beta$ 42 (Hardy and Selkoe, 2002). This hypothesis was originally based on the premise that pathogenic mutations increase the production of A $\beta$ 42 by favoring proteolytic processing of APP by  $\beta$ - or  $\gamma$ -secretase and by heightening the self-aggregation of A $\beta$  into amyloid fibrils (Selkoe and Wolfe, 2007; Steiner *et al.*, 2008). In the present study, fibroblasts from FAD patients carrying APP Val717Ile, PS1 Leu392Val or Met146Leu gene mutations, secreted elevated amounts of A $\beta$ 42 peptide and showed greater membrane permeability and lipid peroxidation with respect to WT fibroblasts from healthy subjects, suggesting partial disruption of membrane integrity and chronic oxidative stress associated with enhanced A $\beta$  production. These findings are in agreement with several other studies, which also provide evidence for excess lipid peroxidation associated with A $\beta$  deposits in APP/PS1-mutant AD brains and mice (Abdul *et al.*, 2008; Varadarajan *et al.*, 2000). Oxidative damage may further increase A $\beta$  binding to the cell surface. Indeed, A $\beta$  is reported to accumulate faster in membranes containing oxidatively damaged phospholipids than in membranes containing only unoxidized or saturated phospholipids (Murray *et al.*, 2007). Our results also showed that the lipoperoxidation was higher in detergent-resistant membranes (DRMs) compared to the entire cell membrane, pointing to lipid rafts as preferential sites for A $\beta$ 42 interaction at the cell surface. Indeed, as observed by contact mode AFM, the increased release of A $\beta$ 42 in FAD fibroblasts was associated with evident alteration of lipid raft morphology, resulting in the formation of steps/cavities in PS1 and, to a greater extent, in APP DRMs. Our observations are in agreement with AFM data obtained in reconstituted planar lipid bilayers, in which A $\beta$ 42 treatment resulted in the formation of multimeric channel-like structures (Lin *et al.*, 2001). On the other hand, other AFM studies have suggested that the amyloidogenic human amylin peptide induces small defects that spread across the lipid surface and result in lipid loss, rather than formation of discrete protein pores (Green *et al.*, 2004). Moreover, A $\beta$  treatment induced greater aggregate-ganglioside colocalization and DRM structure perturbation

in FAD fibroblasts, with respect to WT controls. Our approach allowed us to study the role of lipid rafts in A $\beta$ -induced cytotoxicity in living cells displaying genetic defects in tissues where AD lesions occur. Indeed, mutated fibroblasts displayed enhanced raft damage, suggesting that modified molecular structure is a common feature of cells displaying these genetic mutations. This evidence strengthens the claim that lipid rafts are key cell membrane targets for A $\beta$ 42 oligomers. In agreement with our observations, A $\beta$  has been shown to be highly concentrated in lipid rafts in the brains of Tg2576 transgenic mice (Kawarabayashi *et al.*, 2004). Moreover, the present study provides evidence that two lipidic raft components, that is cholesterol and GM1, affect the susceptibility of FAD fibroblasts to A $\beta$ 42 oligomers in opposite ways, by modulating amyloid binding to lipid rafts and its subsequent toxic effects. In particular, immunofluorescence and FRET analysis revealed that cholesterol-depleted membranes displayed enhanced A $\beta$ 42-GM1 colocalization with respect to cholesterol-enriched lipid rafts. Furthermore, fibroblast treatment with NAA, an enzyme that leaves the content and structure of GM1 unchanged except for the removal of the negatively charged sialic acid moiety, almost completely precluded A $\beta$ 42 binding to the cell surface. In agreement with our observations, a decrease in cholesterol, resulting from downregulated seladin-1 gene expression, and an increase in GM1 have been found in cell membranes purified from AD patients, relative to healthy controls (Greeve *et al.*, 2000; Molander-Melin *et al.*, 2005). Other results indicate that cholesterol depletion promotes the formation of membrane GM1 clusters, which may in turn favor greater interaction of A $\beta$  with the cell membrane (Fujita *et al.*, 2007; Yanagisawa, 2011).

The idea that calcium overload might be the final toxic insult to brain neurons in AD fits with numerous observations. The three major mechanisms of A $\beta$  interaction with cell membranes that have been proposed involve binding to endogenous calcium-permeable channels, disruption of membrane lipid integrity, and the formation of calcium-permeable channels by A $\beta$  (Arispe *et al.*, 2007; Decker *et al.*, 2010; Demuro *et al.*, 2010). We found a sharp increase in cytosolic Ca<sup>2+</sup> levels and extensive alteration of membrane permeability in FAD and WT fibroblasts when exposed to A $\beta$ 42 oligomers. The increase in cytosolic Ca<sup>2+</sup> content and alteration of membrane permeability was much smoother and milder in cholesterol-enriched or GM1-depleted fibroblasts exposed to amyloid oligomers with respect to similarly treated control cells with basal cholesterol or GM1 content. In contrast, membrane cholesterol depletion or GM1 enrichment triggered a greater increase in cytosolic Ca<sup>2+</sup> levels and membrane permeability. Even in rat cortical neurons membrane GM1 content influences A $\beta$ 42 toxicity and intracellular Ca<sup>2+</sup> homeostasis, corroborating our hypothesis at the neuronal level. Moreover, fibroblasts pre-treated with anti-GM1 antibodies, cholera toxin subunit B –a specific GM1 ligand– or with NAA completely suppressed A $\beta$ -induced Ca<sup>2+</sup> spikes and membrane damage, suggesting that the negative charge on GM1 is a key factor determining calcium dyshomeostasis and membrane permeabilization, which results in cell vulnerability to A $\beta$  oligomers. In agreement with our observations, pre-treatment of neurons with either anti-GM1 antibodies or NAA has been shown to prevent Ca<sup>2+</sup> spikes and protect against salm-

on calcitonin oligomer-induced neurotoxicity, probably modifying the plasma membrane region that is susceptible to the formation of pore-like structures (Malchiodi-Albedi *et al.*, 2010). On the other hand, other studies report that GM1 may protect against A $\beta$ 25-35 toxicity in hippocampal slices (Kreutz *et al.*, 2011). Altered ganglioside metabolism, resulting in increased GM1 content, has also been reported in the AD brain (Yamamoto *et al.*, 2008). In addition, an age-dependent local increase in ganglioside density and loss of cholesterol has been reported, showing that high-density GM1 clustering at presynaptic neuritic terminals is a critical step for A $\beta$  deposition in AD (Yamamoto *et al.*, 2008) and for the subsequent increase in membrane lateral pressure (Lin M.S. *et al.*, 2008). Our data also showed that A $\beta$ 42-induced lipoperoxidation is inhibited by depletion of extracellular calcium, suggesting that oligomer-induced membrane oxidation is supported by Ca $^{2+}$  uptake, which ultimately disrupts calcium homeostasis and activates signaling cascades that lead to cellular degeneration. It can therefore be hypothesized that oligomers first increase Ca $^{2+}$  uptake, possibly via amyloid channel formation, resulting in membrane pore formation and/or generalized thinning of the phospholipid bilayer that eventually leads to non-specific alteration of membrane permeability. From this point of view, one might suggest that raft cholesterol and GM1, by modulating membrane fluidity and charge, respectively, may specifically influence the binding of A $\beta$ 42 oligomers, their insertion into the phospholipid bilayer and their ability to disrupt membrane structure, which ultimately triggers cell death. However, the possibility that intracellular calcium overload is in part due to the interaction of oligomers with endogenous calcium-permeable channels cannot be ruled out. Greater knowledge of neuronal calcium dysregulation is needed, as calcium signaling modulators are targets of potential AD therapeutics. Despite using few patients in this study, our findings strongly suggest that the binding of A $\beta$ 42 oligomers to the plasma membrane and the resulting dysregulation of membrane permeability is significantly mediated by lipid raft microdomains.

#### **4.3 Membrane lipid composition and its physicochemical properties define cell vulnerability to aberrant protein oligomers**

A number of previous studies have provided considerable insight into the molecular basis of the structure-toxicity relationship for aberrant protein oligomers, revealing the significance of flexibility, hydrophobic exposure, and overall instability, as determinants of their ability to interact with the plasma membrane of cells disrupting their normal function (Bolognesi *et al.*, 2010; Campioni *et al.*, 2010; Lee *et al.*, 2007). An increasing body of data also highlights the roles of biological surfaces, notably the cell membrane, in promoting protein binding, misfolding, aggregation and fibril disassembly, thereby influencing the morphology, structure and biological activity of the resulting aggregates (Demuro *et al.*, 2005; Gorbenko and Kinnunen, 2006; Koffie *et al.*, 2009; Martins *et al.*, 2008; Xue *et al.*, 2009). Interestingly, however, the ability of protein oligomers to cause cell dysfunction has primarily been relat-

ed simply to the inherent properties of the oligomers, formed either in the presence or in the absence of a range of biological factors.

In the present study we show that the nature of the cell membrane can influence profoundly the degree of toxicity of specific forms of misfolded protein oligomers. To this aim we set out to explore the cytotoxicity to cultured neuroblastoma cells with a normal or a rationally altered content of membrane lipids, of two types of pre-formed HypF-N oligomers that we previously found to display different structural features and toxicities (Campioni *et al.*, 2010; Zampagni *et al.*, 2011). For comparison, we also used A $\beta$ 42 oligomers, whose cytotoxicity is well known (Kayed *et al.*, 2003; Stefani and Dobson, 2003). In particular, we modulated the structural rigidity and/or charge density of the plasma membrane by altering in a variety of ways the levels of either cholesterol or GM1, or of both at one time. Cholesterol and GM1 are two key components of lipid rafts (Lingwood and Simons, 2010), whose importance as sites stimulating peptide and protein misfolding and aggregation, and also as regions where oligomers interact preferentially with membranes, is increasingly recognized (Ehehalt *et al.*, 2003; Malchiodi-Albedi *et al.*, 2010; Molander-Melin *et al.*, 2005).

Our results show that both type A and B oligomers were internalized and sorted into endocytotic vesicles in the exposed cells. However, interaction of oligomer with the cell membrane and internalisation were significantly decreased in cells enriched in membrane cholesterol or with a reduced content of GM1; in particular, type B oligomers, that were unable to cross the plasma membrane of SH-SY5Y cells with a basal lipid content, became increasingly internalised in cells with a reduced content of cholesterol. Moreover, the cytotoxicities of A $\beta$ 42 oligomers and of the two types of misfolded HypF-N oligomers used in this study were dramatically affected by the physicochemical features of the cell membrane. In particular, the oligomers found to be toxic to the cells with basal lipid content became increasingly significantly less toxic as the membrane cholesterol level was increased or that of GM1 was decreased, whereas the opposite effect was found with cells treated so as to reduce their content of membrane cholesterol. Conversely, the oligomers that were not toxic to untreated cells remained harmless to cells with an increased content of cholesterol or a reduced content of GM1, but became increasingly harmful as the content of cholesterol in the membrane was decreased or that of GM1 was increased, reaching levels of toxicity comparable to those shown by the toxic oligomers with untreated cells. A number of characteristic features known to underlie oligomer cytotoxicity were also found to be modified in the cells with an altered membrane lipid composition, including cell membrane permeability, the levels of intracellular Ca<sup>2+</sup> and ROS, and the apoptotic response.

The data obtained using cells with an altered content of both membrane cholesterol and GM1 show that the alteration in the GM1 levels plays a dominant role in determining the resulting effects. The importance of GM1 relative to cholesterol in determining oligomer-mediated cytotoxicity is also supported by our findings of an inverse relationship between the content of cholesterol and of GM1 in the plasma membrane of our cell model. On the basis of these data, we conclude that in the sys-

tem studied here the effects on oligomer cytotoxicity of the modulation of membrane cholesterol results predominantly from the concomitant inverse modification of the content of GM1. In particular, the higher increase of GM1 content induced by cell treatment with 10 µM Mev compared to cells exposure to 2.0 mM β-CD correlates well with the greater cytotoxicity of both types of oligomers under the former condition, although the cholesterol content was similar under both conditions. In addition, we found that cells treated with NAA, an enzyme that remove the negatively charged sialic acid from gangliosides (Malchiodi-Albedi *et al.*, 2010), behaved similarly to those treated with an inhibitor of GM1 synthesis, suggesting that the negative charge carried by the head group of GM1 is one of the key chemical factors determining cell vulnerability to aberrant protein oligomers.

In agreement with our observations, a decrease in cholesterol and an increase in GM1 have been found in cell membranes purified from AD patients relative to healthy controls (Fujita *et al.*, 2007; Molander-Melin *et al.*, 2005). An altered ganglioside metabolism resulting in an increase in GM1 has also been reported in AD brains (Yamamoto *et al.*, 2008). In addition, membrane alterations associated with age-dependent local increases in the density of gangliosides and the loss of cholesterol have been reported, suggesting that high-density GM1 clustering at presynaptic neuritic terminals is a critical step for Aβ deposition in AD (Yamamoto *et al.*, 2008) and for the consequent increase of the membrane lateral pressure (Lin M.S *et al.*, 2008). Finally, GM1-containing membranes have been reported to induce polymorphisms of Aβ fibrils favouring the growth of more cytotoxic species than those formed in solution (Okada *et al.*, 2008).

The data reported here, therefore, lead us to conclude that the level of cytotoxicity of a specific type of protein oligomer, or indeed of other amyloid-related structures, is the result of a complex interplay between two critical factors: the specific properties of the aberrant protein assemblies (e.g., relative stability, disorder, flexibility and exposure of hydrophobic surface) (Bolognesi *et al.*, 2010; Campioni *et al.*, 2010; Lee *et al.*, 2007; Olzsha *et al.*, 2011) and the physicochemical features of the interacting cell membranes that are associated with their lipid composition (e.g. fluidity, electrostatic potential, curvature, lateral pressure) (Martins *et al.*, 2008; McLaurin *et al.*, 1998; Sethuraman and Belfort, 2005; Stefani, 2008). Accordingly, our data can contribute to rationalize the variable susceptibility to deleterious protein oligomers (Nekooki-Machida *et al.*, 2009) of different cell types (Cecchi *et al.*, 2005) or different regions of the same tissue (Demuro *et al.*, 2005) where cells with distinctive membrane characteristics are present (Cecchi *et al.*, 2005). Finally, these results also shed new light on the molecular determinants of protein misfolding and deposition diseases and expand the spectrum of molecular strategies for therapeutic intervention, ranging from those aimed at the inhibition of protein aggregation itself to those designed to increase the resistance of cellular targets to the misfolded forms of proteins.

#### 4.4 Neuronal differentiation of human mesenchymal stromal cells increases their resistance to A $\beta$ 42 aggregate toxicity

Multipotent neural stem cells are the most primordial, least committed cells of the central nervous system, and their transplantation holds the promise of regenerative therapy for a number of neurodegenerative diseases (Lee *et al.*, 2008). However, the propagation efficiency of these cells is often limited, making it difficult to establish large-scale cultures. Moreover, once grafted, these cells may be inefficient at generating the neuronal cells required for reconstruction of the damaged tissue (Pearson *et al.*, 2008). Among other problems, the possible therapeutic use of embryonic or adult neural, or hematopoietic stem cells in AD, Parkinson's disease and other neurodegenerative conditions also raises the question of whether they, like neuronal cells, are susceptible to endogenous amyloid deposits, which would jeopardize their survival *in vivo*. The potential relevance of this issue is further highlighted by recent data showing that amyloid fibrils are not entirely stable entities; rather, they can 'leak' toxic oligomers in the presence of phospholipid bilayers (Martins *et al.*, 2008) and, possibly, other surfaces found in tissue (Koffie *et al.*, 2009). The question of stem cell susceptibility to amyloid species arises from a wealth of data showing that different cells display differential susceptibility to the same amyloid species, not only in culture (Cecchi *et al.*, 2005; Cecchi *et al.*, 2008b; Cecchi *et al.*, 2008c) but also *in vivo*. This is supported by the finding that in neurological disorders with amyloid deposition, only specific neuronal cell populations present in distinct brain areas are functionally impaired and eventually die.

In this study we investigated whether, and to what extent, undifferentiated human mesenchymal stromal cells (hMSCs) and their neuronally differentiated counterparts (hMSC-n) were affected by the of A $\beta$ 42 oligomer toxicity. Our data show that the two cell types displayed differential susceptibility to A $\beta$  aggregate-induced toxicity. We found that undifferentiated cells were much more vulnerable to A $\beta$ 42 oligomers than their differentiated counterparts, in agreement with previous findings in a number of stem cell models (Cecchi *et al.*, 2008a). Actually, several recent studies on the toxic effects of prefibrillar amyloid species on undifferentiated cells have yielded contrasting results, with different stem cell types displaying variable susceptibility to amyloid cytotoxicity. A report published in 1990 showed that A $\beta$  peptides were neurotrophic to undifferentiated neurogenic cells, but neurotoxic to their differentiated counterparts (Yankner *et al.*, 1990). It has also been reported that rat neural stem cells can resist micromolar concentrations of A $\beta$  peptides (Eucher *et al.*, 2007; López-Toledano and Shelanski, 2004). More recently, murine embryonic stem cells and hematopoietic progenitor cells have been shown to be highly resistant to concentrations of A $\beta$ 42 oligomers previously shown to be cytotoxic to several other cell types (Neri *et al.*, 2010). However, other investigations working on neuronal progenitor cells reached opposite conclusions (Haughey *et al.*, 2002; Mazur-Kolecka *et al.*, 2006). A possible explanation for these discrepancies is that, like differentiated cells (Cecchi *et al.*, 2005), even different types of undifferentiated stem cells can display differential susceptibility to toxic amyloid species.

Some of the earliest and most common biochemical modifications seen in cells exposed to toxic amyloid oligomers are the result of oligomer-cell membrane interactions, which result in bilayer disassembly, loss of selective membrane permeability, uptake of free  $\text{Ca}^{2+}$  and the appearance of oxidative stress (Butterfield *et al.*, 2001; Demuro *et al.*, 2005). In this chain of events, the cell membrane, particularly lipid rafts, plays a dominant role in the binding of amyloid oligomers, favoring oligomer insertion into the phospholipid bilayer (Cecchi *et al.*, 2009). Indeed, an increasing number of studies point to the importance of lipid rafts and their cholesterol- and ganglioside-rich composition (Ariga *et al.*, 2008; Arispe and Doh, 2002). However, we previously found that, by modulating both cholesterol and GM1 content in neuroblastoma cell membranes, the overriding contribution to amyloid cytotoxicity is that of GM1 (Evangelisti *et al.*, 2012). In particular, gangliosides are thought to play a key role in recruiting amyloid species, possibly via electrostatic interactions due to their net negative charge (Malchiodi-Albedi *et al.*, 2010). We therefore assessed whether the differential susceptibility of undifferentiated and neuronally differentiated stem cells to A $\beta$ 42 oligomers is determined by the content of monosialoganglioside GM1, the most abundant ganglioside in lipid rafts. The more vulnerable, undifferentiated cells displayed significantly higher membrane GM1 content, thus explaining, at least in part, their ability to bind and to be permeabilized by A $\beta$ 42 oligomers, together with the resulting increase in  $\text{Ca}^{2+}$  and ROS and loss of cell viability. Equally, new functional ion channel features in hMSC-n could increase their resistance to amyloid toxicity (Benvenuti *et al.*, 2006). Yanagisawa *et al.* (Yanagisawa *et al.*, 2010) found that the toxicity of A $\beta$ 40, which is considerably less cytotoxic than A $\beta$ 42 (Jan *et al.*, 2008), increased markedly in the presence of a 4-fold molar excess of GM1 in a murine embryonic neural stem cell model. In contrast, another report found that A $\beta$ 40 exerted a toxic effect on neural progenitor cells even in the absence of gangliosides (Mazur-Kolecka *et al.*, 2006). It is likely that the use of different cells and different experimental conditions are responsible for these conflicting findings.

We report for the first time that a neuronally differentiated cell model is intrinsically more resistant to A $\beta$ 42 oligomer-induced cytotoxicity than the undifferentiated, cognate cell line, and that the molecular basis of this differential susceptibility can be traced, at least in part, to the GM1 content of the plasma membrane. Subsequent biochemical studies should address the molecular basis of this resistance, such that potential cell therapies can be implemented in the treatment of amyloid diseases, particularly neurodegenerative pathologies such as AD and Parkinson's disease.

#### 4.5 Concluding remarks

Taken together, these results provide information useful to depict a mechanism of cell impairment and death that can be common to prefibrillar aggregates of most peptides and proteins. Some of the earliest and most common biochemical modifications induced by amyloid species are the result of oligomer-cell membrane interactions, which result in bilayer disassembly, loss of selective membrane permeability,

uptake of free  $\text{Ca}^{2+}$  and the appearance of oxidative stress. In this chain of events, the cell membrane, particularly lipid rafts, plays a dominant role in the binding of amyloid oligomers, favoring oligomer insertion into the phospholipid bilayer (Cecchi *et al.*, 2009). In particular, our data suggest that raft cholesterol and GM1, by modulating membrane fluidity and charge, respectively, may specifically influence the binding of oligomers, their insertion into the phospholipid bilayer and their ability to disrupt membrane structure, which ultimately triggers cell death. Moreover, the effects on oligomer cytotoxicity of the modulation of membrane cholesterol results predominantly from the concomitant inverse modification of the content of GM1. These results implement the recently published data on the role of membrane cholesterol and GM1 in AD pathogenesis. Furthermore, the data lead us to conclude that the degree of toxicity of the oligomeric species results from a complex interplay between the structural and physicochemical features of both the oligomers (e.g., relative stability, disorder, flexibility and exposure of hydrophobic surface) and physicochemical features of the interacting cell membranes that are associated with their lipid composition (e.g. fluidity, electrostatic potential, curvature, lateral pressure). Moreover, we report that a neuronally differentiated human mesenchymal stromal cells are intrinsically more resistant to  $\text{A}\beta 42$  oligomer-induced cytotoxicity than the undifferentiated, cognate cell line, and that the molecular basis of this differential susceptibility can be traced, at least in part, to the GM1 content of the plasma membrane. Finally, these results also shed new light on the molecular determinants of protein misfolding and deposition diseases and expand the spectrum of molecular strategies for therapeutic intervention, ranging from those aimed at the inhibition of protein aggregation itself to those designed to increase the resistance of cellular targets to the misfolded forms of proteins.



## Abbreviations

**A $\beta$**  amyloid- $\beta$  peptide; **AD** Alzheimer's disease; **ADDL** amyloid  $\beta$ -derived diffusible ligands; **AFM** atomic force microscopy; **AICD** APP intracellular C-terminal domain fragment; **AMPA**  $\alpha$ -amino-3-hydroxy-5-methyl-4-isoxazolepropionic acid receptor; **ApoE** apolipoprotein E; **APP** amyloid precursor protein; **A $\beta$ 42-FAM** A $\beta$ 42 amine-reactive succinimidyl esters of carboxyfluorescein; **BACE** beta site APP cleaving enzyme or  $\beta$ -secretase; **BAPTA-AM** 1,2-bis(2-aminophenoxy)ethane-N,N,N',N'-tetraacetic acid acetoxymethyl ester; **BBB** blood brain barrier; **bFGF** basic fibroblast growth factor; **BME**  $\beta$ -mercaptoethanol; **BODIPY** 4,4-difluoro-3',4adiaza-s-indacene; **BSA** bovine serum albumin;  **$\beta$ -CD** methyl- $\beta$ -cyclodextrin; **Calcein-AM** calcein-acetoxyethyl ester; **Chol** water-soluble cholesterol balanced with methyl- $\beta$ -cyclodextrin; **CM-H<sub>2</sub>DCFDA** 2'-7' dichlorodihydrofluorescein diacetate, acetyl ester; **CNS** central nervous system; **CR** congo red; **CSF** cerebro spinal fluid; **CTX-B** cholera toxin subunit B; **DMEM** Dulbecco's modified Eagle's medium; **DMSO** dimethylsulfoxide; **DPH** 1,6-diphenyl-1,3,5-hexatriene; **DRMs** detergent-resistant membranes; **DTT** dithiothreitol; **ECL** enhanced chemiluminescence; **EDTA** ethylenediaminetetraacetic acid; **EGTA** ethylene glycol-bis( $\beta$  aminoethyl)ether) N,N,N',N'-tetraacetic acid; **ELISA** enzyme-linked immunosorbent assay; **FAD** familial Alzheimer's disease; **FBS** fetal bovine serum; **Fluo3-AM** fluo3-acetoxyethyl ester; **FM4-64** N-(3-triethylammoniumpropyl)-4-(4-(diethylamino)phenyl)hexatrienyl)pyridinium dibromide; **FRET** fluorescence resonance energy transfer; **GD1a** disialoganglioside; **GM1** monosialotetrahexosylganglioside; **GT1b** trisialoganglioside; **HBSS** hank's balanced saline solution; **HEPES** N-(2-hydroxyethyl)piperazine-N'-(2-ethanesulfonic acid); **HFIP** hexafluoro-2-isopropanol; **HMGCoAR** 3-hydroxy-3-methylglutarylCoA reductase; **HRP** horseradish peroxidase; **HypF-N** N-terminal domain of the prokaryotic hydrogenase maturation factor HypF; **HypF-N 5-FITC** HypF-N labelled with fluorescein-5-isothiocyanate; **IAPP** islet amyloid polypeptide; **LDH** lactate dehydrogenase; **MAP2** Microtubule associated protein 2; **Mev** mevastatin; **MSCs** bone marrow-derived mesenchymal stromal cells; **MTT** 3-(4,5-dimethylthiazol-2-yl)-2,5-diphenyltetrazolium bromide; **NAA** neuroaminidase; **NBM** neurobasal medium; **NF-M** neurofilament M; **NMDA** N-methyl D-aspartate receptors; **PBS** phosphate buffer saline; **PDMP** D-Threo-1-phenyl-2-decanoylamino-3-morpholino-1-propanol; **PEG-cholesterol** polyoxyetanyl-cholesteryl sebacate; **PI3-SH3** SH3 domain from bovine phosphatidyl-inositol-3'-kinase; **PMSF** phenylmethylsulpho-Elisa Evangelisti, *Structural and functional aspects of membranes : the involvement of lipid rafts in Alzheimer's disease pathogenesis : the interplay between protein oligomers and plasma membrane physicochemical features in determining cytotoxicity* ISBN 978-88-6655-444-8 (print) ISBN 978-88-6655-445-5 (online) © 2013 Firenze University Press

## Amyloid Cytotoxicity and Membrane Lipid Composition

nylfluoride; **PrP** prion protein; **PS1** Presenilin-1; **PS2** Presenilin-2; **PVDF** polyvinylidene difluoride; **RAGE** receptor for advanced glycation end products; **ROS** reactive oxygen species; **SDS-PAGE** sodiumdodecylsulfate polyacrylamide gel electrophoresis; **TEM** transmission electron microscopy; **TFA** trifluoroacetic acid; **TFE** trifluoroethanol; **ThT** thioflavin T; **TNE** Tris-HCl, NaCl, EGTA and Triton X-100 containing buffer; **Vit E** Vitamin E; **WGA** wheat germ agglutinin.

## References

- Abad-Rodriguez J., Ledesma M.D., Craessaerts K., Perga S., Medina M., Delacourte A., Dingwall C., De Strooper B., Dotti C.G. (2004). Neuronal membrane cholesterol loss enhances amyloid peptide generation. *J. Cell. Biol.* **167**, 953–960.
- Abdul H.M., Sultana R., St Clair D.K., Markesberry W.R., Butterfield D.A. (2008). Oxidative damage in brain from human mutant APP/PS-1 double knock-in mice as a function of age. *Free Radic Biol. Med.* **45**, 1420–1425.
- Abrous D.N., Koehl M., Le Moal M. (2005). Adult neurogenesis: from precursors to network and physiology. *Physiol. Rev.* **85**, 523–569.
- Adamczyk A. and Strosznajder J.B. (2006). Alpha-synuclein potentiates  $\text{Ca}^{2+}$  influx through voltage-dependent  $\text{Ca}^{2+}$  channels. *NeuroReport* **17**, 1883–1886.
- Adler M.J., Coronel C., Shelton E., Seegmiller J.E., Dewji N.N. (1991). Increased gene expression of Alzheimer disease  $\beta$ -amyloid precursor protein in senescent cultured fibroblasts. *Proc. Natl. Acad. Sci. USA* **88**, 16–20.
- Allen J.A., Halverson-Tamboli R.A., Rasenick M.M. (2007). Lipid raft microdomains and neurotransmitter signalling. *Nat. Rev. Neurosci.* **8**, 128–140.
- Alvarez A., Toro R., Cáceres A., Maccioni R.B. (1999). Inhibition of tau phosphorylating protein kinase cdk5 prevents beta-amyloid-induced neuronal death. *FEBS Lett.* **459**, 421–426.
- Alvarez-Buylla A., Garcia-Verdugo J.M., Tramontin A.D. (2001). A unified hypothesis on the lineage of neural stem cells. *Nat. Rev. Neurosci.* **2**, 287–293.
- American Psychiatric Association. (1994). Diagnostic and statistical manual of mental disorders. 4th Ed., Washington DC.
- Amundson D.M. and Zhou M. (1999). Fluorometric method for the enzymatic determination of cholesterol. *J. Biochem. Biophys. Methods* **38**, 43–52.
- Anderton B.H., Dayanandan R., Killick R., Lovestone S. (2000). Does dysregulation of the Notch and wingless/Wnt pathways underlie the pathogenesis of Alzheimer's disease? *Mol. Med. Today* **6**, 54–59.
- Ariga T., Kobayashi K., Hasegawa A., Kiso M., Ishida H., Miyatake T. (2001). Characterization of high-affinity binding between gangliosides and amyloid  $\beta$ -protein. *Arch. Biochem. Biophys.* **388**, 225–230.
- Ariga T., McDonald M.P., Yu R.K. (2008). Role of ganglioside metabolism in the pathogenesis of Alzheimer's disease--a review. *J. Lipid Res.* **49**, 1157–1175.
- Arispe N., Pollard H.B., Rojas E. (1993). Giant multilevel cation channels formed by Alzheimer disease amyloid beta-protein [A beta P-(1-40)] in bilayer membranes. *Proc. Natl. Acad. Sci. USA* **90**, 10573–10577.
- Arispe N. and Doh M. (2002). Plasma membrane cholesterol controls the cytotoxicity of Alzheimer's disease Abeta(1-40) and (1-42) peptides. *FASEB J.* **16**, 1526–1536.

## Amyloid Cytotoxicity and Membrane Lipid Composition

- Arispe N., Diaz, J.C., Simakova O. (2007). Abeta ion channels. Prospects for treating Alzheimer's disease with Abeta channel blockers. *Biochim. Biophys. Acta* **1768**, 1952-1965.
- Baglioni S., Casamenti F., Bucciantini M., Luheshi L.M., Taddei N., Chiti F., Dobson C.M., Stefani M. (2006). Prefibrillar amyloid aggregates could be generic toxins in higher organisms. *J. Neurosci.* **26**, 8160-8167.
- Benvenuti S., Saccardi R., Luciani P., Urbani S., Deledda C., Cellai I., Francini F., Squecco R., Rosati F., Danza G., Gelmini S., Greeve I., Rossi M., Maggi R., Serio M., Peri A. (2006). Neuronal differentiation of human mesenchymal stem cells: changes in the expression of the Alzheimer's disease-related gene seladin-1. *Exp. Cell Res.* **312**, 2592-2604.
- Berson J.F., Theos A.C., Harper D.C., Tenza D., Raposo G., Marks M.S. (2003). Proprotein convertase cleavage liberates a fibrillogenic fragment of a resident glycoprotein to initiate melanosome biogenesis. *J. Cell. Biol.* **161**, 521-533.
- Bezprozvanny I. and Hayden M.R. (2004). Deranged neuronal calcium signaling and Huntington disease. *Biochem. Biophys. Res. Comm.* **322**, 1310-1317.
- Billings L.M., Oddo S., Green K.N., McGaugh J.L., LaFerla F.M. (2005). Intraneuronal A $\beta$  causes the onset of early Alzheimer's disease-related cognitive deficits in transgenic mice. *Neuron* **45**, 675-688.
- Blurton-Jones M., Kitazawa M., Martinez-Coria H., Castello N.A., Müller F.J., Loring J.F., Yamasaki T.R., Poon W.W., Green K.N., LaFerla F.M. (2009). Neural stem cells improve cognition via BDNF in a transgenic model of Alzheimer disease. *Proc. Natl. Acad. Sci. USA* **106**, 13594-13599.
- Bokvist M., Lindström F., Watts A., Gröbner G. (2004). Two types of Alzheimer's  $\beta$ -amyloid (1-40) peptide membrane interactions: aggregation preventing transmembrane anchoring versus accelerated surface fibril formation. *J. Mol. Biol.* **335**, 1039-1049.
- Bolognesi B., Kumita J.R., Barros T.P., Esbjorner E.K., Luheshi L.M., Crowther D.C., Wilson M.R., Dobson C.M., Favrin G., Yerbury J.J. (2010). ANS binding reveals common features of cytotoxic amyloid species. *ACS Chem. Biol.* **5**, 735-740.
- Bradford M.M. (1976). A rapid and sensitive method for the quantitation of microgram quantities of protein utilizing the principle of protein-dye binding. *Anal. Biochem.* **72**, 248-254.
- Brandt M.D. and Storch A. (2008). Neurogenesis in the adult brain: from bench to bedside? *Fortschr. Neurol. Psychiatr.* **76**, 517-529
- Bravo R., Arimon M., Valle-Delgado J.J., Garcia R., Durany N., Castel S., Cruz M., Ventura S., Fernandez-Busquets X. (2008). Sulfated polysaccharides promote the assembly of amyloid  $\beta_{1-42}$  peptide into stable fibrils of reduced cytotoxicity. *J. Biol. Chem.* **283**, 32471-32783.
- Brunelle P. and Rauk A. (2002). The radical model of Alzheimer's disease: specific recognition of Gly29 and Gly33 by Met35 in a beta-sheet model of Abeta: an ONIOM study. *J. Alzheimers Dis.* **4**, 283-289.
- Bucciantini M., Giannoni E., Chiti F., Baroni F., Formigli L., Zurdo J., Taddei N., Ramponi G., Dobson C.M., Stefani M. (2002). Inherent cytotoxicity of aggregates implies a common origin for protein misfolding diseases. *Nature* **416**, 507-511.
- Bucciantini M., Rigacci S., Berti A., Pieri L., Cecchi C., Nosi D., Formigli L., Chiti F., Stefani M. (2005). Patterns of cell death triggered in two different cell lines by HypF-N prefibrillar aggregates. *FASEB J.* **19**, 437-439.
- Buee L., Bussiere T., Buee-Scherrer V., Delacourte A., Hof P.R. (2000). Tau protein isoforms, phosphorylation and role in neurodegenerative disorders. *Brain Res. Brain Res. Rev.* **33**, 95-130.

- Butterfield A.D., Drake J., Pocernich C., Castegna A. (2001). Evidence of oxidative damage in Alzheimer's disease brain: central role for amyloid  $\beta$ -peptide. *Trends Mol. Med.* **7**, 548-554.
- Butterfield S.M. and Lashuel H.A. (2010). Amyloidogenic protein-membrane interactions: mechanistic insight from model systems. *Angew. Chem. Int. Ed. Engl.* **49**, 5628-5654.
- Buxbaum J.D., Liu K.N., Luo Y., Slack J.L., Stocking K.L., Peschon J.J., Johnson R.S., Castner B.J., Cerretti D.P., Black R.A. (1998). Evidence that tumor necrosis factor  $\alpha$  converting enzyme is involved in regulated  $\alpha$ -secretase cleavage of the Alzheimer amyloid protein precursor. *J. Biol. Chem.* **273**, 27765-27767.
- Cai X.D., Golde T.E., Younkin S.G. (1993). Release of excess amyloid beta protein from a mutant amyloid beta protein precursor. *Science* **259**, 514-516.
- Campioni S., Mannini B., Zampagni M., Pensalfini A., Parrini C., Evangelisti E., Relini A., Stefani M., Dobson C.M., Cecchi C., Chiti F. (2010). A causative link between the structure of aberrant protein oligomers and their toxicity. *Nat. Chem. Biol.* **6**, 140-147.
- Canale C., Torrassa S., Rispoli P., Relini A., Rolandi R., Bucciantini M., Stefani M., Gliozi A. (2006). Natively folded HypF-N and its early amyloid aggregates interact with phospholipid monolayers and destabilize supported phospholipid bilayers. *Biophys. J.* **91**, 4575-4588.
- Casalot L. and Rousset M. (2001). Maturation of the [NiFe] hydrogenases. *Trends Microbiol.* **9**, 228-237.
- Cecchi C., Baglioni S., Fiorillo C., Pensalfini A., Liguri G., Nosi D., Rigacci S., Bucciantini M., Stefani M. (2005). Insights into the molecular basis of the differing susceptibility of varying cell types to the toxicity of amyloid aggregates. *J. Cell Sci.* **118**, 3459-3470.
- Cecchi C., Pensalfini A., Baglioni S., Fiorillo C., Caporale R., Formigli L., Liguri G., Stefani M. (2006). Differing molecular mechanisms appear to underlie early toxicity of prefibrillar HypF-N aggregates to different cell types. *FEBS J.* **273**, 2206-2222.
- Cecchi C., Pensalfini A., Liguri G., Baglioni S., Fiorillo C., Guadagna S., Zampagni M., Formigli L., Nosi D., Stefani M. (2008a). Differentiation increases the resistance of neuronal cells to amyloid toxicity. *Neurochem. Res.* **33**, 2516-2531.
- Cecchi C., Rosati F., Pensalfini A., Formigli L., Nosi D., Liguri G., Dichiara F., Morello M., Danza G., Pieraccini G., Peri A., Serio M., Stefani M. (2008b). Seladin-1/DHCR24 protects neuroblastoma cells against Abeta toxicity by increasing membrane cholesterol content. *J. Cell. Mol. Med.* **12**, 1990-2002.
- Cecchi C., Pensalfini A., Stefani M., Baglioni S., Fiorillo C., Cappadona S., Caporale R., Nosi D., Ruggiero M., Liguri G. (2008c). Replicating neuroblastoma cells in different cell cycle phases display different vulnerability to amyloid toxicity. *J. Mol. Med.* **86**, 197-209.
- Cecchi C., Nichino D., Zampagni M., Bernacchioni C., Evangelisti E., Pensalfini A., Liguri G., Gliozi A., Stefani M., Relini A. (2009). A protective role for lipid raft cholesterol against amyloid-induced membrane damage in human neuroblastoma cells. *Biochim. Biophys. Acta* **1788**, 2204-2216.
- Chafekar F.M., Hoozemans J.J., Zwart R., Baas F., Schepers W. (2007). Abeta 1-42 induces mild endoplasmic reticulum stress in an aggregation state-dependent manner. *Antioxid. Redox Signal.* **9**, 2245-2254.
- Chafekar S.M., Baas F., Schepers W. (2008). Oligomer-specific A $\beta$  toxicity in cell models is mediated by selective uptake. *Biochim. Biophys. Acta* **1782**, 523-531.
- Chapman M.R., Robinson L.S., Pinkner J.S., Roth R., Heuser J., Hammar M., Normark S., Hultgren S.J. (2002). Role of *Escherichia coli* curli operons in directing amyloid fiber formation. *Science* **295**, 851-855.

## Amyloid Cytotoxicity and Membrane Lipid Composition

- Chen F., David D., Ferrari A., Götz J. (2004). Posttranslational modifications of tau — role in human tauopathies and modeling in transgenic animals. *Curr. Drug Targets* **5**, 503–515.
- Chen Y. and Kokholyan N. (2005). A single disulfide bond differentiates aggregation pathways of  $\beta$ 2-microglobulin. *J. Mol. Biol.* **354**, 473–482.
- Chen S., Yadav S.P., Surewicz W.K. (2010). Interaction between human prion protein and amyloid-beta (Abeta) oligomers: role of N-terminal residues. *J. Biol. Chem.* **285**, 26377–26383.
- Cheon M., Chang I., Mohanty S., Luheshi L.M., Dobson C.M., Vendruscolo M., Favrin G. (2007). Structural reorganisation and potential toxicity of oligomeric species formed during the assembly of amyloid fibrils. *PLoS Comput. Biol.* **3**, 1727–1738.
- Cherny D., Hoyer W., Subramanian V., Jovin T.M. (2004). Double-stranded DNA stimulates the fibrillation of alpha-synuclein in vitro and is associated with the mature fibrils: an electron microscopy study. *J. Mol. Biol.* **344**, 929–938.
- Chevallier N.L., Soriano S., Kang D.E., Masliah E., Hu G., Koo E.H. (2005). Perturbed neurogenesis in the adult hippocampus associated with presenilin-1 A246E mutation. *Am. J. Pathol.* **167**, 151–159.
- Chi E.Y., Frey S.L., Lee K.Y. (2007). Ganglioside G(M1)-mediated amyloid- $\beta$  fibrillogenesis and membrane disruption. *Biochemistry* **46**, 1913–1924.
- Chiti F., Webster P., Taddei N., Clark A., Stefani M., Ramponi G., Dobson C.M. (1999). Designing conditions for in vitro formation of amyloid protofilaments and fibrils. *Proc. Natl. Acad. Sci. USA* **96**, 3590–3594.
- Chiti F., Bucciantini M., Capanni C., Taddei N., Dobson C.M., Stefani M. (2001). Solution conditions can promote formation of either amyloid protofilaments or mature fibrils from the HypF N-terminal domain. *Protein Sci.* **10**, 2541–2547.
- Chiti F. and Dobson C.M. (2006). Protein misfolding, functional amyloid, and human disease. *Annu. Rev. Biochem.* **75**, 333–366.
- Choi D.W. (1992). Excitotoxic cell death. *J. Neurobiol.* **23**, 1261–1276.
- Choi Y.G., Kim J.L., Lee H.P., Jin J.K., Choi E.K., Carp R.I., Kim Y.S. (2000). Induction of heme oxygenase-1 in the brain of scrapie-infected mice. *Neurosci. Lett.* **11**, 173–176.
- Choo-Smith L., Garzon-Rodriguez W., Glabe C.G., Surewicz W.K. (1997). Acceleration of amyloid fibril formation by specific binding of Abeta-(1-40) peptide to ganglioside-containing membrane vesicles. *J. Biol. Chem.* **272**, 22987–22990.
- Citron M., Oltersdorf T., Haass C., McConlogue L., Hung A.Y., Seubert P., Vigo-Pelfrey C., Lieberburg I., Selkoe D.J. (1992). Mutation of the beta-amyloid precursor protein in familial Alzheimer's disease increases beta-protein production. *Nature* **360**, 672–674.
- Citron M., Vigo-Pelfrey C., Teplow D.B., Miller C., Schenk D., Johnston J., Winblad B., Venizelos N., Lannfelt L., Selkoe D.J. (1994). Excessive production of amyloid beta-protein by peripheral cells of symptomatic and presymptomatic patients carrying the Swedish familial Alzheimer disease mutation. *Proc. Natl. Acad. Sci. USA* **91**, 11993–11997.
- Claessen D., Rink R., de Jong W., Siebring J., de Vreugd P., Boersma F.G., Dijkhuizen L., Wosten H.A. (2003). A novel class of secreted hydrophobic proteins is involved in aerial hyphae formation in *Streptomyces coelicolor* by forming amyloid-like fibrils. *Genes. Dev.* **17**, 1714–1726.
- Cleary J.P., Walsh D.M., Hofmeister J.J., Shankar G.M., Kuskowski M., Selkoe D.J., Ashe K.H. (2005). Natural oligomers of the amyloid- $\beta$  specifically disrupt cognitive function. *Nat. Neurosci.* **8**, 79–84.
- Colbeau A., Elsen S., Tomiyama M., Zorin N.A., Dimon B., Vignais P.M. (1998). Rhodobacter capsulatus HypF is involved in regulation of hydrogenase synthesis through the HupUV proteins. *Eur. J. Biochem.* **251**, 65–71.

- Colucci-D'Amato L., Bonavita V., di Porzio U. (2006). The end of the central dogma of neurobiology: stem cells and neurogenesis in adult CNS. *Neurol. Sci.* **27**, 266–270.
- Companyó M., Iborra A., Villaverde J., Martínez P., Morros A. (2007). Membrane fluidity changes in goat sperm induced by cholesterol depletion using beta-cyclodextrin. *Biochim. Biophys. Acta* **1768**, 2246–2255.
- Conway K.A., Harper J.D., Lansbury P.T. Jr. (2000). Fibrils formed in vitro from alpha-synuclein and two mutant forms linked to Parkinson's disease are typical amyloid. *Biochemistry* **39**, 2552–2563.
- Corder E.H., Saunders A.M., Strittmatter W.J., Schmeichel D.E., Gaskell P.C., Small G.W., Roses A.D., Haines J.L., Pericak-Vance M.A. (1993). Gene dose of apolipoprotein E type 4 allele and the risk of Alzheimer's disease in late onset families. *Science* **261**, 921–923.
- Crameri A., Biondi E., Kuehnle K., Lütjohann D., Thelen K.M., Perga S., Dotti C.G., Nitsch R.M., Ledesma M.D., Mohajeri M.H. (2006). The role of seladin-1/DHCR24 in cholesterol biosynthesis, APP processing and Abeta generation *in vivo*. *EMBO J.* **25**, 432–443.
- Crowther R.A. and Wischik C.M. (1985). Image reconstruction of the Alzheimer paired helical filament. *EMBO J.* **4**, 3661–3665.
- Curtain C.C., Ali F.E., Smith D.G., Bush A.I., Masters C.L., Barnham K.J. (2003). Metal ions, pH, and cholesterol regulate the interactions of Alzheimer's disease amyloid-beta peptide with membrane lipid. *J. Biol. Chem.* **278**, 2977–2982.
- Dahlgren K.N., Manelli A.M., Stine W.B.Jr., Baker L.K., Krafft G.A., LaDu M.J. (2002). Oligomeric and fibrillar species of amyloid-beta peptides differentially affect neuronal viability. *J. Biol. Chem.* **277**, 32046–32053.
- Dal Pozzo S., Urbani S., Mazzanti B., Luciani P., Deledda C., Lombardini L., Benvenuti S., Perri A., Bosi A., Saccardi R. (2010). High recovery of mesenchymal progenitor cells with non-density gradient separation of human bone marrow. *Cyotherapy* **12**, 579–586.
- Danzer K.M., Haasen D., Karow A.R., Moussaud S., Habeck M., Giese A., Kretzschmar H., Hengerer B., Kostka M. (2007). Different species of  $\alpha$ -synuclein oligomers induce calcium influx and seeding. *J. Neurosci.* **271**, 9220–9232.
- Day R., Periasamy A., Schaufele F. (2001). Fluorescence resonance energy transfer microscopy of localized protein interactions in the living cell nucleus. *Methods* **25**, 4–18.
- De Felice F.G., Velasco P.T., Lambert M.P., Viola K., Fernandez S.J., Ferreira S.T., Klein W.L. (2007).  $\text{A}\beta$  oligomers induce neuronal oxidative stress through an N-methyl-D-aspartate receptor-dependent mechanism that is blocked by the Alzheimer drug memantine. *J. Biol. Chem.* **282**, 11590–11601.
- De Ferrari G.V. and Inestrosa N.C. (2000). Wnt signaling function in Alzheimer's disease. *Brain Res. Brain Res. Rev.* **33**, 1–12.
- De Strooper B., Saftig P., Craessaerts K., Vanderstichele H., Guhde G., Annaert W., Von Figura K., Van Leuven F. (1998). Deficiency of presenilin-1 inhibits the normal cleavage of amyloid precursor protein. *Nature* **391**, 387–390.
- De Strooper B. (2003). Aph-1, Pen-2, and nicastrin with presenilin generate an active  $\gamma$ -secretase complex. *Neuron* **38**, 9–12.
- Decker H., Jürgensen S., Adrover M.F., Brito-Moreira J., Bomfim T.R., Klein W.L., Epstein A.L., De Felice F.G., Jerusalinsky D., Ferreira S.T. (2010). N-methyl-D-aspartate receptors are required for synaptic targeting of Alzheimer's toxic amyloid- $\beta$  peptide oligomers. *J. Neurochem.* **115**, 1520–1529.
- Demuro A., Mina E., Kayed R., Milton S.C., Parker I., Glabe C.G. (2005). Calcium dysregulation and membrane disruption as a ubiquitous neurotoxic mechanism of soluble amyloid oligomers. *J. Biol. Chem.* **280**, 17294–17300.

## Amyloid Cytotoxicity and Membrane Lipid Composition

- Demuro A., Parker I., Stutzmann G.E. (2010). Calcium signaling and amyloid toxicity in Alzheimer disease. *J. Biol. Chem.* **285**, 12463-12468.
- Dickson D.W. (1995). Correlation of synaptic and pathological markers with cognition of the elderly. *Neurobiol. Aging* **16**, 285-298.
- Diociaiuti M., Polzi L.Z., Valvo L., Malchiodi-Albedi F., Bombelli C., Gaudiano M.C. (2006). Calcitonin forms oligomeric pore-like structures in lipid membranes. *Biophys. J.* **91**, 2275-2281.
- Doetsch F., Caille I., Lim D.A., García-Verdugo J.M., Alvarez-Buylla A. (1999). Subventricular zone astrocytes are neural stem cells in the adult mammalian brain. *Cell* **97**, 703-716.
- Dougherty J.J., Wu J., Nichols R.A. (2003).  $\beta$ -amyloid regulation of presynaptic nicotinic receptors in rat hippocampus and neocortex. *J. Neurosci.* **23**, 6740-6747.
- Drabikowski W., Lagwińska E., Sarzala M.G. (1973). Filipin as a fluorescent probe for the location of cholesterol in the membranes of fragmented sarcoplasmic reticulum. *Biochim. Biophys. Acta* **291**, 61-70.
- Drapeau E. and Nora Abrous D. (2008). Stem cell review series: role of neurogenesis in age-related memory disorders. *Aging Cell* **7**, 569-589.
- Drummen G.P., Gadella B.M., Post J.A., Brouwers J.F. (2004). Mass spectrometric characterization of the oxidation of the fluorescent lipid peroxidation reporter molecule C11-BODIPY(581/591). *Free Radic. Biol. Med.* **36**, 1635-1644.
- Duff K., Eckman C., Zehr C., Yu X., Prada C.M., Perez-tur J., Hutton M., Buee L., Harigaya Y., Yager D., Morgan D., Gordon M.N., Holcomb L., Refolo L., Zenk B., Hardy J., Younkin S. (1996). Increased amyloid beta42(43) in brains of mice expressing mutant presenilin 1. *Nature* **383**, 710-713.
- Ebneth A., Godemann R., Stamer K., Illenberger S., Trinczek B., Mandelkow E. (1998). Overexpression of tau protein inhibits kinesin-dependent trafficking of vesicles, mitochondria, and endoplasmic reticulum: implications for Alzheimer's disease. *J. Cell Biol.* **143**, 777-794.
- Eckert G.P., Wood W.G., Müller W.E. (2005). Membrane disordering effects of beta-amyloid peptides. *Subcell. Biochem.* **38**, 319-337.
- Egawa H. and Furusawa K. (1999). Liposome adhesion on mica surface studied by atomic force microscopy. *Langmuir* **15**, 1660-1666.
- Ehehalt R., Keller P., Haass C., Thiele C., Simons K. (2003). Amyloidogenic processing of the Alzheimer beta-amyloid precursor protein depends on lipid rafts. *J. Cell. Biol.* **160**, 113-123.
- Eikeleboom R., Bate C., Van Gool W.A., Hoozemans J.J., Rozemuller J.M., Veerhuis, R., Williams A. (2002). Neuroinflammation in Alzheimer's disease and prion disease. *Glia* **40**, 232-239.
- Endo A., Kuroda M., Tanzawa K. (1976). Competitive inhibition of 3-hydroxy-3-methylglutaryl coenzyme A reductase by ML-236A and ML-236B, fungal metabolites having hypocholesterolemic activity. *FEBS Lett.* **72**, 323-326.
- Eucher J.N., Uemura E., Sakaguchi D.S., Greenlee M.H. (2007). Amyloid-beta peptide affects viability but not differentiation of embryonic and adult rat hippocampal progenitor cells. *Exp. Neurol.* **203**, 486-492.
- Evangelisti E., Cecchi C., Cascella R., Sgromo C., Becatti M., Dobson C.M., Chiti F., Stefani M. (2012). Membrane lipid composition and its physicochemical properties define cell vulnerability to aberrant protein oligomers. Accepted for publication *J. Cell Sci.*
- Evers F., Jeworrek C., Tiemeyer S., Weise K., Sellin D., Paulus M., Struth B., Tolan M., Winter R. (2009). Elucidating the mechanism of lipid membrane-induced IAPP fibrillogenesis and

- its inhibition by the red wine compound resveratrol: a synchrotron X-ray reflectivity study. *J. Am. Chem. Soc.* **131**, 9516–9521.
- Fan M.M.Y., Fernandes H. B., Zhang L. Y. J., Hayden M. R., Raymond L. A. (2007). Altered NMDA receptor trafficking in a yeast artificial chromosome transgenic mouse model of Huntington's disease. *J. Neurosci.* **14**, 3768–3779.
- Farzan M., Schnitzler C.E., Vasilieva N., Leung D., Choe H. (2000). BACE2, a  $\beta$ -secretase homolog, cleaves at the  $\beta$  site and within the amyloid- $\beta$  region of the amyloid- $\beta$  precursor protein. *Proc. Natl. Acad. Sci. USA* **97**, 9712–9717.
- Fazzini E., Durso R., Davoudi H., Szabo G.K., Albert M.L. (1990). GM1 gangliosides alter acute MPTP-induced behavioral and neurochemical toxicity in mice. *J. Neurol. Sci.* **99**, 59–68.
- Flanagan L.A., Cunningham C.C., Chen J., Prestwich G.D., Kosik K.S., Janmey P.A. (1997). The structure of divalent cation-induced aggregates of PIP2 and their alteration by gel-solin and tau. *Biophys. J.* **73**, 1440–1447.
- Fodero-Tavoletti M.T., Villemagne V.L., Rowe C.C., Masters C.L., Barnham K.J., Cappai R. (2011). Amyloid- $\beta$ : the seeds of darkness. *Int. J. Biochem. Cell Biol.* **43**, 1247–1251.
- Fu W., Luo H., Parthasarathy S., Mattson M.P. (1998). Catecholamines potentiate amyloid  $\beta$ -peptide neurotoxicity: involvement of oxidative stress, mitochondrial dysfunction, and perturbed calcium homeostasis. *Neurobiol. Dis.* **5**, 229–243.
- Fujita A., Cheng J., Hirakawa M., Furukawa K., Kusunoki S., Fujimoto T. (2007). Gangliosides GM1 and GM3 in the living cell membrane form clusters susceptible to cholesterol depletion and chilling. *Mol. Biol. Cell.* **18**, 2112–2122.
- Gasparini L., Racchi M., Binetti G., Trabucchi M., Solerte S.B., Alkon D., Etcheberrigaray R., Gibson H.G., Blass J., Paoletti R., Govoni S. (1998). Peripheral markers in testing pathophysiological hypotheses and diagnosing Alzheimer's disease. *FASEB J.* **12**, 18–34.
- Gharibyan A.L., Zamotin V., Yanamandra K., Moskaleva O.S., Margulis B.A., Kostanyan I.A., Morozova-Roche L.A. (2007). Lysozyme amyloid oligomers and fibrils induce cellular death via different apoptotic/necrotic pathways. *J. Mol. Biol.* **365**, 1337–13349.
- Glaebe C.G. (2004). Conformation-dependent antibodies target diseases of protein misfolding. *Trends Biochem. Sci.* **29**, 542–547.
- Glaebe C.G. (2008). Structural classification of toxic amyloid oligomers. *J. Biol. Chem.* **283**, 29639–29643.
- Glenner G.G. and Wong C.W. (1984). Alzheimer's disease: Initial report of the purification and characterization of a novel cerebrovascular amyloid protein. *Biochem. Biophys. Res. Commun.* **120**, 885–890.
- Goate A., Chartier-Harlin M.C., Mullan M., Brown J., Crawford F., Fidani L., Giuffra L., Haynes A., Irving N., James L., Mant R., Newton P., Rooke K., Roques P., Talbot C., Pericak-Vance M., Roses A., Williamson R., Rossor M., Owen M., Hardy J. (1991). Segregation of a missense mutation in the amyloid precursor protein gene with familial Alzheimer's disease. *Nature* **349**, 704–706.
- Goedert M., Wischik C.M., Crowther R.A., Walker J.E., Klug A. (1988). Cloning and sequencing of the cDNA encoding a core protein of the paired helical filament of Alzheimer disease: identification as the microtubule-associated protein tau. *Proc. Natl. Acad. Sci. USA* **85**, 4051–4055.
- Goedert M., Spillantini M.G., Cairns N.J., Crowther R.A. (1992). Tau proteins of Alzheimer paired helical filaments: abnormal phosphorylation of all six brain isoforms. *Neuron* **8**, 159–168.

## Amyloid Cytotoxicity and Membrane Lipid Composition

- Goedert M., Spillantini M.G., Jakes R., Crowther R.A., Vanmechelen E., Probst A., Götz, J., Burki K., Cohen P. (1995). Molecular dissection of the paired helical filament. *Neurobiol. Aging* **16**, 325–334.
- Gorbenko G.P. and Kinnunen P. K.. (2006). The role of lipid-protein interactions in amyloid-type protein fibril formation. *Chem. Phys. Lipids* **141**, 72–82.
- Gosal W.S., Morten I.J., Hewitt E.W., Smith D.A., Thomson N.H., Radford S.E. (2005). Competing pathways determine fibril morphology in the self-assembly of beta2-microglobulin into amyloid. *J. Mol. Biol.* **351**, 850–64.
- Gottfries C.G. (1994). Therapy options in Alzheimer's disease. *Br. J. Clin. Pract.* **48**, 327–330.
- Götz J. (2001). Tau and transgenic animal models. *Brain Res. Brain Res. Rev.* **35**, 266–286.
- Götz J., Streffer J.R., David D., Schild A., Hoerndl F., Pennanen L., Kurosinski P., Chen F. (2004). Transgenic animal models of Alzheimer's disease and related disorders: histopathology, behavior and therapy. *Mol. Psychiatr.* **9**, 664–683.
- Gotz M. and Huttner W.B. (2005). The cell biology of neurogenesis. *Nat. Rev. Mol. Cell. Biol.* **6**, 777–788.
- Grace E.A., Rabiner C.A., Busciglio J. (2002). Characterization of neuronal dystrophy induced by fibrillar amyloid  $\beta$ : implications for Alzheimer's disease. *Neuroscience* **114**, 265–273.
- Green J.D., Kreplak L., Goldsbury C., Li Blatter X., Stoltz M., Cooper G.S., Seelig A., Kistler J., Aeby U. (2004). Atomic force microscopy reveals defects within mica supported lipid bilayers induced by the amyloidogenic human amylin peptide. *J. Mol. Biol.* **342**, 877–887.
- Greeve I., Hermans-Borgmeyer I., Brellinger C., Kasper D., Gomez-Isla T., Behl C., Levkau B., Nitsch R.M. (2000). The human DIMINUTO/DWARF1 homolog seladin-1 confers resistance to Alzheimer's disease-associated neurodegeneration and oxidative stress. *J. Neurosci.* **20**, 7345–7352.
- Guentchev M., Voigtlander T., Haberler C., Groschup M.H., Budka H. (2000). Evidence for oxidative stress in experimental prion disease. *Neurobiol. Dis.* **7**, 270–273.
- Guirland C. and Zheng J.Q. (2007). Membrane lipid rafts and their role in axon guidance. *Adv. Exp. Med. Biol.* **621**, 144–155.
- Gujiarro J.I., Sunde M., Jones J.A., Campbell I.D., Dobson C.M. (1998). Amyloid fibril formation by an SH3 domain. *Proc. Natl. Acad. Sci. USA* **95**, 4224–4228.
- Haass C., Schlossmacher M.G., Hung A.Y., Vigo-Pelfrey C., Mellon A., Ostaszewski B.L., Lieberburg I., Koo E.H., Schenk D., Teplow D.B., Selkoe D.J. (1992). Amyloid  $\beta$ -peptide is produced by cultured cells during normal metabolism. *Nature* **359**, 322–325.
- Hadjiconstantinou M. and Neff N.H. (1998). GM1 ganglioside: *in vivo* and *in vitro* trophic actions on central neurotransmitter systems. *J. Neurochem.* **70**, 1335–1345.
- Hakomori S. and Igarashi Y. (1995). Functional role of glycosphingolipids in cell recognition and signaling. *J. Biochem.* **118**, 1091–1103.
- Hakomori S. (2003). Structure, organization, and function of glycosphingolipids in membrane. *Curr. Opin. Hematol.* **10**, 16–24.
- Harder T. and Engelhardt K.R. (2004). Membrane domains in lymphocytes – from lipid rafts to protein scaffolds. *Traffic* **5**, 265 – 275.
- Hardy J. and Selkoe D.J. (2002). The amyloid hypothesis of Alzheimer's disease: progress and problems on the road to therapeutics. *Science* **297**, 353–356.
- Harper J.D., Wong S.S., Lieber C.M., Lansbury P.T. (1997). Observation of metastable Abeta amyloid protofibrils by atomic force microscopy. *Chem. Biol.* **4**, 119–125.
- Harris D.A. (1999). Cellular biology of prion diseases. *Clin. Microbiol. Rev.* **12**, 429–444.
- Haughey N.J., Liu D., Nath A., Borchard A.C., Mattson M.P. (2002). Disruption of neurogenesis in the subventricular zone of adult mice, and in human cortical neuronal precursor

- cells in culture, by amyloid beta-peptide: implications for the pathogenesis of Alzheimer's disease. *Neuromolecular Med.* **1**, 125-135.
- Hayashi H., Kimura N., Yamaguchi H., Hasegawa K., Yokoseki T., Shibata M., Yamamoto N., Michikawa M., Yoshikawa Y., Terao K., Matsuzaki K., Lemere C.A., Selkoe D.J., Naiki H., Yanagisawa K. (2004). A seed for Alzheimer amyloid in the brain. *J. Neurosci.* **24**, 4894-4902.
- He P., Zhong Z., Lindholm K., Berning L., Lee W., Lemere C., Staufenbiel M., Li R., Shen Y. (2004). Tumor necrosis factor death receptor signaling cascade is required for amyloid- $\beta$  protein-induced neuron death. *J. Neurosci.* **24**, 1760-1771.
- Hering H., Lin C.C., Sheng M. (2003). Lipid rafts in the maintenance of synapses, dendritic spines, and surface AMPA receptor stability. *J. Neurosci.* **23**, 3262-3271.
- Hojjati M.R. and Jiang X.C. (2006). Rapid, specific, and sensitive measurements of plasma sphingomyelin and phosphatidylcholine. *J. Lipid Res.* **47**, 673-676.
- Holtzman D.M., Bales K.R., Tenkova T., Fagan A.M., Parsadanian M., Sartorius L.J., Mackey B., Olney J., McKeel D., Wozniak D., Paul S.M. (2000). Apolipoprotein E isoform-dependent amyloid deposition and neuritic degeneration in a mouse model of Alzheimer's disease. *Proc. Natl. Acad. Sci. USA* **97**, 2892-2897.
- Hou X., Parkington H.C., Coleman H.A., Mechler A., Martin L.L., Aguilar M.I., Small D.H. (2007). Transthyretin oligomers induce calcium influx via voltage-gated calcium channels. *J. Neurochem.* **100**, 446-457.
- Hung L.W., Ciccotosto G.D., Giannakis E., Tew D.J., Perez K., Masters C.L., Cappai R., Wade J.D., Barnham K.J. (2008). Amyloid-beta peptide (Abeta) neurotoxicity is modulated by the rate of peptide aggregation: Abeta dimers and trimers correlate with neurotoxicity. *J. Neurosci.* **28**, 11950-11958.
- Hyun D.H., Lee M., Hattori N., Kubo S., Mizuno Y., Halliwell B., Jenner P. (2002). Effect of wild-type or mutant Parkin on oxidative damage, nitric oxide, antioxidant defenses, and the proteasome. *J. Biol. Chem.* **277**, 28572-28577.
- Imahori K. and Uchida T. (1997). Physiology and pathology of tau protein kinases in relation to Alzheimer's disease. *J. Biochem.* **121**, 179-188.
- Inoue S. (2008). In situ Abeta pores in AD brain are cylindrical assembly of Abeta protofilaments. *Amyloid* **15**, 223-233.
- Ionescu-Zanetti C., Khurana R., Gillespie J.R., Petrick J.S., Trabachino L.C., Minert L.J., Carter S.A., Fink A.L. (1999). Monitoring the assembly of Ig light-chain amyloid fibrils by atomic force microscopy. *Proc. Natl. Acad. Sci. USA* **96**, 13175-13179.
- Ishiguro K., Omori A., Takamatsu M., Sato K., Arioka M., Uchida T., Imahori K. (1992). Phosphorylation sites on tau by tau protein kinase I, a bovine derived kinase generating an epitope of paired helical filaments. *Neurosci. Lett.* **148**, 202-206.
- Jahn T.T. and Redford S.E. (2008). Folding versus aggregation: polypeptide conformations on competing pathways. *Arch. Biochem. Biophys.* **469**, 100-117.
- Jan A., Gokce O., Luthi-Carter R., Lashuel H.A. (2008). The ratio of monomeric to aggregated forms of Abeta40 and Abeta42 is an important determinant of amyloid-beta aggregation, fibrillogenesis, and toxicity. *J. Biol. Chem.* **283**, 28176-28189.
- Jarrett J.T., Berger E.P., Lansbury P.T.Jr. (1993). The carboxy terminus of the beta amyloid protein is critical for the seeding of amyloid formation: implications for the pathogenesis of Alzheimer's disease. *Biochemistry* **32**, 4693-4697.
- Jenkins S.M. and Johnson G.V. (1998). Tau complexes with phospholipase C-gamma in situ. *Neuroreport* **9**, 67-71.

## Amyloid Cytotoxicity and Membrane Lipid Composition

- Ji S.R., Wu Y., Sui S.F. (2002). Cholesterol is an important factor affecting the membrane insertion of beta-amyloid peptide (A beta 1-40), which may potentially inhibit the fibril formation. *J. Biol. Chem.* **277**, 6273-6279.
- Jin K., Galvan V., Xie L., Mao X.O., Gorostiza O.F., Bredesen D.E., Greenberg D.A. (2004). Enhanced neurogenesis in Alzheimer's disease transgenic (PDGF-APPs<sub>w</sub>,Ind) mice. *Proc. Natl. Acad. Sci. USA* **101**, 13363-13367.
- Ju Yeon B. and Yeon Hee S. (2005). Blockade of 5-HT(3) receptor with MDL 72222 and Y 25130 reduces beta-amyloid protein (25-35)-induced neurotoxicity in cultured rat cortical neurons *Eur. J. Pharmacol.* **520**, 12-21.
- Jurevics H. and Morell P. (1995). Cholesterol for synthesis of myelin is made locally, not imported into brain. *J. Neurochem.* **64**, 895-901.
- Kagan B.L., Azimov R., Azimova R. (2004). Amyloid peptide channels. *J. Membr. Biol.* **202**, 1-10.
- Kagan B.L. and Thundimadathil J. (2010). Amyloid peptide pores and the beta sheet conformation. *Adv. Exp. Med. Biol.* **677**, 150-167.
- Kaiser R.D. and London E. (1998). Location of diphenylhexatriene (DPH) and its derivatives within membranes: comparison of different fluorescence quenching analyses of membrane depth. *Biochemistry* **37**, 8180-8190.
- Kakio A., Nishimoto S.I., Yanagisawa K., Kozutsumi Y., Matsuzaki K. (2001). Cholesterol-dependent formation of GM1 ganglioside-bound amyloid  $\beta$ -protein, an endogenous seed for Alzheimer amyloid. *J. Biol. Chem.* **276**, 24985-24990.
- Kakio A., Nishimoto S., Yanagisawa K., Kozutsumi Y., Matsuzaki K. (2002). Interactions of amyloid  $\beta$ -protein with various gangliosides in raft-like membranes: importance of GM1 ganglioside-bound form as an endogenous seed for Alzheimer amyloid. *Biochemistry* **41**, 7385-7390.
- Kakio A., Nishimoto S., Kozutsumi Y., Matsuzaki K. (2003). Formation of a membrane-active form of amyloid  $\beta$ -protein in raft-like model membranes. *Biochem. Biophys. Res. Commun.* **303**, 514-518.
- Kalanj S., Kracun I., Rosner H., Cosovic C. (1991). Regional distribution of brain gangliosides in Alzheimer's disease. *Neurol. Croat.* **40**, 269-281.
- Kamiguchi H. (2006). The region-specific activities of lipid rafts during axon growth and guidance. *J. Neurochem.* **98**, 330-335.
- Kaminski Schierle G.S., Van de Linde S., Erdelyi M., Esbjörner E.K., Klein T., Rees E., Bertoni C.W., Dobson C.M., Sauer M., Kaminski, C.F. (2011). In situ measurements of the formation and morphology of intracellular  $\beta$ -amyloid fibrils by super-resolution fluorescence imaging. *J. Am. Chem. Soc.* **133**, 12902-12905.
- Kaneko I., Morimoto K., Kubo T. (2001). Drastic neuronal loss in vivo by  $\beta$ -amyloid racemized at Ser(26) residue: conversion of non-toxic [D-Ser(26)] beta-amyloid 1-14 to toxic and proteinase-resistant fragments. *Neuroscience* **104**, 1003-1011.
- Kang J., Lemaire H.G., Unterbeck A., Salbaum J.M., Masters C.L., Grzeschik K.H., Multhaup G., Beyreuther K., Müller-Hill B. (1987). The precursor of Alzheimer's disease amyloid A4 protein resembles a cell-surface receptor. *Nature* **325**, 733-736.
- Kawahara M., Kuroda Y., Arispe N., Rojas E. (2000). Alzheimer's  $\beta$ -amyloid, human islet amylin, and prion protein fragment evoke intracellular free calcium elevation by a common mechanism in a hypothalamic GnRH neuronal cell line. *J. Biol. Chem.* **275**, 14077-14083.
- Kawarabayashi T., Shoji M., Younkin L.H., Wen-Lang L., Dickson D.W., Murakami T., Matsubara E., Abe K., Ashe K.H., Younkin S.G. (2004). Dimeric amyloid  $\beta$  protein rapidly accumulates in the cytoplasm of hippocampal CA1 pyramidal neurons. *Neuroscience* **124**, 103-112.

- lates in lipid rafts followed by apolipoprotein E and phosphorylated tau accumulation in the Tg2576 mouse model of Alzheimer's disease. *J. Neurosci.* **24**, 3801-3809.
- Kayed R., Head E., Thompson J.L., McIntire T.M., Milton S.C., Cotman C.W., Glabe C.G. (2003). Common structure of soluble amyloid oligomers implies common mechanism of pathogenesis. *Science* **300**, 486-489.
- Kayed R., Sokolov Y., Edmonds B., McIntire T.M., Milton S.C., Hall J.E., Glabe C.G. (2004). Permeabilization of lipid bilayers is a common conformation-dependent activity of soluble amyloid oligomers in protein misfolding diseases. *J. Biol. Chem.* **279**, 46363-46366.
- Kayed R. and Glabe C.G. (2006). Conformation-dependent anti-amyloid oligomer antibodies. *Methods Enzymol.* **413**, 326-344.
- Kayed R., Head E., Sarsoza F., Saing T., Cotman C.W., Necula M., Margol L., Wu J., Breydo L., Thompson J.L., Rasool S., Gurlo T., Butler P., Glabe C.G. (2007). Fibril specific, conformation dependent antibodies recognize a generic epitope common to amyloid fibrils and fibrillar oligomers that is absent in prefibrillar oligomers. *Mol. Neurodegener.* **2**, 1-18.
- Kayed R., Pensalfini A., Margol L., Sokolov Y., Sarsoza F., Head E., Hall J., Glabe C.G. (2009). Annular protofibrils are a structurally and functionally distinct type of amyloid oligomer. *J. Biol. Chem.* **284**, 4230-4237.
- Kempermann G. and Gage F.H. (1999). New nerve cells for the adult brain. *Sci. Am.* **280**, 48-53.
- Kenworthy A.K., Petranova N., Edidin M. (2000). High-resolution FRET microscopy of cholera toxin B-subunit and GPI-anchored proteins in cell plasma membranes. *Mol. Biol. Cell.* **11**, 1645-1655.
- Kenworthy A.K., Nichols B.J., Remmert C.L., Hendrix G.M., Kumar M., Zimmerberg J., Lipincott-Schwartz J. (2004). Dynamics of putative raft-associated proteins at the cell surface. *J. Cell Biol.* **165**, 735 - 746.
- Kim H.Y., Cho M.K., Kumar A., Maier E., Siebenhaar C., Becker S., Fernandez C.O., Lashuel H.A., Benz R., Lange A., Zweckstetter M. (2009). Structural properties of pore-forming oligomers of alpha-synuclein. *J. Am. Chem. Soc.* **131**, 17482-17489.
- Kimura N. and Yanagisawa K. (2007). Endosomal accumulation of GM1 ganglioside-bound amyloid  $\beta$ -protein in neurons of aged monkey brains. *Neuroreport* **18**, 1669-1673.
- Kinoshita A., Fukumoto H., Shah T., Whelan C.M., Irizarry M.C., Hyman B.T. (2003). Demonstration by FRET of BACE interaction with the amyloid precursor protein at the cell surface and in early endosomes. *J. Cell Sci.* **116**, 3339-3346.
- Klyubin I., Walsh D.M., Lemere C.A., Cullen V.K., Shankar G.M., Betts V., Spooner E.T., Jiang L., Amwyll R., Selkoe D.J., Rowan M.J. (2005). Amyloid beta protein immunotherapy neutralizes Abeta oligomers that disrupt synaptic plasticity *in vivo*. *Nat. Med.* **11**, 556-561.
- Koffie R.M., Meyer-Luehmann M., Hashimoto T., Adams K.W., Mielke M.L., Garcia-Alloza M., Micheva K.D., Smith S.J., Kim M.L., Lee V.M., Hyman B.T., Spires-Jones T.L. (2009). Oligomeric amyloid beta associates with postsynaptic densities and correlates with excitatory synapse loss near senile plaques. *Proc. Natl. Acad. Sci. USA* **106**, 4012-4017.
- Koike H., Tomioka S., Sorimachi H., Saido T.C., Maruyama K., Okuyama A., Fujisawa-Sehara A., Ohno S., Suzuki K., Ishiura S. (1999). Membrane-anchored metallopro-tease MDC9 has an  $\alpha$ -secretase activity responsible for processing the amyloid precursor protein. *Biochem. J.* **343**, 371-375.
- Kojro E., Gimpl G., Lammich S., März W., Fahrenholz F. (2001). Low cholesterol stimulates the nonamyloidogenic pathway by its effect on the  $\alpha$ -secretase ADAM 10 *Proc. Natl. Acad. Sci. USA* **98**, 5815-5820.

## Amyloid Cytotoxicity and Membrane Lipid Composition

- Kölsch H., Heun R., Kerksiek A., Bergmann K.V., Maier W., Lütjohann D. (2004). Altered levels of plasma 24S-hydroxycholesterol and 7-hydroxycholesterol in demented patients. *Neurosci. Lett.* **368**, 303-308.
- Koudinov A.R. and Koudinova N.V. (2005). Cholesterol homeostasis failure as a unifying cause of synaptic degeneration. *J. Neurol. Sci.* **230**, 233-240.
- Kourie J.I. (2001). Mechanisms of amyloid  $\beta$  protein-induced modification in ion transport systems: implications for neurodegenerative diseases. *Cell. Mol. Neurobiol.* **21**, 173-213.
- Kourie J.I., Farrelly P.V., Henry C.L. (2001). Channel activity of deamidated isoforms of prion protein fragment 106-126 in planar lipid bilayers. *J. Neurosci. Res.* **66**, 214-220.
- Kourie J.I. and Henry C.L. (2002). Ion channel formation and membrane-linked pathologies of misfolded hydrophobic proteins: the role of dangerous unchaperoned molecules. *Clin. Exp. Pharmacol. Physiol.* **29**, 741-753.
- Kracun I., Kalanj S., Talan-Hranilovic J., Cosovic C. (1992). Cortical distribution of gangliosides in Alzheimer's disease. *Neurochem. Int.* **20**, 433-438.
- Kranenburg O., Bouma B., Kroon-Batenburg L.M.J., Reijerkerk A., Wu Y.P., Voest E.E., Gebbink M.F.B.G. (2002). Tissue-type plasminogen activator is a multiligand cross-beta structure receptor. *Current Biol.* **12**, 1833-1839.
- Kremer J.J., Pallitto M.M., Sklansky D.J., Murphy R.M. (2000). Correlation of beta-amyloid aggregate size and hydrophobicity with decreased bilayer fluidity of model membranes. *Biochemistry* **39**, 10309-10318.
- Kreutz F., Frozza R.L., Breier A.C., de Oliveira V.A., Horn A.P., Pettenuzzo L.F., Netto C.A., Salbego C.G., Trindade V.M (2011). Amyloid- $\beta$  induced toxicity involves ganglioside expression and is sensitive to GM1 neuroprotective action. *Neurochem. Int.* **59**, 648-655.
- Kumar S. and Udgaonkar J.B. (2009). Structurally distinct amyloid protofibrils form on separate pathways of aggregation of a small protein. *Biochemistry* **48**, 6441-6449.
- Lambert M.P., Barlow A.K., Chromy B.A., Edwards C., Freed R., Liosatos M., Morgan T.E., Rozovsky I., Trommer B., Viola K.L., Wals P., Zhang C., Finch C.E., Krafft G.A., Klein, W.L.(1998). Diffusible nonfibrillar ligands derived from Abeta 1-42 are potent central nervous system neurotoxins. *Proc. Natl. Acad. Sci. USA* **95**, 6448-6453.
- Lambert M.P., Viola K.L., Chromy B.A., Chang L., Morgan T.E., Yu J., Venton D.L., Krafft G.A., Finch C.E., Klein W.L. (2001). Vaccination with soluble Abeta oligomers generates toxicity-neutralizing antibodies. *J. Neurochem.* **79**, 595-605.
- Lashuel H.A., Hartley D., Petre B.M., Walz T., Lansbury, P.T.Jr. (2002) Neurodegenerative disease: amyloid pores from pathogenic mutations. *Nature* **418**, 291.
- Lashuel H.A. and Lansbury P.T.Jr. (2006). Are amyloid diseases caused by protein aggregates that mimic bacterial pore-forming toxins? *Q. Rev. Biophys.* **39**, 167-201.
- Lauren J., Gimbel D.A., Nygaard H.B., Gilbert J.W., Strittmatter S.M. (2009). Cellular prion protein mediates impairment of synaptic plasticity by amyloid-beta oligomers. *Nature* **457**, 1128-1132.
- Ledeen R.W., Wu G., Lu Z.H., Kozireski-Chuback D., Fang Y. (1998). The role of GM1 and other gangliosides in neuronal differentiation. Overview and new finding. *Ann. N.Y. Acad. Sci.* **845**, 161-175.
- Ledeen R.W. and Wu G. (2007). GM1 in the nuclear envelope regulates nuclear calcium through association with a nuclear sodiumcalcium exchanger. *J. Neurochem.* **103**, 126-134.
- Ledesma M.D. and Dotti C.G. (2005). The conflicting role of brain cholesterol in Alzheimer's disease: lessons from the brain plasminogen system. *Biochem. Soc. Symp.* **72**, 129-138.
- Ledesma M.D. and Dotti C.G. (2006). Amyloid excess in Alzheimer's disease: what is cholesterol to be blamed for? *FEBS Lett.* **580**, 5525-5532.

- Lee G. and Rook S.L. (1992). Expression of tau protein in non-neuronal cells:microtubule-binding and stabilization. *J. Cell Sci.* **102**, 227–237.
- Lee I.P., McKenzie S., Muller F.J., Snyder E.Y. (2008). Neural stem cell transplantation in mouse brain. *Curr. Protoc. Neurosci.* **3**, 3-10.
- Lee S., Fernandez E.J., Good T.A. (2007). Role of aggregation conditions in structure, stability, and toxicity of intermediates in the Abeta fibril formation pathway. *Protein Sci.* **16**, 723–732.
- Lee S.J., Liyanage U., Bickel P.E., Xia W., Lansbury P.T., Kosik K.S. (2003). A detergent-insoluble membrane compartment contains A beta *in vivo*. *Nat. Med.* **4**, 730–734.
- Lee V.M., Goedert M., Trojanowski J.Q. (2001). Neurodegenerative tauopathies. *Annu. Rev. Neurosci.* **24**, 1121–1159.
- Leissing M.A., Murphy M.P., Mead T.R., Akbari Y., Sugarman M.C., Jannatipour M., Anliker B., Müller U., Saftig P., Strooper B.D., Wolfe M.S., Golde T.E., LaFerla F.M. (2002). A physiologic signaling role for the  $\gamma$ -secretase-derived intracellular fragment of APP. *Proc. Natl. Acad. Sci. USA* **99**, 4697–4702.
- Lentz B.R. (1989). Membrane “fluidity” as detected by diphenylhexatriene probes. *Chem. Phys. Lipids* **50**, 171–190.
- Lentz B.R. (1993). Use of fluorescent probes to monitor molecular order and motions within liposome bilayers. *Chem. Phys. Lipids* **64**, 99–116.
- Lesné S., Koh M.T., Kotilinek L., Kayed R., Glabe C.G., Yang A., Gallagher M., Ashe K.H. (2006). A specific amyloid  $\beta$  protein assembly in the brain impairs memory. *Nature* **440**, 352–357.
- Levison S.W. and Goldman J.E. (1993). Both oligodendrocytes and astrocytes develop from progenitors in the subventricular zone of postnatal rat forebrain. *Neuron* **10**, 201–212.
- Levy-Lahad E., Wasco W., Poorkaj P., Romano D.M., Oshima J., Pettingell W.H., Yu C.E., Jondro P.D., Schmidt S.D., Wang K. (1995). Candidate gene for the chromosome 1 familial Alzheimer’s disease locus. *Science* **269**, 973–977.
- Lewis V. and Hooper N.M. (2011). The role of lipid rafts in prionprotein biology. *Front. Biosci.* **16**, 151–168.
- Li G., Peskind E.R., Millard S.P., Chi P., Sokal I., Yu C.E., Bekris L.M., Raskind M.A., Galasko D.R., Montine T.J. (2009). Cerebrospinal fluid concentration of brain-derived neurotrophic factor and cognitive function in non-demented subjects. *PLoS One* **4**, e5424.
- Li X. and Zuo P. (2005). Effects of Abeta25-35 on neurogenesis in the adult mouse subventricular zone and dentate gyrus. *Neurol. Res.* **27**, 218–222.
- Lichtenberg B., Mandelkow E.M., Hagedstedt T., Mandelkow E. (1988). Structure and elasticity of microtubule-associated protein tau. *Nature* **334**, 359–362.
- Lin H., Bhatia R., Lal R. (2001). Amyloid beta protein forms ion channels: implications for Alzheimer’s disease pathophysiology. *FASEB J.* **15**, 2433–2444.
- Lin M.S., Chen L.Y., Wang S.S., Chang Y., Chen W.Y. (2008). Examining the levels of ganglioside and cholesterol in cell membrane on attenuation the toxicity of beta-amyloid peptide. *Coll. Surf. B Biomem.* **65**, 173–177.
- Lingwood D. and Simons K. (2010). Lipid rafts as a membrane-organizing principle. *Science* **327**, 46–50.
- Litvinovich S.V., Brew S.A., Aota S., Akiyama S.K., Haudenschild C., Ingham K.C. (1998). Formation of amyloid-like fibrils by self-association of a partially unfolded fibronectin type III module. *J. Mol. Biol.* **280**, 245–258.
- Liu Q. and Zhao B. (2004). Nicotine attenuates  $\beta$ -amyloid peptide-induced neurotoxicity, free radical and calcium accumulation in hippocampal neuronal cultures. *Brit. J. Pharmacol.* **141**, 746–754.

## Amyloid Cytotoxicity and Membrane Lipid Composition

- Liu R., McAllister C., Lyubchenko Y., Sierks M.R. (2004). Residues 17–20 and 30–35 of beta-amyloid play critical roles in aggregation. *J. Neurosci. Res.* **75**, 162–171.
- Lledo P.M. and Gheusi G. (2003). Olfactory processing in a changing brain. *Neuroreport* **14**, 1655–1663.
- Lois C. and Alvarez-Buylla A. (1993). Proliferating subventricular zone cells in the adult mammalian forebrain can differentiate into neurons and glia. *Proc. Natl. Acad. Sci. USA* **90**, 2074–2077.
- López-Toledano M.A. and Shelanski M.L. (2004). Neurogenic effect of beta-amyloid peptide in the development of neural stem cells. *J. Neurosci.* **24**, 5439–5444.
- Lopez-Toledano M.A. and Shelanski M.L. (2007). Increased neurogenesis in young transgenic mice overexpressing human APP(Sw, Ind). *J. Alzheimers. Dis.* **12**, 229–240.
- Lunn J.S., Sakowski S.A., Hur J., Feldman E.L. (2011). Stem cell technology for neurodegenerative diseases. *Ann. Neurol.* **70**, 353–361.
- Maas T., Eidenmuller J., Brandt R. (2000). Interaction of tau with the neuralmembrane cortex is regulated by phosphorylation at sites that are modified in paired helical filaments. *J. Biol. Chem.* **275**, 15733–15740.
- MacManus A., Ramsden M., Murray M., Henderson Z., Pearson H.A., Campbell V. A. (2000). Enhancement of (45)Ca<sup>2+</sup> influx and voltage-dependent Ca<sup>2+</sup> channel activity by β-amyloid-(1–40) in rat cortical synaptosomes and cultured cortical neurons. Modulation by the proinflammatory cytokine interleukin-1β. *J. Biol. Chem.* **275**, 4713–4718.
- Mahley RW. (1988). Apolipoprotein E: cholesterol transport protein with expanding role in cell biology. *Science* **240**, 622–630.
- Malchiodi-Albedi F., Contrusciere V., Raggi C., Fecchi K., Rainaldi G., Paradisi S., Matteucci A., Santini M.T., Sargiacomo M., Frank C., Gaudiano M.C., Diociaiuti M. (2010). Lipid raft disruption protects mature neurons against amyloid oligomer toxicity. *Biochim. Biophys. Acta* **1802**, 406–415.
- Malchiodi-Albedi F., Paradisi S., Matteucci A., Frank C., Diociaiuti M. (2011). Amyloid oligomer neurotoxicity, calcium dysregulation, and lipid rafts. *Int. J. Alzheimers Dis.* **8**, 906964.
- Mamikonyan G., Necula M., Mkrtichyan M., Ghochikyan A., Petrushina I., Movsesyan N., Mina E., Kiyatkin A., Glabe C.G., Cribbs D.H., Agadjanyan M.G. (2007). Anti-A beta 1–11 antibody binds to different beta-amyloid species, inhibits fibril formation, and disaggregates preformed fibrils but not the most toxic oligomers. *J. Biol. Chem.* **282**, 22376–22386.
- Mandal P.K. and Pettegrew J.W. (2004). Alzheimer's disease: NMR studies of asialo (GM1) and trisialo (GT1b) ganglioside interactions with Aβ(1–40) peptide in a membrane mimetic environment. *Neurochem. Res.* **29**, 447–453.
- Marcon G., Plakoutsi G., Canale C., Relini A., Taddei N., Dobson C.M., Ramponi G., Chiti F. (2005). Amyloid formation from HypF-N under conditions in which the protein is initially in its native state. *J. Mol. Biol.* **347**, 323–335.
- Martins I.C., Kuperstein I., Wilkinson H., Maes E., Vanbrabant M., Jonckheere W., Van Gelder P., Hartmann D., D'Hooge R., De Strooper B., Schymkowitz J., Rousseau F. (2008). Lipids revert inert Abeta amyloid fibrils to neurotoxic protofibrils that affect learning in mice. *EMBO J.* **27**, 224–33.
- Mason R.P., Shoemaker W.J., Shajenko L., Chambers T.E., Herbette L.G. (1992). Evidence for changes in the Alzheimer's disease brain cortical membrane structure mediated by cholesterol. *Neurobiol. Aging* **13**, 413–419.
- Masters C.L., Cappai R., Barnham K.J., Villemagne V.L. (2006). Molecular mechanisms for Alzheimer's disease: implications for neuroimaging and therapeutics. *J. Neurochem.* **97**, 1700–1725.

- Masters C.L., Simms G., Weinman N.A., Multhaup G., McDonald B.L., Beyreuther K. (1985). Amyloid plaque core protein in Alzheimer disease and Down syndrome. *Proc. Natl. Acad. Sci. USA* **82**, 4245–4249.
- Matsuoka Y., Saito M., LaFrancois J., Saito M., Gaynor K., Olm V., Wang L., Casey E., Lu Y., Shiratori C., Lemere C., Duff K. (2003). Novel therapeutic approach for the treatment of Alzheimer's disease by peripheral administration of agents with an affinity to  $\beta$ -amyloid. *J. Neurosci.* **23**, 29–33.
- Matsuzaki K. (2007). Physicochemical interactions of amyloid beta-peptide with lipid bilayers. *Biochim. Biophys. Acta* **1768**, 1935–1942.
- Matsuzaki K., Kato K., Yanagisawa K. (2010). Abeta polymerization through interaction with membrane gangliosides. *Biochim. Biophys. Acta* **1801**, 868–877.
- Mattson M.P. (1999). Impairment of membrane transport and signal transduction systems by amyloidogenic proteins. *Methods Enzymol.* **309**, 733–768.
- Mayeux R. (2010). Clinical practice. Early Alzheimer's disease. *N. Engl. J. Med.* **362**, 2194–2201.
- Mazur-Kolecka B., Golabek A., Nowicki K., Flory M., Frackowiak J. (2006). Amyloid-beta impairs development of neuronal progenitor cells by oxidative mechanisms. *Neurobiol. Aging* **27**, 1181–1192.
- McLaurin J. and Chakrabarty A. (1996). Membrane disruption by Alzheimer  $\beta$ -amyloid peptides mediated through specific binding to either phospholipids or gangliosides. Implications for neurotoxicity. *J. Biol. Chem.* **271**, 26482–26489.
- McLaurin J., Franklin T., Fraser P.E., Chakrabarty A. (1998). Structural transitions associated with the interaction of Alzheimer beta-amyloid peptides with gangliosides. *J. Biol. Chem.* **273**, 4506–4515.
- McLaurin J., Yang D., Yip C.M., Fraser P.E. (2000) Review: modulating factors in amyloid-beta fibril formation. *J. Struct. Biol.* **130**, 259–270.
- Mehta T. K., Dougherty J. J., Wu J., Choi C. H., Khan G. M., Nichols R. A. (2008). Defining pre-synaptic nicotinic receptors regulated by beta amyloid in mouse cortex and hippocampus with receptor null mutants. *J. Neurochem.* **109**, 1452–1458.
- Michel G., Mercken M., Murayama M., Noguchi K., Ishiguro K., Imahori K., Takashima A. (1998). Characterization of tau phosphorylation in glycogen synthase kinase-3beta and cyclin dependent kinase-5 activator (p23) transfected cells. *Biochim. Biophys. Acta* **1380**, 177–182.
- Mirzabekov T.A., Lin M.C., Kagan B.L. (1996). Pore formation by the cytotoxic islet amyloid peptide amylin. *J. Biol. Chem.* **271**, 1988–1992.
- Mizuno T., Nakata M., Naiki H., Michikawa M., Wang R., Haass C., Yanagisawa K. (1999). Cholesterol-dependent generation of a seeding amyloid  $\beta$ -protein in cell culture. *J. Biol. Chem.* **274**, 15110–15114.
- Mohanty J.G., Jaffe J.S., Schulman E.S., Raible D.G. (1997). A highly sensitive fluorescent micro-assay of  $H_2O_2$  release from activated human leukocytes using a dihydroxyphenoazine derivative. *J. Immunol. Methods* **202**, 133–141.
- Molander-Melin M., Blennow K., Bogdanovic N., Dellheden B., Mansson J.E., Fredman P. (2005). Structural membrane alterations in Alzheimer brains found to be associated with regional disease development; increased density of gangliosides GM1 and GM2 and loss of cholesterol in detergent-resistant membrane domains. *J. Neurochem.* **92**, 171–182.
- Monoi H., Futaki S., Kugimiya S., Minakata H., Yoshihara K. (2000). Poly-L-glutamine forms cation channels: relevance to the pathogenesis of the polyglutamine diseases. *Biophys. J.* **78**, 2892–2899.

## Amyloid Cytotoxicity and Membrane Lipid Composition

- Moreira P.I., Santos M.S., Moreno A., Rego A.C., Oliveira C. (2002). Effect of amyloid beta-peptide on permeability transition pore: a comparative study. *J. Neurosci. Res.* **15**, 257–267.
- Mori T., Buffo A., Gotz M. (2005). The novel roles of glial cells revisited: the contribution of radial glia and astrocytes to neurogenesis. *Curr. Top. Dev. Biol.* **69**, 67–99.
- Morishima-Kawashima M. and Kosik K.S. (1996). The pool of map kinase associated with microtubules is small but constitutively active. *Mol. Biol. Cell.* **7**, 893–905.
- MRC/BHF Heart Protection Study of cholesterol lowering with simvastatin in 20,536 high-risk individuals: a randomized placebo-controlled trial. (2002). *Lancet* **360**, 7–22.
- Murray I.V., Liu L., Komatsu H., Uryu K., Xiao G., Lawson J.A., Axelsen P.H. (2007). Membrane-mediated amyloidogenesis and the promotion of oxidative lipid damage by amyloid beta proteins. *J. Biol. Chem.* **282**, 9335–9345.
- Mutoh T., Hirabayashi Y., Mihara T., Ueda M., Koga H., Ueda A., Kokura T., Yamamoto H. (2006). Role of glycosphingolipids and therapeutic perspectives on Alzheimer's disease. *CNS Neurol. Disord. Drug Targets* **5**, 375–380.
- Naguib Y.M. (1998). A fluorometric method for measurement of peroxyl radical scavenging activities of lipophilic antioxidants. *Anal. Biochem.* **265**, 290–298.
- Necula M., Kayed R., Milton S., Glabe C.G. (2007). Small molecule inhibitors of aggregation indicate that amyloid beta oligomerization and fibrillization pathways are independent and distinct. *J. Biol. Chem.* **282**, 10311–10324.
- Nekooki-Machida Y., Kurosawa M., Nukina N., Ito K., Oda T., Tanaka M. (2009). Distinct conformations of *in vitro* and *in vivo* amyloids of huntingtin-exon1 show different cytotoxicity. *Proc. Natl. Acad. Sci. USA* **106**, 9679–9684.
- Nelson R., Sawaya M.R., Balbirnie M., Madsen, A.Ø., Riek C., Grothe R., Eisenberg D. (2005). Structure of the cross- $\beta$  spine of amyloid-like fibrils. *Nature* **435**, 773–778.
- Neri T., Bucciantini M., Rosti V., Raimondi S., Relini A., Massa M., Zuccotti M., Donadei S., Stefani M., Redi C.A., Merlini G., Stoppini M., Garagna S., Bellotti V. (2010). Embryonic stem and haematopoietic progenitor cells resist to A $\beta$  oligomer toxicity and maintain the differentiation potency in culture. *Amyloid* **17**, 137–145.
- Ngamukote S., Yanagisawa M., Ariga T., Ando S., Yu R.K. (2007). Developmental changes of glycosphingolipids and expression of glycogenes in mouse brains. *J. Neurochem.* **103**, 2327–2341.
- Nicolet Y., Piras C., Legrand P., Hatchikian C.E., Fontecilla-Camps J.C. (1999). Desulfovibrio desulfuricans iron hydrogenase: the structure shows unusual coordination to an active site Fe binuclear center. *Structure* **7**, 13–23.
- Novitskaya V., Bocharova O.V., Bronstein I., Baskakov I.V. (2006). Amyloid fibrils of mammalian prion protein are highly toxic to cultured cells and primary neurons. *J. Biol. Chem.* **281**, 13828–13836.
- O'Nuallain B. and Wetzel R. (2002). Conformational Abs recognizing a generic amyloid fibril epitope. *Proc. Natl. Acad. Sci. USA* **99**, 1485–1490.
- Okada T., Wakabayashi M., Ikeda K., Matsuzaki K. (2007). Formation of toxic fibrils of Alzheimer's amyloid beta-protein-(1-40) by monosialoganglioside GM1, a neuronal membrane component. *J. Mol. Biol.* **371**, 481–489.
- Okada T., Ikeda K., Wakabayashi M., Ogawa M., Matsuzaki K. (2008). Formation of toxic Abeta(1-40) fibrils on GM1 ganglioside-containing membranes mimicking lipid rafts: polymorphisms in Abeta(1-40) fibrils. *J. Mol. Biol.* **382**, 1066–1074.
- Olzscha H., Schermann S.M., Woerner A.C., Pinkert S., Hecht M.H., Tartaglia G.G., Ven-druscolo M., Hayer-Hartl M., Hartl F.U., Vabulas R.M. (2011). Amyloid-like aggregates sequester numerous metastable proteins with essential cellular functions. *Cell* **144**, 67–78.

- Oma Y., Kino Y., Sasagawa N., Ishiura S. (2005). Comparative analysis of the cytotoxicity of homopolymeric amino acids. *Biochim. Biophys. Acta* **1748**, 174-179.
- Orrenius S., Zhovotovsky B., Nicotera P. (2003). Regulation of cell death: the calcium-apoptosis link. *Nat Rev* **4**, 552–565.
- Pappolla M.A., Omar R.A., Chyan Y.J., Ghiso J., Hsiao K., Bozner P., Perry G., Smith M.A., Cruz-Sanchez F. (2001). Induction of NADPH cytochrome P450 reductase by the Alzheimer  $\beta$ -protein. Amyloid as a “foreign body. *J. Neurochem.* **78**, 121–128.
- Parton R.G. (1994). Ultrastructural localization of gangliosides; GM1 is concentrated in caveolae. *J. Histochem. Cytochem.* **42**, 155–166.
- Paschos A., Glass R.S., Böck A. (2001). Carbamoylphosphate requirement for synthesis of the active center of [NiFe]-hydrogenases. *FEBS Lett.* **488**, 9-12.
- Paterson J.A., Privat A., Ling E.A., Leblond C.P. (1973). Investigation of glial cells in semithin sections. 3 Transformation of subependymal cells into glial cells, as shown by radioautography after 3 H-thymidine injection into the lateral ventricle of the brain of young rats. *J. Comp. Neurol.* **149**, 83–102.
- Patrick G.N., Zukerberg L., Nikolic M., de da Monte S., Dikkes P., Tsai L.H. (1999). Conversion of p35 to p25 deregulates Cdk5 activity and promotes neurodegeneration. *Nature* **402**, 615–622.
- Pearson X.H., Teng Y.D., Snyder E.Y. (2008). Important precautions when deriving patient-specific neural elements from pluripotent cells. *Cyotherapy* **11**, 815-824.
- Pedersen J.S., Christensen G., Otzen D.E. (2004). Modulation of S6 fibrillation by unfolding rates and gatekeeper residues. *J. Mol. Biol.* **341**, 575-588.
- Pellistri F., Bucciantini M., Relini A., Glizzi A., Robello M., Stefani M. (2008). Generic interaction of pre-fibrillar amyloid aggregates with NMDA and AMPA receptors results in free  $\text{Ca}^{2+}$  increase in primary neuronal cells. *J. Biol. Chem.* **283**, 29950-29960.
- Pensalfini A., Zampagni M., Liguri G., Becatti M., Evangelisti E., Fiorillo C., Bagnoli S., Cellini E., Naemias B., Sorbi S., Cecchi C. (2011). Membrane cholesterol enrichment prevents  $\text{A}\beta$ -induced oxidative stress in Alzheimer's fibroblasts. *Neurobiol. Aging* **32**, 210-22.
- Petkova A.T., Leapman R.D., Guo Z., Yau W.M., Mattson M.P., Tycko R. (2005). Self-propagating, molecular-level polymorphism in Alzheimer's beta-amyloid fibrils. *Science* **307**, 262-265.
- Pfrieger F.W. (2003). Cholesterol homeostasis and function in neurons of the central nervous system. *Cell. Mol. Life Sci.* **60**, 1158-11571.
- Pike L.J. (2003). Lipid rafts: bringing order to chaos. *J. Lipid Res.* **44**, 655 – 667.
- Poirier J., Baccichet A., Dea D., Gauthier S. (1993). Cholesterol synthesis and lipoprotein reuptake during synaptic remodelling in hippocampus in adult rats. *Neuroscience* **55**, 81-90.
- Poirier J., Davignon J., Bouthillier D., Kogan S., Bertrand P., Gauthier S. (1993). Apolipoprotein E polymorphism and Alzheimer's disease. *Lancet* **342**, 697–699.
- Poirier J. (2003). Apolipoprotein E and cholesterol metabolism in the pathogenesis and treatment of Alzheimer's disease. *Trends Mol. Med.* **9**, 94-101.
- Pollard H.B., Arispe N., Rojas E. (1995). Ion channel hypothesis for Alzheimer amyloid peptide neurotoxicity. *Cell. Mol. Neurobiol.* **15**, 513-526.
- Pope-Coleman A., Tinker J.P., Schneider J.S. (2000). Effects of GM1 ganglioside treatment on pre- and postsynaptic dopaminergic markers in the striatum of parkinsonian monkeys. *Synapse* **36**, 120–128.
- Porat Y., Kolusheva S., Jelinek R., Gazit E. (2003). The human islet amyloid polypeptide forms transient membrane-active prefibrillar assemblies. *Biochemistry* **42**, 10971–10977.

## Amyloid Cytotoxicity and Membrane Lipid Composition

- Postina R., Schroeder A., Dewachter I., Bohl J., Schmitt U., Kojro E., Prinzen C., Endres K., Hiemke C., Blessing M., Flamez P., Dequenne A., Godaux E., Leuven F.V., Fahrenholz F. (2004). A disintegrin-metalloproteinase prevents amyloid plaque formation and hippocampal defects in an Alzheimer disease mouse model. *J. Clin. Invest.* **113**, 1456–1464.
- Prusiner S.B., Scott M.R., deArmond S.J., Cohen F.E. (1998). Prion protein biology. *Cell* **93**, 337–348.
- Puglielli L., Tanzi R.E., Kovacs D.M. (2003). Alzheimer's disease: the cholesterol connection. *Nat. Neurosci.* **6**, 7212–7212.
- Qin L., Liu Y., Cooper C., Liu B., Wilson B., Hong J.S. (2002). Microglia enhance  $\beta$ -amyloid peptide-induced toxicity in cortical and mesencephalic neurons by producing reactive oxygen species. *J. Neurochem.* **83**, 973–983.
- Qiu L., Lewis A., Como J., Vaughn M.W., Huang J., Somerharju P., Virtanen J., Cheng K.H. (2009) Cholesterol modulates the interaction of beta-amyloid peptide with lipid bilayers. *Bioophys. J.* **20**, 4299–3407.
- Quintas A., Vaz D.C., Cardoso I., Saraiva M.J., Brito R.M. (2001). Tetramer dissociation and monomer partial unfolding precedes protofibril formation in amyloidogenic transthyretin variants. *J. Biol. Chem.* **276**, 27207–27213.
- Quist A., Doudevski I., Lin H., Azimova R., Ng D., Frangione B., Kagan B., Ghiso J., Lal R. (2005). Amyloid ion channels: a common structural link for protein-misfolding disease. *Proc. Natl. Acad. Sci. USA* **102**, 10427–10432.
- Rasband W.S. (1997-2008). ImageJ. U.S. National Institutes of Health, Bethesda, Maryland, USA, <http://rsb.info.nih.gov/ij/>.
- Reissmann S., Hochleitner E., Wang H., Paschos A., Lottspeich F., Glass R.S., Böck A. (2003). Taming of a poison: biosynthesis of the NiFe-hydrogenase cyanide ligands. *Science* **299**, 1067–10670.
- Reixach N., Deechingkit S., Jiang X., Kelly J.W., Buxbaum J.N. (2004). Tissue damage in the amyloidoses: transthyretin monomers and nonnative oligomers are the major cytotoxic species in tissue culture. *Proc. Natl. Acad. Sci. USA* **101**, 2817–2822.
- Relini A., Torrassa S., Rolandi R., Glioza A., Rosano C., Canale C., Bolognesi M., Plakoutsi G., Bucciantini M., Chiti F., Stefani M. (2004). Monitoring the process of HypF fibrillization and liposome permeabilization by protofibrils. *J. Mol. Biol.* **338**, 943–957.
- Relini A., Canale C., De Stefano S., Rolandi R., Giorgetti S., Stoppini M., Rossi A., Fogolari F., Corazza A., Esposito G., Glioza A., Bellotti V. (2006). Collagen plays an active role in the aggregation of beta2-microglobulin under physiopathological conditions of dialysis-related amyloidosis. *J. Biol. Chem.* **281**, 16521–16529.
- Repetto E., Russo C., Venezia V., Nizzari M., Nitsch R.M., Schettini G. (2004). BACE1 over-expression regulates amyloid precursor protein cleavage and interaction with the ShcA adapter. *Ann. NY Acad. Sci.* **1030**, 330–338.
- Resende R., Pereira C., Agostinho P., Vieira A.P., Malva J.O., Oliveira C.R. (2007). Susceptibility of hippocampal neurons to  $\text{A}\beta$  peptide toxicity is associated with perturbation of  $\text{Ca}^{2+}$  homeostasis. *Brain Res.* **1143**, 11–21.
- Reszka A.A., Seger R., Diltz C.D., Krebs E.G., Fischer E.H. (1995). Association of mitogen-activated protein kinase with the microtubule cytoskeleton. *Proc. Natl. Acad. Sci. USA* **92**, 8881–8885.
- Richardson J.S. and Richardson D.C. (2002). Natural beta-sheet proteins use negative design to avoid edge-to-edge aggregation. *Proc. Natl. Acad. Sci. USA* **99**, 2754–2759.
- Rinia H.A., Kik R.A., Demel R.A., Snel M.M.E., Killian J.A., van der Eerden J.P.J.M., de Kruijff B. (2000). Visualization of highly ordered striated domains induced by transmembrane peptides in supported phosphatidylcholine bilayers. *Biochemistry* **39**, 5852–5858.

- Rodriguez J.J., Jones V.C., Verkhratsky A. (2009). Impaired cell proliferation in the subventricular zone in an Alzheimer's disease model. *Neuroreport* **20**, 907–912.
- Romiti E., Meacci E., Tanzi G., Becciolini L., Mitsutake S., Farnararo M., Ito M., Bruni P. (2001). Localization of neutral ceramidase in caveolin-enriched light membranes of murine endothelial cells. *FEBS Lett.* **506**, 163–168.
- Rosano C., Zuccotti S., Bucciantini M., Stefani M., Ramponi G., Bolognesi M. (2002). Crystal structure and anion binding in the prokaryotic hydrogenase maturation factor HypF acylphosphatase-like domain. *J. Mol. Biol.* **321**, 785–796.
- Rosenberg R.N. (2000). The molecular and genetic basis of AD: the end of the beginning: the 2000 Wartenberg lecture. *Neurology* **54**, 2045–2054.
- Rothblat D.S. and Schneider J.S. (1999). Regional differences in striatal dopamine uptake and release associated with recovery from MPTP-induced parkinsonism: an *in vivo* electrochemical study. *J. Neurochem.* **72**, 724–733.
- Rovira C., Arbez N., Mariani J. (2002).  $\text{A}\beta(25\text{-}35)$  and  $\text{A}\beta(1\text{-}40)$  act on different calcium channels in CA1 hippocampal neurons. *Biochem. Biophys. Res. Commun.* **296**, 1317–1321.
- Sakono M. and Zako T. (2010). Amyloid oligomers: formation and toxicity of Abeta oligomers. *FEBS J.* **277**; 1348–1358.
- Sasaki N., Takeuchi M., Chowei H., Kikuchi S., Hayashi N., Nakano H., Ikeda S., Yamagishi T., Kitamoto T., Saito T., Makita Z. (2002). Advanced glycation end products (AGE) and their receptor (RAGE) in the brain of patients with Creutzfeldt-Jakob disease with prion plaques. *Neurosci. Lett.* **326**, 117–120.
- Satija N.K., Singh V.K., Verma Y.K., Gupta P., Sharma S., Afrin F., Sharma M., Sharma P., Tripathi R.P., Gurudutta G.U. (2009). Mesenchymal stem cellbased therapy: a new paradigm in regenerative medicine. *J. Cell. Mol. Med.* **13**, 4385–4402.
- Saulino M.F. and Schengrund C.L. (1994). Differential accumulation of gangliosides by the brains of MPTP-lesioned mice. *J. Neurosci. Res.* **37**, 384–391.
- Scheuner D., Eckman C., Jensen M., Song X., Citron M., Suzuki N., Bird T.D., Hardy J., Hutton M., Kukull W., Larson E., Levy-Lahad E., Viitanen M., Peskind E., Poorkaj P., Schellenberg G., Tanzi R., Wasco W., Lannfelt L., Selkoe D.J., Younkin S. (1996). Secreted amyloid beta-protein similar to that in the senile plaques of Alzheimer's disease is increased *in vivo* by the presenilin 1 and 2 and APP mutations linked to familial Alzheimer's disease. *Nat Med.* **2**, 864–870.
- Schneider J.S., Pope A., Simpson K., Taggart J., Smith M.G., DiStefano L. (1992). Recovery from experimental Parkinsonism in primates with GM1 ganglioside treatment. *Science* **256**, 843–846.
- Schweers O., Schonbrunn-Hanebeck E., Marx A., Mandelkow E. (1994). Structural studies of tau protein and Alzheimer paired helical filaments show no evidence for beta-structure. *J. Biol. Chem.* **269**, 24290–24297.
- Seaberg R.M. and van der Kooy D. (2002). Adult rodent neurogenic regions: the ventricular subependyma contains neural stem cells, but the dentate gyrus contains restricted progenitors. *J. Neurosci.* **22**, 1784–1793.
- Selkoe D.J. (2001). Alzheimer's disease: genes, proteins, and therapy. *Physiol. Rev.* **81**, 741–766.
- Selkoe D.J. (2007). Developing preventive therapies for chronic diseases: lessons learned from Alzheimer's disease. *Nutr. Rev.* **65**, S239–S243.
- Selkoe D.J. and Wolfe M.S. (2007). Presenilin: running with scissors in the membrane. *Cell* **131**, 215–221.

## Amyloid Cytotoxicity and Membrane Lipid Composition

- Serio T.R., Kashikar A.G., Kowal A.S., Sawicki G.J., Moslehi J.J., Serpell L., Arnsdorf M.F., Lindquist S.L. (2000). Nucleated conformational conversion and the replication of conformational information by a prion determinant. *Science* **289**, 1317-1321.
- Serpell L.C., Sunde M., Benson M.D., Tennent G.A., Pepys M.B., Fraser P.E. (2000). The protofilament substructure of amyloid fibrils. *J. Mol. Biol.* **300**, 1033-1039.
- Sethuraman A. and Belfort G. (2005). Protein structural perturbation and aggregation on homogeneous surfaces. *Biophys. J.* **88**, 1322-1333.
- Seubert P., Vigo-Pelfrey C., Esch F., Lee M., Dovey H., Davis D., Sinha S., Schlossmacher M., Whaley J., Swindlehurst C., McCormack R., Selkoe D.J., Lieberburg I., Schenk D. (1992). Isolation and quantitation of soluble Alzheimer's  $\beta$ -peptide from biological fluids. *Nature* **359**, 325-327.
- Shadek G.M., Kummer M.P., Lu D.C., Galvan V., Bredesen D.E., Koo E.H. (2006).  $\text{A}\beta$  induces cell death by direct interaction with its cognate extracellular domain on APP (APP 597-624). *FASEB J.* **20**, 1254-1266.
- Sherrington R., Rogaeva E.I., Liang Y., Rogaeva E.A., Levesque G., Ikeda M., Chi H., Lin C., Li G., Holman K., Tsuda T., Mar L., Foncin J.F., Bruni A.C., Montesi M.P., Sorbi S., Rainero I., Pinessi L., Nee L., Chumakov I., Pollen D., Brookes A., Sanseau P., Polinsky R.J., Wasco W., Da Silva H.A., Haines J.L., Perkicak-Vance M.A., Tanzi R.E., Roses A.D., Fraser P.E., Rommens J.M., St George-Hyslop P.H. (1995). Cloning of a gene bearing missense mutations in early-onset familial Alzheimer's disease. *Nature* **375**, 754-760.
- Shinitzky M. and Barenholz Y. (1974). Dynamics of the hydrocarbon layer in liposomes of lecithin and sphingomyelin containing dicetylphosphate. *J. Biol. Chem.* **249**, 2652-2657.
- Shobab L.A., Hsiung G.Y.R., Feldman H.H. (2004). Cholesterol in Alzheimer's disease. *Lancet Neurol.* **5**, 841-852.
- Shoji M., Golde T.E., Ghiso J., Cheung T.T., Estus S., Shaffer L.M., Cai X.D., McKay D.M., Tintner R., Frangione B., Younkin S.G. (1992). Production of the Alzheimer amyloid  $\beta$  protein by normal proteolytic processing. *Science* **258**, 126-129.
- Shruster A., Melamed E., Offen D. (2010). Neurogenesis in the aged and neurodegenerative brain. *Apoptosis* **15**, 1415-1421.
- Simakova O. and Arispe N.J. (2007). The cell-selective neurotoxicity of the Alzheimer's Abeta peptide is determined by surface phosphatidylserine and cytosolic ATP levels. Membrane binding is required for Abeta toxicity. *J. Neurosci* **27**, 13719-13729.
- Simons K. and Ikonen E. (1997). Functional rafts in cell membranes. *Nature* **387**, 569-572.
- Simons K. and Toomre D. (2000). Lipid rafts and signal transduction. *Nat. Rev. Mol. Cell Biol.* **1**, 31-39.
- Sirangelo I., Malmo C., Iannuzzi C., Mezzogiorno A., Bianco M.R., Papa M., Irace G. (2004). Fibrillogenesis and cytotoxic activity of the amyloid-forming apomyoglobin mutant W7FW14F. *J. Biol. Chem.* **279**, 13183-13189.
- Sjögren M., Vanderstichele H., Agren H., Zachrisson O., Edsbagge M., Wikkelsø C., Skoog I., Wallin A., Wahlund L.O., Marcusson J., Nägga K., Andreasen N., Davidsson P., Vanmechelen E., Blennow K. (2001). Tau and Abeta42 in cerebrospinal fluid from healthy adults 21-93 years of age: establishment of reference values. *Clin. Chem.* **47**, 1776-1781.
- Sjögren M., Mielke M., Gustafson D., Zandi P., Skoog I. (2006). Cholesterol and Alzheimer's disease—is there a relation? *Mech. Ageing. Develop.* **127**, 138-147.
- Skovronsky D.M., Moore D.B., Milla M.E., Doms R.W., Lee V.M.Y. (2000). Protein kinase C-dependent  $\alpha$ -secretase competes with  $\beta$ -secretase for cleavage of amyloid- $\beta$  precursor protein in the trans-golgi network. *J. Biol. Chem.* **275**, 2568-2575.

- Sokolov Y., Kozak J.A., Kayed R., Chanturiya A., Glabe C., Hall J.E. (2006). Soluble amyloid oligomers increase bilayer conductance by altering dielectric structure. *J. Gen. Physiol.* **128**, 637–647.
- Sokolova T.V., Zakharova I.O., Furaev V.V., Rychkova M.P., Avrova N.F. (2007). Neuroprotective effect of ganglioside GM1 on the cytotoxic action of hydrogen peroxide and amyloid  $\beta$ -peptide in PC12 cells. *Neurochem. Res.* **32**, 1302–1313.
- Song H., Stevens C.F., Gage F.H. (2002). Astroglia induce neurogenesis from adult neural stem cells. *Nature* **417**, 39–44.
- Sontag E., Nunbhakdi-Craig V., Lee G., Brandt R., Kamibayashi C., Kuret J., White III C.L., Mumby M.C., Bloom G.S. (1999). Molecular interactions among protein phosphatase 2A, tau, and microtubules. Implications for the regulation of tau phosphorylation and the development of tauopathies. *J. Biol. Chem.* **274**, 25490–25498.
- Squier T.C. (2001). Oxidative stress and protein aggregation during biological aging. *Exp. Gerontol.* **36**, 1539–1550.
- Stefani M., Taddei N., Ramponi G. (1997). Insights into acylphosphatase structure and catalytic mechanism. *Cell. Mol. Life Sci.* **53**, 141–151.
- Stefani M. and Dobson C.M. (2003). Protein aggregation and aggregate toxicity: new insights into protein folding, misfolding diseases and biological evolution. *J. Mol. Med.* **81**, 678–699.
- Stefani M. (2004). Protein misfolding and aggregation: new examples in medicine and biology of the dark side of the protein world. *Biochim. Biophys. Acta* **1739**, 5–25.
- Stefani M. (2007). Generic cell dysfunction in neurodegenerative disorders: role of surfaces in early protein misfolding, aggregation, and aggregate cytotoxicity. *Neuroscientist* **13**, 519–531.
- Stefani M. (2008). Protein folding and misfolding on surfaces. *Int. J. Mol. Sci.* **9**, 2515–2542.
- Stefani M. and Liguri G. (2009). Cholesterol in Alzheimer's disease: unresolved questions. *Curr. Alzh. Res.* **6**, 15–29.
- Stefani M. (2010a). Structural polymorphism of amyloid oligomers and fibrils underlies different fibrillization pathways: immunogenicity and cytotoxicity. *Curr. Protein Pept. Sci.* **11**, 343–354.
- Stefani M. (2010b). Biochemical and biophysical features of both oligomer/fibril and cell membrane in amyloid cytotoxicity. *FEBS J.* **277**, 4602–4613.
- Steiner H., Winkler E., Haass C. (2008). Chemical cross-linking provides a model of the gamma-secretase complex subunit architecture and evidence for close proximity of the C-terminal fragment of presenilin with APH-1. *J. Biol. Chem.* **283**, 34677–34686.
- Suk J.Y., Zhang F., Balch W.E., Linhardt R.J., Kelly J.W. (2006). Heparin accelerates gelsolin amyloidogenesis. *Biochemistry* **45**, 2234–2242.
- Suzuki N., Cheung T.T., Cai X.D., Odaka A., Otvos L. Jr., Eckman C., Golde T.E., Younkin S.G. (1996). An increased percentage of long amyloid beta protein secreted by familial amyloid beta protein precursor (beta APP717) mutants. *Science* **264**, 1336–1340.
- Svennerholm L. and Gottfries C.G. (1994). Membrane lipids, selectively diminished in Alzheimer brains, suggest synapse loss as a primary event in early-onset form (type I) and demyelination in late-onset form (type II). *J. Neurochem.* **62**, 1039–1047.
- Tabner B.J., Turnbull S., El-Agnaf O.M.A., Allsop D. (2002). Formation of hydrogen peroxide and hydroxyl radicals from A $\beta$  and  $\alpha$ -synuclein as a possible mechanism of cell death in Alzheimer's disease and Parkinson's disease. *Free Radic. Biol. Med.* **32**, 1076–1083.
- Takashima A., Noguchi K., Sato K., Hoshino T., Imahori K. (1993). Tau protein kinase I is essential for amyloid beta-protein-induced neurotoxicity. *Proc. Natl. Acad. Sci. USA* **90**, 7789–7793.

## Amyloid Cytotoxicity and Membrane Lipid Composition

- Tamboli I.Y., Prager K., Barth E., Heneka M., Sandhoff K., Walter J. (2005). Inhibition of glycosphingolipid biosynthesis reduces secretion of the  $\beta$ -amyloid precursor protein and amyloid  $\beta$ -peptide. *J. Biol. Chem.* **280**, 28110-28117.
- Taupin P. and Gage F.H. (2002). Adult neurogenesis and neural stem cells of the central nervous system in mammals. *J. Neurosci. Res.* **69**, 745-749.
- Teller H.W., Waring A.J., Lehrer R.I., Harroun T.A., Weiss T.M., Yang L., Huang H.W. (2000). Membrane thinning effect of the  $\beta$ -sheet antimicrobial peptide protegrin. *Biochemistry* **39**, 139-145.
- Terzi E., Holzemann G., Seelig J. (1995). Self-association of  $\beta$ -amyloid peptide (1-40) in solution and binding to lipid membranes. *J. Mol. Biol.* **252**, 633-642.
- Tesco G., Vergelli M., Amaducci L., Sorbi S. (1993). Growth properties of familial Alzheimer skin fibroblasts during in vitro aging. *Exp. Gerontol.* **28**, 51-58.
- The dementia study group of the italian neurological society. (2000). Guidelines for the diagnosis of dementia and Alzheimer's disease. *Ital. J. Neurol. Sci.* **21**, 87-194.
- Tjernberg L., Hosia W., Bark N., Thyberg J., Johansson J. (2002). Charge attraction and  $\beta$  propensity are necessary for amyloid fibril formation from tetrapeptides. *J. Biol. Chem.* **277**, 43243-43246.
- Tsai L.H., Delalle I., Caviness V.S. Jr., Chae T., Harlow E. (1994). p35 is a neural-specific regulatory subunit of cyclin-dependent kinase 5. *Nature* **371**, 419-423.
- Turley S.D., Burns D.K., Rosenfeld C.R., Dietschy J.M. (1996). Brain does not utilize low density lipoprotein-cholesterol during fetal and neonatal development in the sheep. *J. Lipid Res.* **37**, 1953-1961.
- Varadarajan S., Yatin S., Aksanova M., Butterfield D.A. (2000). Review: Alzheimer's amyloid  $\beta$ -peptide-associated free radical oxidative stress and neurotoxicity. *J. Struct. Biol.* **130**, 184-208.
- Verret L., Jankowsky J.L., Xu G.M., Borchelt D.R., Rampon C. (2007). Alzheimer's-type amyloidosis in transgenic mice impairs survival of newborn neurons derived from adult hippocampal neurogenesis. *J. Neurosci.* **27**, 6771-6780.
- Volles M.J., Lee S.J., Rochet J.C., Shtilerman M.D., Ding T.T., Kessler J.C., Lansbury P.T.Jr. (2001). Vesicle permeabilization by protofibrillar alpha-synuclein: implications for the pathogenesis and treatment of Parkinson's disease. *Biochemistry* **40**, 7812-7819.
- Volles M.J. and Lansbury P.T.Jr. (2002). Vesicle permeabilization by protofibrillar alpha-synuclein is sensitive to Parkinson's disease-linked mutations and occurs by a pore-like mechanism. *Biochemistry* **41**, 4595-4602.
- Wakabayashi M. and Matsuzaki K. (2007). Formation of amyloids by  $A\beta$ (1-42) on NGF-differentiated PC12 cells: roles of gangliosides and cholesterol. *J. Mol. Biol.* **371**, 924-933.
- Wakabayashi M. and Matsuzaki K. (2009). Gangliosideinduced amyloid formation by human islet amyloid polypeptide in lipid rafts. *FEBS Lett.* **583**, 2854-2858.
- Walsh D.M., Hartley D.M., Kusumoto Y., Fezoui Y., Condron M.M., Lomakin A., Benedek G.B., Selkoe D.J., Teplow D.B. (1999). Amyloid beta-protein fibrillogenesis. Structure and biological activity of protofibrillar intermediates. *J. Biol. Chem.* **274**, 25945-25952.
- Walsh D.M., Klyubin I., Fadeeva J.V., Cullen W.K., Anwyl R., Wolfe M.S., Rowan M.J., Selkoe D.J. (2002). Naturally secreted oligomers of amyloid  $\beta$  protein potently inhibit hippocampal longterm potentiation in vivo. *Nature* **416**, 535-539.
- Wang S.S., Good T.A., Rymer D.L. (2005). The influence of phospholipid membranes on bovine calcitonin peptide's secondary structure and induced neurotoxic effects. *Int. J. Biochem. Cell. Biol.* **37**, 1656-1669.

- Weisblum B. and Haensler E. (1974). Fluorometric properties of the bibenzimidazole derivative Hoechst 33258, a fluorescent probe specific for AT concentration in chromosomal DNA. *Chromosoma* **46**, 255-260.
- Williams T.L. and Serpell L.C. (2011). Membrane and surface interactions of Alzheimer's A $\beta$  peptide--insights into the mechanism of cytotoxicity. *FEBS J.* **278**, 3905-3917.
- Williamson M.P., Suzuki Y., Bourne N.T., Asakura T. (2006). Binding of amyloid  $\beta$ -peptide to ganglioside micelles is dependent on histidine-13. *Biochem. J.* **397**, 483-490.
- Williamson R., Usardi A., Hanger D.P., Anderton B. H. (2008). Membrane-bound  $\beta$ -amyloid oligomers are recruited into lipid rafts by a Fyn-dependent mechanism *FASEB J.* **22**, 1552-1559.
- Wischik C.M., Crowther R.A., Stewart M., Roth M. (1985). Subunit structure of paired helical filaments in Alzheimer's disease. *J. Cell. Biol.* **100**, 1905-1912.
- Wisniewski K.E., Wisniewski H.M., Wen G.Y. (1985). Occurrence of neuropathological changes and dementia of Alzheimer's disease in Down's syndrome. *Ann. Neurol.* **17**, 278-282.
- Wolfe M.S., Xia W., Ostaszewski B.L., Diehl T.S., Kimberly W.T., Selkoe D.J. (1999). Two transmembrane aspartates in presenilin-1 required for presenilin endoproteolysis and gamma-secretase activity. *Nature* **398**, 513-517.
- Wood W.G., Schroeder F., Avdulov N.A., Chochina S.V., Igbaavboa U. (1999). Recent advances in brain cholesterol dynamics: transport, domains and Alzheimer's disease. *Lipids* **34**, 225-234.
- Wytttenbach A., Swartz J., Kita H., Thykjaer T., Carmichael J., Bradley J., Brown R., Maxwell M., Schapira A., Orntoft T.F., Kato K., Rubinsztein D.C. (2001). Polyglutamine expansions cause decreased CRE-mediated transcription and early gene expression changes prior to cell death in an inducible cell model of Huntington's disease. *Hum. Mol. Genet.* **10**, 1829-1845.
- Xia W., Zhang J., Kholodenko D., Citron M., Podlisny M.B., Teplow D.B., Haass C., Seubert P., Koo E.H., Selkoe D.J. (1997). Enhanced production and oligomerization of the 42-residue amyloid beta-protein by Chinese hamster ovary cells stably expressing mutant presenilins. *J. Biol. Chem.* **272**, 7977-7982.
- Xuan A.G., Long D.H., Gu H.G., Yang D.D., Hong L.P., Leng S.L. (2008). BDNF improves the effects of neural stem cells on the rat model of Alzheimer's disease with unilateral lesion of fimbria-fornix. *Neurosci. Lett.* **440**, 331-335.
- Xue W.F., Hellewell A.L., Gosal W.S., Homans S.W., Hewitt E.W., Radford S.E. (2009). Fibril fragmentation enhances amyloid cytotoxicity. *J. Biol. Chem.* **284**, 34272-34282.
- Yamamoto N., Igbaavboa U., Shimada Y., Ohno-Iwashita Y., Kobayashi M., Wood W.G., Fujita S.C., Yanagisawa K. (2004). Accelerated A $\beta$  aggregation in the presence of GM1-ganglioside-accumulated synaptosomes of aged apoE4-knock-in mouse brain. *FEBS Lett.* **569**, 135-139.
- Yamamoto N., Yokoseki T., Shibata M., Yamaguchi H., Yanagisawa K. (2005). Suppression of A $\beta$  deposition in brain by peripheral administration of Fab fragments of anti-seed antibody. *Biochem. Biophys. Res. Commun.* **335**, 45-47.
- Yamamoto N., Matsubara T., Sato T., Yanagisawa K. (2008). Age-dependent high density clustering of GM1 ganglioside at presynaptic neuritic terminals promotes amyloid beta-protein fibrilllogenesis. *Biochim. Biophys. Acta* **1778**, 2717-2726.
- Yan S.D., Chen X., Fu J., Chen M., Zhu H., Roher A., Slattery T., Zhan M., Nagashima J., Morser A., Migheli P., Nawroth D., Stern A.M., Schmidt A.M. (1996). RAGE and amyloid-beta peptide neurotoxicity in Alzheimer's disease. *Nature* **382**, 685-691.

## Amyloid Cytotoxicity and Membrane Lipid Composition

- Yan S.D., Stern D., Kane M.D., Kuo Y.M., Lampert H.C., Roher A.E. (1998). RAGE-Abeta interactions in the pathophysiology of Alzheimer's disease. *Resto. Neurol. Neurosci.* **12**, 167-173.
- Yan S.D., Zhu H., Zhu A., Golabek A., Du H., Roher A., Yu J., Soto C., Schmidt A.M. Stern D., Kindy M. (2000). Receptor-dependent cell stress and amyloid accumulation in systemic amyloidosis. *Nat. Med.* **6**, 643-651.
- Yanagisawa K., Odaka A., Suzuki N., Ihara Y. (1995). GM1 ganglioside-bound amyloid  $\beta$ -protein (A $\beta$ ): a possible form of preamyloid in Alzheimer's disease. *Nat. Med.* **1**, 1062-1066.
- Yanagisawa K. (2007). Role of gangliosides in Alzheimer's disease. *Biochim. Biophys. Acta* **1768**, 1943-1951.
- Yanagisawa M. and Yu R.K. (2007). The expression and functions of glycoconjugates in neural stem cells. *Glycobiology* **17**, 57R-74R.
- Yanagisawa M., Ariga T., Yu R.K. (2010). Cytotoxic effects of G(M1) ganglioside and amyloid beta-peptide on mouse embryonic neural stem cells. *ASN Neuro* **15**, 2(1):e00029.
- Yanagisawa K. (2011). Pathological significance of ganglioside clusters in Alzheimer's disease. *J. Neurochem.* **116**, 806-812.
- Yancey P.G., Rodriguez W.V., Kilsdonk E.P., Stoudt G.W., Johnson W.J., Phillips M.C., Rothblat G.H. (1996). Cellular cholesterol efflux mediated by cyclodextrins. Demonstration of kinetic pools and mechanism of efflux. *J. Biol. Chem.* **271**, 16026-16034.
- Yang L.J., Zeller C.B., Shaper N.L., Kiso M., Hasegawa A., Shapiro R.E., Schnaar R.L. (1996). Gangliosides are neuronal ligands for myelin-associated glycoprotein. *Proc. Natl. Acad. Sci. USA* **93**, 814-818.
- Yankner B.A., Duffy L.K., Kinschner D.A. (1990). Neurotrophic and neurotoxic effects of amyloid beta protein: reversal by tachykinin neuropeptides. *Science* **250**, 279-282.
- Yip C.M., Elton E.A., Darabie A.A., Morrison M.R., McLaurin J. (2001). Cholesterol, a modulator of membrane-associated Abeta-fibrillogenesis and neurotoxicity, *J. Mol. Biol.* **311**, 723-734
- Younkin S.G. (1998). The role of A beta 42 in Alzheimer's disease. *J. Physiol. Paris* **92**, 289-292.
- Yu R.K. (1994). Development regulation of ganglioside metabolism. *Prog. Brain Res.* **101**, 31-44.
- Yu R.K., Usuki S., Ariga T. (2006). Ganglioside molecular mimicry and its pathological roles in Guillain-Barre' syndrome and related diseases. *Infect. Immun.* **74**, 6517-6527.
- Yu R.K., Yanagisawa M., Ariga.T. (2007). Glycosphingolipid structures. In Comprehensive Glycoscience. Elsevier Oxford UK. 73-122.
- Yuyama K., Yamamoto N., Yanagisawa K. (2006). Chloroquine-induced endocytic pathway abnormalities: cellular model of GM1 ganglioside-induced A $\beta$  fibrillogenesis in Alzheimer's disease. *FEBS Lett.* **580**, 6972-6976.
- Zampagni M., Cascella R., Casamenti F., Grossi C., Evangelisti E., Wright D., Becatti M., Ligure G., Mannini B., Campioni S., Chiti F., Cecchi C. (2011). A comparison of the biochemical modifications caused by toxic and nontoxic protein oligomers in cells *J. Cell. Mol. Med.* **15**, 2106-2116.
- Zandi P.P., Sparks D.L., Khachaturian A.S., Tschanz J., Norton M., Steinberg M., Steinberg M., Welsh-Bohmer K.A., Breitner J.C. (2005). Do statins reduce the risk of incident dementia and Alzheimer's disease? *Arch. Gen Psychiatry* **62**, 217-224.
- Zhang H., Li Q., Graham R. K., Slow E., Hayden M. R., Bezprozvanny I. (2008). Full length mutant huntingtin is required for altered Ca $^{2+}$  signaling and apoptosis of striatal neurons in the YAC mouse model of Huntington's disease. *Neurobiol. Dis.* **31**, 80-88.

Elisa Evangelisti

- Zhao H., Tuominen E.K.J., Kinnunen P.K.J. (2004). Formation of amyloid fibers triggered by phosphatidylserine-containing membranes. *Biochemistry* **43**, 10302–10307.
- Zhao C., Deng W., Gage F.H. (2008). Mechanisms and functional implications of adult neurogenesis. *Cell* **132**, 645–660.



PREMIO TESI DI DOTTORATO

ANNO 2007

- Bracardi M., *La Materia e lo Spirito. Mario Ridolfi nel paesaggio umbro*  
Coppi E., *Purines as Transmitter Molecules. Electrophysiological Studies on Purinergic Signalling in Different Cell Systems*  
Mannini M., *Molecular Magnetic Materials on Solid Surfaces*  
Natali I., *The Ur-Portrait. Stephen Hero ed il processo di creazione artistica in A Portrait of the Artist as a Young Man*  
Petretto L., *Imprenditore ed Università nello start-up di impresa. Ruoli e relazioni critiche*

ANNO 2008

- Bemporad F., *Folding and Aggregation Studies in the Acylphosphatase-Like Family*  
Buono A., *Esercito, istituzioni, territorio. Alloggiamenti militari e «case Herme» nello Stato di Milano (secoli XVI e XVII)*  
Castenasi S., *La finanza di progetto tra interesse pubblico e interessi privati*  
Colica G., *Use of Microorganisms in the Removal of Pollutants from the Wastewater*  
Gabbiani C., *Proteins as Possible Targets for Antitumor Metal Complexes: Biophysical Studies of their Interactions*

ANNO 2009

- Decorosi F., *Studio di ceppi batterici per il biorisanamento di suoli contaminati da Cr(VI)*  
Di Carlo P., *I Kalasha del Hindu Kush: ricerche linguistiche e antropologiche*  
Di Patti F., *Finite-Size Effects in Stochastic Models of Population Dynamics: Applications to Biomedicine and Biology*  
Inzitari M., *Determinants of Mobility Disability in Older Adults: Evidence from Population-Based Epidemiologic Studies*  
Macrì F., *Verso un nuovo diritto penale sessuale. Diritto vivente, diritto comparato e prospettive di riforma della disciplina dei reati sessuali in Italia*  
Pace R., *Identità e diritti delle donne. Per una cittadinanza di genere nella formazione*  
Vignolini S., *Sub-Wavelength Probing and Modification of Complex Photonic Structures*

ANNO 2010

- Fedi M., *«Tuo lumine». L'accademia dei Risvegliati e lo spettacolo a Pistoia tra Sei e Settecento*  
Fondi M., *Bioinformatics of genome evolution: from ancestral to modern metabolism. Phylogenomics and comparative genomics to understand microbial evolution*  
Marino E., *An Integrated Nonlinear Wind-Waves Model for Offshore Wind Turbines*  
Orsi V., *Crisi e Rigenerazione nella valle dell'Alto Khabur (Siria). La produzione ceramica nel passaggio dal Bronzo Antico al Bronzo Medio*  
Polito C., *Molecular imaging in Parkinson's disease*  
Romano R., *Smart Skin Envelope. Integrazione architettonica di tecnologie dinamiche e innovative per il risparmio energetico*

ANNO 2011

- Acciaioli S., *Il trompe-l'œil letterario, ovvero il sorriso ironico nell'opera di Wilhelm Hauff*  
Bernacchioni C., *Sfingolipidi bioattivi e loro ruolo nell'azione biologica di fattori di crescita e citochine*  
Fabbri N., *Bragg spectroscopy of quantum gases: Exploring physics in one dimension*  
Gordillo Hervás R., *La construcción religiosa de la Hélade imperial: El Panhelenion*  
Mugelli C., *Indipendenza e professionalità del giudice in Cina*  
Pollastri S., *Il ruolo di TAF12B e UVR3 nel ciclo circadiano dei vegetali*  
Salizzoni E., *Paesaggi Protetti. Laboratori di sperimentazione per il paesaggio costiero euro-mediterraneo*

ANNO 2012

- Evangelisti E., *Structural and functional aspects of membranes: the involvement of lipid rafts in Alzheimer's disease pathogenesis. The interplay between protein oligomers and plasma membrane physicochemical features in determining cytotoxicity*
- Bondi D., *Filosofia e storiografia nel dibattito anglo-americano sulla svolta linguistica*
- Petrucci F., Petri Candidi Decembrii *Epistolarum iuvenilium libri octo.* A cura di Federico Petrucci
- Alberti M., *La 'scoperta' dei disoccupati. Alle origini dell'indagine statistica sulla disoccupazione nell'Italia liberale (1893-1915)*
- Gualdani R., *Using the Patch-Clamp technique to shed light on ion channels structure, function and pharmacology*
- Adessi A., *Hydrogen production using Purple Non-Sulfur Bacteria (PNSB) cultivated under natural or artificial light conditions with synthetic or fermentation derived substrates*
- Ramalli A., *Development of novel ultrasound techniques for imaging and elastography. From simulation to real-time implementation*



